THE OLEOPHILICITY/HYDROPHOBICITY OF GALENA AND PYRITE IN TWO-LIQUID FLOTATION

A thesis submitted for the degree of
Doctor of Philosophy of the University of London

and

The Diploma of Imperial College

by

DURAN KOCABAĞ

Department of Mineral Resources Engineering
Royal School of Mines
Imperial College
University of London

May 1983

To my parents

ABSTRACT

The different processing methods for the treatment of fine mineral particles are reviewed, with special emphasis on the use of non-polar oils. The thermodynamic conditions for the wetting of a mineral by a liquid have been discussed and the various forces at mineral/oil/water interfaces have been analysed.

An investigation has been made of the concentration of fine galena and pyrite particles at the oil/water interface in a two-liquid flotation system, in the absence of any surfactant. Due to the Eh-pH dependent behaviour of mineral sulphides, electrochemical techniques were used to define the possible redox reactions and surface phases present at the mineral/water interface at different pH values.

Both unoxidised galena and pyrite were found to be naturally oleophilic, but hydrophilic with respect to gas bubbles. More than 70% of the galena and 90% of the pyrite were concentrated at the oil/water interface with maximum recovery at pH 5.5 and 6.5-9.5 respectively. Contact angle measurements were congruent with the flotation results. The maximum contact angles were 70^{o} and 90^{o} for galena and pyrite respectively.

Oxidation in acidic solution below pH 5 increased the oleophilicity of both galena and pyrite due to the formation of S^{o}, whereas in neutral and alkaline solutions their oleophilicity decreased with oxidation, due to the

formation of metal hydroxides. Sulphidation of oxidised minerals with aqueous Na_2S solution restored the oleophilicity.

The initial oxidation of galena took place at pH < 5 by the reaction

$$PbS \longrightarrow Pb^{2+} + S^{o} + 2e$$

and in neutral and alkaline solutions by

$$PbS + 2H_2O \longrightarrow Pb(OH)_2 + S + 2H^{+} + 2e$$

With pyrite, initial oxidation occurred by

$$FeS_2 \longrightarrow Fe^{2+} + 2S + 2e$$

at pH I and 4.6, and by

$$FeS_2 + 3H_2O \longrightarrow Fe(OH)_3 + 2S + 3H^{+} + 3e$$

at higher pH values.

Two-liquid flotation experiments were carried out using a feeder electrode held under potential control, in an attempt to control the surface phase of the sulphide mineral pulp, with which it was in contact, i.e. to carry out controlled potential two-liquid flotation. However, separate contact potential measurements showed that the assumption of the sulphide mineral particles adopting the potential of the feeder electrode by collision was not wholly valid. It was found that the chemistry of metal/metal sulphide or oxide formation was important as well as the mineral-feeder electrode collision efficiency.

ACKNOWLEDGEMENTS

I wish to express my sincere gratitude to Dr H L Shergold and Dr G H Kelsall for their guidance, encouragement and unfailing support during the course of this work.

I would also like to express my thanks to my colleagues in the Royal School of Mines, especially P W Page, for many useful discussions.

I am indebted to the Scientific and Technical Research Council of Turkey (TUBITAK) for financial assistance. I am also indebted to the Department of Mineral Resources Engineering for the provision of financial assistance during the writing of this thesis.

Finally, I should like to thank my wife, Şükran, for her inexhaustible support and patience during the past three years.

CONTENTS

Page

LIST OF FIGURES

Page

Page

LIST OF TABLES

CHAPTER ONE

INTRODUCTION

1 INTRODUCTION

1.1 Treatment of fine particles in mineral processing

Industrial processing of fine particles is a problem in many areas, not least in mineral processing. What is meant by 'slime' or 'fine particle' depends on the method by which the ore has to be treated, and can be defined as that material too fine for efficient treatment by the process under consideration. Thus in gravity concentration generally, although it will depend on the density of the minerals involved, a particle size below 50 μm can be called a slime, whereas in flotation, in salt-type mineral flotation with a relatively unselective collector it is usual to deslime at about 10-15 μm. With sulphides, however, there are examples where desliming is not carried out and the particle size is, say, 90% - 20 μm. Therefore in mineral processing the term 'slimes' or 'fine particles' depends on the process and the mineralogy of the ore, and they are not only difficult to treat but also have adverse effects on the processing of coarser particles.

Slimes are produced by the decomposition of certain rock components of the ore body due to weathering before it is mined (primary slimes) and during crushing and grinding to liberate the valuable minerals from the gangue minerals (secondary slimes). Therefore the slime fraction in an ore will depend on the amount of grinding, and might be as high as 30%, such as in some phosphate ores[1] or even much higher, as it is in the clay industry where the valuable mineral, kaolin, occurs mostly in fine size, 90-95% - 2 μm.[2,3]

As the amount of high grade ores decreases and demand grows for raw materials in the world, man can no longer afford to lose the value contained in slimes. There are also deposits, not treated at present due to their very fine liberation sizes. Therefore the need for the treatment of slimes is increasing. The development of new methods as well as further progress in existing methods for the treatment of slimes is gaining importance.

1.2 Methods exploiting differences in the bulk properties of minerals

These include gravity separation, magnetic separation and electrostatic separation. In spite of claims that gravity separation can be applied to the particles as fine as 10-15 μm range,[5-8] or even finer[6,8], gravity separation is normally limited to particles about 20 μm. Magnetic separation operates over a fairly wide size range[9-16] and can be as effective as flotation in recovering particles down to 5 μm[11] by using a high magnetic field strength.[11] However, electrostatic separation has been effective down to 75 or 50 μm sizes,[17,18] although claims have been made for its applicability to finer sizes.[19-21] With the decrease of particle size with these methods, forces, i.e. liquid drag forces, other than main separating forces, i.e. the differences in density, magnetic susceptibility and electronic conductivity of minerals, become predominant, decreasing the effectiveness of the methods.

1.3 Surface chemical methods

1.3.1 Froth flotation

Of the mineral separation techniques in common use, flotation treats the finest particles. Even in this process, however, not all the particles can be treated to the same degree. The optimum particle size for flotation is between 20 and 100 μm, both below and above which the flotation rate decreases.[22-25,47] This does not mean that the particles at these limiting sizes become less hydrophobic but that the collection of particles by bubbles and the formation of stable aggregates becomes less favourable.

Two characteristics begin to dominate as particle size is reduced. The specific surface becomes larger and the mass of the particle becomes smaller. Hydrodynamic conditions show that the reduction in flotation rates with particle size is related to the decreased probability of bubble-particle collisions.[24,26] The probability of particle-bubble collision is dependent on the mass of the particle, and hence on its size. The greater the particle size the higher the energy of impact that can be utilised in rapturing the liquid film that separates the particle and bubble during collision.[27] The mass of fine particles, however, does not confer sufficient energy for disruption of the liquid layer.[39,43]

The rising bubble forms an integral body with the liquid.[28-31] The streamlines around the bubble make it difficult for fine particles to approach bubble surfaces. Dergaguin and Dukhin[31] suggested that below a certain critical size, particles might

never collide with a bubble either because they will be swept away in the streamlines or because of the presence of 'diffusiophoretic' forces. Recently, the same authors[40] have discussed the peculiar features of fine particle flotation, suggesting that as opposed to the formation of a three phase wetting perimeter as a prerequisite in coarse particle flotation, fine particles can be floated without this contact. There is a possibility of this contactless flotation because long range surface forces such as electrostatic forces together with van der Waals forces might overcome the disjoining forces and bubble particle association is established. Furthermore, the role of electrical double layer forces is very important in the attachment of fine particles to bubbles[40-42] and becomes dominant with colloid size particles.[1] This dominance of surface electrical effects causes the lack of selectivity in fine particle flotation.

Fine mineral particles have higher specific surface energy because of their increased number of edges, corners and crystallographic imperfections[44] which cause increased dissolution of mineral.[1,3] Thus, concentration of certain ions, such as metal cations, might be high enough to cause unintentional activation of undesirable minerals or depression of desired minerals.

Prolonged grinding to produce very fine particles might cause crystallographic and chemical changes, such as amorphisation, decrystallisation and polymorphic transition on the surfaces of fine particles.[45,46] This might lead to the loss of selectivity in their flotation.

Fine particles are not only difficult to float but they are also detrimental to the flotation of coarser particles because of the presence of slime coating,[33-35] entrainment of very fine gangue particles in the froth[25,36] and consumption of large amounts of collector due to their large specific surface area.[37] Nonselective agglomeration of fine particles is also detrimental to their flotation.

1.3.2 Modified flotation techniques for fine particles

During recent years, new methods[1,3,9,18,24,48] have been developed to overcome the problems in the flotation of fine particles.

1.3.2.1 Methods of improving the chemistry of flotation

It has been suggested that using chemisorbing collectors, i.e. collectors that react by specific chemical reactions between the collector ion or molecule and metallic cation sites on the mineral surface, or increasing the pulp temperature, can improve the flotation recovery and grade of fine size ranges, probably by enhancing the selective adsorption of the collector.[1,58] Successful results have been obtained by using chelating agents with 70% - 15 μm hematite[49] and oxidised lead and zinc ores[50] without desliming. One micron scheelite particles have also been floated successfully with sodium oleate, a chemisorbing collector.[51,52]

The beneficial effects of increased conditioning temperature have been demonstrated by Cooke et al[53] in the flotation of hematite from quartz, by Parkins and Shergold[54] with ilmenite,

and by others in the separation of magnetite from quartz[55] and chalcopyrite from galena.[56]

Recently, Miller and Ackerman[57] treated an alunite ore with a grade of 35%, the main gangue mineral being quartz. Using oleic acid, which chemisorbs on alunite, and heating the pulp to 323K, they obtained a rougher recovery of 88% with 65% grade using a -400 mesh (-38μm) particle size. Desliming at 11 μm, however, increased the concentrate grade to 95% with a recovery of 58% in the cleaned product. Lai[58] obtained 83% recovery with a grade of 35% by floating -500 mesh manganese nodule tailings at high ionic strength (sea water) with fatty acids (75% oleic acid) at a pulp temperature of 333K.

1.3.2.2 Methods of improving bubble-particle collision efficiency

This can be obtained either by increasing the effective particle size, by using smaller bubbles or forming bubbles on particles. The first approach is used in 'ultraflotation' or carrier flotation, floc-flotation and emulsion flotation. The second approach is used in electroflotation, vacuum flotation and dissolved air flotation.

a) 'Ultraflotation' or carrier flotation

Carrier flotation is based on the principle of using an auxiliary carrier mineral of fine but floatable size to recover the slimes.[59,60,101] The fine particles to be floated form slime coatings on the carrier mineral and the coated particles are then floated. The rate of adhesion of ultrafine particles to large particles of the carrier mineral may be a factor of 10^3 to 10^4 higher than the rate of cohesion between ultrafine particles in turbulent flow.[62,63] Although the method is said by its inventors[59,61] to be promising for the treatment

of slime particles; so far it has found very few industrial applications. It has been applied to 98% - 15 μm kaolinite on plant scale using calcite as the carrier mineral.[59,61] Good recovery of kaolinite has been obtained by floating the anatase impurities. The method has also been applied to phosphate slimes[61] with sulphur as the carrier, and to quartz by using two coarser size fractions (75-40 μm and 30-21 μm) as carriers for the 5-10 μm fraction.

Warren[51] studied the shear flocculation of ultrafine 1 μm and larger 10-40 μm sheelite particles in sodium oleate solution. The degree of slime coating was determined both by the rate of shear flocculation and by the rate of removal of the coating by attrition and shear redispersion. The most dense slime coatings were observed at the lowest concentration of coarse particles, but the greatest removal of ultrafines from suspension occurred at an intermediate concentration of the coarser fraction. The main drawbacks of this process in mineral beneficiation operations are high reagent consumption and the necessity for subsequent separation of valuables from the carrier particles.[9]

b) Floc-flotation

Selective flocculation[64-67] may be used to increase the effective particle size of slimes, which may then be floated by a conventional flotation technique.

Gaudin and Malezemof[64] found that by selectively flocculating sulphide minerals with heteropholar sulphur-bearing substances, fine sulphide particles could be floated with high recovery.

Osborne[67] investigated the flotation of sulphides with quartz as gangue mineral and for the flotation of flocs, the use of low turbulence flotation units was necessary to avoid the breakage of flocs. The method has also been applied to water clarification,[68] to a hematitic-goethitic taconite ore[69] and to the removal of insoluble slimes from a potash ore.[70]

c) Electroflotation

At a given gas supply rate, more efficient removal of the particles is effected if the bubbles are small,[41,48] due to their increased residence time and specific surface area.[71] One way of producing smaller bubbles is electroflotation,[72-76] in which bubbles are produced by electrolysis of water.

Various applications of electroflotation and the effect of different variables have been reviewed and discussed.[72,73] Glembotsky et al[72] floated both an 86% - 10 μm manganese oxide slime and fine diamonds (0.5-0.042 mm and finer) that could not be treated with conventional flotation. Electroflotation enabled[72] 99% recovery with -5 μm copper sulphide particles from a thickener overflow containing copper/molybdenum sulphides which had been concentrated by conventional flotation. The method has also been applied to cassiterite[75] and chalcopyrite.[289] Bhaskar and Khangoankar[289] floated -20 μm chalcopyrite by electroflotation and obtained 400% and 250% increase in recovery using electro-generated oxygen and hydrogen respectively, compared to dispersed gas flotation with the same gases.

The method is widely used for the treatment of effluents.[76,77] However, in mineral flotation it has yet to find industrial application.

d) Column flotation

The technique of column flotation has been developed to utilise the principle of counter current flow to improve separation in a flotation process. Solids are kept in suspension by settling against rising air bubbles and spray pipes situated a few inches below the froth surface are used for washing purposes. The advantages of using a column are to decrease the entrainment of fine gangue particles by counter current flow, and to increase the bubble-particle collision frequency by increasing the residence time of the bubble in the pulp.[1,3,78]

The technique has been applied to molybdenum.[78] to the separation of fine graphite particles from clay impurities[79] and to a uranium ore.[80] Sastry and Fuerstenau[81] have developed a theoretical model to analyse the performance of a column flotation unit.

e) Vacuum and dissolved air flotation

Nucleation of bubbles from solution on solid particles may be achieved by application of a vacuum or pressure release, thus eliminating the bubble-particle collision step in conventional flotation.[82,83]

In vacuum flotation, the solution is saturated with air at atmospheric pressure and the air bubbles are generated by applying a vacuum to the flotation tank, releasing dissolved air as small bubbles. The process has several disadvantages such as the limited supply of air and difficulty in achieving continuous process.[84]

In dissolved air flotation, pressurised air-saturated water is introduced into a flotation pulp under atmospheric pressure, so releasing small air bubbles. The method is widely used in water purification[83-86] but has yet to find application in mineral processing. Saavedra[87] studied the dissolved air flotation of fine cassiterite (-10 μm) from quartz and found that for effective separation, an adequate control of the surface chemistry of system was necessary, to render the valuable particles hydrophobic and flocculated to some extent. The main factors contributing to a low selectivity were hetero-coagulation of cassiterite and quartz particles, non-selective adsorption of collector and entrainment of quartz particles in the froth. Adhesion of bubbles to particles was found to be by particle-bubble collision.

f) Emulsion flotation

In emulsion flotation, a mixture of collector reagent and neutral (non-polar) oil is used,[88-91] usually in an emulsified form. The total amount of reagent is many times greater than that employed in ordinary flotation. The collector renders the mineral particles hydrophobic, thereby enabling the oil droplets to adhere to the particles. The oil-coated particles then become attached to one another and form a selective agglomerate. The amount of reagent required depends upon the floatable mineral content of the ore, the solubility of gangue minerals in water, and on the total surface area of the desired mineral.

The effect of a range of variables on the conditioning of emulsion flotation of ilmenite,[54,91-93] apatite[89] and iron

ore[94] have been studied. A conditioning mechanism involving a flocculation-deflocculation process has been described,[54,98,92,94] during which first non-selective flocculation of ore takes place, followed by a deflocculation period. Both recovery and selectivity were highest at the end of the deflocculation period during which redistribution of reagents takes place, resulting in hydrophobic mineral and hydrophilic gangue particles. Conditioning requires intense agitation at high pulp density and so a considerable amount of power.

Although it has been claimed that very fine particles can be treated by the process[88,89] and it has been applied to manganese,[95] hematite[96] and ilmenite ores[91,97] without desliming, usually ore is deslimed before flotation.[98-100]

1.3.3 Selective flocculation

In the floc-flotation of fine particles the flocculation of fine particles into flocs improved their flotation, since a floc acts as a coarse particle, overcoming the difficulties due to the small mass of a fine particle.[64-70]

If selective flocculation of one mineral can be obtained while keeping the rest of the solids dispersed, the separation of the flocs might be obtained by means of methods other than flotation, such as elutriation[102,103,111] or the use of a floc cleaning tank.[104]

Aggregation of fine particles can be obtained by: i) coagulation[105-107,110] by adjusting the concentration of potential determining ions or by increasing the ionic strength of electolytes or both; ii) flocculation[106-109] involving use of high

molecular weight long chain polymers that bind the particles together by a bridging mechanism.

Coagulation has several practical limitations. The process depends mainly on inter-particle collisions forming weak aggregates which are liable to disintegrate when subjected to shearing. By contrast, flocculation is far more effective.[106,109] The flocculation rate of particles is faster, as the resultant floc sizes are larger, and the flocs formed are stronger.

In selective flocculation, like flotation, the suspended particles have to be conditioned in such a way that functional groups of added molecules attach only to the surfaces of the particles to be flocculated. Therefore problems are to be expected similar to those encountered in conditioning fine particles for flotation.

The adsorption of polymers in flocculation can take place due to coulombic interaction, hydrophobic bonding and hydrogen bonding.[110] For successful selective flocculation, a good dispersion of at least one component, selective polymer adsorption and removal of the flocs are all necessary.

Read[103] achieved selective flocculation of either hematite or silicate from a mixture, which was stably dispersed prior to flocculant addition. However, Yarar and Kitchener[108] achieved selective flocculation of galena from quartz under conditions in which the galena was initially slowly coagulating and the quartz was stably dispersed.

Flocculant adsorption has been inhibited in different cases by electrostatic repulsion,[103,108,112] preadsorbed species[103,108]

and removal of free hydroxyls from the surface of quartz by heating.[162] The presence of dissolved ions also affect the selective adsorption of flocculants.[113]

Read and Whitehead[111] have described an elutriation separator for the separation of flocs in the selective flocculation of feldspar from hematite. Friend et al[104] separated calcite ($< 10\ \mu m$) from quartz ($< 20\ \mu m$) by using a floc cleaning tank.

It has been suggested that polymer molecules containing the types of functional groups used in flotation collectors might give better selectivity.[114-116] Attia and Kitchener[114] flocculated various minerals with a number of water-soluble polymers of high molecular weight, incorporating sulphydryl (-SH) or other active groups. Selective flocculation of $-10\ \mu m$ cassiterite from $-37\ \mu m$ quartz was achieved[115-116] with a flocculant that was obtained by introducing carboxylic acid groups into Cyanamur - 250, a nominally pure polyacrylamide. Rubio and Kitchener[117] have suggested that selective flocculation can be obtained by treating the mineral with a collector prior to adding polymeric flocculants that are surface active by virtue of hydrophobic groups which associate with the adsorbed collector. They demonstrated the validity of this principle by separating chrysocolla and malachite from quartz, calcite and dolomite, using potassium ethyl xanthate as collector and poly [ethylene oxide $(-CH_2\ CH_2\ O-)_n$] as the flocculant which forms hydrophobic bonds with the collector.

Various applications have been reviewed[1,102,118] for selective flocculation which has also been applied to iron

ores,[119-122] bauxites[123,124] and calcite-quartz, magnesite-quartz and dolomite-quartz systems.[125] The main problem at present with the treatment of fine particles by selective flocculation is in achieving selective adsorbtion of a flocculant on the mineral to be flocculated. As with flotation, it is necessary to employ auxiliary reagents to modify the action of flocculants and each ore needs detailed investigation to establish suitable conditions.[126]

1.3.4 Concentration of minerals at the oil/water interface

When a mixture of two immiscible or partially immiscible liquids is shaken, a dispersion of one in the other results. To obtain any degree of stability, a third component which can be either an emulsifying agent or a finely divided solid[127,128] is necessary. If the two immisciple liquids are a neutral oil and water, and the solid particles are partially wetted by both fluids, then the solid particle will concentrate at the oil/water interface and stabilise oil drops by preventing their coalescence.

The methods involving oil are analogous to the other surface chemical methods. They require that the mineral to be separated should be made selectively hydrophobic/oleophilic by the use of collectors, activators and depressants, as in flotation. However, the use of oil drops instead of air bubbles as the carrier phase has several advantages. The lower oil/water interfacial tension compared to the air/water surface tension means that oil in water dispersions are energetically more favourable than air in water dispersions. Much higher oil/water interfacial areas can be

obtained than in air/water systems, which results in a greater probability of particle-drop collisions and hence attachment. Furthermore, oil drops have a greater momentum than air bubbles, which should favour collection of fine particles. Two methods are available for the treatment of fine particles, depending on the amount of oil used.

1.3.4.1 Spherical agglomeration

In spherical agglomeration, the amount of oil used varies from 1.5 to 6%[129] and depends on the particle size, the type of mineral treated and the size of agglomerates required.[130] The oil is added to the slurry of the ore together with an appropriate collector, if the particles to be collected are not naturally oleophilic. The pulp is conditioned, preferably under a slow shearing action, until the oil phase has loaded the desired particles at a pulp density of about 30%. During shearing, the oil drops coat oleophilic particles. The oil-coated particles then adhere to each other on collision, forming agglomerates.[130-134] With the aid of a suitable tumbling action, compact and approximately spherical agglomerates of up to 20 mm diameter or more can be obtained, which then can be separated by screening or sedimentation. For spherical agglomeration to take place, a contact angle of $> 90^{\circ}$, measured through the aqueous phase, is required.[137]

Collisions between oil-coated particles result in the formation of oil bridges which bind the particles together. For this reason the second liquid is usually called 'bridging liquid'. The form and strength of the agglomerates formed is dependent

on the amount of bridging liquid added, the degree and type of agitation and on size, size distribution and surface conditioning of relevant particles.[135-137] Addition of too little bridging liquid results in the formation of flocs and very small agglomerates, which are quite weak and difficult to separate. As the amount of bridging liquid is increased the agglomerates change progressively to larger and densified spheres and eventually to pasty lumps, in which the solids are essentially dispersed in the bridging liquid.[133]

The type and degree of agitation applied to the suspension influences the size and size distribution of agglomerates formed, because it must not only distribute the bridging liquid uniformly but also promote interparticulate collision and agglomerate growth.[132,135,136] Sirianni and co-workers[132] have reviewed the various agglomeration equipment and their application. They include ball mills, inclined pans, grease kettles, horizontal drums, etc.

A review of the application of spherical agglomeration methods in mineral beneficiation and in other fields such as separation of solids from liquids and pelletisation, is given by Puddington and Sparks.[133]

Spherical agglomeration has been applied, at laboratory and pilot plant scales, to the treatment of mineral mixtures containing hematite,[131] alumina,[137] graphite and zinc sulphide[130] and to germanium ore,[138] gold ore,[139] two different iron-apatite ores,[140] tin ore,[141,142] ilmenite concentrates,[143] and barite.[144] No desliming was necessary and successful results have been reported.

It was found[142-144] that as the agglomerates grew they became more selective towards the hydrophobic mineral. Hydrophobic particles forced less hydrophobic particles out of the agglomerate in the competition to contact the organic bridging liquid.

Meadus and Puddington[144] treated the tailings from a lead-zinc mine (65% - 325 mesh) to produce a high grade barite. Four stage flotation of barite produced a grade of 95% but with a recovery of only 25%. In comparison a two stage agglomeration process yielded the same grade of barite at a recovery of over 80%. Kavouridis et al[137] found that fine alumina particles (-10 μm) could be agglomerated provided that a preconditioning step was used. They also found that the degree of agglomeration and type of agglomerate obtained at a given collector concentration, pH and tumbling speed were dependent on the bridging liquid volume and the size distribution of alumina particles.

Spherical agglomeration has also been applied to coal processing[135,136,145-147] and was found to be effective when the grinding time was such that the feed was 95% minus 400 mesh.[145]

1.3.4.2 Two-liquid flotation

The two-liquid flotation is similar to froth flotation except that oil droplets collect the hydrophobic particles in the pulp instead of air bubbles. The amount of oil may vary from 10 to 30% and forms a separate phase. At higher oil to water ratios there is the possibility that the emulsion obtained will change from the oil-in-water to the water-in-oil type, which is undesirable.[148] However, this is dependent not only on the oil to water phase ratio

but also on the type of surfactant used and the contact angle established between the oil, water and solid phases.[128,149] After being made selectively hydrophobic and collected by oil droplets, the hydrophobic components of the slurry are carried upwards, forming an oil-rich layer above the slurry and separating from the aqueous phase.

According to von Reinders,[150] three situations may occur in an oil/water/solid system:

i) if $\gamma_{s/o} > \gamma_{o/w} + \gamma_{s/w}$, the solid will be dispersed in the aqueous phase.

ii) if $\gamma_{s/w} > \gamma_{o/w} + \gamma_{s/o}$, the solid will be dispersed in the oil phase.

iii) if $\gamma_{o/w} > \gamma_{s/o} + \gamma_{s/w}$, or none of the three interfacial tensions is greater than the sum of the other two, the solid will be concentrated at the oil/water interface. The $\gamma_{o/w}$, $\gamma_{s/o}$ and $\gamma_{s/w}$ are the interfacial tensions at oil/water, solid/oil and solid/water interfaces respectively.

If the interfacial tension between the three phases is modified by use of suitable surfactants, such that for a particular mineral component condition (ii) or (iii) is satisfied, it should be possible to 'extract' the mineral particles into the oil phase[128,160,161] or concentrate them at the oil/water interface.[149-159]

Schulman and Lega[128] investigated the stabilisation of emulsions by barium sulphate particles with alkyl sulphates and other surfactants. When the contact angle was $<90^{\circ}$, an oil-in-water emulsion was formed and when it was $>90^{\circ}$, a water-in-oil emulsion was obtained. At high concentrations of long-chain

surfactants the contact angle approached 180° and some barium sulphate particles became dispersed in the oil phase.

Takakuwa and Takamori[149] used the occurrence of phase inversion to establish whether the contact angle was bigger or smaller than 90° in a study of the flotation of sulphides.

Two-liquid flotation has been applied to the separation of many minerals at both laboratory and pilot plant scales.[150,151] Shergold and Mellgren[152,153] applied the process to the separation of hematite and quartz particles of 50 and 57% - 10 μm respectively, using iso-octane as the oil phase and either alkyl sulphates or alkyl amines as collector. Lai and Fuerstenau[154] concentrated fine alumina particles at the iso-octane/water interface using sodium dodecyl sulphonate as collector. Similarly, Raghavan and Fuerstenau[155] concentrated 0.2 μm hematite particles by oil flotation, using potassium octylhydroxamate to control the wettability of the hematite particles, and demonstrated the superiority of oil flotation over froth flotation in separating the hematite from quartz. Coleman and co-workers[156] used the two-liquid flotation method to separate calcite from ground shale.

The recovery of cassiterite slimes have also been studied with two-liquid flotation.[157,158] Zambrana and co-workers[157] investigated the recovery of cassiterite from a -10 μm fraction containing 1.5% Sn, with gasolene as the oil phase and Aerosol 22, a sulpho-succinamate, as the collector. They reported rougher tin recoveries of about 80% at a grade of 6.5% Sn and cleaner concentrates of 14% Sn at recoveries of about 60%.

Two-liquid flotation has been applied to the removal of impurities, such as anatase, rutile and iron oxide, from -1 μm

kaolin clays.[2,159] A pilot plant for the process has been developed by English China Clays Ltd[2] using kerosene as the oil phase and oleic acid as collector.

The extraction of rutile (titanium dioxide) particles into various organic liquids have been achieved by Stratton-Crawley and Shergold[160,161] with cationic and anionic collectors. A 180^{o} receding contact angle was a prerequisite for the extraction to occur. Although in general, nonpolar oils with an interfacial tension against pure water of less than 49.6 mN m^{-1} extracted TiO_2, there was no obvious relationship between the extraction and the oil/water interfacial tension.

It has been suggested that the process may also be applied to the concentration of sulphide minerals and diamond.[129] The concentration of pyrite, sphalerite and chalcopyrite at the oil/water interface was observed using paraffin as the oil phase without any collector. However, although detailed studies have been carried out on two-liquid flotation of various oxide minerals, no such study has been made on sulphide minerals. These are of particular interest because in addition to the need to develop new processes for the treatment of finely disseminated complex sulphide ores, they are also substantially different from oxides and silicates. This is reflected in the length of the hydrocarbon chain in the collectors used to float these minerals. Sulphides require short chain thiols or their oxidation products, whereas long chain electrolytes are used to float the oxides and silicates. They are even suggested to be naturally hydrophobic.[217,221,225]

CHAPTER TWO

WETTABILITY IN MINERAL/WATER/OIL SYSTEMS

2.1 Thermodynamics of wetting

The thermodynamic condition for floatability, i.e. for a finite contact angle, in a froth flotation system is that the work of adhesion of water to the solid (Ww/s) should be less than the work of cohesion of water (Wco):[163]

$$Ww/s < Wco \tag{2.1}$$

The work of adhesion per unit area of a liquid to a solid is defined by the Dupré equation:

$$Ww/s = \gamma_{s/v} + \gamma_{w/v} - \gamma_{s/w} \tag{2.2}$$

and the work of cohesion of the water is

$$W_{co} = 2\ \gamma_{w/v} \tag{2.3}$$

where $\gamma_{s/v}$, $\gamma_{w/v}$ and $\gamma_{s/w}$ are the interfacial energies, as defined in figure 1a.

If the water is replaced with a nonpolar oil, the same condition should prevail for the formation of a contact angle at the solid/oil/vapour interface:

$$W_{o/s} < W_{o-o} \tag{2.4}$$

$$W_{o/s} = \gamma_{s/v} + \gamma_{o/v} - \gamma_{s/o} \tag{2.5}$$

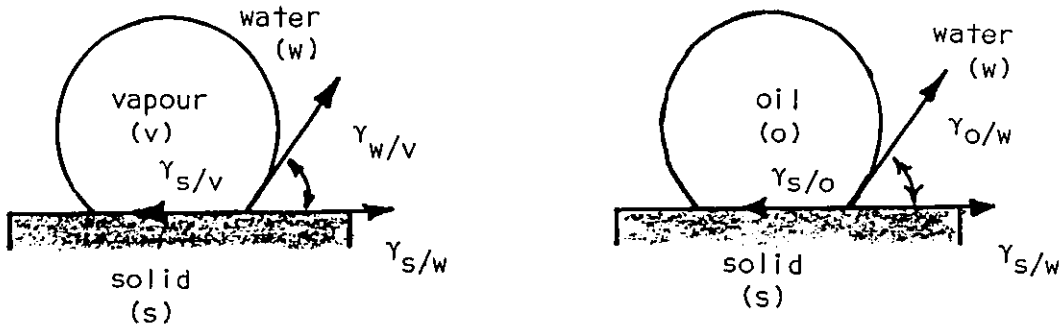

Figure 2.1. Contact angle and interfacial tension forces (a) at the solid/water/vapour interface, (b) at the solid/water/oil interface. θ , contact angle, $\gamma_{s/w}$, $\gamma_{s/v}$, $\gamma_{w/v}$, $\gamma_{s/o}$ and $\gamma_{o/w}$ are the interfacial tensions or energies at the solid/water, solid/vapour, water/vapour, solid/oil and oil/water interfaces respectively.

and

$$W_{o-o} = 2\gamma_{o/v} \qquad (2.6)$$

where $W_{o/s}$ is the work of adhesion of oil to the solid. W_{o-o} is the work of cohesion of oil and $\gamma_{o/v}$ and $\gamma_{s/o}$ are the interfacial energies at the oil/vapour and solid/oil interfaces respectively.

The two conditions (2.1) and (2.4) indicate that in a two-liquid flotation system, where the solid surface is in contact with water and a nonpolar oil, the liquid with the higher work of adhesion to the solid should replace the liquid with the lower work of adhesion, and form a contact angle at

the mineral/oil/water interface (figure 1b). If the work of adhesion of oil to the solid is larger than the work of adhesion of water, then the solid should be wetted by the oil:

$$W_{o/s} > W_{w/s} \qquad (2.7)$$

$$(\gamma_{o/v} - \gamma_{s/o}) > (\gamma_{w/v} - \gamma_{s/w}) \qquad (2.8)$$

Since in all cases $\gamma_{o/v} < \gamma_{w/v}$ and therefore $W_{co} > W_{o-o}$, equation (2.8) can hold only if $\gamma_{s/w} >> \gamma_{s/o}$. The liquid of polarity closer to that of the solid will preferentially wet that solid.[164]

If dispersion forces alone are assumed to be involved at the interfaces when the solid surface is naturally hydrophobic, as with graphite, sulphur and wax,[165] then according to Fowkes[166]

$$\gamma_{s/w} = \gamma_{s/v} + \gamma_{w/v} - 2\sqrt{\gamma^{d}_{s/v}\ \gamma^{d}_{w/v}} \qquad (2.9)$$

and

$$\gamma_{s/o} = \gamma_{s/v} + \gamma_{o/v} - 2\sqrt{\gamma^{d}_{s/v}\ \gamma^{d}_{o/v}} \qquad (2.10)$$

where $\gamma^{d}_{s/v}$, $\gamma^{d}_{w/v}$ and $\gamma^{d}_{o/v}$ are the dispersion force components of $\gamma_{s/v}$, $\gamma_{w/v}$ and $\gamma_{o/v}$ respectively. Substitution of $\gamma_{s/w}$ and $\gamma_{s/o}$ from equations (2.9) and (2.10) into (2.8) gives

$$\gamma^{d}_{o/v} > \gamma^{d}_{w/v} \qquad (2.11)$$

For a non polar oil the surface energy/tension is equal to its dispersion component, i.e. $\gamma_{o/v} = \gamma^{d}_{o/v}$, so that if $\gamma_{o/v} > \gamma^{d}_{w/v}$, the solid will be wetted preferentially by the oil. The value of $\gamma^{d}_{w/v}$ has been determined by Fowkes[166,167] as 21.8 ± 0.7 mJ m^{-2} at 293 K. Hence condition (2.11) becomes

$$\gamma_{o/v} > 21.8 \pm 0.7 \text{ mJ } m^{-2} \qquad (2.12)$$

In a two-liquid flotation system in which one of the liquids is a non polar oil, in the absence of long chain reagents or any other electrolytes which adsorb at the oil water interface,[161,168] the assumption that dispersion forces alone are present will hold at the oil/water and mineral/oil interfaces.[166] However, for mineral/water interfaces it applies only to naturally hydrophobic minerals, e.g. graphite, molybdenite, sulphur and talc.[165,169]

The mineral/water/vapour and mineral/water/oil systems differ in that dispersion interactions are absent in the vapour.[198] This constrains the maximum contact angle to 120° in the former system, while it is 180° in the latter.

2.2 Other forces at the mineral/water interface

With most of the minerals, the work of adhesion ($W_{w/s}$) of water to the mineral involves forces in addition to dispersion interactions,[170-172] which exist at all interfaces:

$$W_{w/s} = W_d + W_h + W_i \qquad (2.13)$$

where W_d is the contribution from London-van der Waals (dispersion) forces, W_h is the contribution from the hydration of non-ionic polar sites, as with hydrogen bonding of water to surface groups, and W_i is the contribution from ionic sites.

The work of cohesion of water from equation (2.3) is 144 mJ m^{-2} ($\gamma_{w/v}$ = 72 mN m^{-1}), of which 43.6 mJ m^{-2} is due to dispersion forces and the remainder to polar forces, mainly hydrogen bonding.[170] All solids would be naturally hydrophobic/oleophilic if only dispersion forces were involved.[165] Therefore, the hydrophilicity/oleophobicity of mineral/water interfaces is due to the hydration (W_h) and ionisation (W_i) energies which lead to the formation of an electrical double layer.[173-176] For oxygen containing minerals, (W_h + W_i) is large compared with W_{co} and W_d,[170, 171, 199] so that oxide minerals have a strongly bound surface hydration layer and are hydrophilic.[177,199]

The particular importance of hydrogen bonding at the silica/water interface has been demonstrated by Laskowski and Kitchener.[170] For that interface, W_d = 102 mJ m^{-2}, (W_h + W_i) = 368 mJ m^{-2} and except at very high pH values, $W_h >> W_i$. These strong bonding forces arise from the interaction between water and silanol groups, Si-OH, which result when a newly formed silica surface is exposed to water. They form hydrogen bonds with water molecules, thus markedly increasing the strength of attachment of water to the surface.[162,178,179]

In this hydrated state silica is extremely hydrophilic. However, if it is heated to temperatures of 923-1123 K, the polar groups giving rise to W_h are removed from the surface with the formation of siloxane bonds, Si-O-Si, which are basically covalent in nature.[180] The siloxane oxygens are very much less electronegative than hydroxyl oxygens and consequently show little or no tendency to form hydrogen bonds. In this form silica is hydrophobic.[170,181] It has been shown[162] that such dehydrated quartz surfaces do not adsorb flocculants such as polyacrylamides, whose adsorption is known to depend on hydrogen bonding. McCafferty and Zettlomeyer[199] have confirmed the existence of a hydration layer with an ice-like structure on α-Fe_2O_3. The water molecules are doubly hydrogen bonded to two surface hydroxyl groups and are immobile at the surface.

In the industrial flotation of hydrophilic minerals, surfactants known as 'collectors' are used to make the mineral surfaces hydrophobic/oleophilic. The main function of the collector is to eliminate polar sites from the solid surface,[182] producing a lower energy surface.[183] The interaction of water with the mineral surface decreases and the hydration layer becomes unstable or metastable,[196] easing the way for the attachment of air bubbles or oil drops to the mineral surface.

2.2.1 Electrical forces at the interfaces

The W_l factor in equation (2.13) is responsible for the formation of an electrical double layer at the interface[176,185] and is due to[184]

a) differences in the affinity of two phases for electrons;

b) differences in the affinity of two phases for anions and cations, i.e. dissolution or adsorption;

c) ionisation of surface groups;

d) physical entrapment of non-mobile charge in one phase;

e) adsorption of dipoles.

Figure 2.2 shows a schematic representation of the electrical double layer at the mineral/water interface, assuming preferential dissolution of cations which act as counter ions in the liquid phase. This figure also shows the distribution of potential across the double layer. The closest approach of hydrated counter ions to the surface (δ) defines the Stern or outer Helmholtz plane.[164] If there are specifically adsorbed dehydrated ions, these will be located at the inner Helmholtz plane[227] (IHP) (figure 2.2).

The potential difference between the surface and the bulk solution (usually referred to as the surface potential) is ψ_o. The double layer potential is constituted by a potential difference in the Stern layer ($\Psi\delta$) and a potential drop across the diffuse layer or Gouy layer, which is considered to approximate to the zeta potential $-\zeta$. The potential changes linearly with distance from the surface to the Stern plane and from there decays exponentially, at low ψ_o, to zero in the bulk solution. When the specifically adsorbed ions are of opposite charge to that of the solid surface, charge reversal can take place, as seen in figure 2.2d (superequivalent adsorption).[227]

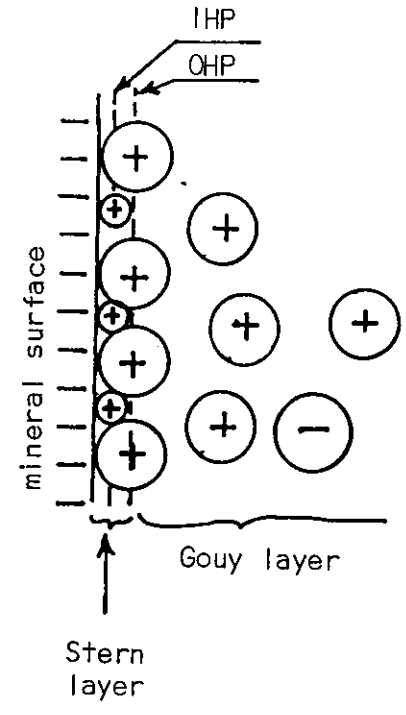

(a) Distribution of ions in the double layer

Hydrated counter ions

Hydrated co-ions

Specifically adsorbed cations

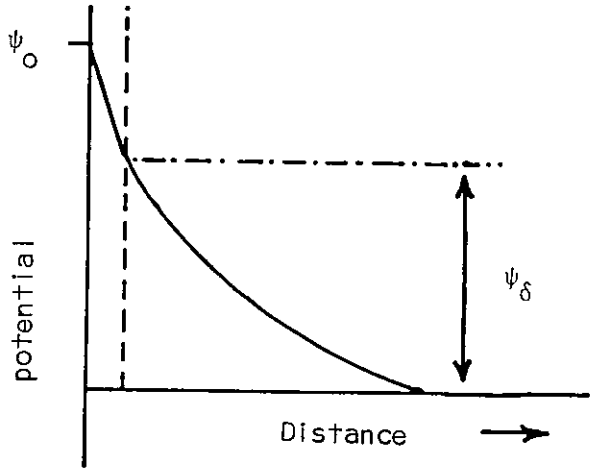

(b) The change of potential in the absence of specific adsorption

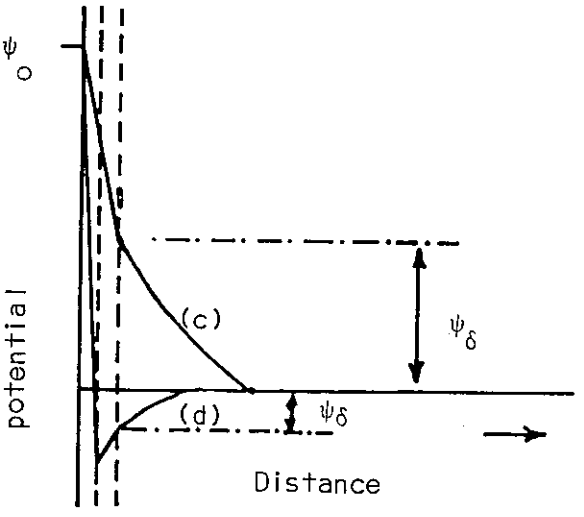

(c) The change of potential in the presence of specific adsorption

(d) in the presence of superequivalent adsorption

Figure 2.2. Schematic representation of the electrical double layer and the change of potential across the mineral/solution interface

Those ions that are free to pass between the two phases and establish the electrical double layer are called potential determining ions. In the case of ionic solids such as $BaSO_4$, AgI and CaF_2, the surface charge arises from a preference of one of the lattice ions for sites at the solid surface as compared with the aqueous phase.[185] Equilibrium is reached when the electrochemical potential (μ) of these ions in the solid and aqueous phases are equal. The potential determining ions for oxide[177,186] and silicate[187] minerals are H^+ and OH^- ions. For salt type minerals, they could be lattice ions as for barite ($BaSO_4$), or both lattice ions and H^+/OH^- ions as for calcite ($CaCO_3$) and apatite $\left[Ca_{10}(PO_4)_6(OH)_2\right]$, because of the hydrolysis reactions that the lattice ions undergo.[188,226] Therefore flotation of these minerals is pH dependent. For sulphide minerals, lattice ions are potential determining[185,189,191] as are H^+/OH^- ions, in that their activity controls the activity of lattice ions by the $H_2S/HS^-/S^{2-}$ equilibria. When the concentration of cation and anion are equal at the interface, the surface charge is zero, and the corresponding solution condition is referred to as the point of zero charge (pzc).[192] The pzc of an oxide is considered generally to correspond to the pH of minimum solubility.[188]

The surface charge density σ_s on a solid in water is determined by the adsorption density of potential determining ions on the solid surface. In the case of a univalent salt σ_s is given by

$$\sigma_s = F(\Gamma_{M^+} - \Gamma_{A^-}) \qquad (2.15)$$

where F is the Faraday constant, Γ_{M^+} and Γ_{A^-} (mol. m^{-2}) are the adsorption densities of the potential determining cation and anion respectively.

The electrical double layer forces, arising from the presence of surface charge on the mineral, affects the equilibrium thickness of the wetting films on the surface of minerals[172,175] and therefore the attachment of mineral particles to oil drops or air bubbles. Derjaguin et al[193,194] have suggested a disjoining pressure concept to explain the stability of liquid films between a solid surface and an approaching air bubble. The disjoining pressure (Π) has three main independent components:[181]

$$\Pi = \Pi_{vdw} + \Pi_{el} + \Pi_s \qquad (2.16)$$

where Π_{vdw} is the pressure due to van der Waals forces, Π_{el} is the pressure due to electrical double layer forces and Π_s is a structural component. As the electrical component is repulsive in all flotation systems, the overall Π will be positive if the Π_{el} term is large. In this condition the liquid film will not break to allow the particle-bubble attachment to take place.[195] This implies that for the solution conditions pH < pzc or pH > pzc, the resultant surface charge will make the mineral more hydrophilic. This has been demonstrated with the collectorless flotation of molybdenite[194] and antimonite.[197]

Read and Kitchener[174,175] suggested that for films thicker than 30 nm on solid surfaces, the electrical double

layer forces should be the predominant component of the disjoining pressure, while Derjaguin and Churaev[290] suggested for films <10 nm the main role was played by the structural component of the disjoining pressure.

2.3 Sulphide minerals

Although the hydrophilic nature of most oxide and silicate minerals is well proven, the position of sulphide minerals, such as galena (PbS), pyrite (FeS_2) and chalcopyrite ($CuFeS_2$) is not yet clear, with the exception of molybdenite (MoS_2), which is naturally hydrophobic. Gaudin[214] suggested that unoxidised sulphides were naturally hydrophobic and could be floated with a frother alone. This was rejected by Taggart et al[215] and Sutherland and Wark,[216] who claimed sulphides were naturally hydrophilic, the observed hydrophobicity being due to contamination. 'Unoxidised' galena has been reported to float without any reagent[218] and with a frother alone.[217,218] Stewart[220] and Fuerstenau and Sabacky[221] floated copper-activated sphalerite and various sulphide minerals respectively, without using any reagent. Lepetic[222] floated a dry, autogeneously ground chalcopyrite with a frothing agent, while Heyes and Trahar[223] found that chalcopyrite was floatable under oxidising conditions, but hydrophilic under reducing conditions. The observed natural hydrophobicity was found to be due to the sulphur formed by oxidation of the mineral surface.[224] A recent study by Yoon[225] showed that chalcopyrite and activated sphalerite could float with a frother

alone. Plaksin[219] explained the observed natural hydrophobicity of sulphide minerals with the adsorption of oxygen which dehydrated the surface.

Sulphide minerals, unlike oxides and silicates, are predominantly covalently bonded[200-201] and do not form hydrogen bonds with water.[171] Their solubilities in water are extremely low,[188,203] reflected in the solubility product values for PbS, CuS, ZnS and HgS of 10^{-28}, 10^{-45}, 10^{-23} and $10^{-52.4}$ respectively. Such low solubility products suggest that sulphide minerals should be relatively inert in aqueous solutions. However, this is not the case, since they are not only pH dependent as with oxides, but also redox potential (E_h) dependent.[204-206] They are thermodynamically unstable in the presence of oxygen as surface oxidation to S_n^{2-}, S^o, $S_2O_3^{2-}$, SO_3^{2-}, SO_4^{2-} and metal ions or oxides/hydroxides occurs depending on the pH. The oxidation products are more soluble than the underlying sulphides.

As sulphide minerals are semiconductors,[207,208] they can act as sources or sinks for electrons and so support electrode reactions, such as their surface oxidation.[232]

In the presence of oxygen or other dissolved oxidants, the conducting mineral/solution potential adopts a 'mixed' value (E_m) between the reversible potentials (EO_2/H_2O) and $E_{\text{mineral ox/red}}$ (E_a), such that cathodic oxygen (oxidant) reduction occurs at a rate equal and opposite to the rate of anodic mineral oxidation, so maintaining an electron balance. The potential differences ($EO_{2/H_2O} - E_m = \eta_c$) and ($E_m - E_a = \eta_a$)

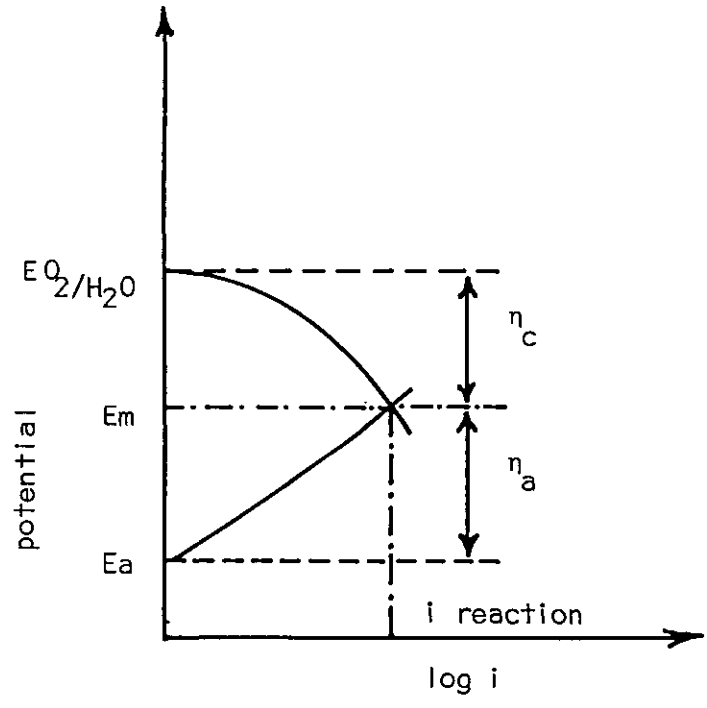

Figure 2.3. Schematic Evans diagram representing the change of anodic and cathodic current with potential. The intersection of the curves defines the reaction current and potential.

provide the driving forces/overpotentials (η) (figure 2.3), which cause the cathodic and anodic half cell reactions to depart from equilibrium and occur at a significant net rate, i.e. oxygen cathodically polarises the mineral surface, the high electronic conductivity of which 'shorts out' the two half cells, as in the corrosion of metals.

$$\tfrac{1}{2}O_2 + 2H^+ + 2e \rightleftharpoons H_2O \qquad (2.17)$$

$$Eh = 1.229 - 0.0591\ pH + 0.01448 \log P_{O_2}$$

$$Pb^{2+} + S^o + 2e \rightleftharpoons PbS \qquad (2.18)$$

$$Eh = 0.354 + 0.0295 \log \left[Pb^{2+}\right]$$

The thermodynamically favoured reactions of a sulphide mineral in contact with aqueous solution of selected composition may be represented in the form of a potential-pH diagram, originally devised by Pourbaix[243] for metals and extended to minerals by Garrels and Christ.[244] Peters[245] has also derived Eh-pH diagrams for metal-sulphur-water systems. By comparing the rest potential for a particular mineral with the appropriate Eh-pH diagram the stability of the mineral and its surface phase(s) can be predicted. However, these diagrams contain no kinetic information about the thermodynamically possible reactions.

Pourbaix's[243] diagrams for the Pb-H_2O and Fe-H_2O systems are presented in figures 2.4 and 2.5. Figures 2.6 and 2.7 show the Eh-pH diagrams of Pb-S-H_2O and Fe-S-H_2O systems respectively. The redox reactions defining the mineral/solution equilibria for galena and pyrite are given in appendices I and II.

Electrochemical methods have been used widely to study surface reactions on sulphide minerals,[212,237] such as adsorption of flotation collectors,[233,236] dissolution in hydrometallurgical processes,[238] non-oxidative dissolution[239] and reduction of oxygen.[235,240-242]

The concept of chemical interactions between sulphide mineral surfaces and collectors occurring by an electrochemical mechanism in flotation was first proposed in 1953 by Salamy and Nixon.[246] Tolun and others[247,248] studied the adsorption of ethyl xanthate at galena[247] and pyrite[248] electrodes using a steady-state potentiodynamic technique. Recently non-steady-state cyclic voltammetry[212,249] has been used to study

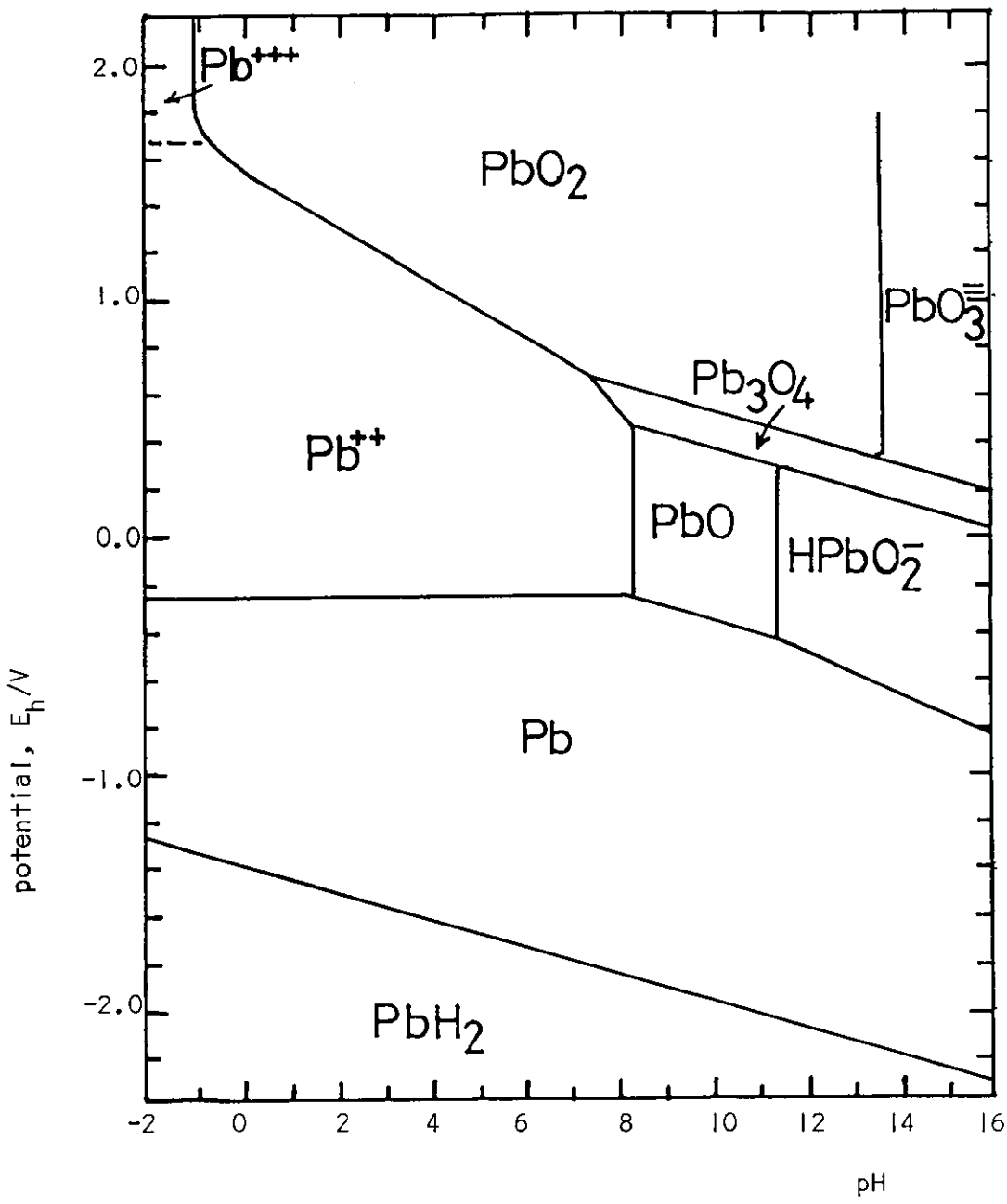

Figure 2.4. Eh-pH diagram of Pb-H_2O system at 298 K and 10^{-4}M solution species

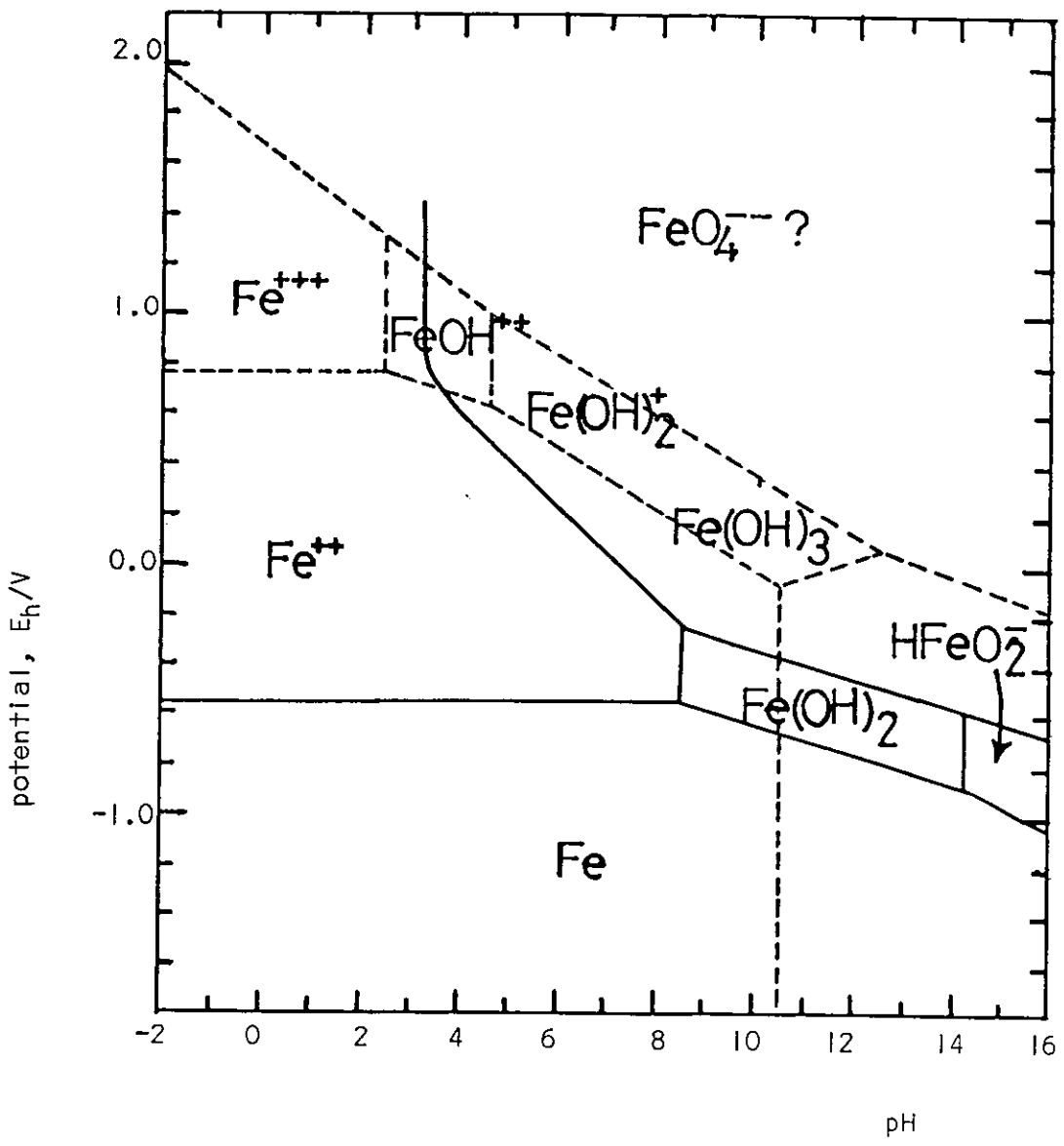

Figure 2.5. Eh-pH diagram of Fe-H_2O system at 298 K and 10^{-4}M solution species

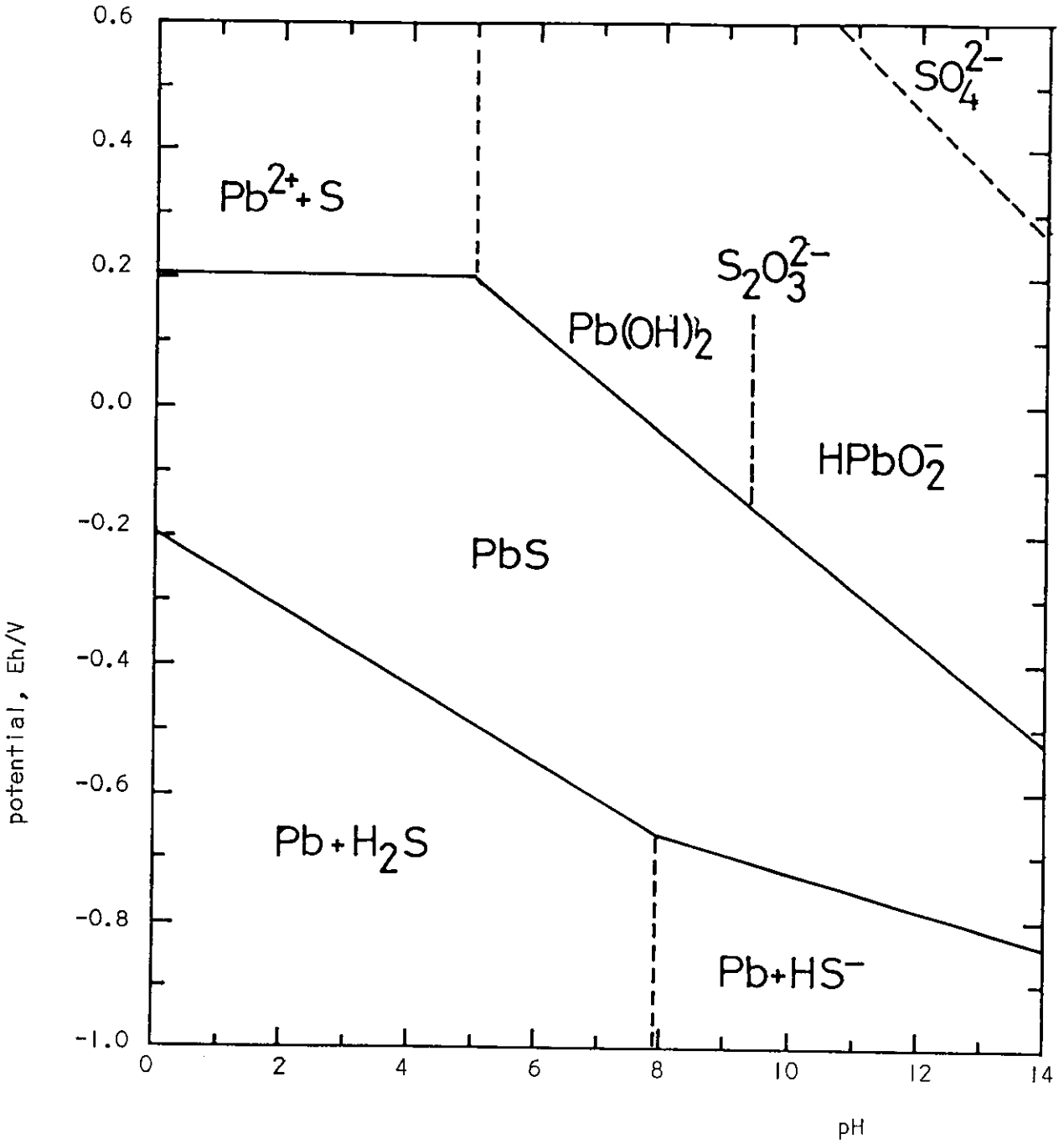

Figure 2.6. Eh-pH diagram of Pb-S-H_2O system at 298 K and 10^{-5}M dissolved species

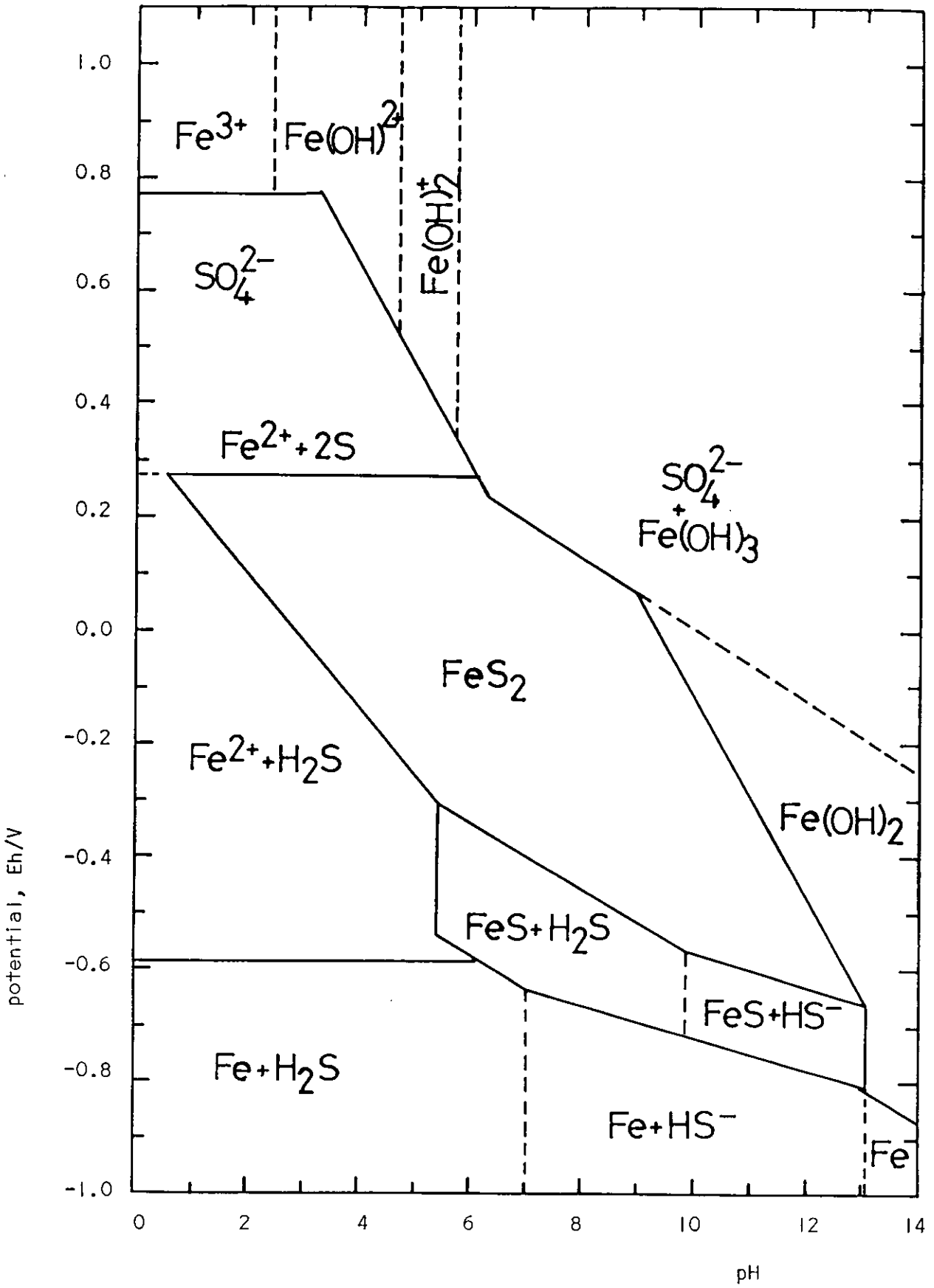

Figure 2.7. Eh-pH diagram of Fe-S-H_2O system at 298 K and 10^{-5}M dissolved species

adsorption processes at sulphide mineral electrodes as it is sufficiently sensitive to detect charge transfer adsorption processes at the monolayer level.[212] This technique has also been applied to identifying the oxidation and reduction reactions and products on galena,[249-251] pyrite and pyrrhotite[213,253] and chalcopyrite[254] electrodes in aqueous systems.

Chander and Fuerstenau[255] studied the change of contact angle and flotation of chalcocite with potential in 2×10^{-3}M potassium diethyldithiophosphate solution and concluded that the hydrophobic species was an oxidation product of the collector. Gardner and Woods[256] recorded contact angles for different degrees of dixanthogen coverage on platinum and gold electrodes and found that platinum and gold were hydrophilic when the potential was more cathodic than the reversible xanthate/dixanthogen potential (Er), but hydrophobic when the potential was above Er. Multilayer adsorption of dixanthogen was required before the maximum contact angle was reached. The results were substantiated with flotation results with gold particles in a particulate bed electrode system.

They also[288] studied galena and pyrite by the same techniques and found that the initial chemisorbed xanthate layer on galena was hydrophobic when ethyl or butyl xanthate were employed, but hydrophilic for the methyl homologue. The presence of dixanthogen enhanced the contact angle whereas the metal xanthate diminished it. These conclusions were supported

by contact angle studies on a lead electrode. Pyrite was hydrophilic except when dixanthogen was formed at its surface, though a substantial quantity of dixanthogen was required before a finite contact angle was observed. This behaviour was interpreted in terms of the presence of hydrated iron oxide on pyrite surface in addition to dixanthogen. The potential at which galena began to float in a particulate bed electrode corresponded to the region where chemisorption of xanthate took place. This occurred at > 0.06 and 0.0 V vs SHE for ethyl and butyl xanthates respectively. On pyrite, however, significant quantities of dixanthogen were necessary before flotation began, at > 0.15 and 0.06 V with ethyl (Er = 0.07 V) and butyl (Er = 0.01 V) xanthates respectively.

Particulate bed electrode systems have been used to study the flotation of sulphide minerals both in the presence and absence of collectors.[254-258] Gardner and Woods[254] studied natural floatability of chalcopyrite using cyclic voltammetry and a particulate bed electrode system, identifying the hydrophobic species as sulphur formed by anodic oxidation.

2.4 Objective of the project

The aim of the project was to define and explain the conditions under which galena and pyrite will concentrate at the oil/water interface in two-liquid flotation systems. The following techniques were used to that end:

i) Two-liquid flotation tests

ii) Contact angle measurements

iii) Electrochemical studies

a) Rest potential measurements

b) Steady state voltammetry

c) Contact angle measurements under controlled potential conditions

d) Cyclic voltammetry

e) Particulate bed electrode studies.

CHAPTER THREE

EXPERIMENTAL

3.1 Materials

High purity galena (PbS) of UK origin and Spanish pyrite (FeS_2) were obtained from Gregory Bottley Ltd, UK. XRF analysis results for galena and pyrite are shown in Table 3.1 below.

Galena		Pyrite	
Impurities	Amount, %	Impurities	Amount, %
Fe, Ca	0.05-0.5	As, Cu	0.5 - 5
Sb, Ag, Cu	500 ppm	Sb	0.05-0.5
		Ca, Ti, Zn	0.05

Table 3.1. XRF analyses of galena and pyrite

Both minerals were received in the form of large pieces which were broken with a hammer and then with a laboratory jaw crusher. Appropriately sized samples were hand-picked to make mineral electrodes and for contact angle measurements. The remainder was stored in plastic containers. For each experiment 30 grams of mineral was ground in a stainless steel Tema mill for 10 minutes under deoxygenated water unless otherwise stated. The particle size range of the product was determined with a cyclosizer and was 95 and 75% - 20 μm for galena and pyrite respectively.

Of the various analytical grade oil phases, iso-octane (2.2.4 Trimethyl pentane) was used most extensively. Before use,

organic liquids were purified by passing through activated alumina columns and kept in the presence of activated alumina. The purity of oils was checked using the drop volume method[228,230] to measure the oil/water interfacial tension, which was found to be independent of drop formation time, indicating the absence of polar impurities.

High purity conductivity water was used throughout the work. This was prepared by passing distilled water through a mixed bed of ion-exchange resins and then through a column of activated charcoal followed by redistillation. The conductivity of the water was less than 4.0×10^{-4} ohm^{-1} m^{-1} and bubble persistence tests[174] indicated that there were no surface active impurities present. Deoxygenated water was prepared by bubbling oxygen-free nitrogen through purified water for at least six hours before use in a clean glass container to remove dissolved oxygen.

Oxygen-free nitrogen was further purified by passing over activated charcoal and soda asbestos to remove organic impurities and CO_2 respectively. It was then passed through two flasks of acidified hypovanadous (V^{2+}) solution[229] which had been prepared by dissolving 0.5 M of vanadium pentoxide in 0.05 M sulphuric acid followed by reduction with zinc amalgam. Oxygen removal was achieved by the following reaction:

$$2V^{2+} + O_{2(aq)} \longrightarrow 2VO^{2+} \qquad (3.1)$$

the vanadyl ion, VO^{2+}, then being re-reduced by excess zinc:

$$VO^{2+} + Zn + 2H^{+} \longrightarrow V^{2+} + Zn^{2+} + H_2O \qquad (3.2)$$

Finally, the nitrogen was passed over copper turnings heated to 900°C in a tube furnace to remove final traces of oxygen.[229]

All the reagents used were analytical grade, though extra purification processes were applied, which will be reported in the relevant sections.

All glassware was cleaned with chromic or nitric acid. When oil had been used the glass was cleaned with 0.5 M NaOH + 10% ethanol mixture followed by acid. After washing with distilled water, conductivity water was used for rinsing.

3.2 Two-liquid flotation studies

3.2.1 Apparatus and experimental procedure

For the two-liquid flotation studies of galena and pyrite, the cell shown in figure 3.1 was used. It consisted of a 300 cm^3 tall glass beaker equipped with stainless steel baffles and a stainless steel stirrer. The cell had a perspex lid with three openings to allow entry of the impellor and the introduction of nitrogen, mineral and oil. An O-ring sealed the cell from the atmosphere.

A speed-controller motor was used for stirring. Preliminary studies indicated that the best recovery was obtained by stirring at 1000 rpm and at phase ratios of about 25% oil/75% aqueous solution.

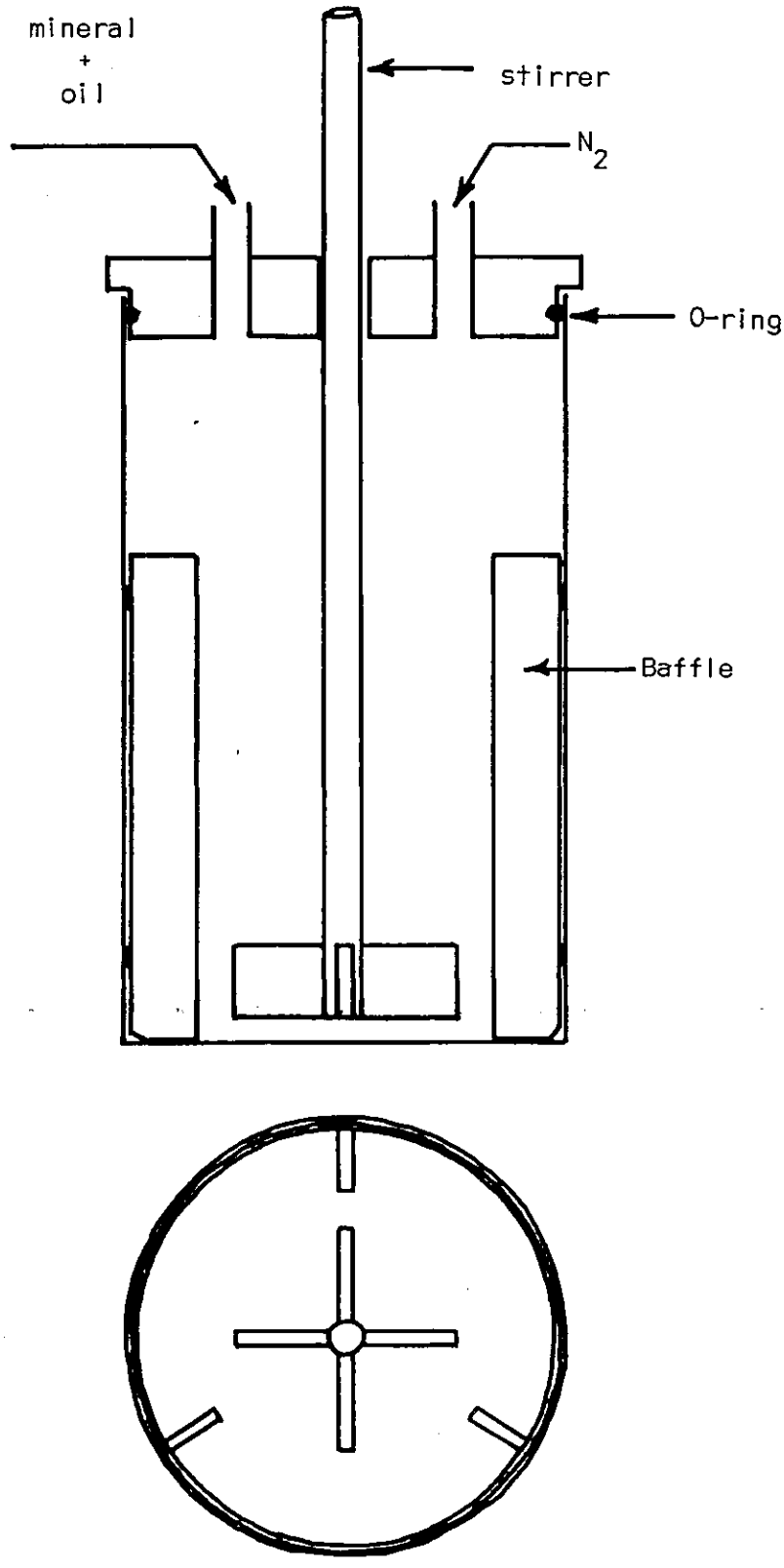

Figure 3.1. Two-liquid flotation cell

The following samples of galena and pyrite were prepared:

a) Wet ground with deoxygenated water. The product was stored in deoxygenated water under a nitrogen atmosphere and is referred to as 'unoxidised'.

b) Wet ground with oxygen-saturated water and stored under the same.

c) The same as (a) but the product was oxidised with 10% H_2O_2 solution.

d) The same as (b) but the product was oxidised with 10% H_2O_2 solution.

e) Dry ground.

Sample (e) was kept in a glass bottle whereas samples (a) - (d) were kept under 250 cm^3 water in a 500 cm^3 sealed conical glass flask under a nitrogen atmosphere. The oxidation of samples (c) and (d) was carried out with H_2O_2 at the natural pH of 5.5-6.5.

In the two-liquid flotation tests 25 cm^3 of mineral suspension was transferred with a pipette to the cell and 50 cm^3 of deoxygenated water was added. After purging the cell with nitrogen for 10 minutes to remove dissolved oxygen, the pH was changed by adding HCl or NaOH and measured after 2 minutes equilibration time. After conditioning for 5 minutes at 500 rpm, 25 cm^3 of iso-octane was added to the cell and its contents mixed for 10 minutes at 1000 rpm while purging with nitrogen. After 10 minutes of mixing the resulting emulsion was transferred to a separating funnel, in which the organic and aqueous phases separated. The amount of solid

associated with each phase was determined after drying. 2 g of sample were used in the 'dry ground' tests.

3.3 Stability of galena and pyrite suspensions

Minerals might report with the organic phase because either they are oleophilic or they coagulate and trap small oil drops which then rise, taking the coagules with them. Suspension stability tests were therefore carried out to determine whether or not the latter process would account for the two-liquid flotation results obtained. Two methods were employed to determine the stability of mineral suspensions.

With the more concentrated (1.5% solids) suspensions, the rate of settlement was measured. Galena and pyrite suspensions were prepared by pipetting measured quantities of mineral from the flask in which the ground sample was kept under deoxygenated water, into a 100 cm^3 conical flask. The solids concentration was adjusted by adding deoxygenated water. The flask was purged with nitrogen for 5 minutes following the adjustment of pH, closed with a glass stopper and shaken for 5 minutes. The suspension was then transferred to a 50 cm^3 sedimentation cylinder and the settling rate was determined by observing the descent of the 'mud line'. Suspensions of dry ground sample were prepared by placing a weighed quantity of the powdered sample in a 100 cm^3 flask to which deoxygenated water was added. The measurements were also done with galena sulphidised after having been oxidised with H_2O_2. The galena suspension was prepared by using 0.05 M Na_2S solution

instead of deoxygenated water to adjust the solids concentration.

With dilute suspensions (0.4% solids) which were prepared as in previous tests, the light absorbance of mineral suspensions was measured as a function of time. The suspensions were first treated with an ultrasonic probe (Dawe Instruments Ltd) for 2 minutes to ensure complete dispersion. The light absorbance was then followed in a 40 cm^3 cell for 30 minutes, readings being taken at 10 minute intervals with an absorptiometer (Evans Electroselenium Ltd).

3.4 Contact angle measurements at galena and pyrite/oil/water interfaces

Contact angle measurements at mineral/oil (or gas)/water interfaces is a widely used technique for studying the wettability of minerals. In this work the measurements were made by the captive bubble/drop technique[273] on samples of galena and pyrite under similar conditions to those used in the two-liquid flotation tests.

3.4.1 Apparatus

The contact angle apparatus was the same as described previously[274] and consisted of a silica spectrophotometer cell held on the modified stage of a Beck 6000 microscope mounted in a horizontal plane. Illumination was provided in the same horizontal plane as the microscope and sample. Light

passed through the cell at a small angle of incidence to the surface of the sample. Heat from the light source was minimised by a copper sulphate filter placed between the light source and the sample. Angles were measured by rotating the eyepiece to line up the cross-wires.

Oil droplets were formed at the tip of a stainless steel capillary and brought into contact with the sample surface by means of an 'Agla' micrometer syringe, mounted in the same vertical plane as the spectrophotometer cell in which the sample was placed. The syringe was mounted on an extension and could be moved vertically and horizontally by means of two micromanipulators (Research Instruments Ltd). All angles were measured through the aqueous phase.

3.4.2 Experimental procedure

Selected pieces of galena and pyrite were cut into rectangular prisms to fit into the spectrophotometer cell. Prior to each measurement the mineral surface was polished by wet grinding on 800 grade silicon carbide paper and then with 0.3 μm alumina on 'Selvyt' cloth. After polishing, the sample was washed with deoxygenated water and kept under deoxygenated water. Utmost care was taken in handling the sample and surgeon's gloves were worn to avoid contamination.

50 cm^3 of deoxygenated water of adjusted pH was shaken/equilibrated with 15 cm^3 of oil for 20 minutes and then the two phases were separated. The aqueous phase was kept under nitrogen in a 100 cm^3 conical flask and the organic phase added

to the syringe. The mineral sample was conditioned in deoxygenated water of the same pH for 5 minutes, after which the water was replaced with the aqueous phase previously shaken with the oil. The contact angle was then measured.

An oil drop of fixed volume was formed on the tip of the stainless steel capillary dipping in the aqueous medium. The drop was brought into contact with the mineral surface, equilibrated for one minute and then its volume increased by a known amount. After a further equilibration period, the contact angle between the three phases was measured through the aqueous phase. This angle was termed the 'receding contact angle' (θ_{RC}). The drop was then returned to its original volume and the 'advancing contact angle' (θ_{Ad}) measured.

When advancing contact angles were larger than about 50^{o}, the attempt to remove the oil drop from the mineral surface by lifting the micrometer syringe left part or the whole of the oil drop stuck to the mineral surface. These samples were washed with acetone prior to polishing, to remove the oil from the surface.

With oxidised samples, the mineral surface was reacted with 10% H_2O_2 solution at natural pH (5.5-6.5) for 30 minutes prior to conditioning. Contact angle measurements were also made with nitrogen bubbles using similar conditions.

3.5 Interfacial tension and contact angle measurements with different organic liquids

3.5.1 General

The interfacial tension between various oil phases and water were determined at the natural pH for the purpose of:

a) determining the relation between the interfacial tension and the contact angle at the sulphide/oil/water interfaces;

b) substituting the value of interfacial tension into the Young-Dupre equation

$$W_{ad} = \gamma_{o/w}(1 + \cos\theta) \qquad (3.1)$$

for the work of adhesion of a liquid on a solid.

The interfacial tension measurements were made using the drop-volume method.[230] This consisted of measuring the volume of a drop and associated satellite drops that broke away from the capillary tip. This volume was then related to the surface or interfacial tension by an empirical relationship, the origin of which is a force balance between the gravitational force (mg) on a pendent drop and the surface or interfacial force ($2\gamma r$), which gives the equation:

$$\gamma = \frac{\Delta\rho . V . g . F}{r} \qquad (3.2)$$

where

γ = surface or interfacial tension;

$\Delta\rho$ = difference between the density of the pendent drop and the density of supporting medium;

F = a correction factor for the deviation of the pendent drop from the ideal drop;

V = volume of the drop;

r = radius of capillary tip.

The factor F, for which values have been tabulated by Harkins,[231] is dependent on the ratio V/r^3.

3.5.2 Experimental procedure

25 cm^3 of oil was shaken with 50 cm^3 of conductivity water in a 150 cm^3 conical flask for 10 minutes, and transferred into a 20 mm diameter test tube placed in a constant temperature bath at 25 ± 0.1°C. A glass capillary was attached to a micrometer syringe and the free end of the capillary polished, so that its cross-section was at right-angles to its length, and there were no edge imperfections when viewed under the microscope. With a travelling microscope the mean outer diameter of the capillary tube was measured as 2.92 ± 0.01 mm.

The micrometer syringe was filled with the aqueous phase and positioned so that the capillary tip was about 5 mm below the surface of oil phase. After 15 minutes of thermal equilibration, a drop of aqueous phase was formed at the tip of the capillary and its volume slowly increased until it became detached. At the point of detachment the micrometer reading was recorded, and the procedure was repeated. After the detachment of the second drop, the difference in the micrometer reading between the detachment of the first drop and the second drop was calculated. This value corresponded to

the volume of the drop from which the interfacial tension was calculated using equation (3.2).

To determine whether the oil phase contained surface active impurities, the effect of drop formation time on interfacial tension was studied. 70% of the volume of the drops was formed within 60 seconds and the remaining 30% after different ageing times. If surface active contaminants were present they should have adsorbed at the oil/water interface and changed the interfacial tension.

The contact angle measurements with different oils were made at unoxidised galena/oil/water interfaces at pH 5.6 and pyrite/oil/water interfaces at pH 9.2, as described in section (3.4.2).

3.6 Electrochemical studies

3.6.1 Experimental procedure

Galena and pyrite electrodes were prepared by cutting hand picked mineral specimens into rectangular prisms with an area of about 30-50 mm^2 and ground to a thickness of about 3 mm. The faces of samples were ground on successively finer grades of silicon carbide paper, down to 800 grade, taking care to avoid cracks and voids. The resistance across each mineral specimen was measured using a power supply with a built-in voltmeter and ammeter incorporating a clamp arrangement to hold the sample. It was found that the resistance of galena varied between 0.2-10Ω depending on the specimen, while that of pyrite lay between 100-400 Ω . Since the resistance of pyrite

was high, the faces of pyrite were vacuum sputtered with gold to minimise the contact resistance. After coating with gold, the pyrite resistance was 20-100 Ω, depending on the specimen.

The type of semiconductivity was established from the sign of thermoelectric voltage by a hot-probe method.[208] Two copper wires were contacted to two opposite faces of the mineral sample. One of the copper wires was heated with a soldering iron, causing a temperature gradient and the potential difference between the two wires was measured (Seebeck voltage). The polarity of this thermoelectric voltage was used to determine the sign of majority carriers, since electrons would give rise to a negative Seebeck voltage whereas holes would result in a positive potential. Both the galena and the pyrite were found to be n-type semiconductors.

To fabricate the electrodes, two contact wires were cemented to one of the faces of the mineral specimens with silver-loaded epoxy resin. The contact wires were threaded through a length of glass tubing, and the mineral with about 10 mm of tubing embedded in epoxy resin in a silicone rubber mould. After hardening, the electrode was removed from the mould, and the resin coating on the surface of the mineral specimen was ground away (Fig 3.2a). This surface was then wet ground on successively finer grades of silicon carbide paper down to 800 grade, followed by wet polishing with 0.3 μm alumina on 'Selvyt' cloth. Care was taken to avoid inclusions, cracks and voids, as well as to remove alumina particles from the surface.

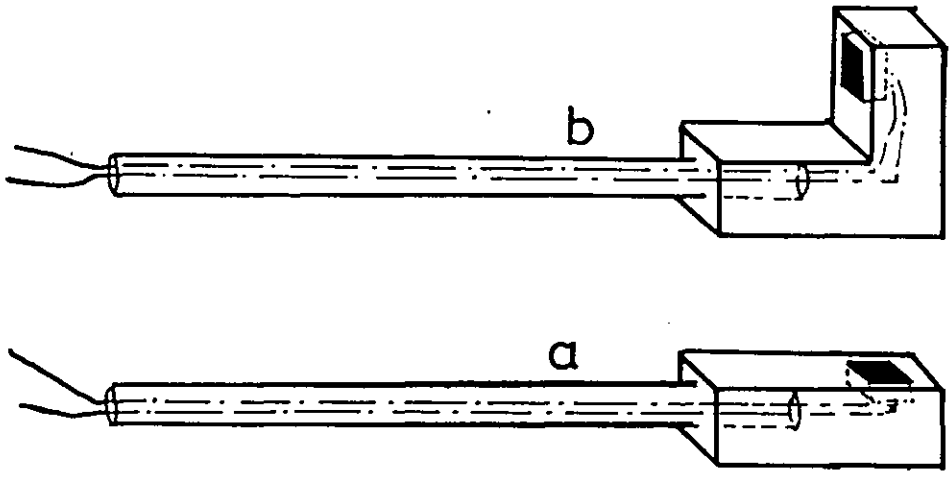

Figure 3.2. Mineral electrodes.

a - used in electrochemical studies;
b - used in contact angle measurements under controlled potential.

A new surface was produced on the mineral surface before each experiment by wet grinding on a silicon carbide paper followed by polishing with 0.3 μm alumina. The electrode was then washed with deoxygenated water and transferred immediately to the eletrochemical cell.

Experiments were carried out in the three compartment glass cells, shown in figure 3.3. The rectangular cross section cell (figure 3.3A) had optically flat surfaces to allow the measurement of contact angles as a function of electrode potential. A Luggin probe in a syringe barrel connected the working electrode and the reference electrode compartments. A saturated calomel electrode (SCE) was used as the reference electrode though all quoted potentials have been converted to the standard hydrogen electrode (SHE) scale, assuming that the SCE has a reversible potential of 0.245 V vs SHE.[264] Both

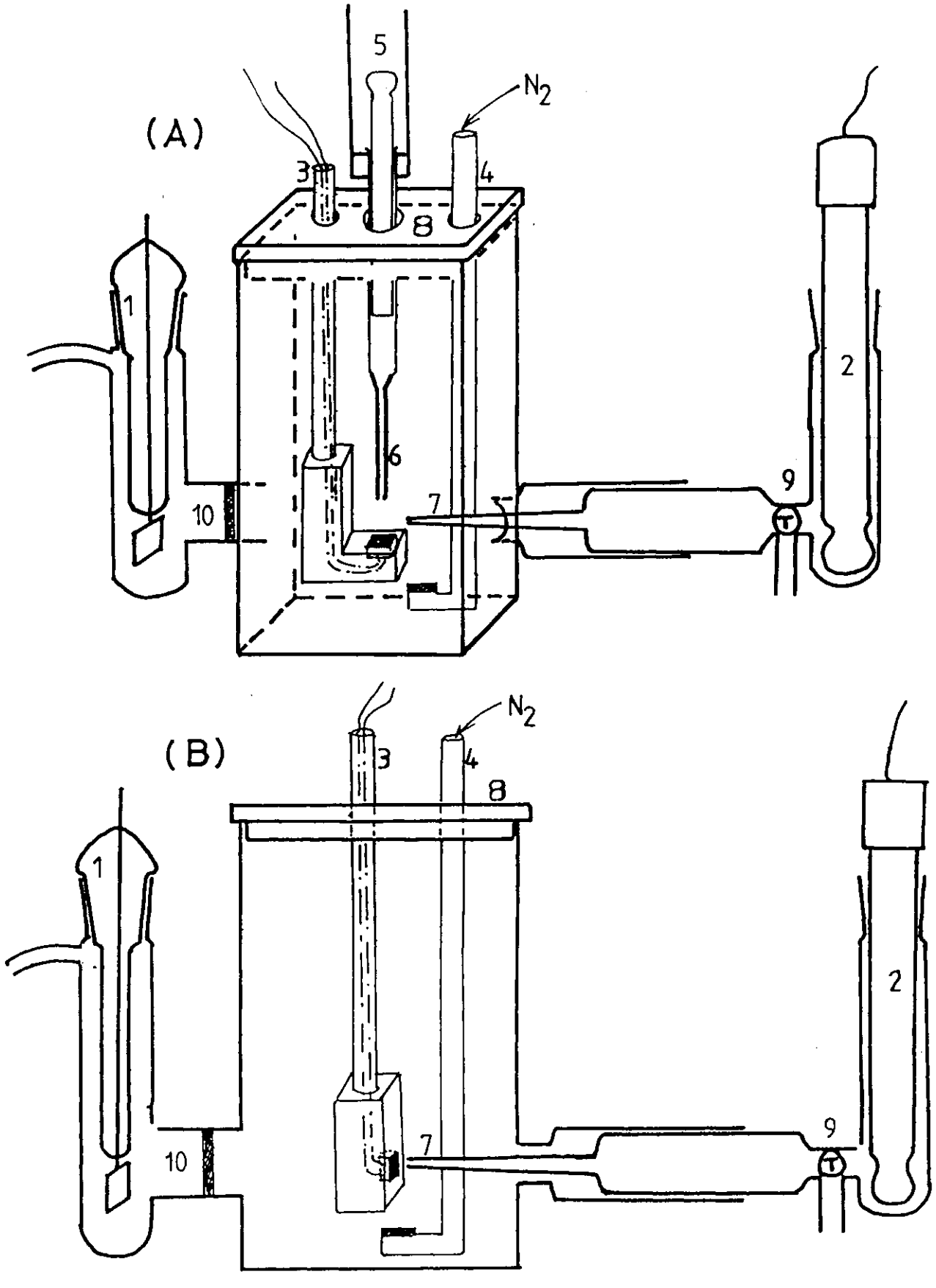

Figure 3.3. Electrochemical cells

A - rectangular; B - cylindrical. 1 - counter electrode; 2 - reference electrode; 3 - mineral electrode; 4 - gas bubbler; 5 - micrometer syringe; 6 - stainless steel capillary; 7 - Luggin capillary; 8 - cell lid; 9 - T-tap; 10 - sintered glass disc.

cells had tightly fitting polythene lids with the necessary openings for the mineral electrode, gas bubbler, and in the case of contact angle measurements for the micrometer syringe.

3.6.2 Rest potential studies

3.6.2.1 General

The rest potential can be defined as the potential between a given electrode and reference electrode in a solution when the external current is zero. The observed potential cannot always be related to the thermodynamic reversible potentials,[232] since there may be internal currents due to a net reaction occurring between solution species and the sulphide electrode surface.[209] This would cause departure from equilibrium and result in a mixed electrode potential being adopted. However, the rest potential does provide information about possible processes taking place on the electrode surface. Because such processes would require the potential to be in an Eh-pH region where the rate of reaction is finite, i.e. allowing for an overpotential.

The rest potential of galena and pyrite electrodes were measured with a digital voltmeter (Sinclair Ltd). Nitrogen was bubbled through the cell during measurements except when the mineral electrodes were oxidised with H_2O_2 within the cell.

3.6.2.2 Experimental procedure

Nitrogen was bubbled for 20 minutes in the cell before introduction of the electrode. The rest potential of galena was measured in 150 cm^3 of deoxygenated water of adjusted pH

before and after oxidation with H_2O_2. The electrode was repolished and its rest potential measured before and after sulphidising in 100 cm^3 of 0.05 M Na_2S for 5 minutes.

With oxidised electrodes, the mineral was reacted in 50 cm^3 of 10% H_2O_2 solution for 30 minutes and then transferred to the electrochemical cell.

To determine the stability of the oxidation products of galena reacted with H_2O_2 at the natural pH (5.5-6.5), the galena electrode was transferred to solutions of different pH in a second cell. The potential was measured at each pH after 5 minutes of conditioning.

The rest potential of galena was also measured in buffer solutions of different pH to minimise the pH change at the mineral/solution interface during oxidation. The electrode was oxidised within the cell by adding H_2O_2, so avoiding the transfer of the electrode between cells.

The rest potentials of pyrite electrodes were measured in the same way as for galena, in buffer electrolytes with freshly polished, sulphidised and oxidised electrodes. The change in the pyrite potential was measured during 30 minutes of oxidation and after the electrode was transferred from the oxidising environment in the first cell to the deoxygenated solution in the second cell. The composition of buffer electrolytes used are shown in table 3.2 below.

pH	Composition of electrolyte
1.0	0.1 M $HClO_4$
1.68	0.05 M $KH_3(C_2O_4)\ 2H_2O$
4.0	0.05 M $KHC_8O_4H_4$
4.6	0.5 M CH_3COOH + 0.5 M $CH_3\ COO\ Na$
6.89	0.025 M KH_2PO_4 + 0.025 M $Na_2\ HPO_4$
9.2	0.05 M $Na_3B_4O_7$
11.0	0.025 M $NaHCO_3$ + 0.023 M NaOH

Table 3.2. The composition of buffer electrolytes

3.6.3 Steady-state potentiostatic studies

Quasi steady state polarisation curves of galena and pyrite were determined in the three compartment glass electrochemical cell shown in figure 3.3B using a potentiostat to control the potential and two digital multimeters to measure the potential and the current. The applied potential was changed in 0.05 v steps starting from the rest potential. Deoxygenated buffer electrolytes were used and the cell was purged for 20 minutes with nitrogen prior to the introduction of the electrode. The electrodes were polarised first in the cathodic direction and then polished before polarising anodically. The currents were taken arbitrarily after three minutes of polarisation. The distance between Luggin capillary and the electrode surface was kept to a minimum to avoid an 'uncompensated' ohmic drop between the Luggin probe tip and mineral electrode. Constant agitation was produced by bubbling nitrogen during polarisation.

3.6.4 Determination of wettability as a function of redox potential

3.6.4.1 Experimental procedure

Contact angle measurements were carried out in the rectangular shaped electrochemical cell (figure 3.3A) by controlling the electrode potential by the steady-state potentiostatic technique described in the previous section (3.6.3). The cell was mounted on the optical bench described in section (3.4.1). The upward facing mineral electrodes (figure 3.2b) were polarised for 3 minutes and then isolated. The advancing contact angles (θ_{Ad}) were measured as described in section (3.4.2). Nitrogen was bubbled in the cell during polarisation but stopped during the measurement of contact angle to avoid shaking the electrode.

To ascertain the cleanliness of the system, the contact angle measurements were repeated in 0.5 M solutions of 'Aristar' KCl which had been heated in a furnace to 500^{o}C in a silica dish and kept under vacuum in a desiccator. The pH was adjusted with HCl and NaOH. The iso-octane was triply distilled after passing through an activated alumina column and was kept in the presence of activated alumina.

Since lead phthalate was found to be oleophilic, this buffer solution was not used in contact angle measurements.

3.6.5 Cyclic voltammetric studies

3.6.5.1 Experimental procedure

The cell in figure 3.3B and the mineral electrode in figure 3.2a, described in section (3.6.1), were used. The

potential was controlled by a Wenking St.72 potentiostat programmed by a voltage sweep generator (Oxford Electrodes). Current potential curves were recorded on a JJ Ltd PL4 XY/t recorder. All the potentials were measured against a saturated calomel electrode (SCE), and reported here against the saturated hydrogen electrode (SHE).

Buffer electrolytes of different composition/pH values (table 3.1) were deoxygenated by bubbling nitrogen for 30 minutes through the cell before the introduction of the electrode. Mineral electrodes were polished wet on 800 grade silicon carbide paper and then on 0.3 μm alumina before each experiment. Galena electrodes were then sulphidised in 100 cm^3 of 0.05 M Na_2S solution for 5 minutes, washed with deoxygenated water and transferred to the cell. Cyclic voltammograms were recorded after 5 minutes of conditioning. Constant stirring was provided during experiments by nitrogen bubbling unless otherwise stated.

To gain more insight into the reactions taking place on galena electrodes, cyclic voltammograms were also obtained for lead electrodes, which were prepared and polished as for mineral electrodes.

The cyclic voltammograms of pyrite were recorded by Mr P Page in the same laboratory using the same procedure as for galena, except that prior to each experiment the pyrite electrodes were held for 60 seconds at a potential more negative than the thermodynamic stability field of ferric oxide (i.e. $E_h = 0.271 - 0.059$ pH V vs SHE) to cause its reduction.

3.6.6 Mineral pulp/suspension electrode studies

3.6.6.1 General

Controlled potential flotation[254,255,257,258] in the absence of surfactants has been used to determine the conditions under which sulphide particles are floatable and hence hydrophobic or oleophilic. The technique assumes that the mineral particle slurry will adopt the potential of a suitable feeder electrode by point contact.

3.6.6.2 Apparatus

Two particulate bed electrode cells were used, the first of which, shown in figure 3.4, was a three electrode modified Hallimond tube electrochemical cell in which particles were kept in suspension by a magnetic stirrer. The second cell was similar to that used by Walker et al[277] and was a modified form of the Partridge-Smith flotation cell[278] (figure 3.5), in which the particles were present as a sedimented or compacted bed.

The counter electrode section was a separate tube within the cell and could be used as a plunger to compact the mineral bed. The connection between the counter electrode and the cell was through a sintered glass disc. Pt foil and Pt wire electrodes were used as the counter electrodes in the first and second cells respectively, and saturated calomel electrodes (SCE) were used as the reference electrodes. Different combinations of feeder electrode were tested in the first cell, while a Pt wire was used with the second cell.

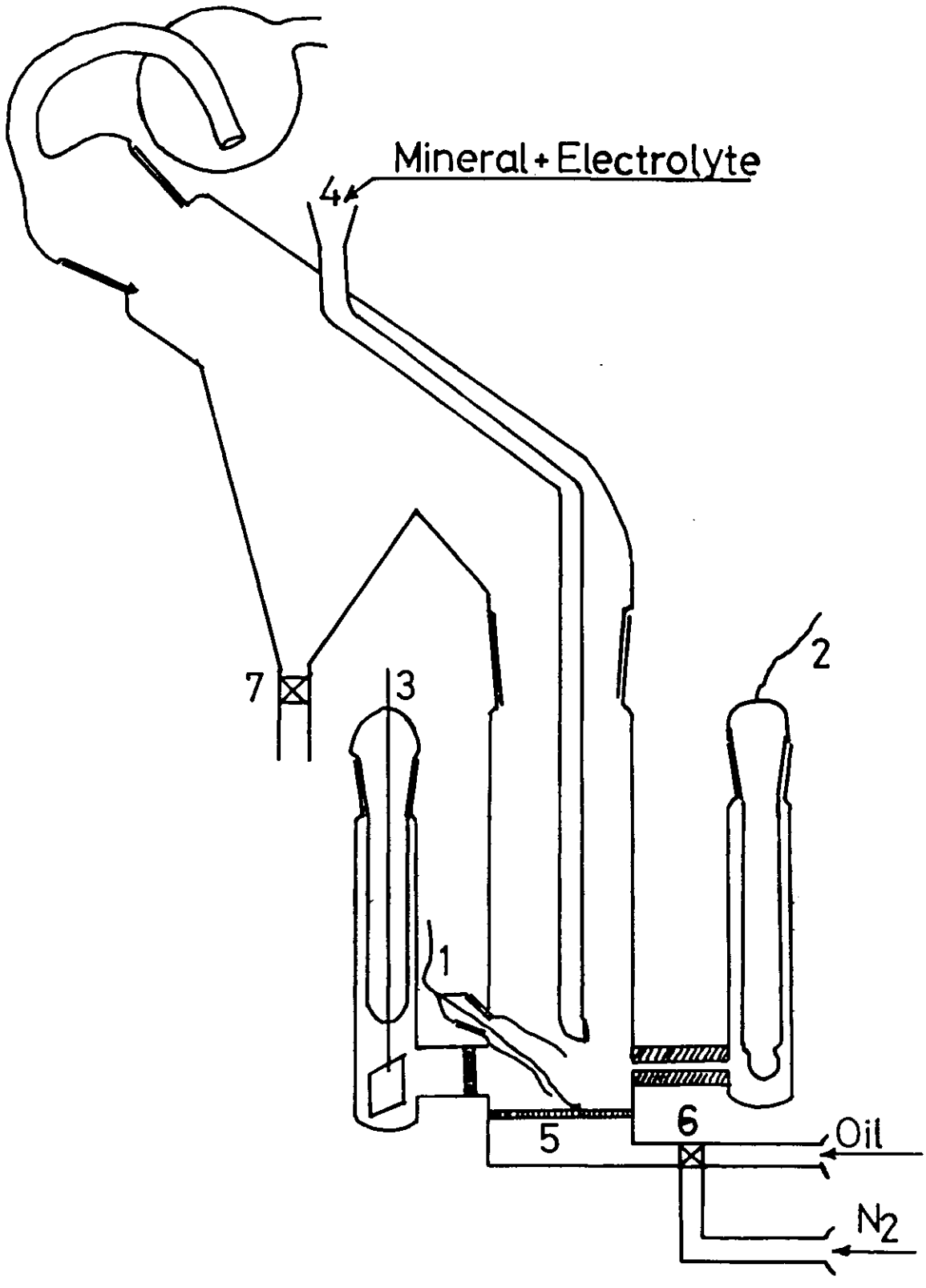

Figure 3.4. Electro Hallimond cell incorporating a particulate mineral electrode. 1 - feeder electrode; 2 - reference electrode; 3 - counter electrode; 4 - sample introduction tube; 5 - sintered glass bottom; 6 - T-tap; 7 - Tap.

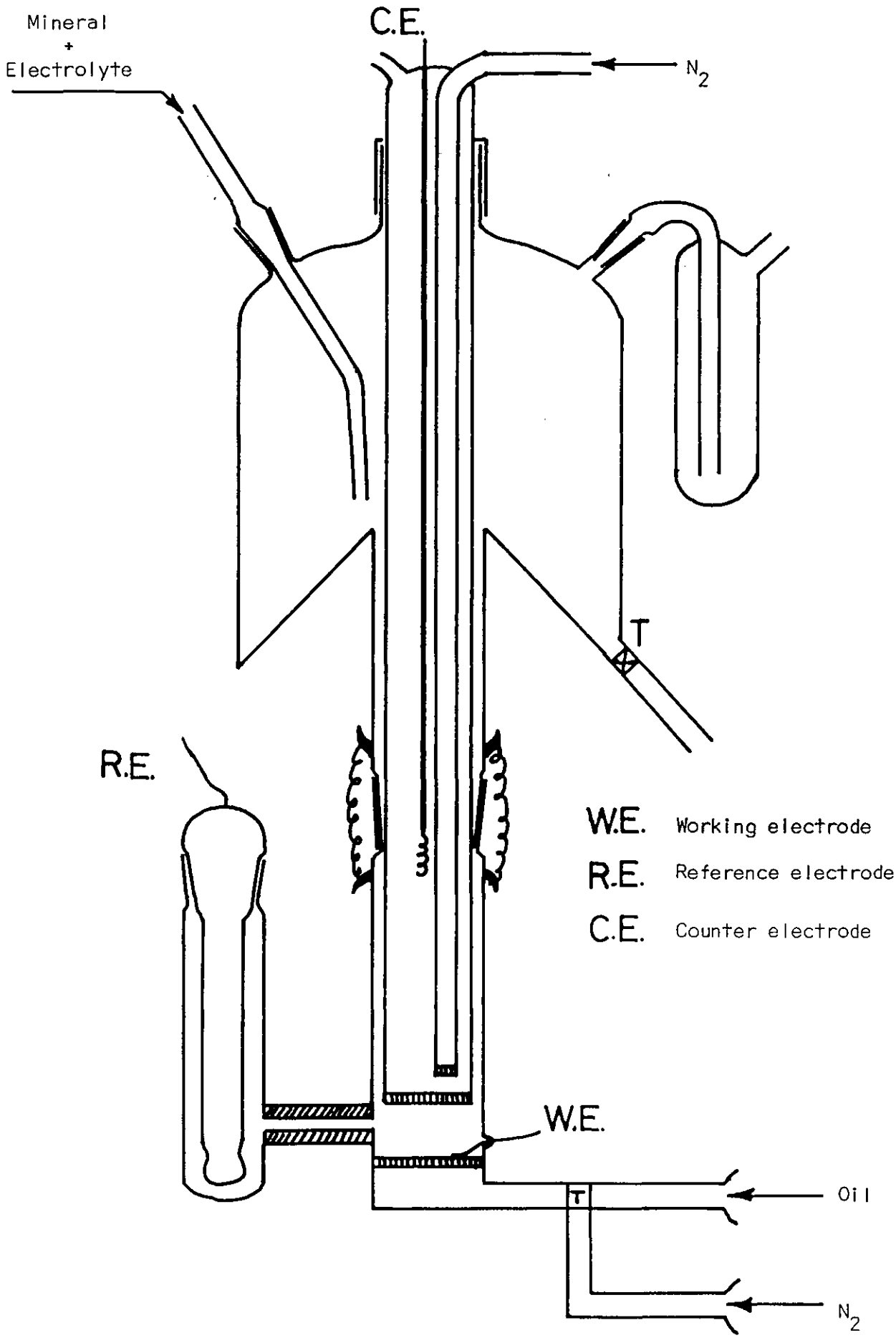

Figure 3.5. Electrochemical cell with a compacted bed of sulphide mineral particles as the working electrode.

The whole system was kept under nitrogen atmosphere, as shown in figure 3.6.

3.6.6.3 Experimental procedure

Preliminary studies were made with coarse galena (-300 + 106 μm) to determine the effectiveness of the system. The mineral was dry ground in a porcelain mortar and the -300 + 106 μm fraction was separated by sieving. It was washed several times with deoxygenated water and sulphidised in 0.05 M Na_2S solution for 5 minutes in a 250 cm^3 conical flask. The sulphide solution was replaced with deoxygenated water and the sample was washed until the pH of the water was 6-7.

Fine samples of galena and pyrite were prepared as described in section (3.1). For each experiment, 60 grams of mineral was ground in two 30 gram batches and kept in a modified Andreason pipette (E) under nitrogen atmosphere (see figure 3.6).

Fine samples were sulphidised by adding 250 cm^3 of 0.05 M Na_2S solution to the Andreason pipette, put into suspension for 5 minutes with a magnetic stirrer and then allowed to settle for 10 minutes. The process was repeated four times replacing the solution with fresh sulphide solution, using gas pressure by adjusting T-taps 2, 3 and 4 in figure 3.6. The sulphide solution and the sample were washed with deoxygenated water until the pH of the wash water was 6-7.

Before each test, the cell was cleaned with nitric acid, and after placing the cell into the circuit (figure 3.6), nitrogen was passed through it for 15 minutes. Some deoxygenated

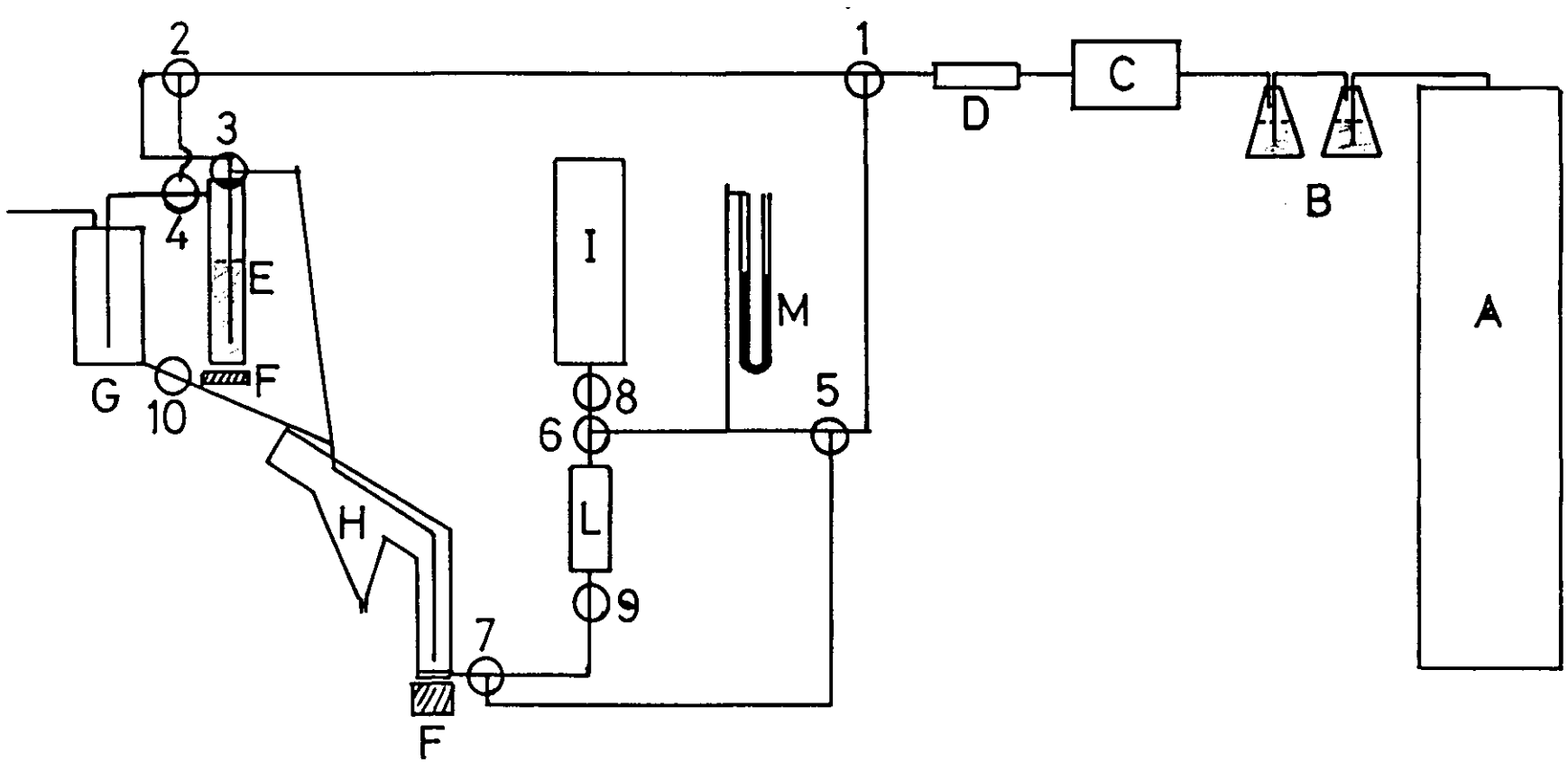

Figure 3.6. System used in particulate bed electrode studies to exclude oxygen. A - nitrogen cylinder; B - acidified vanadous solution with Zn; C - tube furnace; D - condenser; E - Andreason pipette; F - magnetic stirrer; G - electrolyte container; H - electro flotation cell; I - oil container; L - oil measuring funnel; M - monometer; 1-7 - T-taps; 8-10 - two way taps.

buffer electrolyte was transferred from the container G to the cell by opening tap 10. The feeder electrode was cathodically polarised in the hydrogen evolution region to remove any oxidation layer on the surface of the electrode. After purging the cell with nitrogen for another 10 minutes the Andreason pipette (E) was stirred with a magnetic stirrer (F), and by adjusting T-taps 2, 3 and 4, some slurry was transferred to the cell by gas pressure. Additional electrolyte was then added from container G. After 5 minutes conditioning the slurry was polarised at the chosen potential for 60 minutes with nitrogen passing through the cell (first cell only) and the PTFE-coated magnetic stirrer in operation. The coarse sample was added to the cell by a glass spoon through the sample introduction tube 4 (figure 3.4).

During polarisation the cell was not filled completely with buffer electrolyte, so enhancing the collision rate of particles with the feeder electrode, but sufficient solution was present to cover the reference and counter electrodes.

At the end of the polarisation period the applied potential was removed. 50 cm^3 of oil was transferred from the oil container (I) to the oil measuring funnel (L) and forced through the sinterred glass bottom of the cell by gas pressure, having adjusted taps 1, 5, 6, 7 and 9. The cell was then filled with deoxygenated electrolyte raising the oil phase to the separation section of the cell (figure 3.4). The oil phase was removed via tap 7 and the solid in each phase was determined.

With the second cell (figure 3.5), the particulate bed was not stirred during polarisation and 0.5 M KCl was used as

a background electrolyte to decrease electrolyte/cell resistance. Nitrogen was bubbled through the counter electrode compartment to remove oxygen formed during cathodic polarisation of the bed electrode. The cell was filled up with deoxygenated buffer electrolyte before the introduction of oil to allow the oil phase to be taken from tap T. During the passage of the oil the magnetic stirrer was turned on but since the diameter of the cell was small (15 mm) the solid was not suspended. However, it eased the passage of oil by loosening the bed. The amount of solid floated by a constant amount of oil (50 cm^3) was determined.

3.6.6.4 Contact measurements

To gain more insight into the charging mechanism of mineral particles in a pulp/suspension electrode system, a four electrode glass cell was constructed as shown in figure 3.7. A saturated calomel electrode (SCE) was used as the reference electrode and a Pt foil as the counter electrode. The feeder electrode was a Pt wire sealed through a glass capillary connected to the end of the plunger of a 10 cm^3 glass syringe (figure 3.8a). The mineral electrodes were made by cementing of galena and pyrite into a cavity at the end of a glass capillary (figure 3.8b). Two wires had previously been cemented to the back of the mineral specimen with silver-loaded epoxy resin, and threaded through the capillary and syringe plunger.

The mineral electrodes were wet polished on 800 grade silicon carbide paper and alumina, then introduced into the

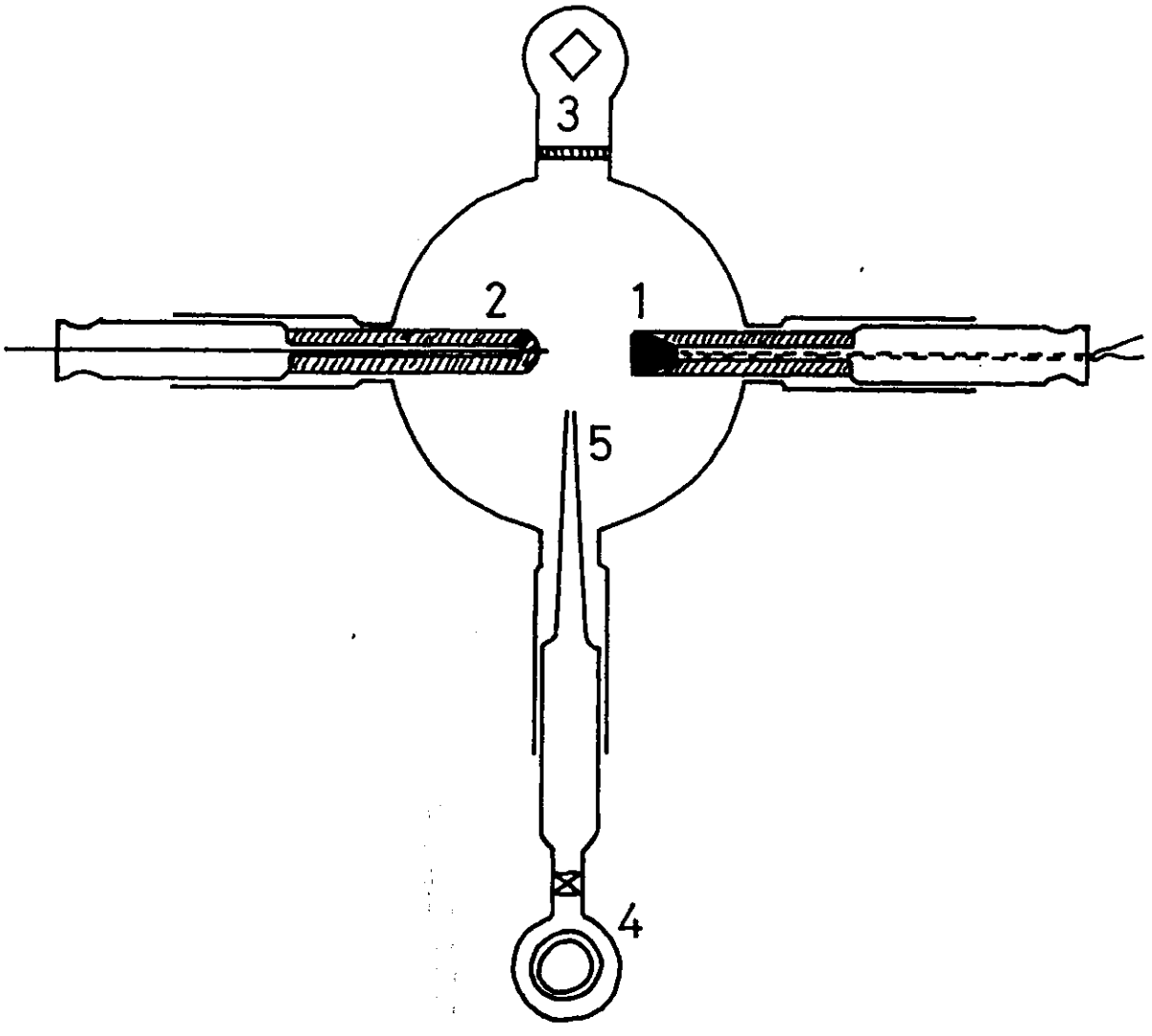

Figure 3.7. Electrochemical cell used in contact measurements. 1 - mineral electrode; 2 - feeder electrode; 3 - counter electrode; 4 - reference electrode; 5 - Luggin probe

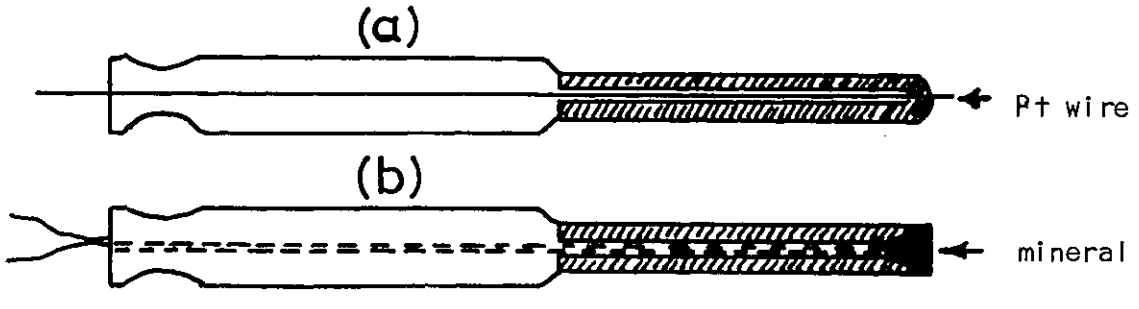

Figure 3.8. Feeder (a) and mineral (b) electrodes used in contact measurements

cell, which had been purged with nitrogen for 20 minutes. Deoxygenated buffer electrolyte of pH 6.89 was added to the cell.

The Pt feeder electrode was polarised at a chosen potential and the mineral electrode contacted with it. The change in the potential of the mineral electrode and the current in the potentiostated Pt feeder electrode circuit was recorded with a digital storage oscilloscope (Nicolet Explorer I) and a XY/t recorder.

CHAPTER FOUR

RESULTS AND DISCUSSION

4.1 Two-liquid flotation studies

The recovery from the oil/water interface of galena, subject to different pretreatments is shown as a function of pH in figure 4.1. Over 70% of the unoxidised galena reported to the oil/water interface at all pH values studied, the maximum recovery being obtained at pH 5.5. Oxidation of galena reduced the recovery and a minimum was obtained at neutral pH values. The Eh-pH diagram of the Pb-S-H_2O system (figure 2.6) shows that in acid solutions galena could oxidise to produce a surface of elemental sulphur which, being hydrophobic, could be responsible for the increase in recovery of oxidised galena.

Similar results were obtained with pyrite (figure 4.2), but the recovery of unoxidised pyrite went through a minimum at pH 4, and maximum recovery was obtained between pH 5.5 and 9.5. A similar minimum was obtained by Fuerstenau et al[272,280] in the flotation of pyrite with xanthate collectors between pH 4 and 5.5. They found that the recovery was dependent on the ratio of ferrous and ferric ion concentrations in solution and explained the results by invoking the formation of colloidal ferric hydroxide, which adsorbed dixanthogen. The Eh-pH diagram of the Fe-S-H_2O system (figure 2.7) shows that oxidation of pyrite yields S^o, Fe^{2+}, $Fe(OH)^{2+}$ and $Fe(OH)_2^+$ in the solution depending on pH, for pH < 6. Although in the present work the oxygen content of the system was minimised, the depression of the two-liquid flotation of pyrite around pH 4 (figure 4.2) could be due to the adsorption of these ferric hydroxide species on

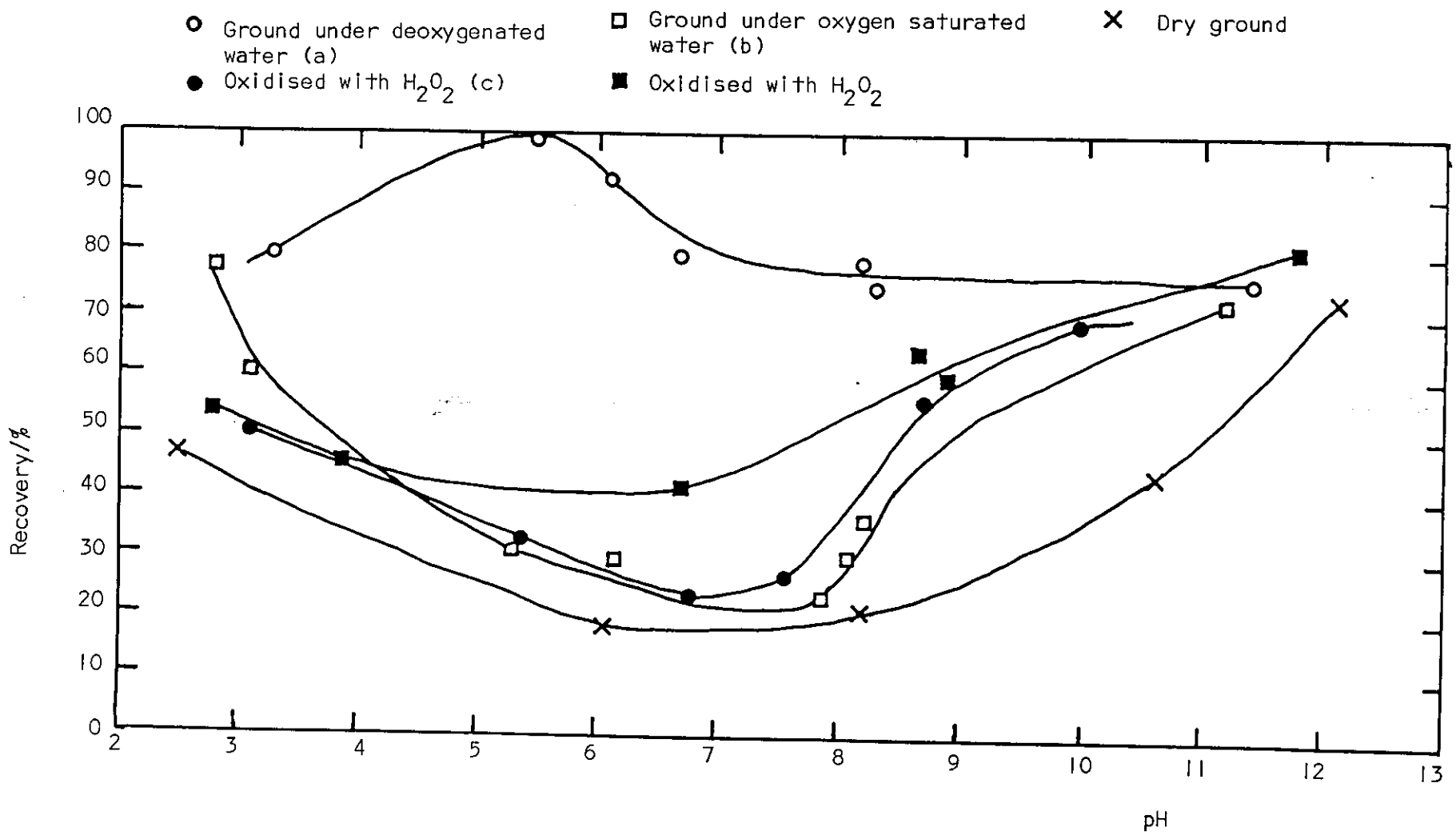

Figure 4.1. The recovery of galena subjected to different pretreatments at the oil/water interface

the surface of pyrite. At pH values < 3 the recovery increased again as ferric hydroxide does not form in acid solutions. The decrease in the recovery of pyrite above pH 9.5 was due to the formation of $Fe(OH)_2$, as the Fe-S-H_2O Eh-pH diagram (figure 2.7) shows that $Fe(OH)_2$ is the thermodynamically favoured oxide species in equilibrium with pyrite.

In acid media the results with oxidised pyrite were similar to those of oxidised galena. However, with oxidised pyrite in alkaline solutions there was no increase in recovery as observed with galena. As for galena, at low pH elemental sulphur could be the oleophilic species on pyrite according to the Eh-pH diagram of the Fe-S-H_2O system (figure 2.7).

4.2 Stability of galena and pyrite suspensions

Although the suspensions of galena were unstable compared to pyrite, both light absorbance (figure 4.4) and settling rate (figure 4.5) measurements showed that the unoxidised galena sample was more stable than the oxidised samples, especially at pH values above 5. The zero point of charge (zpc) of galena has been reported to be around pH 3,[270,271] therefore the decrease in the stability of galena with decreasing pH could be due to a decrease in surface charge. The results are converse to those expected by extrapolation of the flotation results, if the recovery was then due to the entrapment of oil drops in coagules.

In the pH range 5.5 to 9.5 where maximum recovery of pyrite was obtained, all of the pyrite suspensions were reasonably

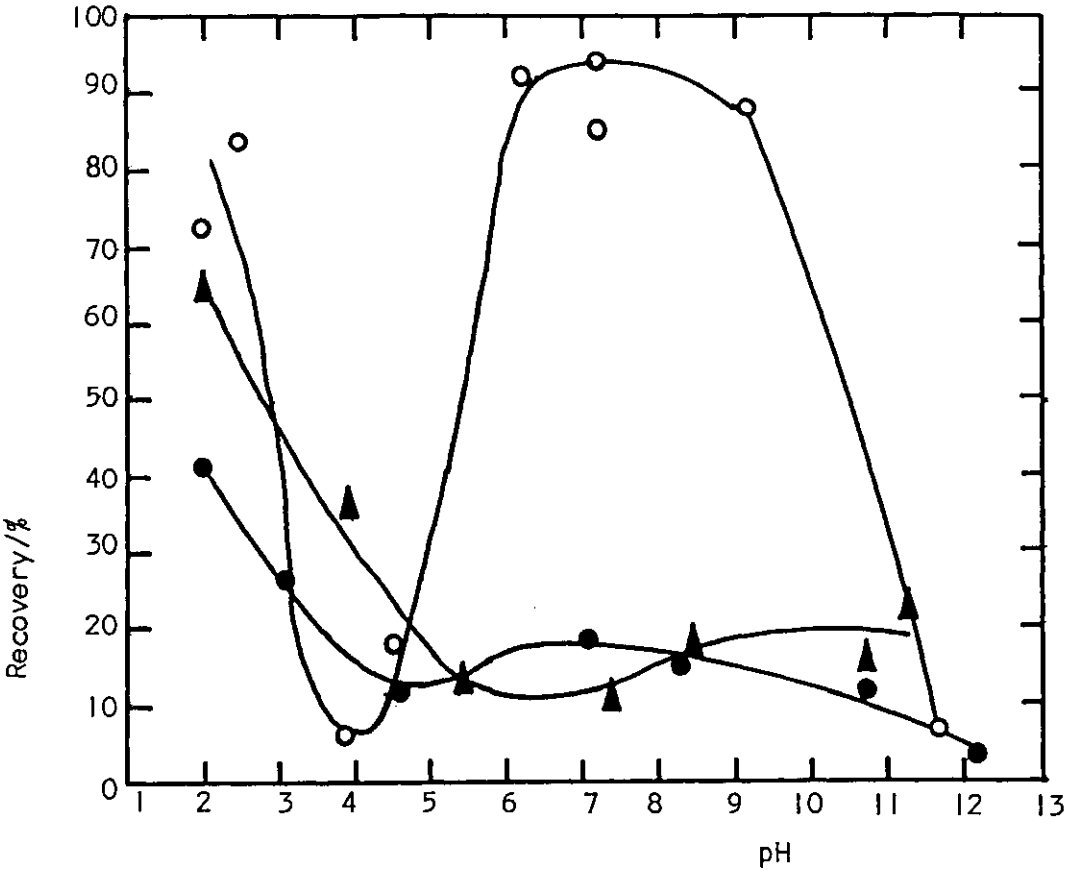

Figure 4.2. The recovery at the oil/water interface of pyrite samples subject to different pretreatments. (o) unoxidised; (●) oxidised with H_2O_2; (▲) dry ground

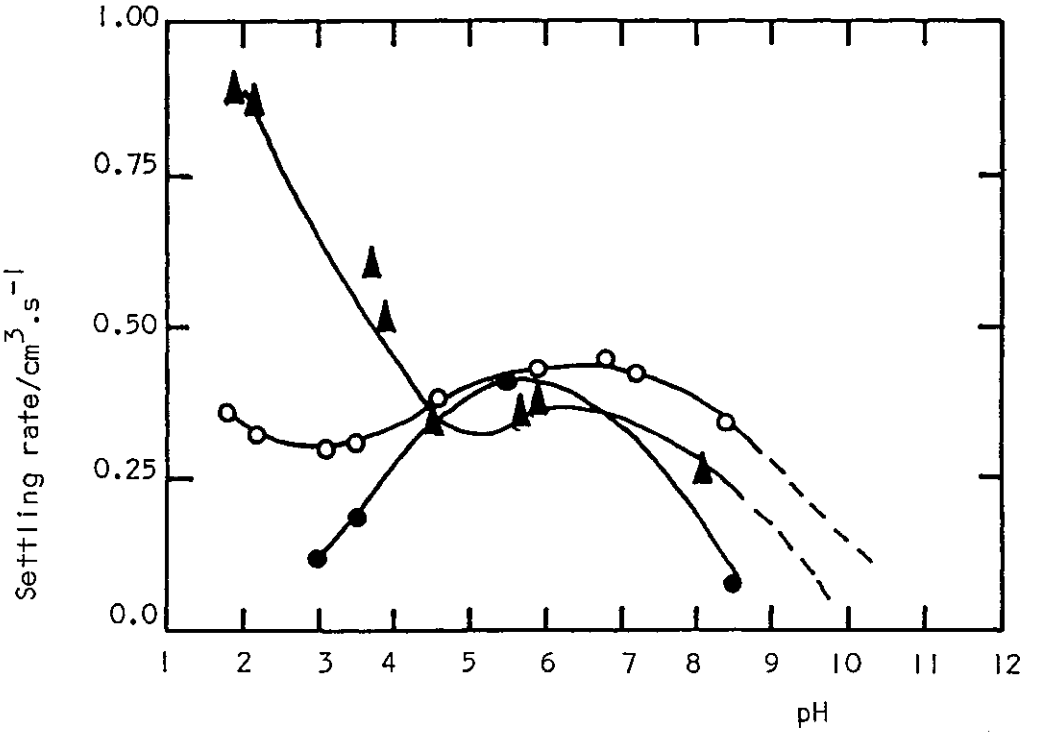

Figure 4.3. Settling rate vs pH for pyrite samples subject to different pretreatments. (o) unoxidised; (●) oxidised with H_2O_2; (▲) dry ground

stable, independent of sample preparation (figure 4.3). The dry ground pyrite differed from unoxidised and H_2O_2 oxidised pyrite in acid solutions, as its stability decreased with decreasing pH, whereas the stability of unoxidised and H_2O_2 oxidised samples increased slightly. The difference might be due to the presence of sulphur on the surface of dry ground pyrite or to the physical adsorption of oxygen as suggested by Plaksin[219] and Lepetic.[222] Pyrite surfaces produced by dry grinding were given sufficient time to adsorb atmospheric oxygen. It has been suggested that this would increase surface hydrophobicity by decreasing the hydration of mineral surface,[219,222] for relatively short exposures to water of this surface. The surface of dry ground pyrite would be less hydrated, and therefore more hydrophobic compared with H_2O_2 oxidised samples.

Thus such pyrite suspensions were found to be less stable. This would also be expected if sulphur, formed by oxidation, was present on the surface. The slightly lower stability of pyrite samples around pH 6 can be explained as the pzc of pyrite is about pH 6.5,[270,272] hence pyrite suspensions tend to coagulate in that pH region.

The results with both galena and pyrite therefore show that coagulation of the minerals was not responsible for the two-liquid flotation results obtained. Hence it would appear that galena and pyrite are oleophilic to a degree dependent on the state of oxidation of their surfaces.

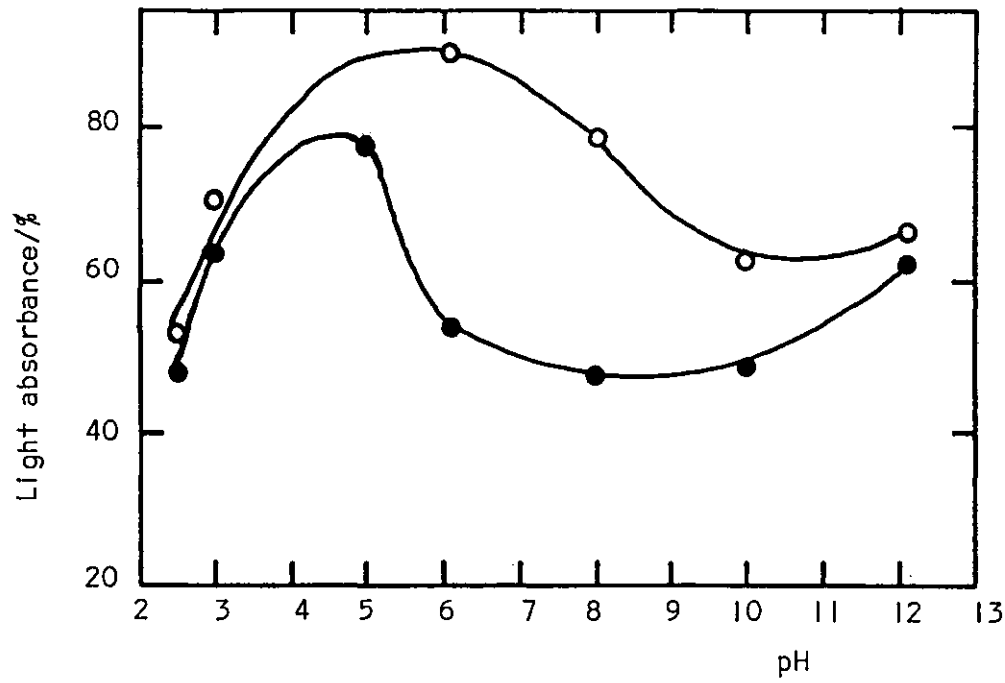

Figure 4.4. Light absorbance as a function of pH for galena suspensions. (o) unoxidised; (●) oxidised with H_2O_2.

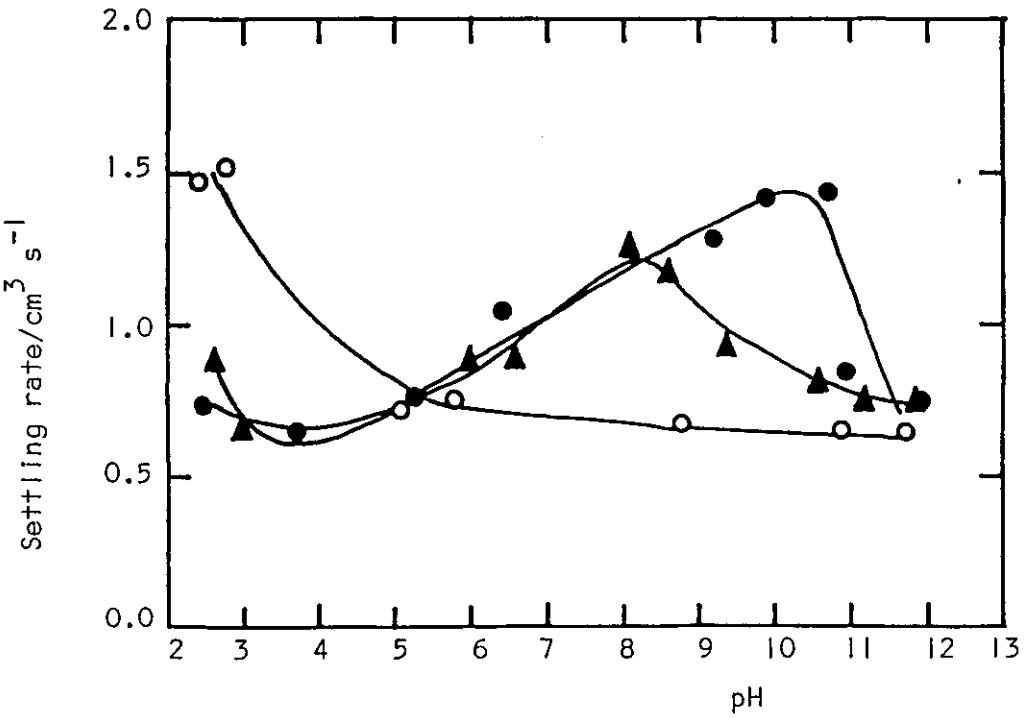

Figure 4.5. Settling rates as a function of pH for galena suspensions subject to different pretreatments. (o) unoxidised; (●) oxidised with H_2O_2; (▲) sulphidised following oxidation

4.3 Contact angle measurements at galena and pyrite/oil/water interfaces

The results obtained are summarised in figure 4.6 and 4.7 in which advancing contact angles, as a function of pH, are plotted for galena and pyrite respectively. The receding contact angles were about 50% of the advancing contact angles. This hysteresis of contact angles could have been due to surface roughness[275,276] or the chemical heterogeneity[276] of the surfaces, which might result from the existence of local cells[209] on the surface of sulphide minerals.

Both unoxidised galena ($\theta \simeq 70^{o}$) and pyrite ($\theta \simeq 90^{o}$) were highly oleophilic under pH conditions where the maximum concentration of similarly treated samples occurred at the oil/water interface. Oxidation of mineral samples resulted in a decrease in contact angles, and in neutral solutions galena was oleophilic, i.e. the contact angle was zero. With pyrite, surface oleophobicity due to oxidation was observed at pH values > 7. The galena and pyrite broken under deoxygenated water at natural pH (5.5-6.5) were also oleophilic. Measurements made with nitrogen bubbles under similar conditions gave zero contact angles. This suggested that the angles measured with the oil drops were not caused by contamination.

To further ascertain whether or not the iso-octane used as the oil phase contained surface active impurities which were responsible for the measured contact angles, measurements were also made on quartz, fluorite and calcite at various pH

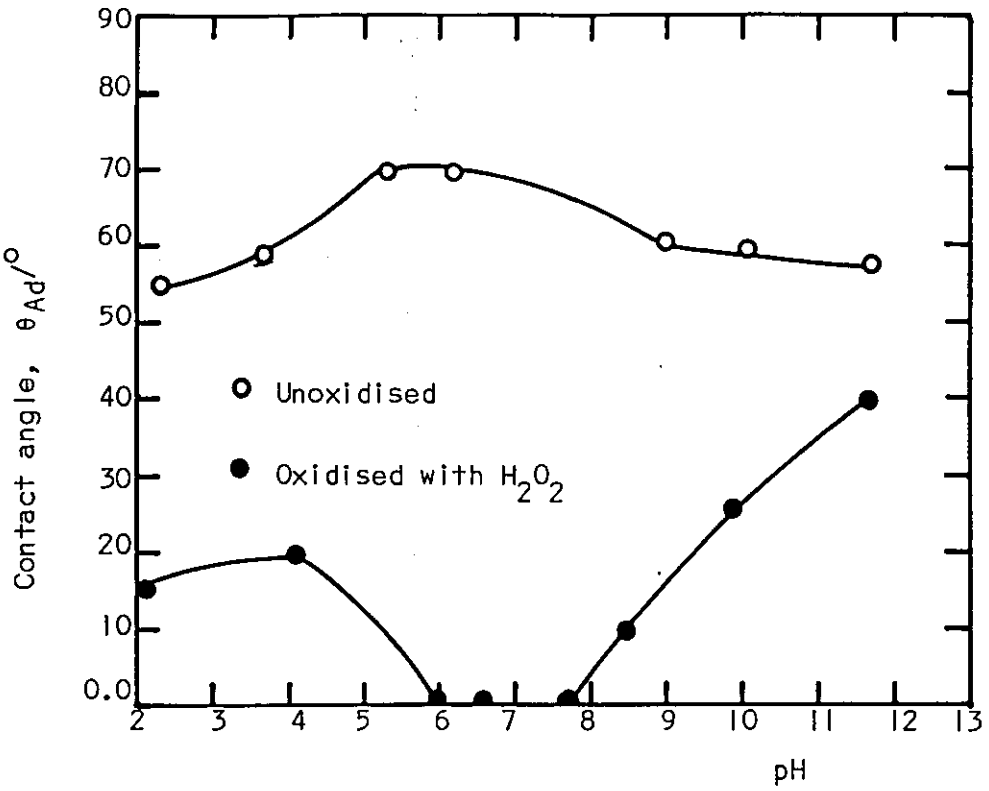

Figure 4.6. The contact angle at the galena/oil/water interface as a function of pH

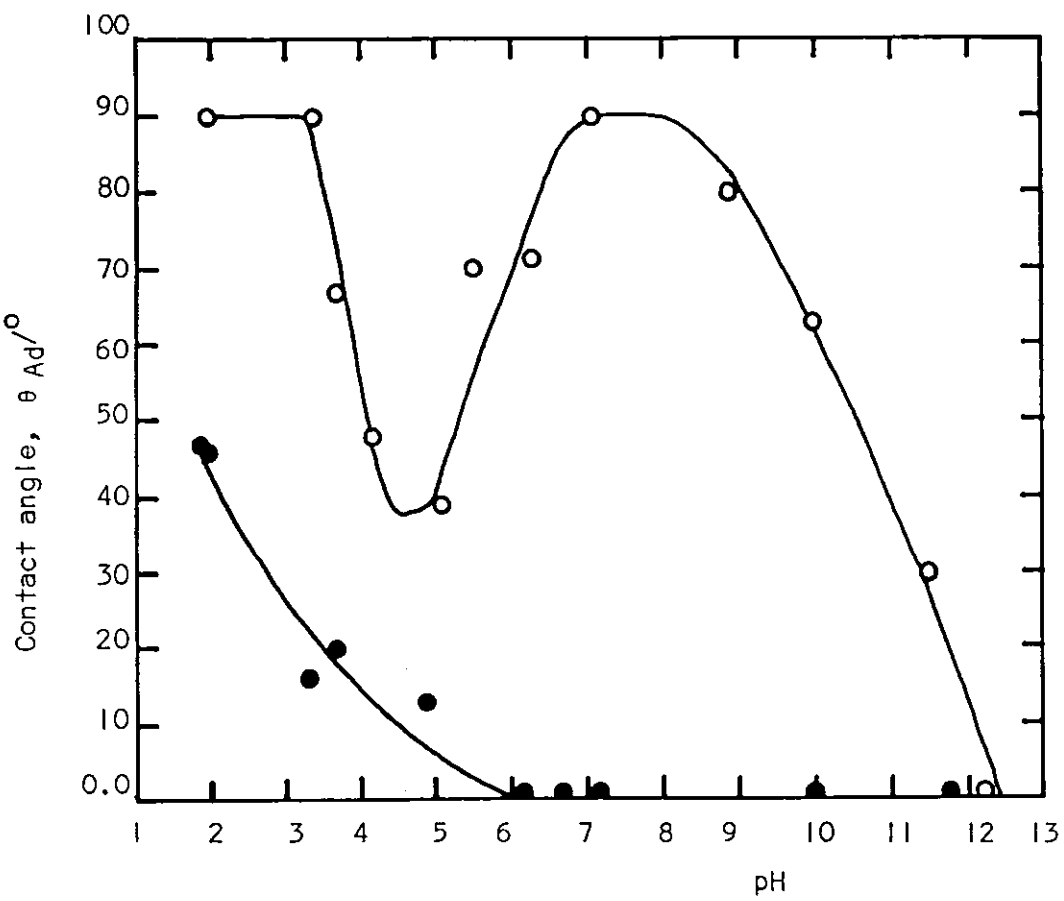

Figure 4.7. The contact angle at the pyrite/oil/water interface as a function of pH. (o) Unoxidised; (●) oxidised with H_2O_2

values. In all cases a zero contact angle was obtained. Therefore it would appear that under certain redox conditions, both pyrite and galena are oleophilic but hydrophobic with respect to gas bubbles. Crystalline sulphur gave 75^{o} and 180^{o} contact angles with nitrogen bubbles and iso-octane drops respectively.

4.4 Interfacial tension and contact angle measurements with different organic liquids

The results of interfacial tension and contact angle measurements are summarised in table 4.1, together with literature values[161] of dipole moments and water solubility of oils.

Measured interfacial tensions were in accordance with values reported in the literature.[161] Both galena and pyrite were oleophilic with respect to all the oils studied. The contact angle from oil to oil was qualitatively similar, though pyrite gave larger contact angles. There was no direct relationship between the interfacial tension, dipole moment, water solubility of the oils and the contact angle.

The change of drop formation time had no effect on the interfacial tension of oils with water, indicating that there was an insignificant concentration of surface active contaminant within the system.

Oil	$\gamma_{o/w}$ (mNm^{-1})	Dipole moment (Debye)	Solubility of water (wt %)	Galena		Pyrite	
				θ_{Rc}	θ_{Ad}	θ_{Rc}	θ_{Ad}
n - heptane	50.60	0.0	0.009	19	31	29	48
cyclohexane	49.80	0.2	0.012	-	23	21	47
iso-octane	48.23	0.0	0.006	25	65	42	70
toluene	36.30	0.3	0.033	-	25	23	50
benzene	34.75	0.0	0.063	20	39	40	69
diethylether	10.70	1.15	1.46	21	40	25	50
n-butanol	2.19	1.75	20.5	60	110	104	119

Table 4.1. Interfacial tensions and contact angles at various oil/water and mineral/oil/water interfaces

4.5 Electrochemical studies

4.5.1 Rest potentials

The rest potential of both unoxidised and oxidised galena are in agreement with the values reported in the literature.[204-5,279] Figure 4.8 shows that the galena rest potential was pH independent in neutral and acid solutions (a), and in alkaline solutions it was pH dependent (b), with a slope of 40 $mV.pH^{-1}$ for unoxidised and 60 $mV.pH^{-1}$ for oxidised electrodes. Reduction of the electrode surface with aqueous Na_2S solution did not affect the electrode potential at neutral and acid pH values, whereas it produced more negative potentials in alkaline solutions, as shown in figure 4.8.

The potential for reaction (a) (see Appendix I)

$$Pb^{2+} + S + 2e \rightleftharpoons PbS \qquad (a)$$

$$Eh = 0.354 + 0.0295 \log \left[Pb^{2+}\right]$$

is represented by the horizontal line (I) in figure 4.8 and agrees well with the measured potentials of galena oxidised with H_2O_2. The region (b) corresponds to the potential of a mineral surface passivated by the formation of oxides or hydroxides. Such a passive oxide electrode may function as a pH electrode[259] with a slope of 0.059 V pH^{-1}:

$$Pb(OH)_2 + S + 2H^+ + 2e \rightleftharpoons PbS + H_2O \qquad (e)$$

$$Eh = 0.765 - 0.059\ pH$$

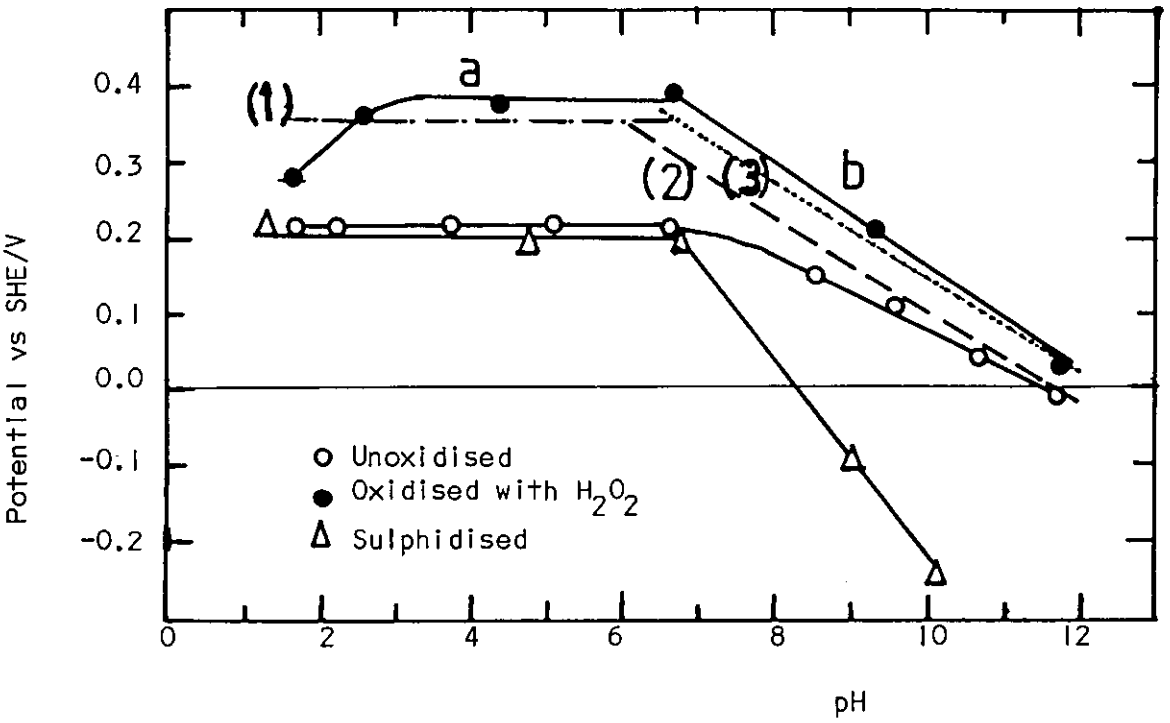

Figure 4.8. The rest potential of galena electrodes - subject to different pretreatments vs pH

This is in reasonable agreement with the potential/pH slope of an oxidised galena electrode in the alkaline region. The oxidation of galena in neutral and alkaline solutions can occur by reaction d or e[204,250,267] represented by the pH dependent lines 2 and 3 in figure 4.8. The potential for reaction e agrees well with the measured potentials.

When oxidised galena electrodes were transferred to various deoxygenated solutions of different pH, their potential decreased, approaching their preoxidation value as the pH was changed to acid and back to alkali pH values or vice versa, as shown in figure 4.9. The $Pb(OH)_2 + S^o$ oxidation products of

galena formed by reaction e at the natural pH (5.5-6.5) were not stable at all pH values and were removed from the surface as the pH changed. The Eh-pH diagram of the Pb-H_2O system (figure 2.4) shows that $Pb(OH)_2$ could be removed from the surface as $HPbO_2^-$ in alkaline solutions and as Pb^{2+} in acidic solutions. Therefore the increase in flotation recovery and contact angle of oxidised galena (figure 4.1 and 4.6) could be due to the removal of an oxide layer in alkaline solutions and to the removal of oxide layer as well as to the presence of sulphur in acid solutions.

The rest potential of galena electrodes measured in buffer solutions showed different features (figure 4.10). The potential of an unoxidised electrode was slightly lower than the potential shown in figure 4.8 for the same surface and did not show a pH independent region in acidic solutions. When H_2O_2 was added to the cell, the electrode potential increased, falling on a line parallel to the original potential response. Comparison of curves (2) and (3) in figure 4.10 shows that, although the electrode potential becomes time invariant after one minute below pH 9.2, at pH 11 the potential continued to increase for 30 minutes, possibly indicating that more than one oxidation stage was involved. With the transfer of the electrode to fresh deoxygenated solution from the oxidising environment, its potential decreased, but showed a maximum at pH 9.2. This could be due to the control of the electrode potential by solution species formed during oxidation below and above pH 9.2. By transferring the electrode these species would have been removed from the surface and the electrode

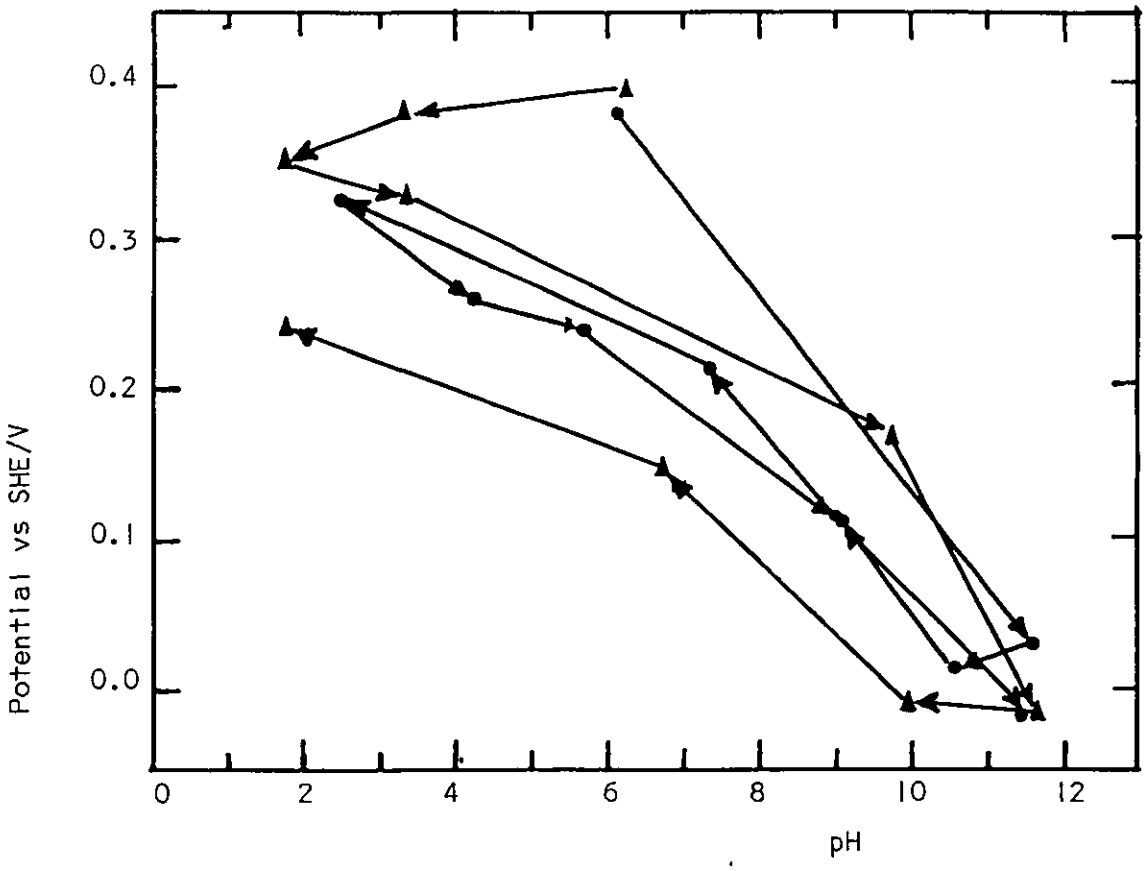

Figure 4.9. The change of the rest potential of a galena electrode when it was transferred to solutions of various pH values after being oxidised at the natural pH

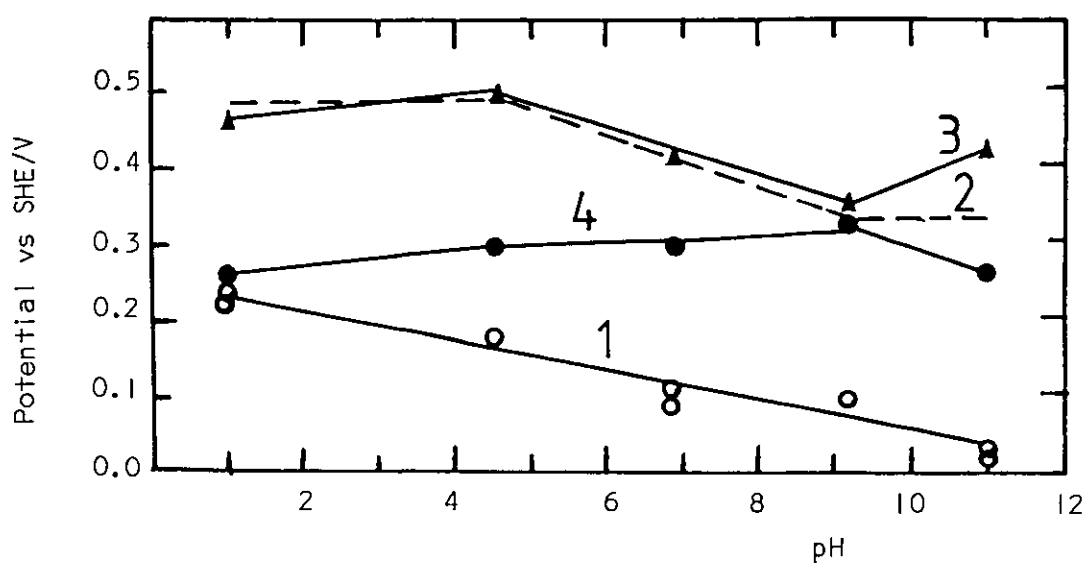

Figure 4.10. The change of the rest potential of a galena electrode oxidised in buffered H_2O_2 solutions. 1 - unoxidised; 2 - after 1 minute of oxidation; 3 - after 30 minutes of oxidation; 4 - after electrode transferred from oxidising environment to fresh solutions

potential would be expected to decrease. The Eh-pH diagram of the Pb-S-H_2O system (figure 2.6) indicates that at pH values < 5 reaction a is possible, while at pH values higher than 9.2 reaction h can occur, producing $2HPbO_2^-$ + $S_2O_3^{2-}$. The Eh-pH diagram for Pb-H_2O system (figure 2.4) shows $HPbO_2^-$, formed by reaction p, as the dominant Pb species at high pH. Therefore, it is possible that at pH 11, while the initial oxidation of galena occurs by reaction e, further oxidation of the mineral involves reaction h.

The rest potential of unoxidised, oxidised and sulphidised pyrite electrodes are shown in figure 4.11. Oxidation with H_2O_2 increased the potential by about 0.2 V at all pH values, whereas sulphidisation with aqueous Na_2S solution produced more negative potentials. The potential did not show a pH independent region in acid solutions as observed with galena. As pyrite is a good electrocatalyst for oxygen reduction[240,241] it is likely that a surface iron oxide or hydroxide would be formed during polishing and washing, even in nominally 'deoxygenated' solutions. At low pH values this hydroxide would dissolve by reaction v':

$$Fe(OH)_3 + 3H^+ \rightleftharpoons Fe^{3+} + 3H_2O \qquad (v')$$

$$\log \left[Fe^{3+}\right] = 4.84 - 3pH$$

The lack of a pH independent potential in acidic solutions could imply that 5 minutes conditioning time was too short for the removal of the oxide layer from the surface by reaction v'.

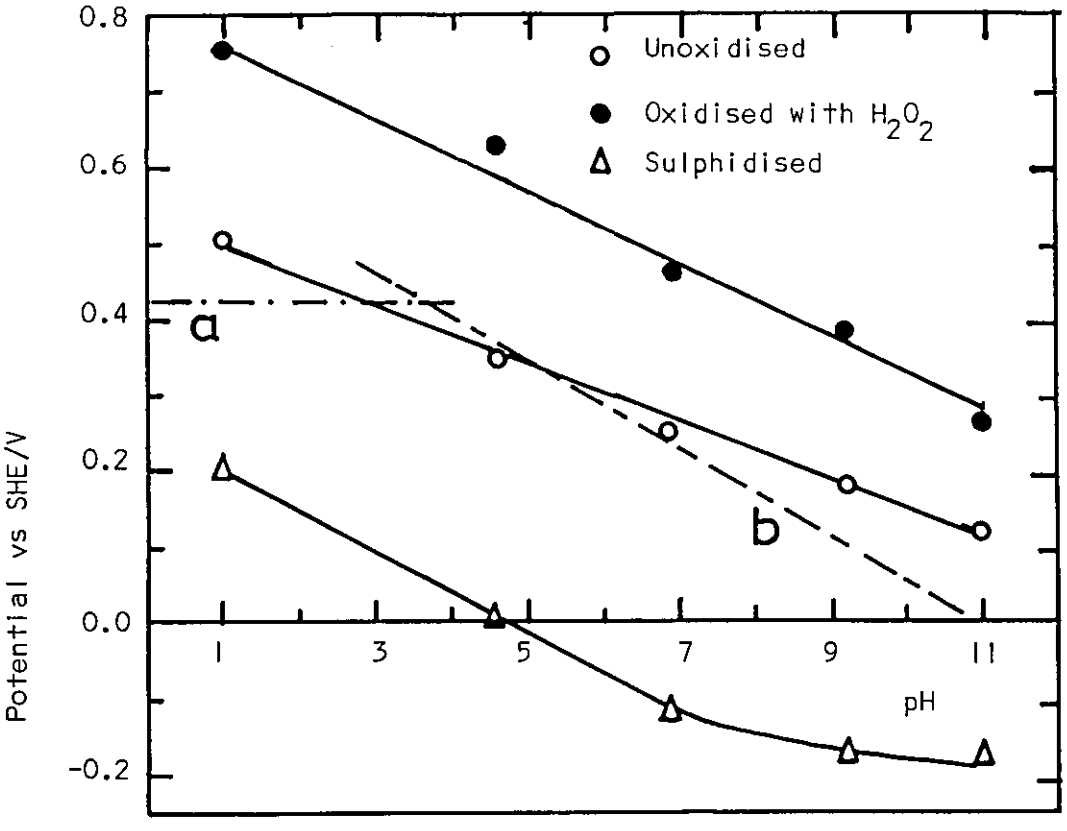

Figure 4.11. The rest potential vs pH for a pyrite electrode subject to different pretreatments

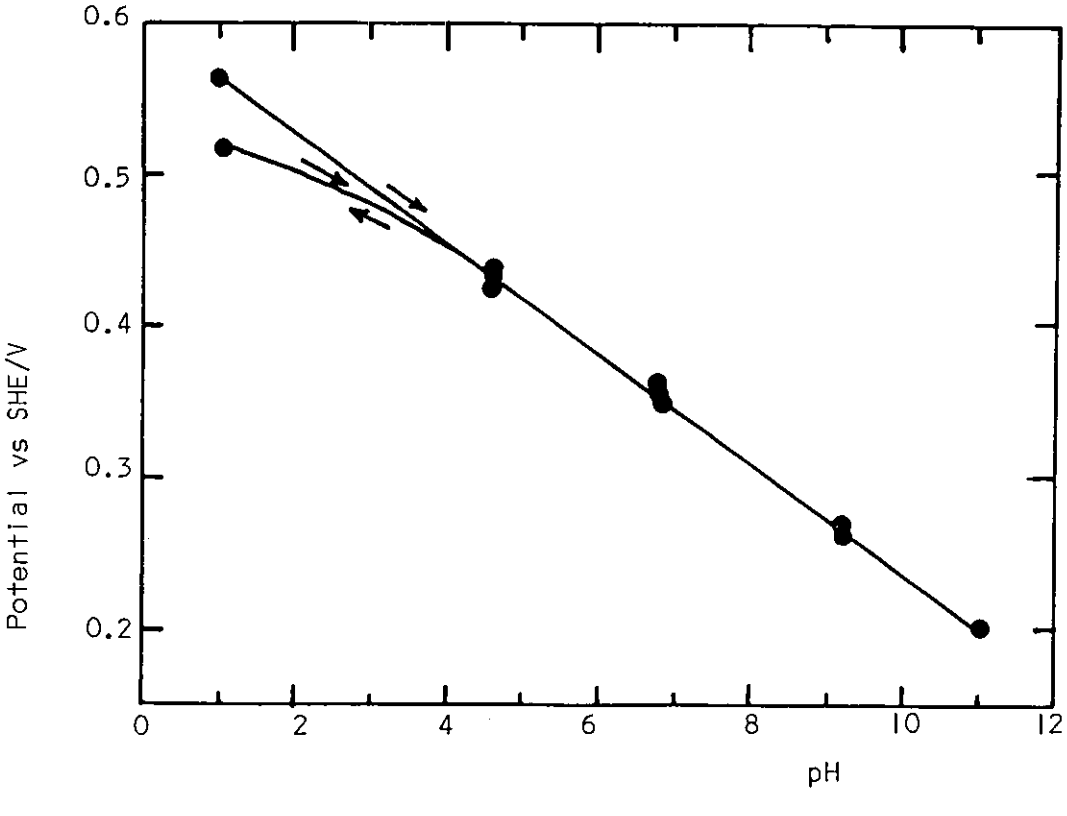

Figure 4.12. The change of pyrite potential when it was transferred to various pH values after being oxidised at natural pH

Peters and Majima[281] studied pyrite electrodes in 1 M $HClO_4$ solution and described a 'passive' and 'active' form of pyrite. They measured a rest potential of 0.62 V for 'passive' pyrite (exposed to air), and 0.2-0.3 V for 'active' pyrite (cathodically reduced). The rest potential of freshly polished and sulphidised pyrite electrodes (figure 4.11) agrees well with the above values for 'passive' and 'active' pyrite respectively.

In 10% H_2O_2 solution, the solution potential will be controlled by[282]

$$H_2O_2 + 2H^+ + 2e \rightleftharpoons 2H_2O \qquad (4.1)$$

$$Eh = 1.77 - 0.059\ pH + 0.0295\ \log[H_2O_2]$$

During oxidation of pyrite with H_2O_2 the electrode potential increased sharply (region I in figure 4.13) and after 5 to 10 minutes, depending on the pH, it became constant. However, when the electrode was transferred from the oxidising environment to deoxygenated solution (region II in figure 4.13), the potential decreased and became constant after 20 minutes. Figure 4.14 shows the final value of the pyrite potential after 30 minutes oxidation in buffered H_2O_2 solutions at various pH values, the equilibrium potential after the electrode was transferred to fresh deoxygenated solutions, and the preoxidation potential. With the removal of the electrode from the oxidising environment, the pyrite potential decreased

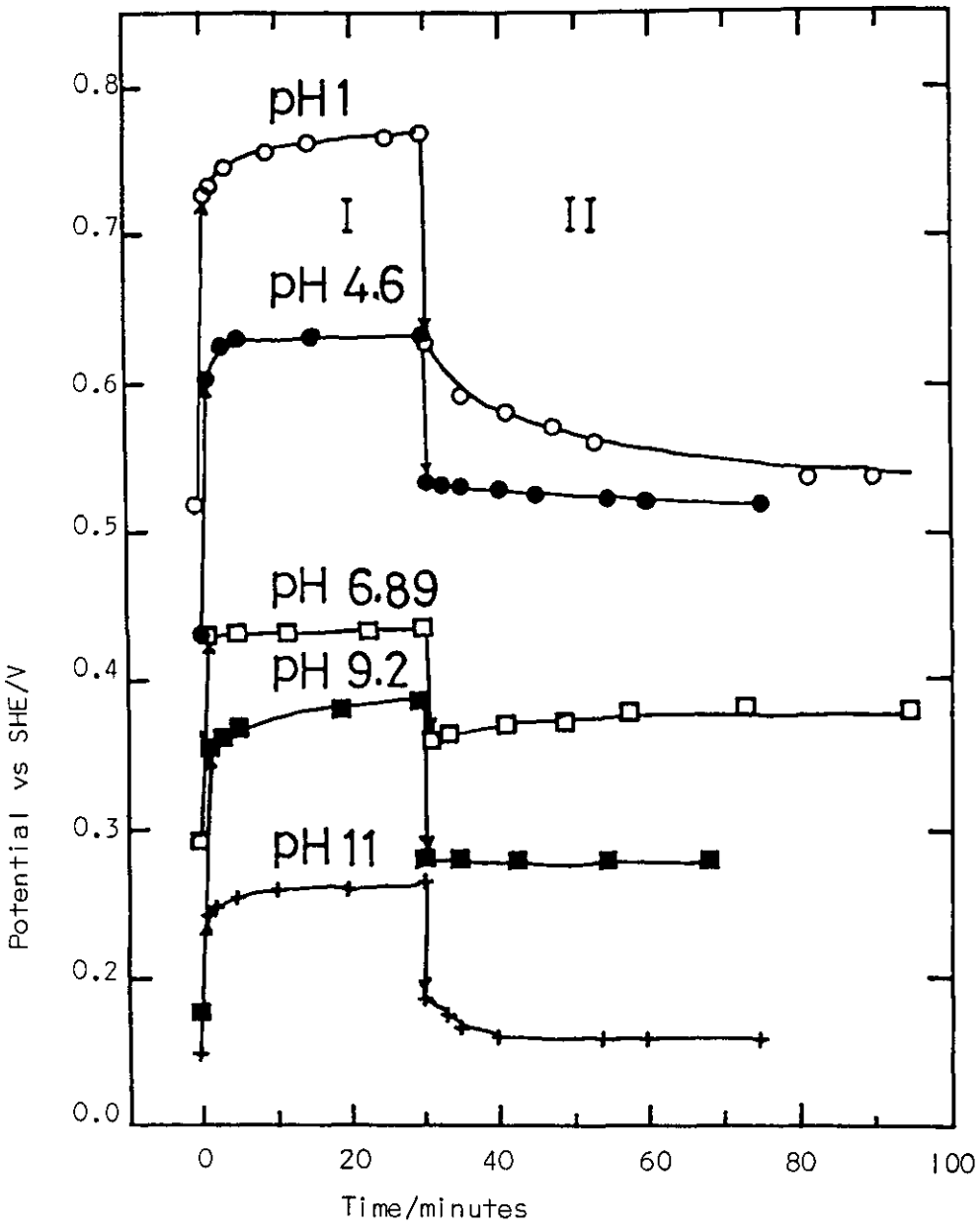

Figure 4.13. The change of pyrite potential during 30 minutes of oxidation in H_2O_2 solution (I) and after electrode was transferred to fresh solution (II) at various pH values.

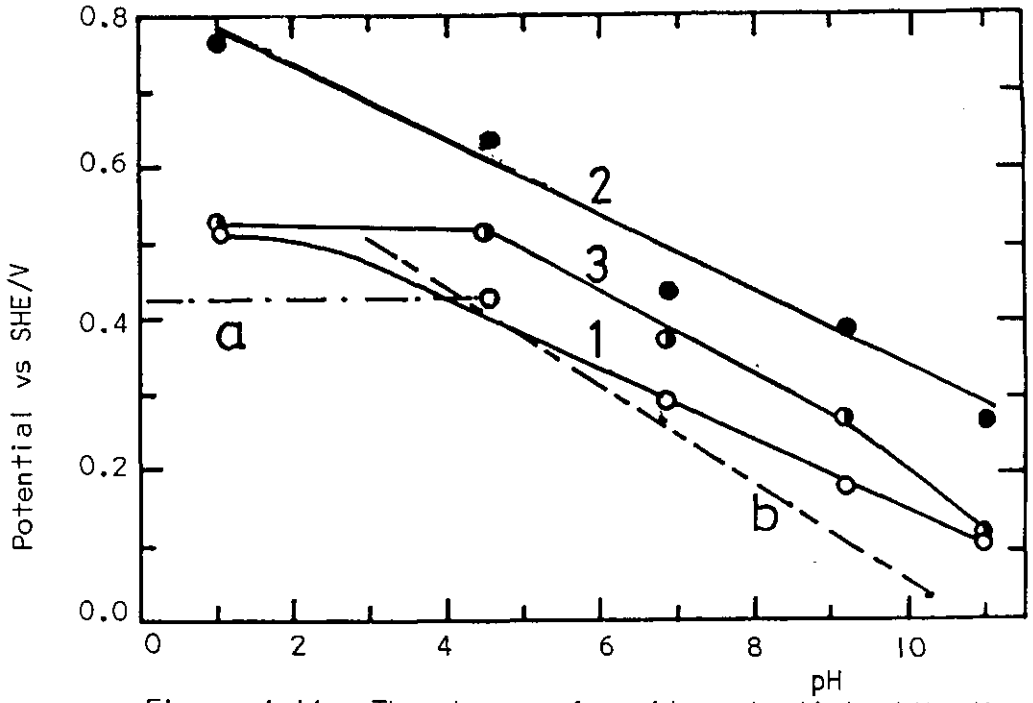

Figure 4.14. The change of pyrite potential with pH. 1 - before oxidation (o); 2 - after 30 minutes of oxidation in 10% H_2O_2 solution (●); 3 - after electrode was transferred to fresh solution (◑).

in deoxygenated solutions, almost to the preoxidation potential at pH I and II, whereas at neutral pH values it remained at higher potentials. This difference at pH I and II might be due to the control of the electrode potential by the solution species formed during oxidation and removed from the surface with the transfer of electrode.

It is possible that the potential of freshly polished unoxidised pyrite under oxygen-free conditions is controlled by reaction a' (see Appendix II):

$$Fe^{2+} + 2S + 2e \rightleftharpoons FeS_2 \qquad (a')$$

$$Eh = 0.423 + 0.0295 \log[Fe^{2+}]$$

in acid solutions, whereas in neutral and alkaline solutions reaction e' determines the potential

$$Fe(OH)_3 + 2S + 3H^+ + 3e \rightleftharpoons FeS_2 + 3H_2O \qquad (e')$$

$$Eh = 0.64 - 0.059\ pH$$

The reactions a' and e' are represented in figures 4.11 and 4.14 by the lines a and b which are in reasonable agreement with the experimental values. This would also explain the decrease of the pyrite potential, when the electrode was transferred from an oxidising environment to the deoxygenated solutions at pH I (figure 4.14), since then the pyrite potential would be controlled by Fe^{2+} concentration. However,

at pH 11 the incomplete Eh-pH diagram of the Fe-S-H_2O system (figure 2.7) shows that above pH 9.5 $Fe(OH)_2$ is the iron oxidation species in equilibrium with a pyrite surface whereas the Eh-pH diagram of Fe-H_2O system (figure 2.5) indicates that some $Fe(OH)_2$ can be removed from the surface as $HFeO_2^-$ above pH 10.53.

When an oxidised pyrite electrode was transferred to deoxygenated solutions of different pH values, the electrode potential did not change with pH in alkaline solutions but it decreased with pH in acidic solutions (figure 4.12). Therefore, unlike galena, the oxidation products of pyrite at the natural pH (5.5-6.5) were stable in alkaline solutions and unstable only at pH values < 4.6. Hence the increase in the recovery and contact angle below this pH (figure 4.2 and 4.7) could be due to the removal of the oxide layer from the surface as well as to the presence of sulphur.

4.5.2 Steady-state potentiostatic studies

The polarisation curves obtained with galena and pyrite at different pH values are shown in figure 4.15 and 4.16 respectively.

With galena the current decreased during 3 minutes of polarisation, while it first increased then decreased with increasing potential, indicating passivation at all pH values. At cathodic potentials the current gradually increased below a certain potential, depending on pH. The surface oxidation product which caused passivation in acidic solutions was S^o formed by reaction a, whereas in neutral and alkaline solutions

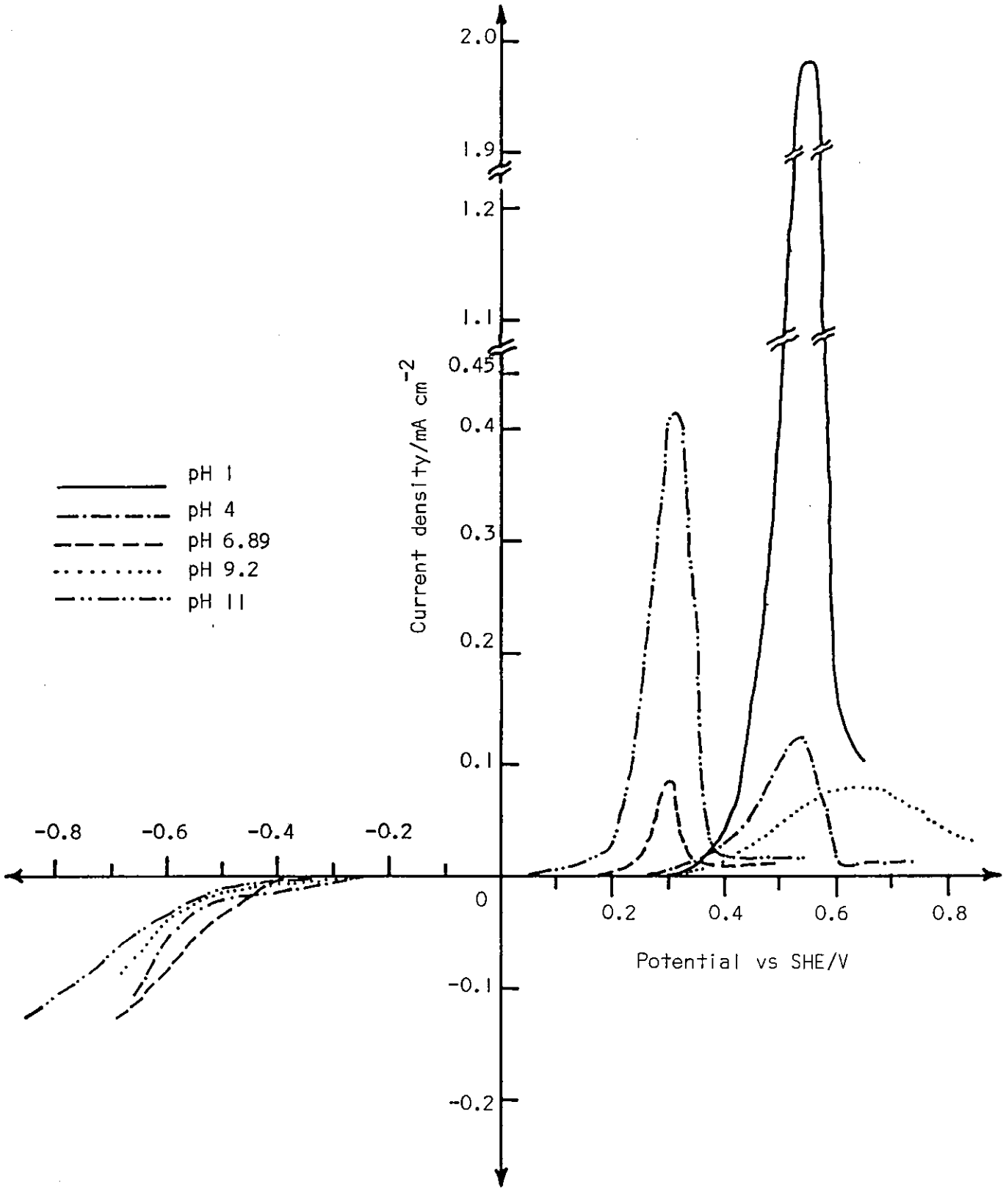

Figure 4.15. Polarisation behaviour of galena at various pH values

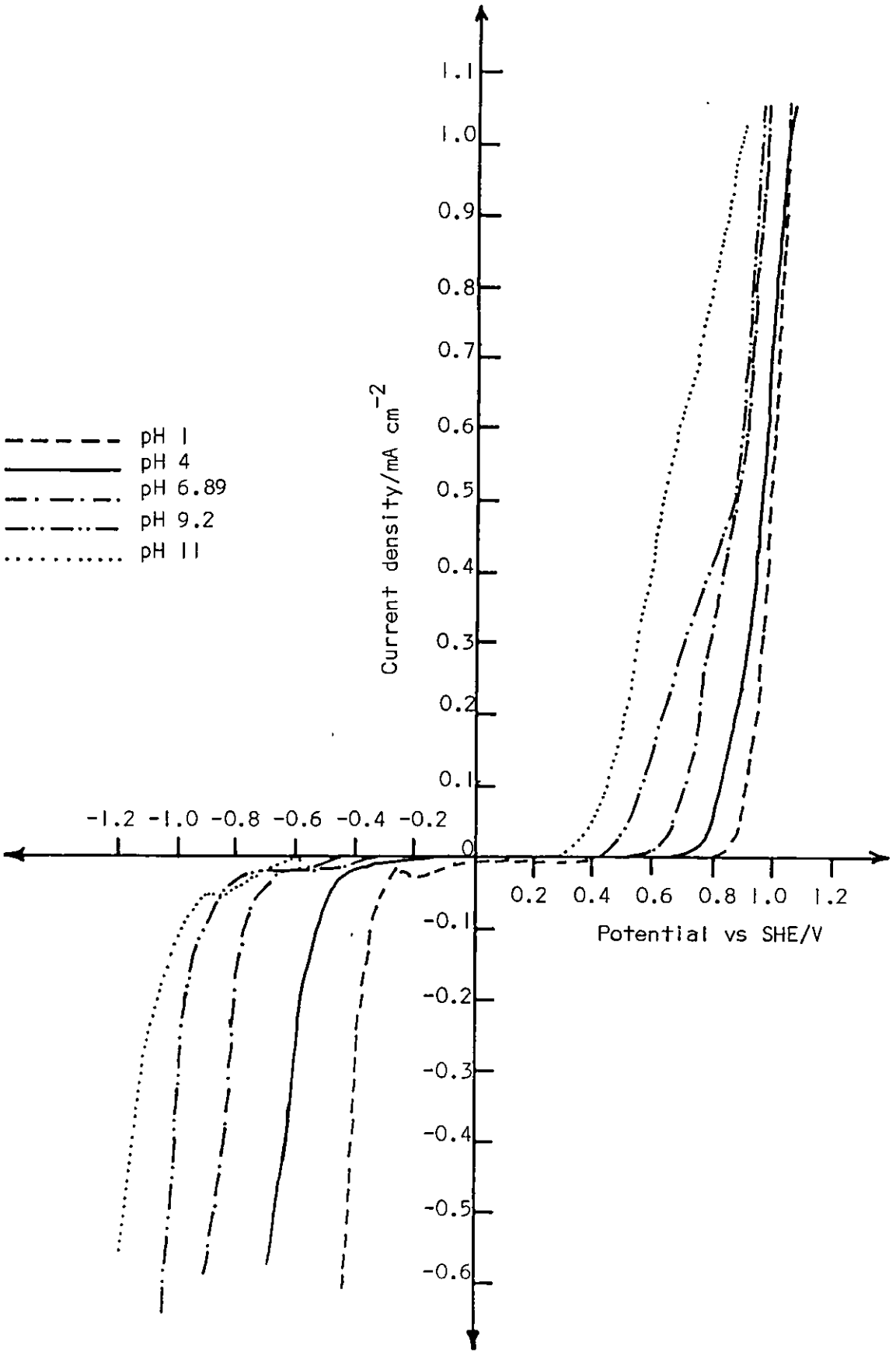

Figure 4.16. Polarisation behaviour of pyrite electrode at various pH values

it could have been $Pb(OH)_2 + S^o$, formed by reaction e.

With pyrite, the current at all pH values increased with increase of potential in both anodic and cathodic directions (figure 4.16). Bigger cathodic currents were obtained with pyrite and gas bubbles formed on the electrode surface. This was due to the greater cathodic activity/lower overpotential for hydrogen evolution on the iron compared with lead, formed by mineral decomposition[260] by reactions k and o for galena and k', l', m', n' and o' for pyrite, depending on the pH. The potential of the increase in the cathodic current on pyrite (figure 4.16) showed a shift of 59 mv per pH unit towards more cathodic potentials, which is the same as the slope of reaction r':

$$2H^+ + 2e \rightleftharpoons H_2 \qquad (r')$$

$$Eh = -\ 0.059\ pH$$

Polarisation of the mineral electrodes resulted in lower or higher rest potentials following cathodic and anodic polarisation respectively. This occurred after wet grinding and polishing on successive grades of silicon carbide paper and then with fine alumina to remove the new phase formed by polarisation.

When the electrode was isolated after 3 minutes of polarisation, the subsequent open circuit potential of the electrode returned towards the prepolarisation potential but there was still some difference between the initial and

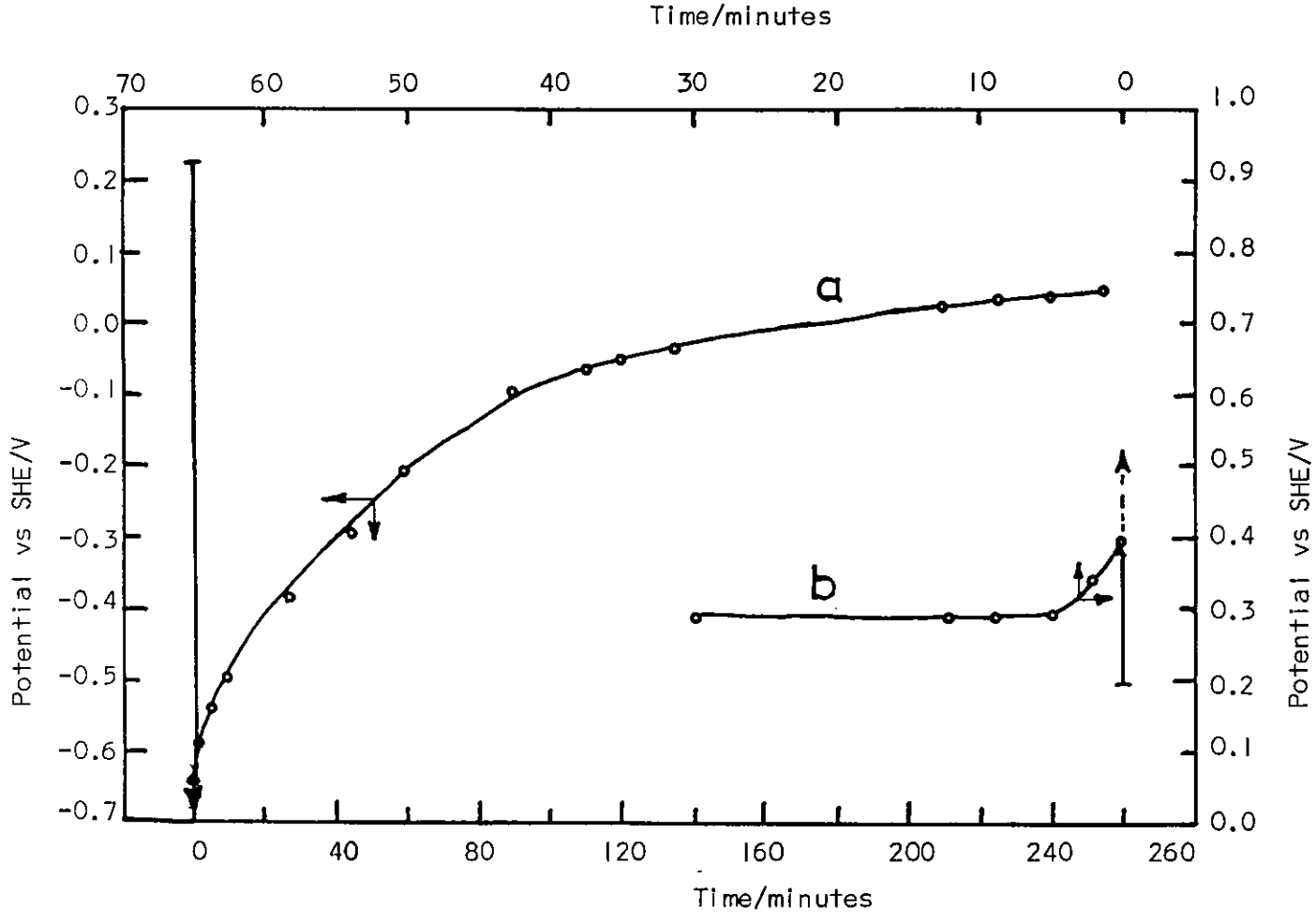

Figure 4.17. The change of the electrode potential of pyrite vs time after being polarised for 3 minutes, a - at -0.985 V; b - at +1.0 V

final potential. Figure 4.17 shows the change of pyrite potential with time, following polarisation at +1.0 V and -0.985 V. During cathodic polarisation at low pH values, H_2S was smelt in the outgoing gas.

4.5.3 The effect of redox potential on wettability

When the electrodes were polished in air with 800 grade silicon carbide paper and alumina, the reduction or oxidation did not produce any change in the wettability of pyrite electrodes which were oleophobic. This could be due to the formation during polishing of a $Fe(OH)_3$ surface layer, the reduction of which yielded $Fe(OH)_2$ and Fe^o by reaction h' and q' (see Appendix II), so pyrite remained oleophobic even when cathodically reduced.

With galena, however, although the mineral was oleophobic at its rest potential, oxidation in acidic solutions (pH 1, 1.68 and 4.0) produced an oleophilic surface. At pH 1.68 [0.05 M potassium tetroxalate, $KH_3(C_2O_4)_2.2H_2O$] the contact angle first increased then decreased with potential (figure 4.18). This could be due to the formation of S^o and lead oxalate, which has very low solubility (0.0015 $g.dm^{-3}$ at 18°C),[283] whereas at pH 1 (0.1 M $HClO_4$) and 4 (0.5 MKCl) lead ions produced by reaction a (Appendix I) dissolved leaving only S^o on the surface, making it oleophilic. Cathodic reduction of galena produced an oleophilic surface, but the degree of oleophilicity, according to contact angle measurements, was not reproducible and seemed highly dependent on the degree of initial oxidation. However, when the electrodes were polished

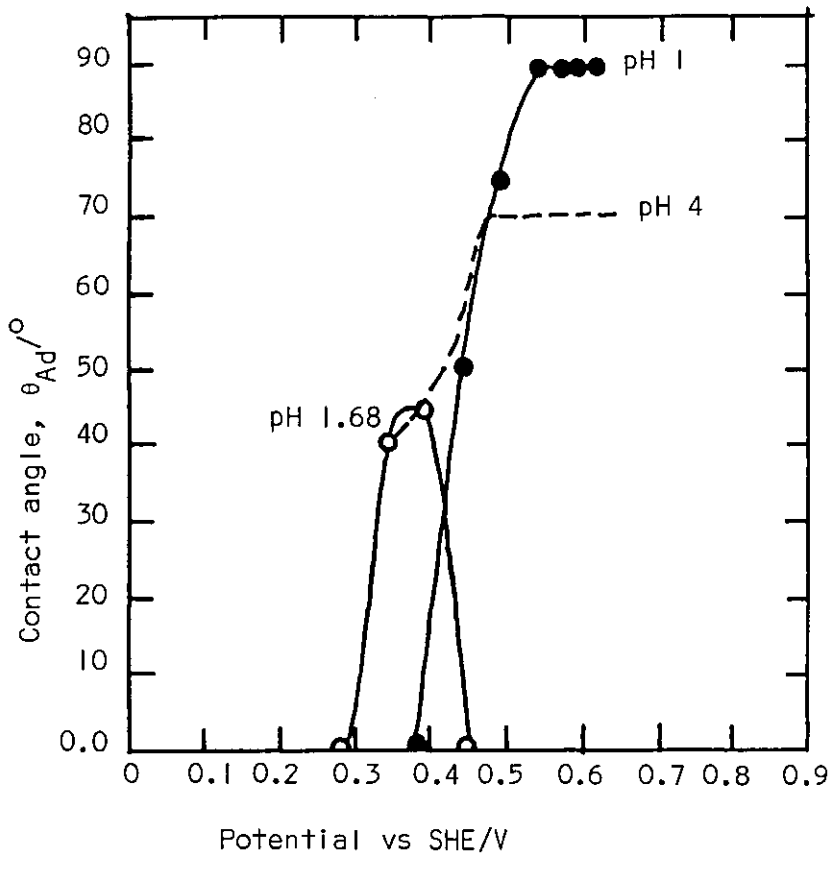

Figure 4.18. The change of contact angle with anodic potential at galena (polished in air)/oil/water interface at acid pH values

under deoxygenated water with 800 grade silicon carbide paper (stuck to the end of a glass rod with araldite) followed by polishing with an alumina pad in Selvyt cloth (tied at the end of a glass rod with acid cleaned copper wire), both galena and pyrite were oleophilic at their rest potential.

As demonstrated in figure 4.19 and 4.20, the galena electrodes were oleophilic at the open circuit potential at all pH values. When oxidised at pH 1, 3 and 4 their contact angle increased with increasing anodic potential. At pH 6.89,

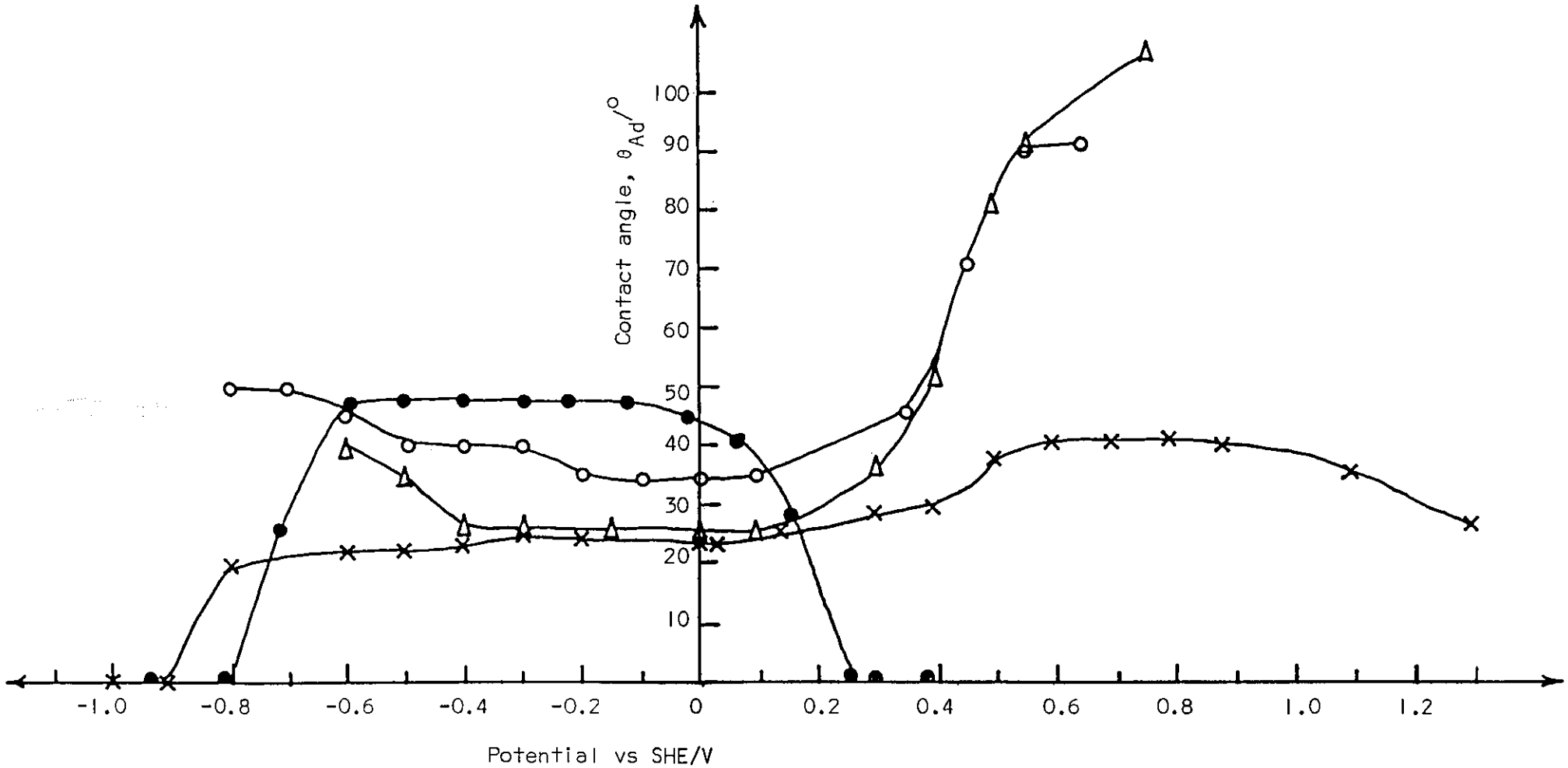

Figure 4.19. The change of contact angle with potential of the galena/oil/water interface at various pH values (in buffer electrolytes). (Δ) pH 1; (o) pH 4; (●) pH 6.89; (x) pH 9.2

oxidation decreased the contact angle and the galena became oleophobic. At pH 9.2, the contact angle increased slightly then decreased with increasing anodic potential. A similar phenomenon was observed at pH 11, when the surface became oleophobic above 0.75 V. At cathodic potentials, reduction caused little change in acidic solutions, whereas in neutral and alkaline solutions, reduction at potentials below a certain pH dependent value produced an oleophobic surface. The results obtained in various buffer electrolytes (figure 4.19) and in 0.5 M heat treated 'Aristar' KCl (figure 4.20) were similar, indicating absence of contamination from the buffer electrolytes.

The increase in the contact angle with anodic oxidation at acid pH values (pH 1, 3, 4 and 5.2) was due to the formation of sulphur[204,249,250,267] on the surface by reaction a. However, in neutral and alkaline solutions $Pb(OH)_2$ formed in addition to S^o by reaction e, so the surface became oleophobic. The initial slight increase in contact angle with oxidation at pH 9.2 and 11 may have been due to the partial removal of $Pb(OH)_2$ as $HPbO_2^-$ by reaction r.

The reduction of galena in acid solutions did not have any effect on the contact angle though lead should have been formed by reaction k. Therefore, contact angles were measured on pure lead electrodes. As figure 4.21 indicates, lead was oleophilic when it was reduced (except at pH 6.89), and oleophobic when it was oxidised, at all pH values. The contact angles measured on unoxidised lead decreased with increasing

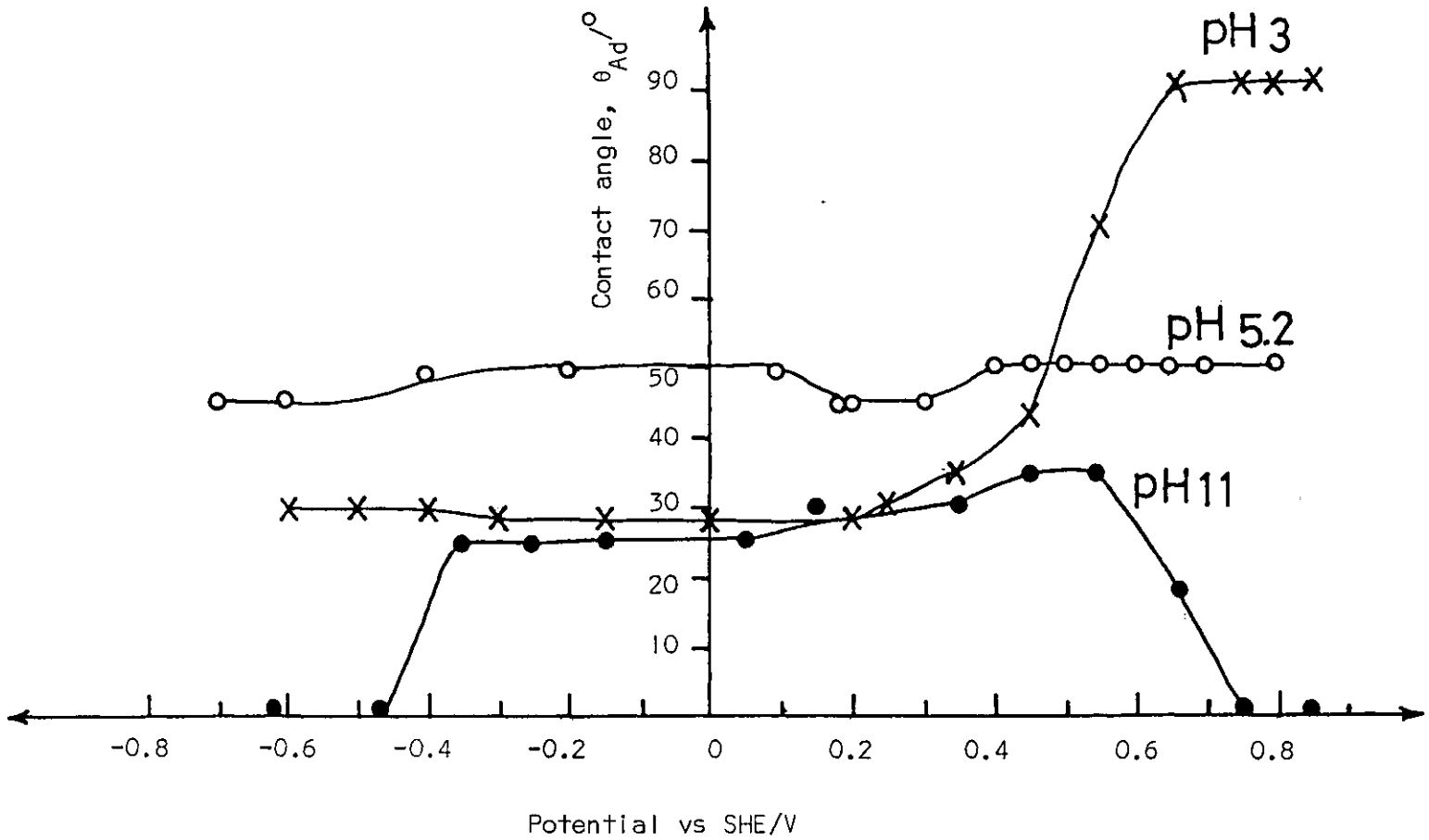

Figure 4.20. The change of contact angle with potential of the galena/oil/water interface at various pH values (in 0.5 M 'Aristar' KCl solution)

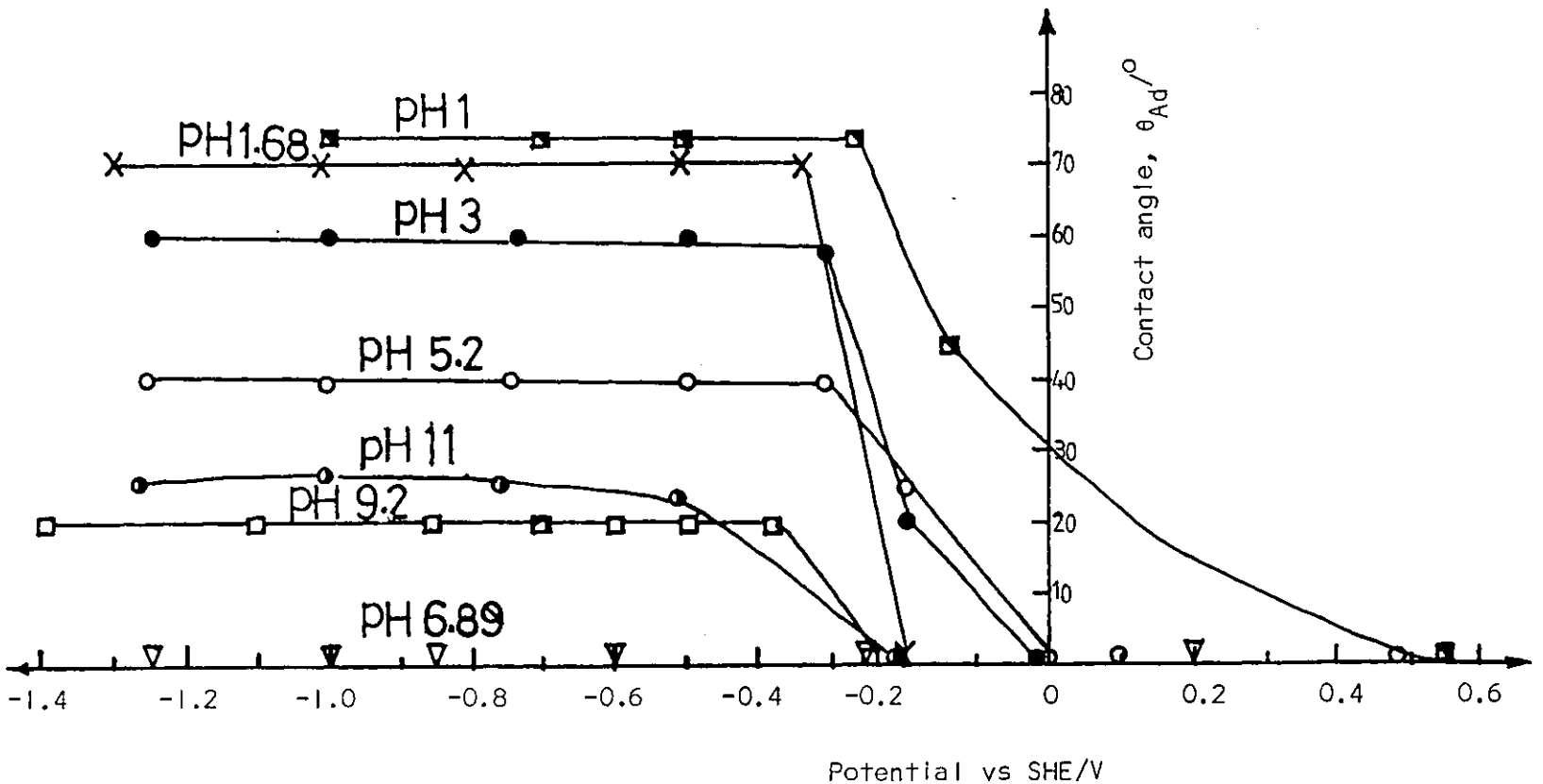

Figure 4.21. The change of contact angle with potential of the lead/oil/water interface at various pH values.

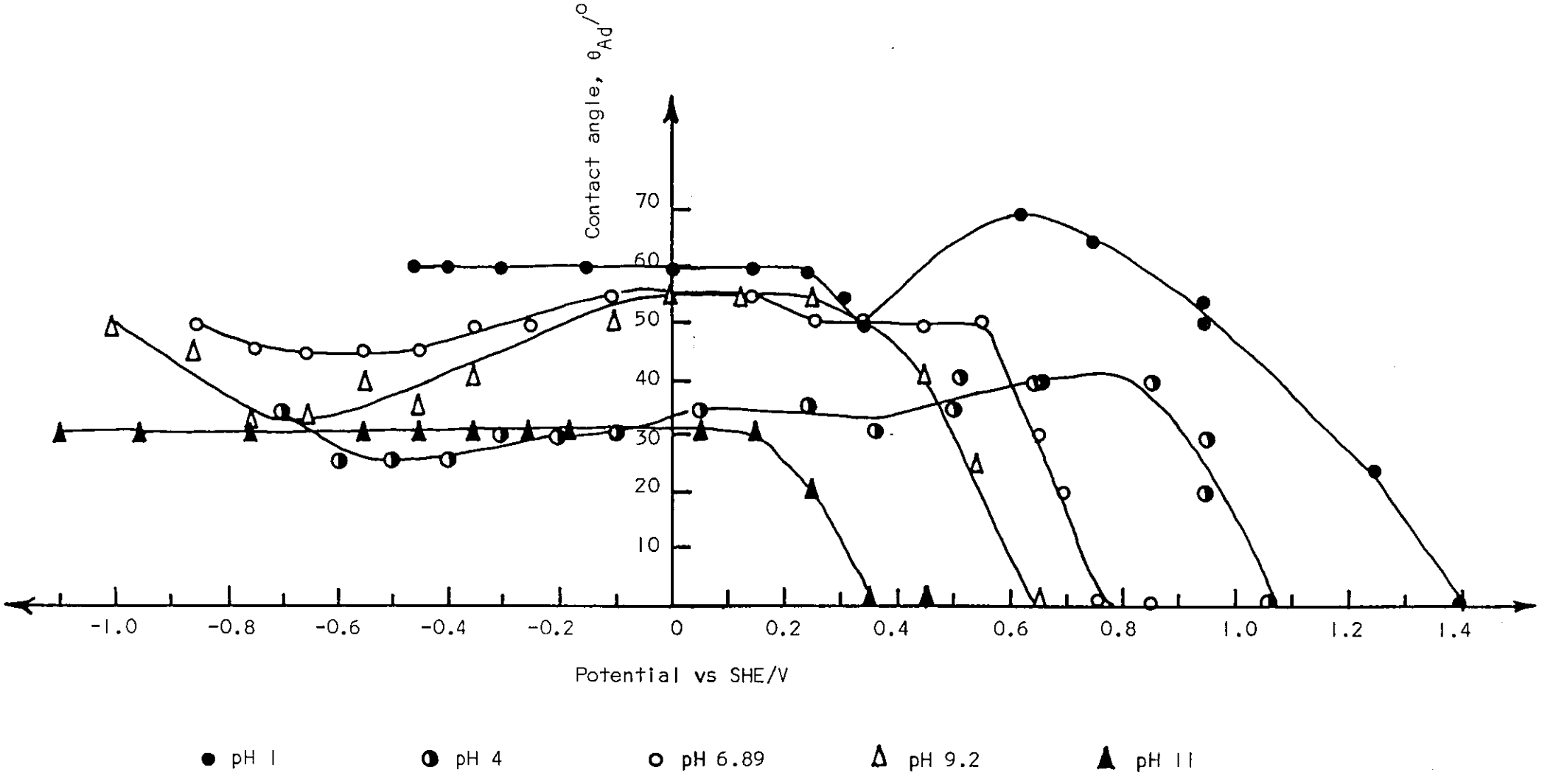

Figure 4.22. The change of contact angle with potential of the pyrite/oil/water interface at various pH values

pH, becoming zero at neutral pH and increasing again in alkaline solutions, but to smaller contact angles than those measured in acidic solutions.

The change of contact angle with potential on pyrite is demonstrated in figure 4.22. At pH 1 and 4 the contact angle first increased then decreased and became zero with increasing anodic potential. At higher pH values, the contact angle decreased with increasing anodic potential and pyrite became oleophobic. On the cathodic side, the potential had little effect on the contact angle except at neutral pH values when it decreased then increased at more cathodic potentials.

The increase in the contact angle at the pyrite/oil/water interface at pH 1 and 4 was due to the formation of sulphur on the surface[213,284,285] by reaction a' (Appendix II). However, with further increase of anodic potential reaction b' became predominant and the contact angle decreased. With increase of pH, the oxidation of pyrite occurred by reaction e' and $Fe(OH)_3$ formed in addition to sulphur, so pyrite became oleophobic.

4.5.4 Cyclic voltammetric studies

4.5.4.1 Cyclic voltammetry of galena

Anodic and cathodic reactions of galena at pH 1 (0.1 M $HClO_4$)

As shown in figure 4.23, when a galena electrode was anodically oxidised on a potential sweep starting from the rest potential, a surface oxidation product was formed which

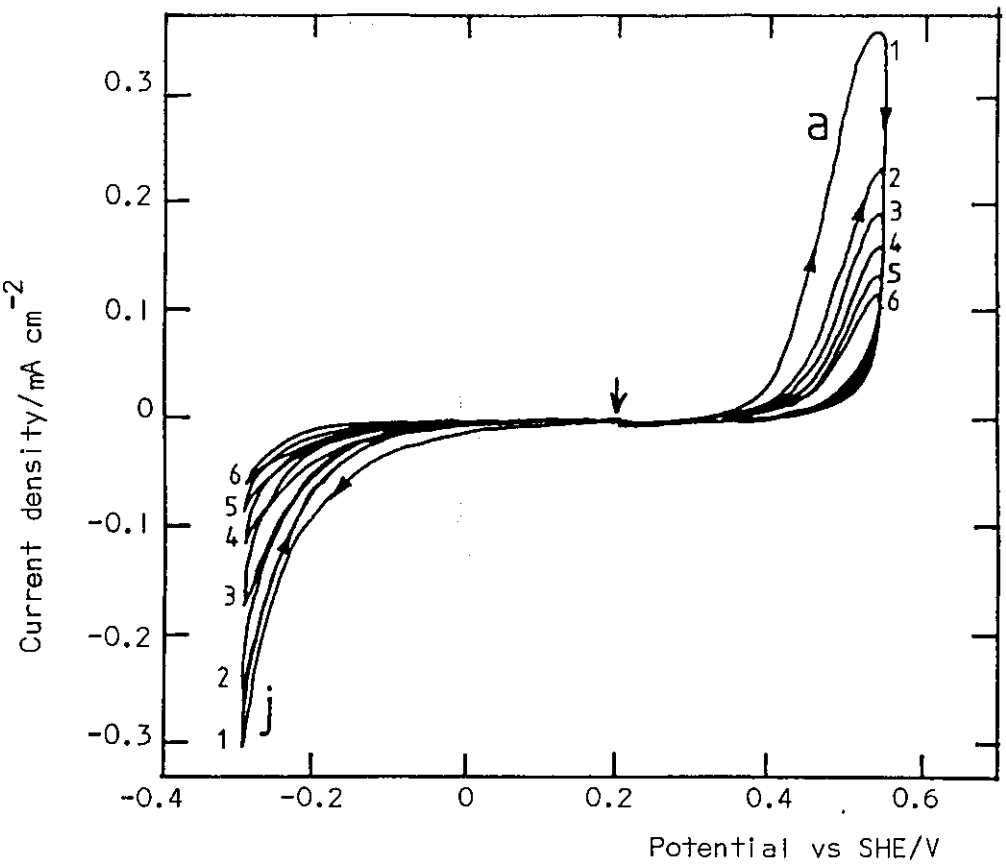

Figure 4.23. Six consecutive cyclic voltammograms of galena at pH 1 (0.1 M $HClO_4$), starting from the rest potential, first cycled anodically then cathodically at 20 mV s^{-1}

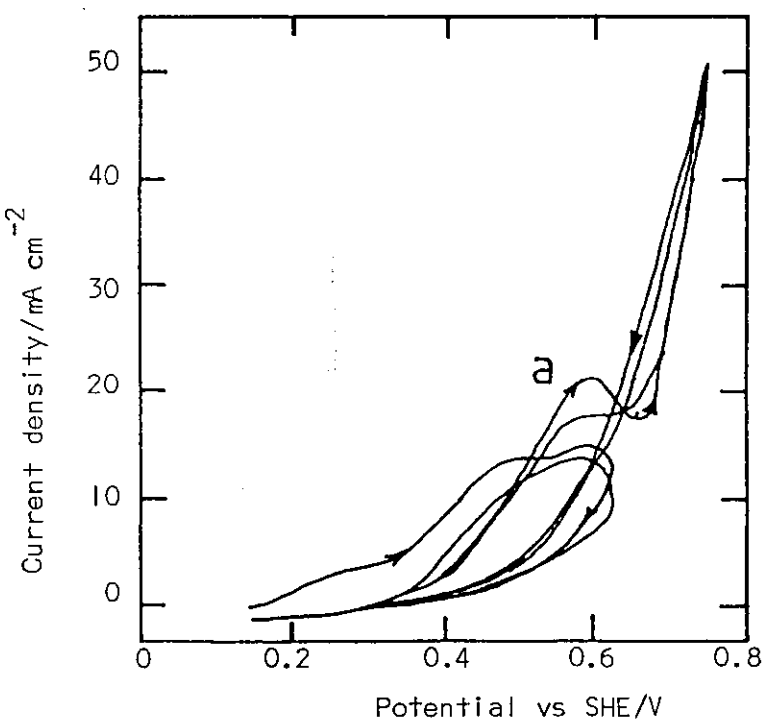

Figure 4.24. The effect of increasing the anodic potential limit on the anodic oxidation of galena with consecutive potential cycles starting from the rest potential

caused passivation as the current decreased on successive cycles. Following oxidation, when the same electrode was reduced on successive cathodic cycles down to -0.3 V, the current decreased as the amount of oxidation product decreased with each successive potential cycle.

The anodic oxidation wave in figure 4.23 to 4.27 started at a potential consistent with reaction a (see Appendix I), forming S^{o} on the surface. The current decreased with increasing anodic potential indicating passivation. The decrease in current appeared in both stirred and unstirred solutions (figure 4.26 and 4.27), hence passivation is unlikely to be associated with the accumulation of lead ions at the electrode surface, as suggested by Paul et al.[251,265] The formation of an insoluble $PbSO_4$ layer by reaction b is thermodynamically possible. However, the rate of this reaction is significant only at high overpotential[250] and $PbSO_4$ is formed only above 1.05 V.[232] Furthermore, the reduction of $PbSO_4$ on the return cathodic sweep would produce Pb with the release of SO_4^{2-} ions[250] and hence a much higher charge would be passed in the formation of $PbSO_4$ than in its reduction, which is not the case. Therefore sulphur would appear to be the surface oxidation product, formed by reaction a.

The more cathodic peak at $\sim$ - 0.2 V on the cathodic sweep was due to the reduction of the anodically formed sulphur by reaction j. Since the solution was stirred by bubbling nitrogen, Pb^{2+} ions were removed from the surface. However, at high sweep rates (figure 4.25) and in unstirred solutions (figure 4.27), a second cathodic peak appeared at more positive

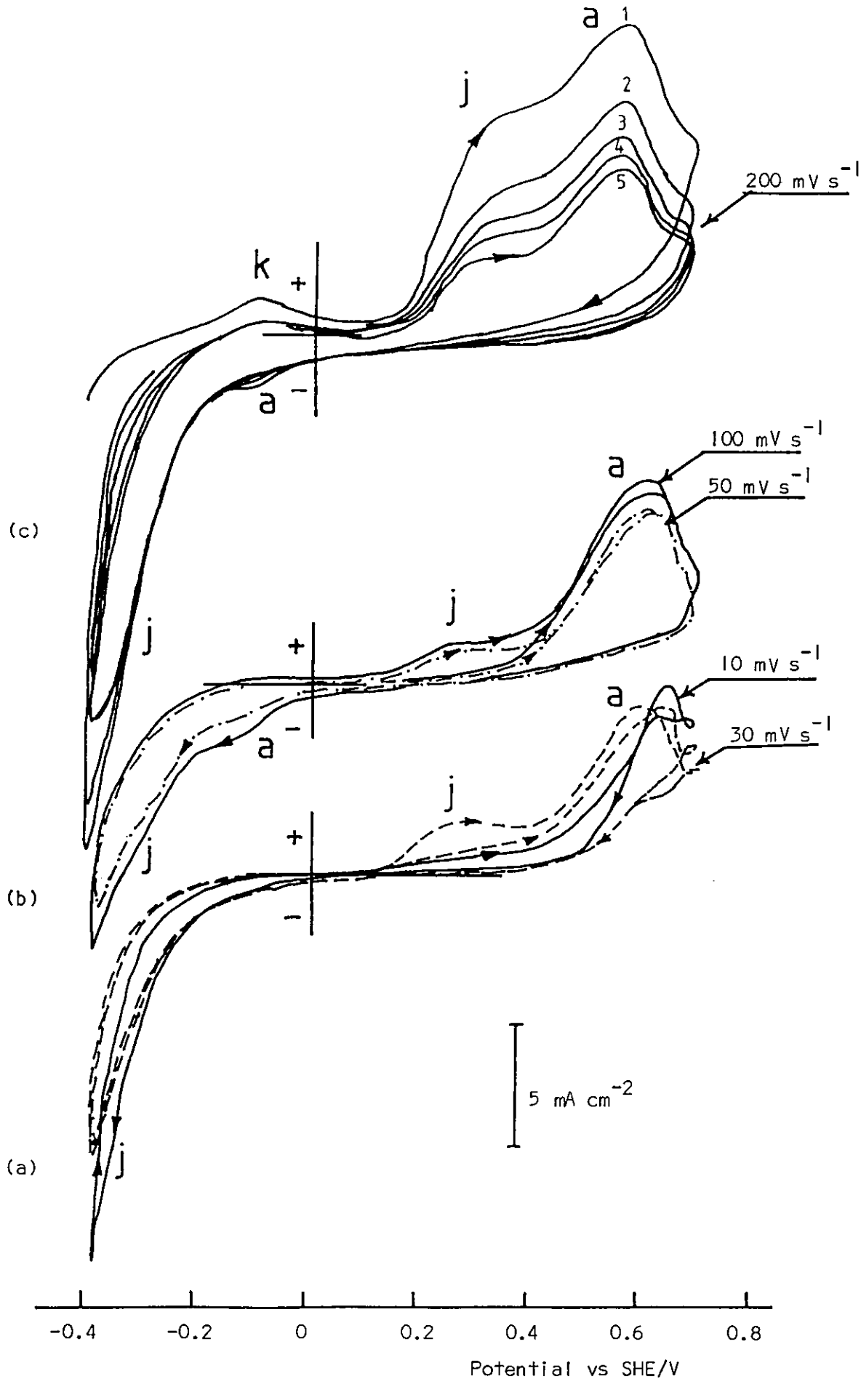

Figure 4.25. Cyclic voltammograms of galena at pH 1 (0.1 M $HClO_4$) at various scan rates

potentials ($\sim$ -0.05 V), indicating the involvement of a solution species formed during anodic oxidation. In unstirred solutions and at high sweep rates, lead ions would have been present at the electrode surface and so reacted with a portion of sulphur by reaction a.

At high scan rates, the decrease in the anodic sulphur formation peak current (figure 4.25 c) with the number of cycles was due to the incomplete reduction of sulphur during the cathodic scan, as the effect disappeared when the cathodic potential limit was extended (figure 4.28).

With further increase of the anodic potential limit (figure 4.24 - 4.28) above 0.65 V, the passivating effect of sulphur disappeared and the anodic current increased again. Also the current on the cathodic scan was higher than on anodic-going scan. The increase of the anodic current started at lower potentials at lower potential sweep rates (figure 4.25a), suggesting that a sulphur layer inhibited further oxidation and that the effect of this layer on the anodic process diminished with time and increasing potential.

It is thermodynamically possible for sulphur to be oxidised to SO_4^{2-} by reaction c, so activating the surface for further oxidation. However, if this was the case, the Pb^{2+} ions formed by reaction a should precipitate with SO_4^{2-} ions[291] forming $PbSO_4$, which would further passivate the surface due to its low solubility (0.040 $g.dm^{-3}$ at 18°C),[292] and would be reduced on the cathodic-going scan. Also, the amount of $PbSO_{4(s)}$ should have increased in unstirred solutions. This did not occur and the process was independent of stirring as

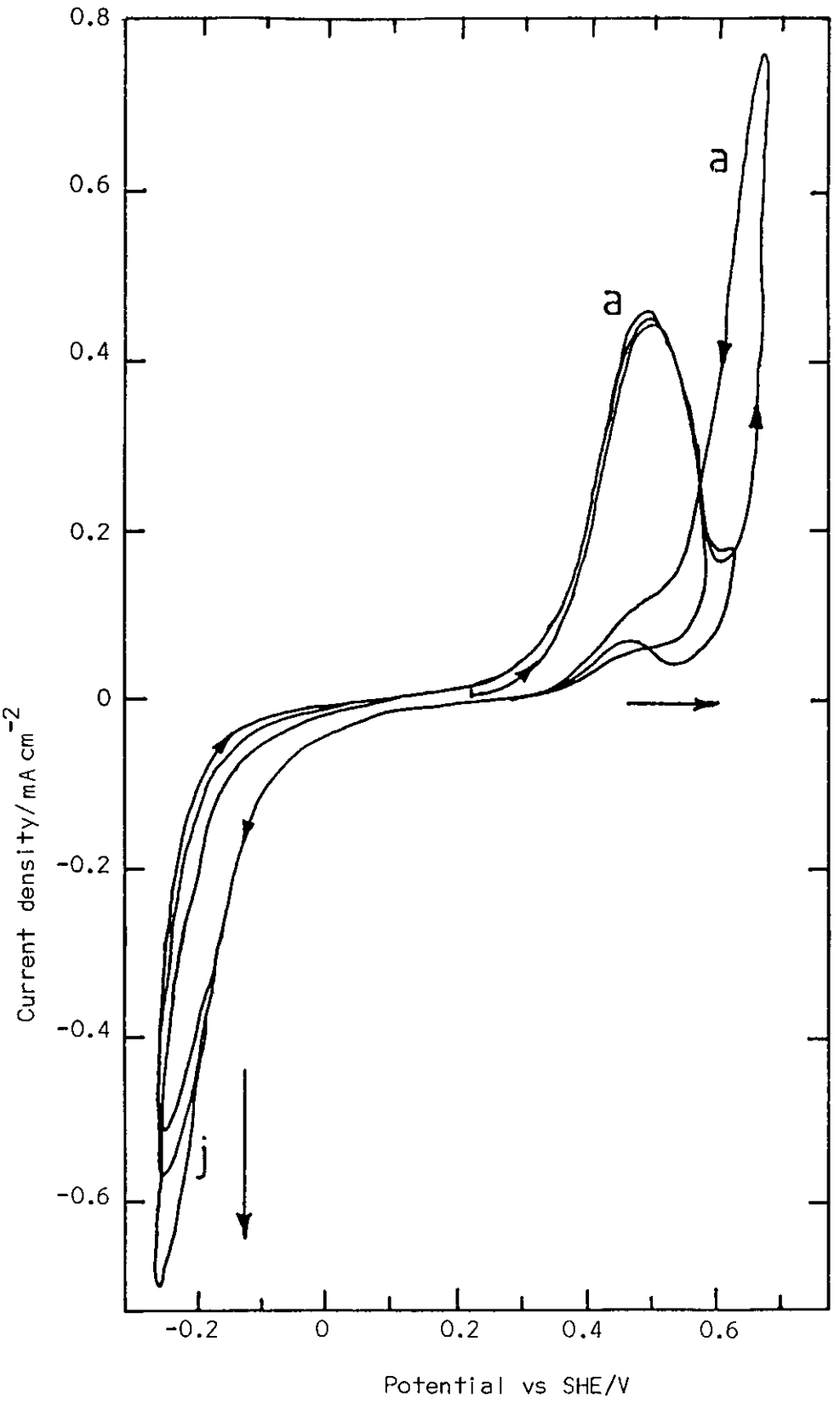

Figure 4.26. Cyclic voltammogram of a galena electrode at pH 1 (0.1 M $HClO_4$) and a scan rate of 0.1 V s^{-1}

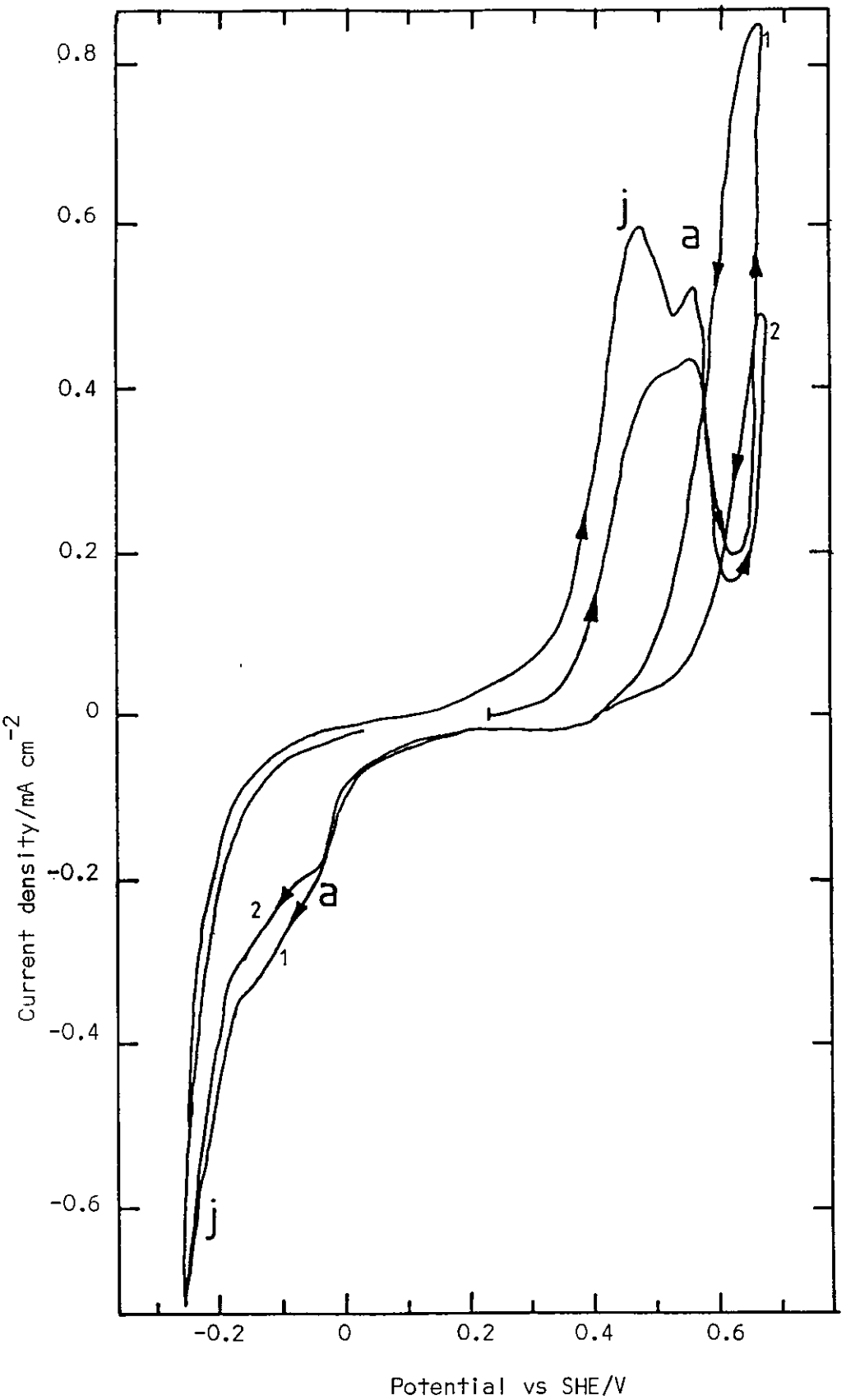

Figure 4.27. Cyclic voltammogram of a galena electrode at pH 1 (0.1 M $HClO_4$) in unstirred solution at a scan rate of 0.1 V S^{-1}

seen from figure 4.26 and 4.27.

Johnson et al[263] suggested that the first anodic process could be due to the oxidation of a substance formed at open circuit potential, while the second anodic process above $\sim$ 0.6 V was the formation of sulphur by reaction a. However, this seems to be unjustified, since the first anodic process at $\sim$ 0.4 V appeared even after several wide potential cycles as shown in figure 4.28.

A phase transition process has been suggested for the sulphur formed by the oxidation of chalcopyrite[264] and of galena.[250] It was proposed that the sulphur formed initially by reaction a could be in an amorphous or plastic form, and passivated the surface when it reached a critical thickness. The amorphous sulphur layer could be slowly converted into a crystalline form, which is sufficiently porous not to inhibit the further oxidation of galena.

This would explain the sweep rate dependence of the potential at which the anodic current started increasing again (figure 4.25). On rapid potential sweeps the initial formation of sulphur would be relatively fast and a passive layer of amorphous sulphur would be built up. On slow sweeps, however, sufficient time would elapse for the sulphur to crystallise and hence the current could start increasing at lower potentials. To clarify this potentiostatic I-t transients are needed. The rate of change in the physical form of sulphur apparently increased with increase in potential. A rapid increase was found[264] in current with potential for chalcopyrite which

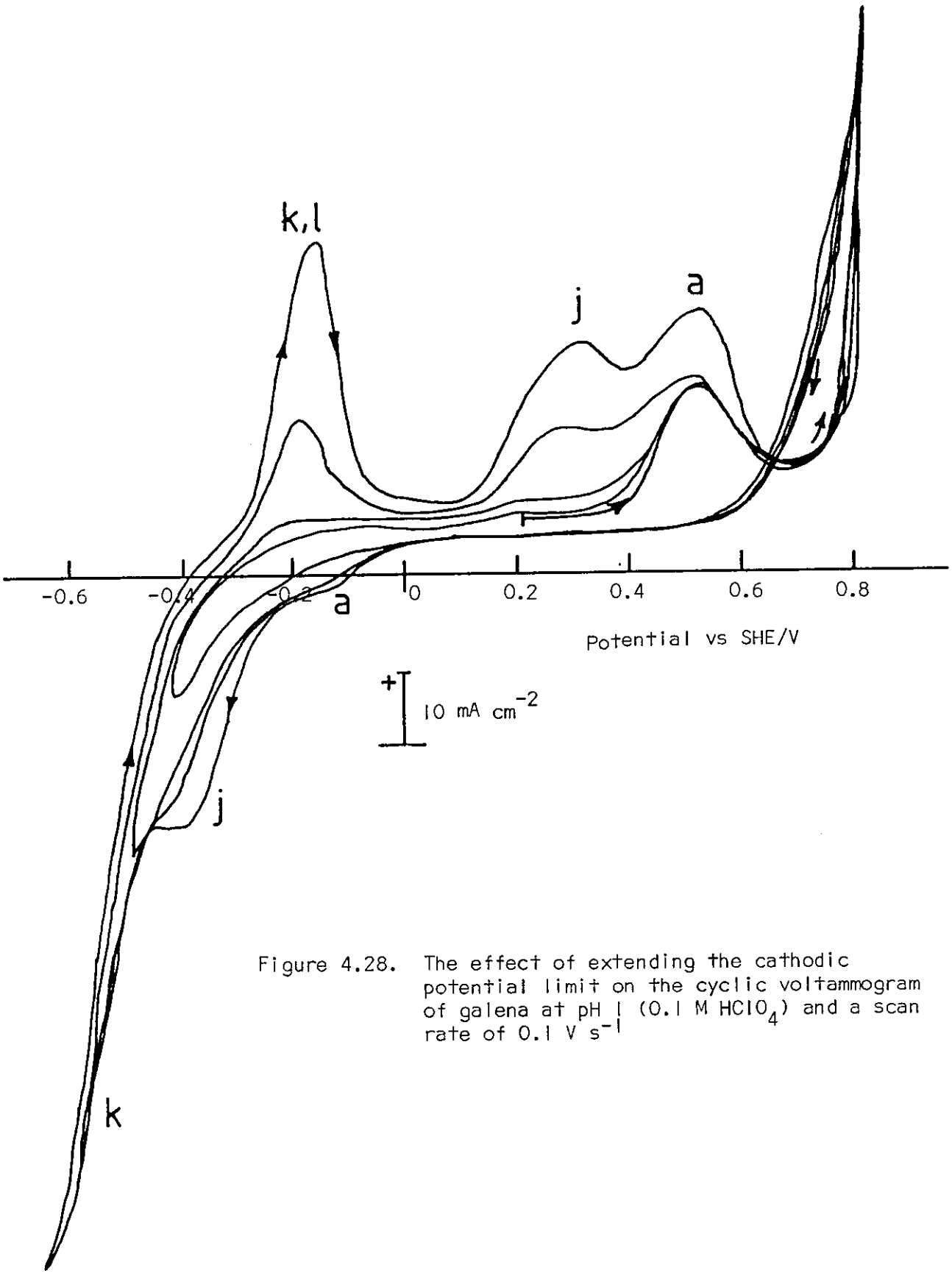

Figure 4.28. The effect of extending the cathodic potential limit on the cyclic voltammogram of galena at pH 1 (0.1 M $HClO_4$) and a scan rate of 0.1 V s^{-1}

was suggested to be due to the increase of the number of sulphur nucleation sites.

Another anodic peak appeared at $\sim$ 0.2 V on the second and subsequent anodic scans and grew with increasing sweep rate (figure 4.25), with decreased stirring (figure 4.27) and with extension of the cathodic potential limit (figure 4.28). This was due to the oxidation of H_2S by reaction j. The H_2S was formed by the reduction of sulphur on the succeeding cathodic going scan and remained in the vicinity of the electrode. The amount of H_2S oxidised would increase with increasing sweep rate and decrease in stirring, since there would be more H_2S at the surface.

The increase in the amount of H_2S oxidised when the cathodic potential limit was extended below $\sim$ -0.4 V (figure 4.28), was due to the formation of additional H_2S from the reductive PbS lattice decomposition by reaction k, which gave rise to a cathodic current below -0.4 V. With the extension of the cathodic potential limit below the reversible potential of reaction k, the anodic peak at $\sim$ -0.2 V appeared on the anodic-going scan and its current increased with further extension of the cathodic potential limit. This anodic process was due to the reverse of reaction k forming PbS. If there was H_2S deficiency at the electrode surface due to stirring, then some of the Pb formed by reaction k dissolved as Pb^{2+} by reaction l at the same potential region. The Pb formed by PbS reduction was completely removed from the surface by the reverse of reaction k and l, so it had no effect on the oxidation processes of galena, as shown in figure 4.28.

pH 1.68 0.05 $MKH_3(C_2O_4)_2.2H_2O$

Anodic oxidation of galena at this pH also produced sulphur by reaction a, resulting in the anodic current above 0.3 V as shown in figure 4.29. Sulphur was reduced by reaction j on the cathodic scan at about $\sim$ -0.18 V. However, when the anodic and cathodic limits were extended, as shown in figure 4.30, the anodic and cathodic currents grew and the potential of the cathodic process shifted to more cathodic potentials. A second cathodic peak below $\sim$ -0.475 V and a second anodic peak at -0.27 V, appeared. All the peaks grew with the number of potential cycles.

At pH 0, Paul et al[265] observed that during the anodic oxidation of galena, the potential of the sulphur reduction peak shifted to more cathodic potentials with increasing anodic potential limits. They explained this by postulating the anodic formation of increased amounts of sulphur which became more difficult to reduce, i.e. the reduction of bulk sulphur is self-inhibiting due to its poor conductivity.[266] It was proposed that the sulphur in the immediate vicinity of the galena was easily reducible or active whereas bulk sulphur was passive.

The shift in the potential of the sulphur reduction peak can be explained by a similar mechanism, since more sulphur will be formed with increasing anodic potential, and become more difficult to reduce, shifting the reduction process to more cathodic potentials. The more cathodic process was the reduction of PbS by reaction k (figure 4.30).

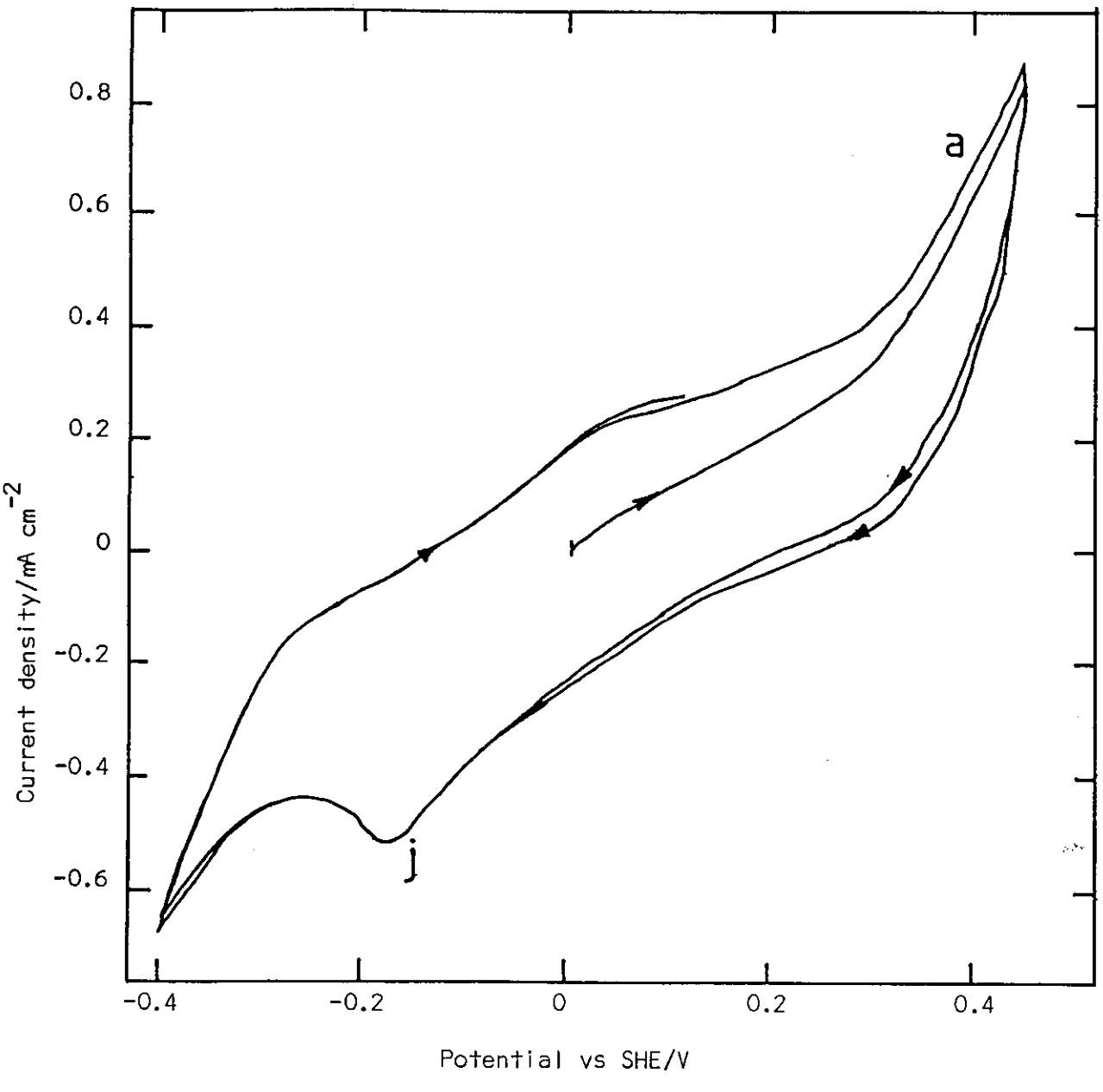

Figure 4.29. Cyclic voltammogram of galena at pH 1.68, 0.05 M$KH_3(C_2O_4)_2.2H_2O$, scan rate 20 mV s^{-1}

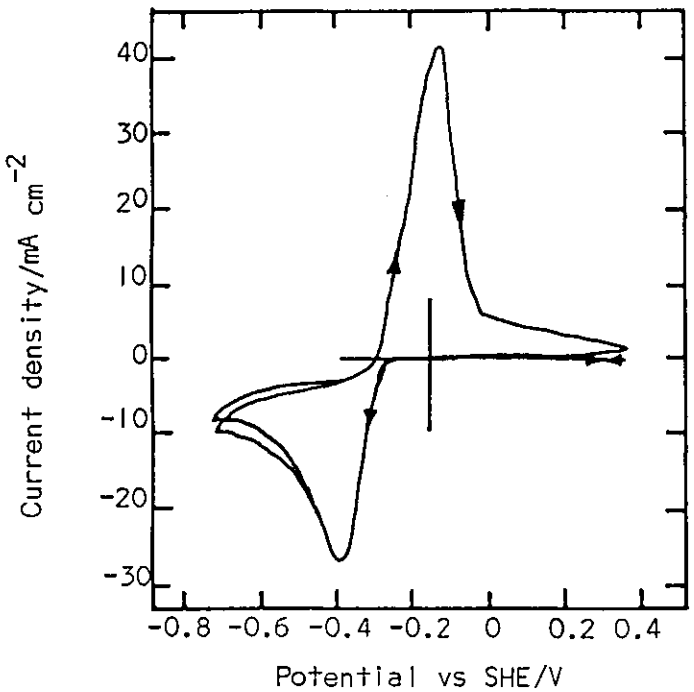

Figure 4.31. Cyclic voltammogram of a lead electrode at pH 1.68 [0.05 M $KH_3(C_2O_4).2H_2O$] , and a scan rate of 20 mV s^{-1}

Figure 4.30. Cyclic voltammogram of a galena electrode when the anodic and cathodic potential limits were extended at pH 1.68 [0.05 M $KH_3(C_2O_4).2H_2O$] and a scan rate of 20 mV s^{-1}

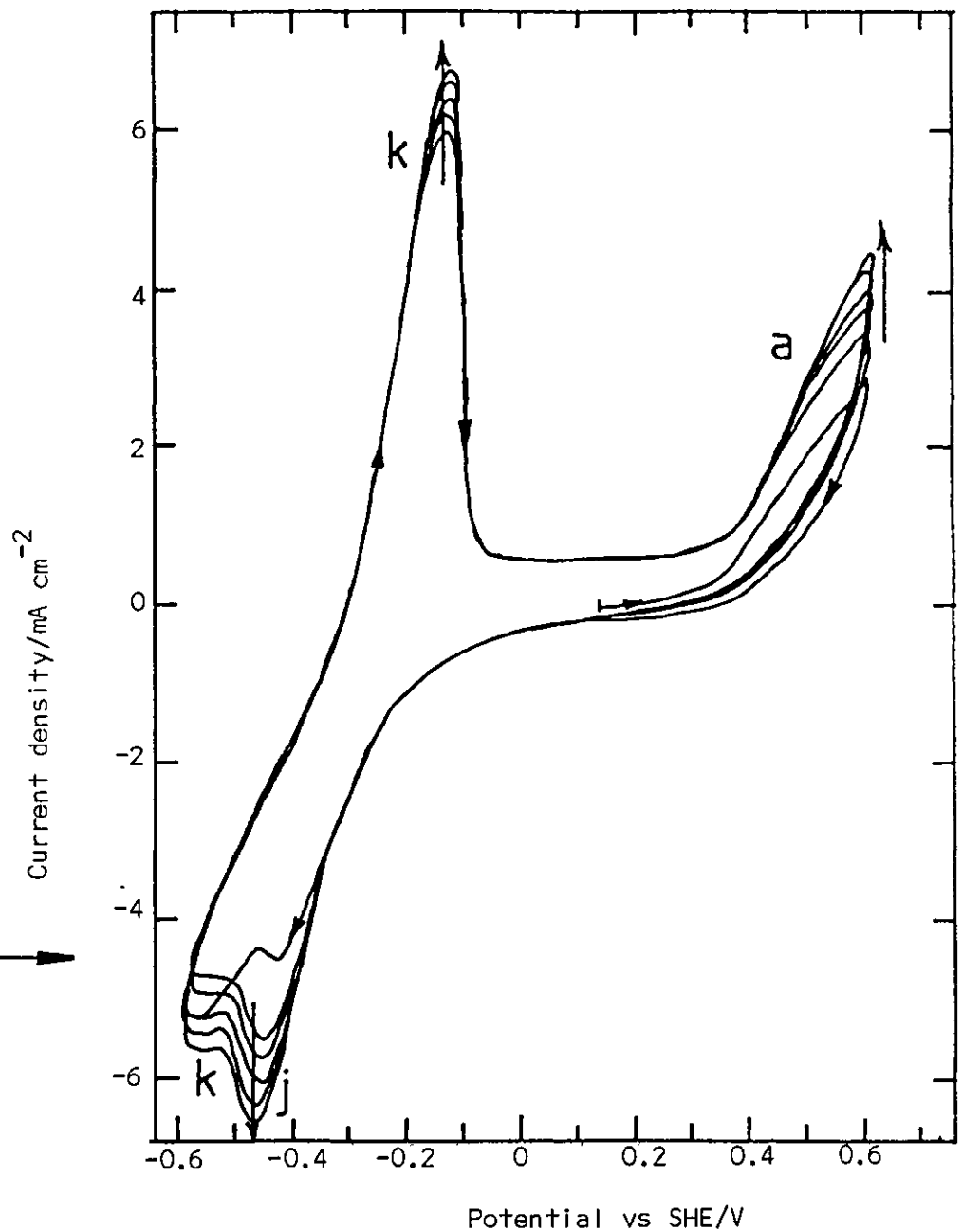

The voltammogram of a lead electrode at this pH is given in figure 4.31, which shows the anodic formation of a species that passivates the surface, the oxidation product being reduced on the following cathodic scan. The same species seemed to form by oxidation at open circuit, since on the first anodic scan starting from the rest potential, there was no anodic current. The electrode was passivated but a cathodic peak appeared on the subsequent cathodic scan and the peak current did not change on the second scan.

The Eh-pH diagram of Pb-H_2O system in figure 2.5 shows that it is thermodynamically possible for Pb to dissolve as Pb^{2+} at the potential of the anodic process on the lead electrode, and the formation of PbO or $Pb(OH)_2$ is not possible. Therefore it seems that the anodic process on the lead electrode was due to the formation of lead oxalate, PbC_2O_4, which passivated the electrode due to its low solubility (0.0015 g/litre).[283]

The same passivation process was not observed on a galena electrode following the reduction of PbS to Pb + H_2S by reaction k (figure 4.30). Therefore the anodic process at -0.27 V on the galena electrode can be assigned to the reverse of reaction k, which at pH 1.68 has a reversible potential of -0.29 V in reasonable agreement with the potential of the peak current.

pH 4 (0.05 M $KHC_8O_4H_4$)

At pH 4 the oxidation/reduction mechanism of the galena electrode is similar to that at pH 1 and 1.68. When the electrode was anodically oxidised, S^o was formed on the surface by reaction a and reduced on the subsequent cathodic scan (figure 4.32) at -0.4 V by reaction j. When the cathodic potential limit was extended below -0.45 V, PbS was reduced to Pb + H_2S by reaction k and on the subsequent anodic scan Pb was oxidised in the presence of H_2S to form PbS at $\sim$ -0.15 V, or when there was H_2S deficiency due to stirring, Pb dissolved as Pb^{2+} by reaction l.

pH 6.89 (0.025 M KH_2PO_4 + 0.025 M Na_2HPO_4)

The anodic dissolution of galena in neutral and alkaline solutions is considerably more involved than in acid, since lead hydroxy complexes ($PbOH^+$, $HPbO_2^-$, $Pb(OH)_2$, $Pb_3(OH)_4^{2+}$, $Pb_4(OH)_4^{4+}$, $Pb_6(OH)_8^{4+}$), oxidises (PbO, PbO_2, Pb_2O_3, P_3O_4), mixed compounds ($PbSO_4$. PbO, $PbSO_4$.2PbO, $PbSO_4$.3PbO) and many other lead-sulphur-oxygen compounds (PbS_2O_3, PbS_2O_6, PbS_3O_6, $PbSO_4$ and others) may form.(265)

Thermodynamic relationships of the type below (reaction d and e in Appendix 1) indicate that oxidation of galena at pH 6.89 can occur by(250)

$$PbS + H_2O \rightleftharpoons PbO + S + 2H^+ + 2e \qquad (d)$$

$$Eh = 0.732 - 0.059\ pH$$

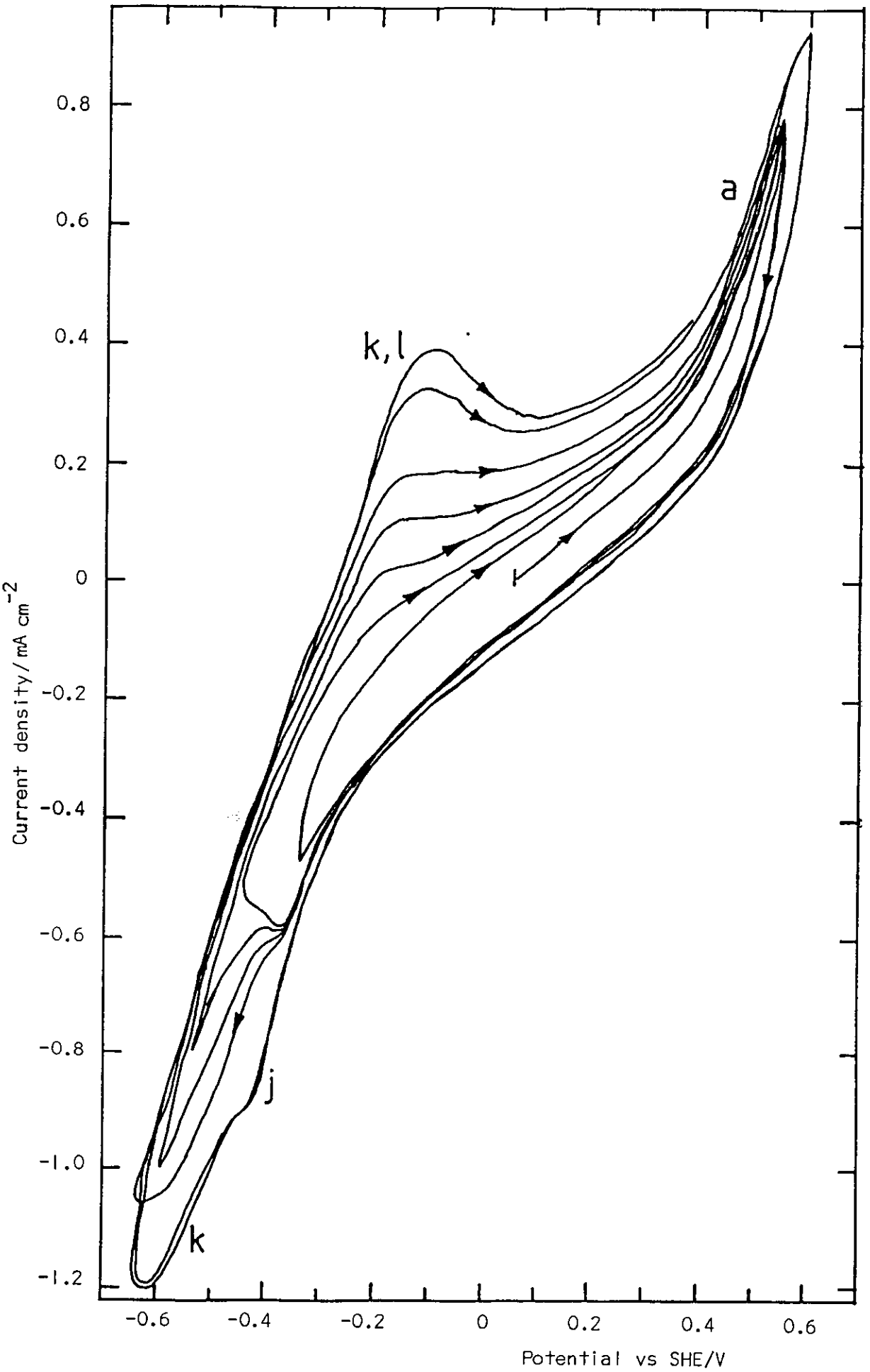

Figure 4.32. Cyclic voltammograms of galena at pH 4 (0.05 M $KHC_8O_4H_4$) and a scan rate of 20 mV s^{-1}

or by[267]

$$PbS + 2H_2O \rightleftharpoons Pb(OH)_2 + S + 2H^+ + 2e \qquad (e)$$

$$Eh = 0.765 - 0.059\ pH$$

The reversible potential of these reactions at pH 6.89 are 0.326 and 0.359 V respectively, both of which are in the potential region of the anodic reaction in figure 4.33. As shown in figure 4.33a, all the peaks grew with the number of potential cycles. This was probably due to a degree of oxidation of the electrode before cycling started, as the same passivation was not observed when cycling restarted from the rest potential in the anodic direction (figure 4.33b) after four consecutive cycles (figure 4.33a).

The cathodic peak at -0.5 V on the cathodic scan was due to the reverse of the anodic process e. Galena was reduced to Pb + H_2S by reaction k when the cathodic potential was extended below $\sim$ -0.7 V and a second anodic peak at -0.3 V appeared on the subsequent anodic going scan (figure 4.33).

The voltammogram of lead in the same electrolyte is shown in figure 4.34, in which there are two anodic peaks at -0.5 V and 0.0 V and a cathodic peak at -0.8 V. The more negative anodic reaction on the lead electrode occurred at about the same potential as anodic reaction I on galena. The Pourbaix diagram for the Pb-H_2O system (figure 2.4) indicates that lead can oxidise to Pb^{2+} at this pH by reaction I which, taking the Pb^{2+} activity as 10^{-6}, has a reversible potential

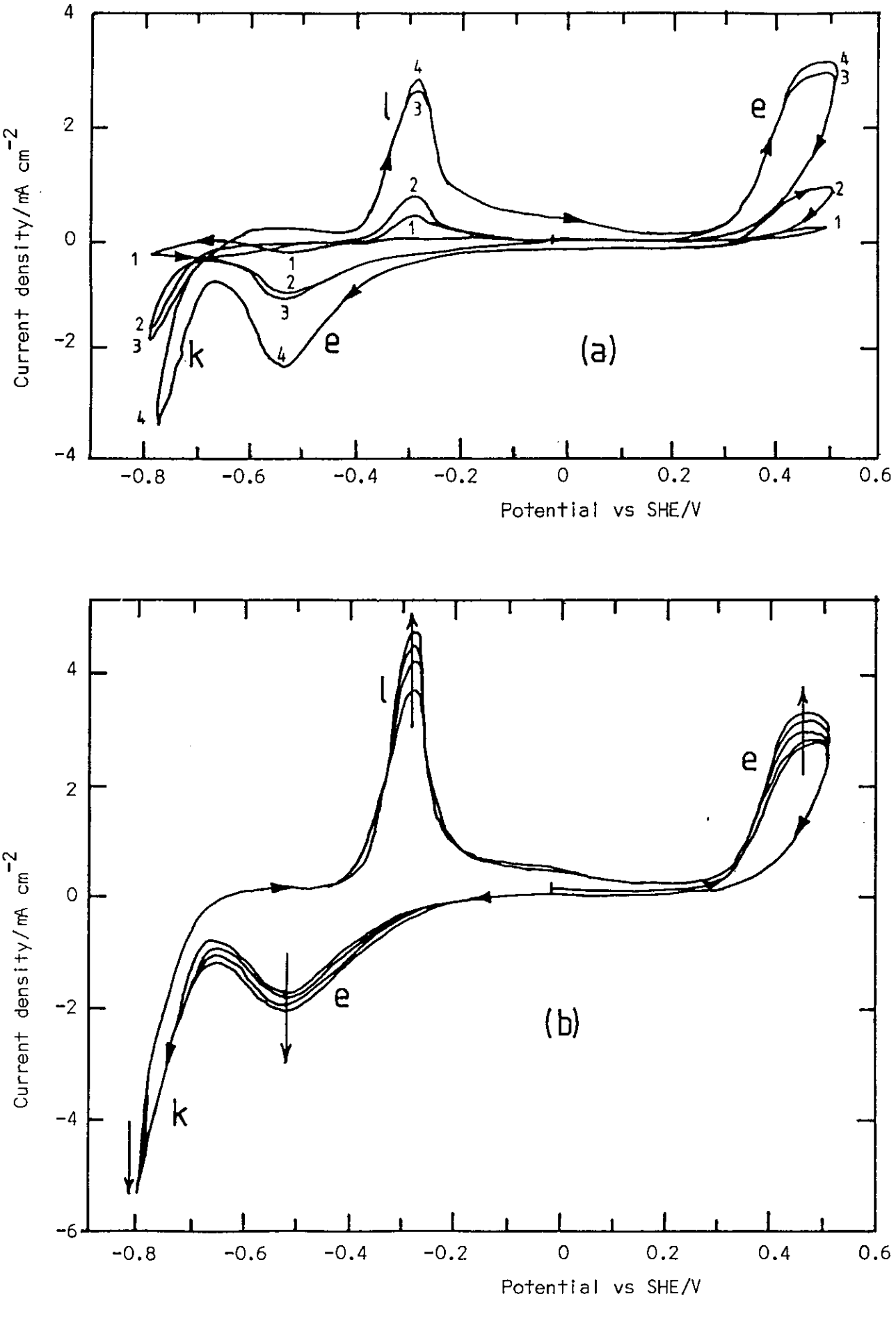

Figure 4.33. Cyclic voltammograms of galena at pH 6.89 (0.025 M KH_2PO_4 + 0.025 M Na_2HPO_4) and a scan rate of 0.1 V s^{-1}. a - the first 4 cycles; b - the cycling started into anodic direction following the first four cycles in a

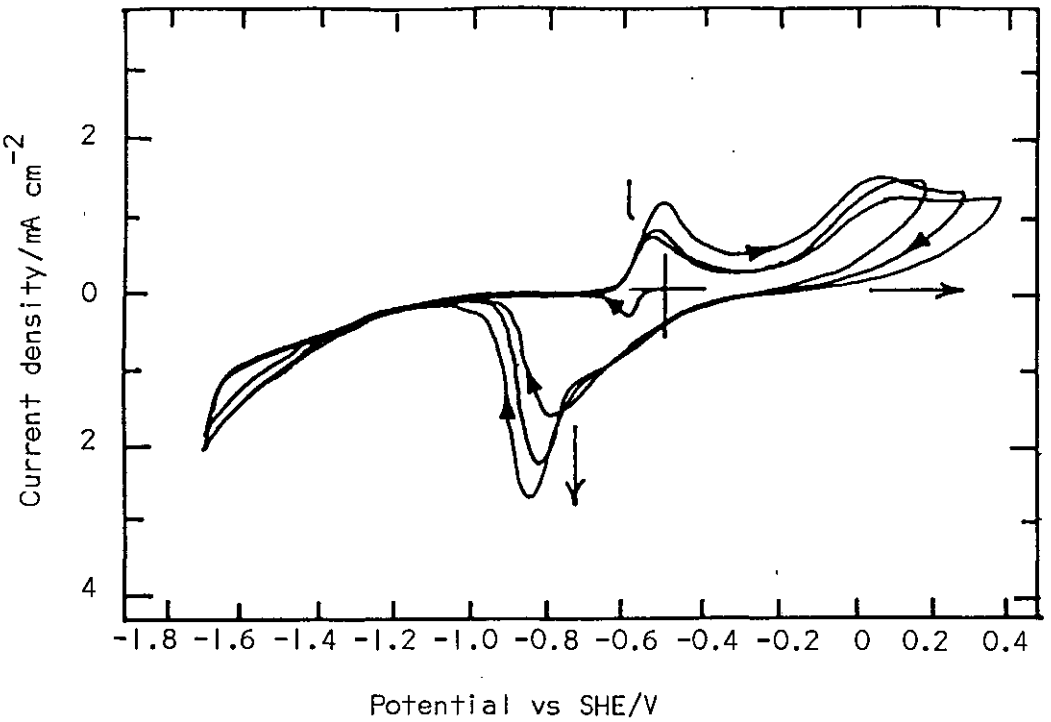

Figure 4.34. Cyclic voltammogram of lead at pH 6.89 (0.025 M KH_2PO_4 + 0.025M Na_2HPO_4) and a sweep rate of 50 mV s^{-1}

of -0.303 V corresponding to the potential of the less positive anodic peaks on galena. This would also explain why the anodic process had no effect on the anodic oxidation of PbS (figure 3.33).

It is possible that a surface oxidation product, i.e. $PbHPO_4$, formed on the lead electrode surface at open circuit and was reduced on the first cathodic sweep (figure 4.34). The formation of this $PbHPO_4$ has been confirmed by Awad and Elhady,[294] who studied the behaviour of lead in different concentrations of phosphate solutions. They found that the presence of phosphate ions modified the electrode behaviour so that the slope of the potential - pH relation was only half of an oxide or hydrogen electrode. They explained this with the formation of $PbHPO_4$ by

$$PbHPO_4 + 2e \rightleftharpoons Pb + HPO_4^{2-} \qquad (4.2)$$

$$Eh = -0.461 - 0.0295 \log HPO_4^{2-}$$

driven by H_2 evolution. The presence of this $PbHPO_4$, which is only slightly soluble in water[291] ($K = 8.7 \times 10^{-12}$) would explain the oleophobicity of lead at pH 6.89 (figure 4.21) since as soon as the circuit was opened to measure the contact angle, a $PbHPO_4$ surface phase was formed. Therefore the more positive peak and cathodic peak (figure 4.34) may be due to reaction (4.2).

pH 9.2 (0.05 M $Na_2B_4O_7$)

As shown in figure 4.35, at pH 9.2 the voltammogram of galena showed only one cathodic peak at -0.6 V, following an anodic sweep to 0.2 V, starting from the rest potential. On the second anodic sweep a second anodic peak appeared at $\sim$ -0.1 V. However, when the anodic potential limit was increased (figure 4.36), a second cathodic peak appeared at -0.3 V.

The oxidation of galena can take place by reaction e, producing $Pb(OH)_2$ + S, the reversible potential of which is 0.222 V at pH 9.2. The cathodic peak at -0.3 V could then be due to the reverse of reaction e.

If the initial oxidation of PbS occurred by the same reactions at all pH values, forming a soluble metal species and sulphur by reaction a, as suggested by Richardson and Maust,[267] then the cathodic peak at -0.6 V could be due to

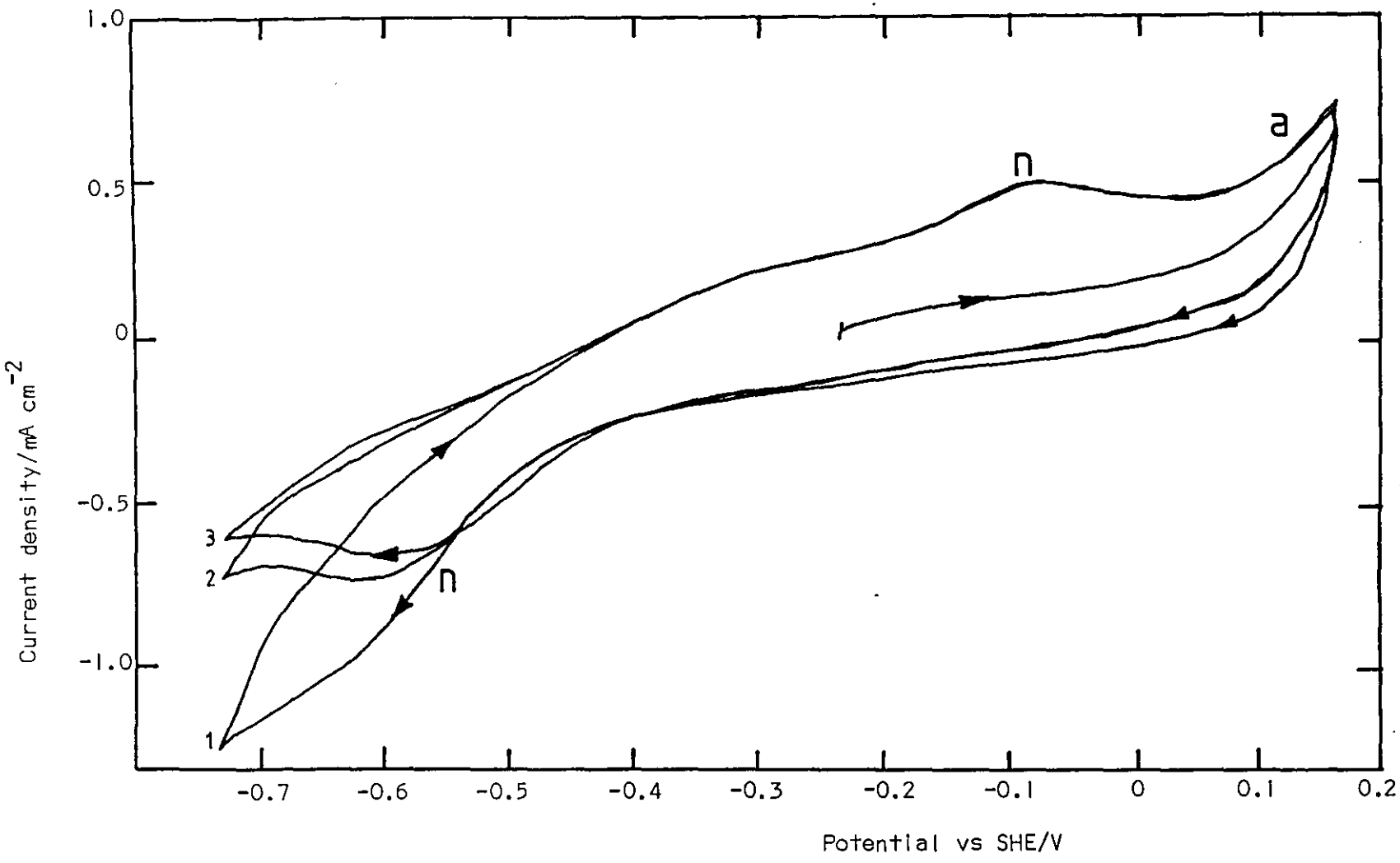

Figure 4.35. Cyclic voltammograms of galena at pH 9.2 (0.05 M $Na_2B_4O_7$) and a scan rate of 0.1 V s^{-1}

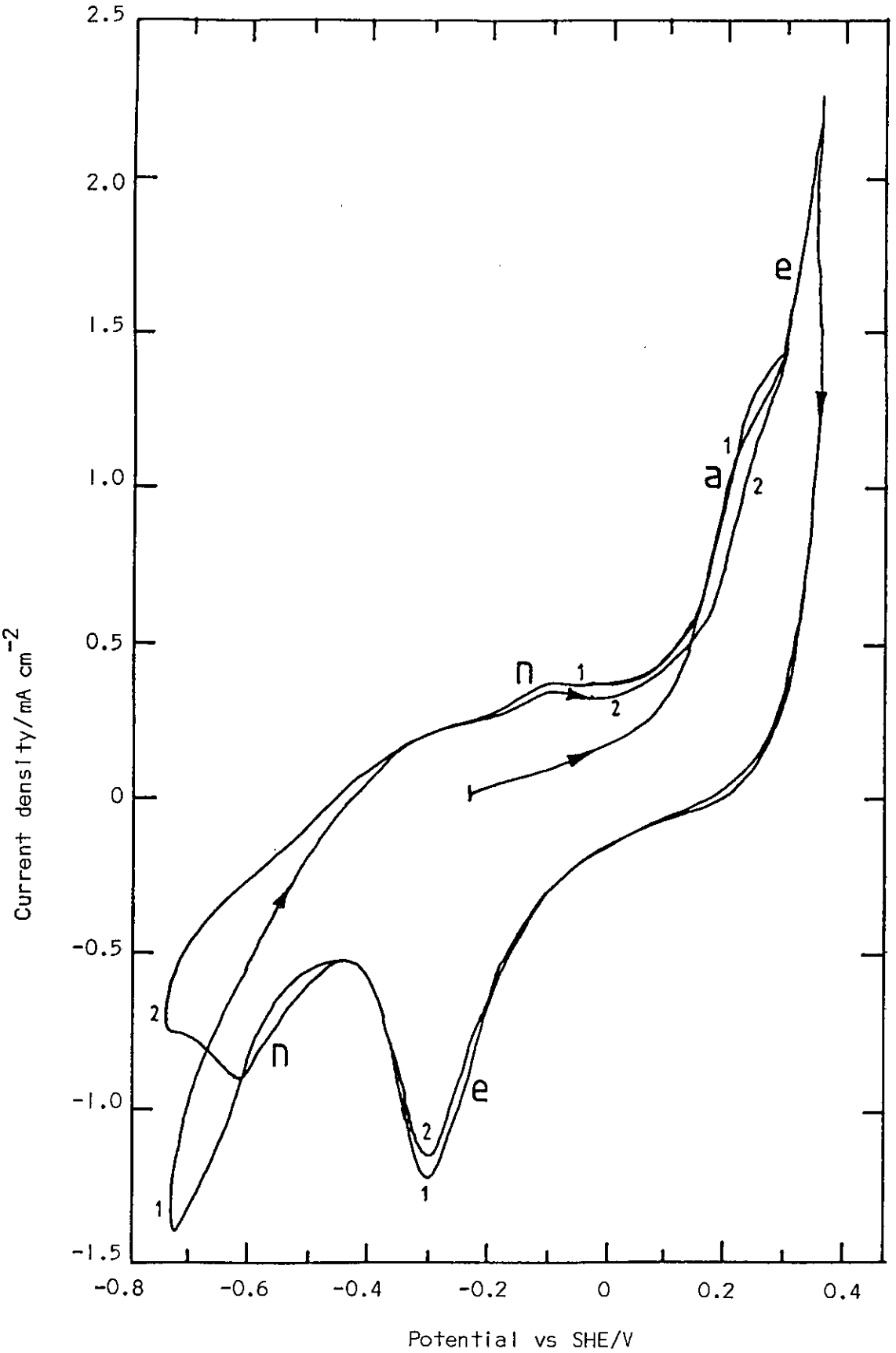

Figure 4.36. Cyclic voltammograms of galena when the anodic potential limit was extended to 0.35 V at pH 9.2 (0.05 M $Na_2B_4O_7$) and a scan rate of 0.1 V s^{-1}

the reduction of excess sulphur by reaction n:

$$S + H^+ + 2e \rightleftharpoons HS^- \qquad (n)$$

$$Eh = 0.065 - 0.0295\ pH - 0.0295\ \log\left[HS^-\right]$$

Assuming an HS^- activity of 10^{-6}, the reversible potential of reaction n is -0.513 V, which corresponds to the potential of the more negative cathodic peak n. The anodic peak at $\sim$ -0.1 V which appeared on the second and subsequent anodic scans could then be due to the oxidation of HS^- by reaction n.

A wave appeared at 0.15 V on the first anodic sweep starting from the rest potential and became smaller with the number of potential cycles (figure 4.36). This wave can be assigned to reaction a, forming excess sulphur while at higher anodic potentials (> 0.3 V), $Pb(OH)_2$ and S^o were formed by reaction e.

pH 11 (0.025 M $NaHCO_3$ + 0.023 M NaOH)

Figure 4.37a shows only one cathodic and one anodic process in the voltammogram of galena at pH 11. However, when the cathodic potential limit was extended below -0.6 V a second anodic peak appeared at -0.5 V on the anodic scan, and both the second anodic peak and cathodic peak at -0.4 V grew with extension of the cathodic potential limit (figure 4.37b).

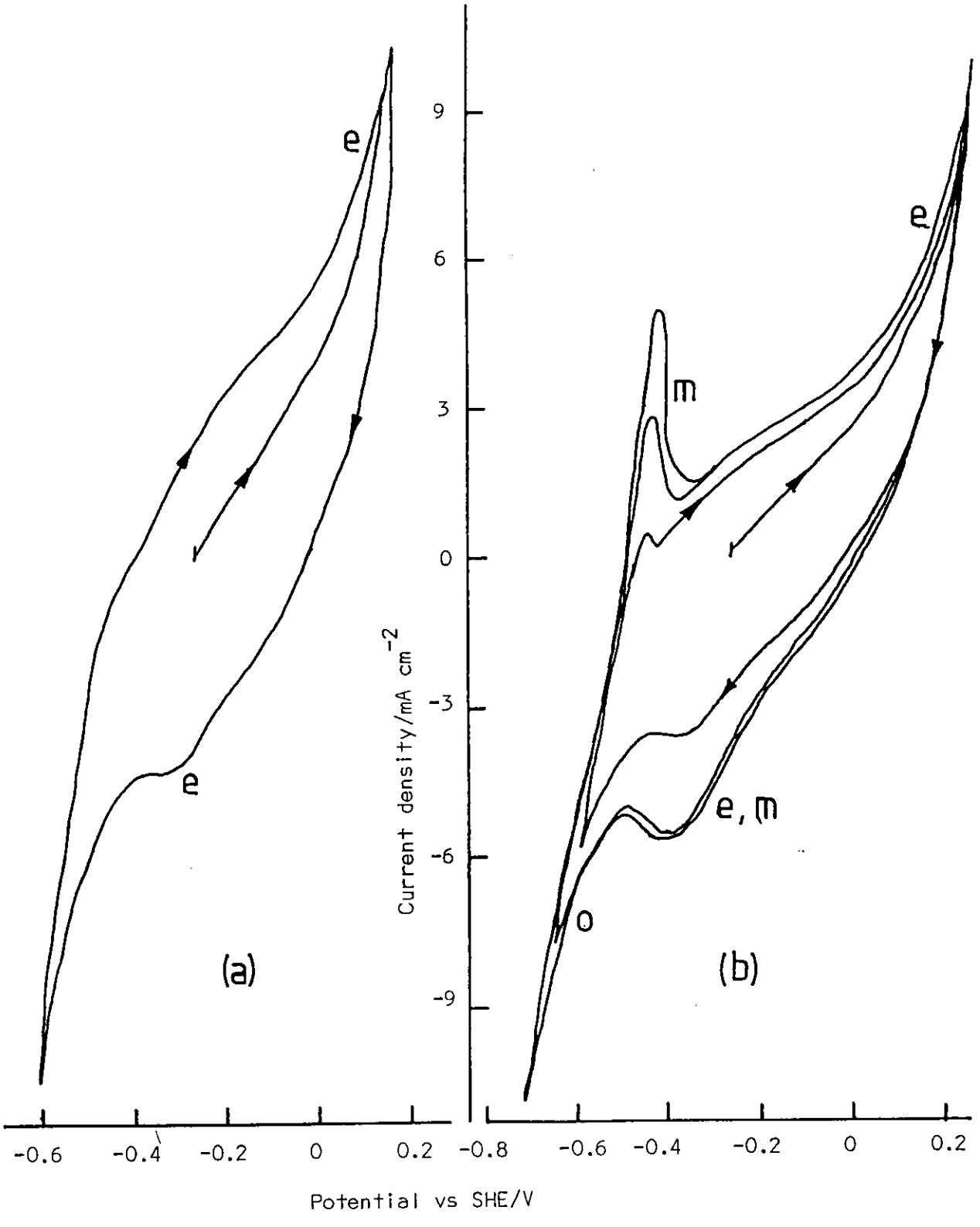

Figure 4.37. Cyclic voltammograms of galena at pH 11 (0.025 M $NaHCO_3$ + 0.023 M NaOH) and a scan rate of 0.1 V s^{-1}. a - potential limit (-0.6 V) - (0.15 V); b - potential limit (-0.7 V) - (0.2 V)

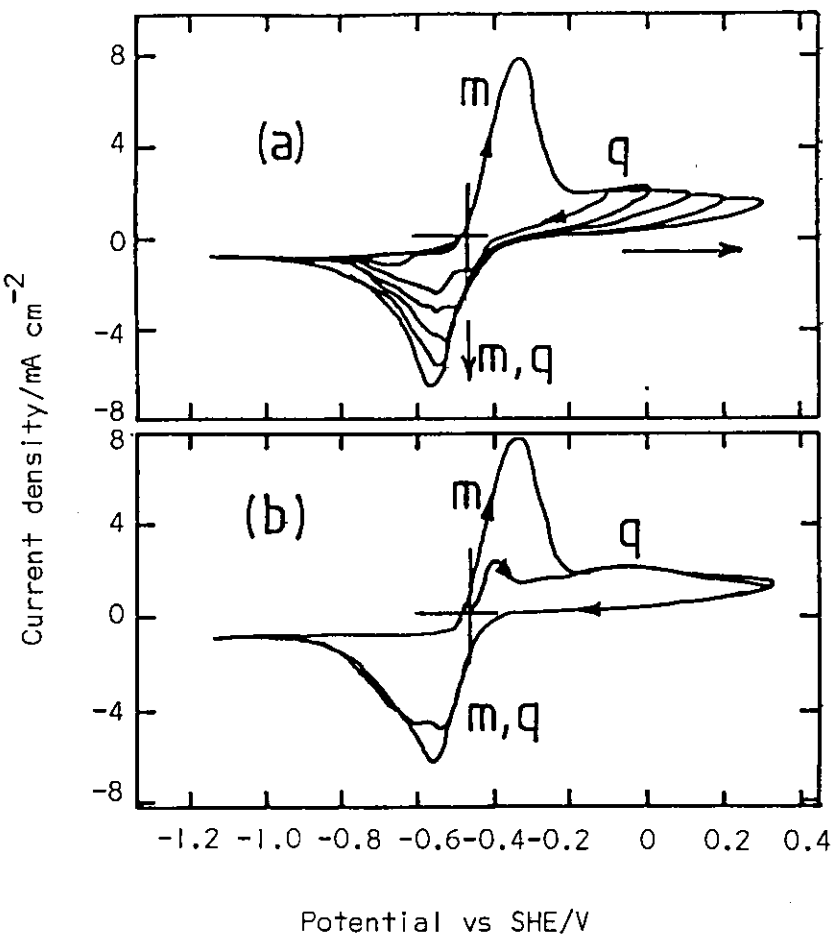

Figure 4.38. Cyclic voltammograms of lead at pH 11 (0.025 M $NaHCO_3$ + 0.023 M NaOH) and a scan rate of 0.1 V^3s^{-1}. a - first scan into cathodic direction; b - first scan into anodic direction

The anodic process at -0.5 V in the galena voltammogram (figure 4.37b) was the oxidation by reaction m of Pb formed at potentials below -0.6 V by reaction o:

$$PbS + H^+ + 2e \rightleftharpoons HS^- + Pb \qquad (o)$$

$$Eh = -0.575 - 0.0295\ pH - 0.0295\ \log\left[HS^-\right]$$

Galena oxidised by reaction e forming $Pb(OH)_2$ + S which was reduced at $\sim$ -0.4, together with PbO formed by the

oxidation of Pb by reaction m. Hence the cathodic peak grew with the extension of the cathodic potential limit, since more Pb was formed by the reduction of PbS.

The voltammogram of a lead electrode at this pH showed an anodic and a cathodic process in the same potential region (figure 4.38). Pb can oxidise to $Pb(OH)_2$ by reaction q, the reversible potential of which is -0.372 V which corresponds to the potential of the anodic peak on the voltammogram of lead electrode. Therefore, the cathodic process in figure 4.38 was due to the reduction of $Pb(OH)_2$ to Pb by reaction q.

4.5.4.2 Cyclic voltammetry of pyrite

Anodic and cathodic reactions of pyrite at pH 1 (0.1 M HCl)

As shown in figure 4.39, on anodic potential sweeps starting from the rest potential an anodic current appeared at potentials > 0.3 V. The reduction of the anodic oxidation products on the subsequent cathodic sweep gave rise to two cathodic peaks at $\sim$ -0.1 V and $\sim$ -0.2 V. With increase of scan rate a broad second anodic peak and a third cathodic peak at 0.35 V appeared.

According to the Eh-pH diagram of the Fe-S-H_2O system (figure 2.7) pyrite can oxidise by reaction a' or b' (see Appendix II):

$$FeS_2 \rightleftharpoons Fe^{2+} + 2S^o + 2e \qquad (a')$$

$$Eh = 0.423 + 0.0295 \log \left[Fe^{2+}\right]$$

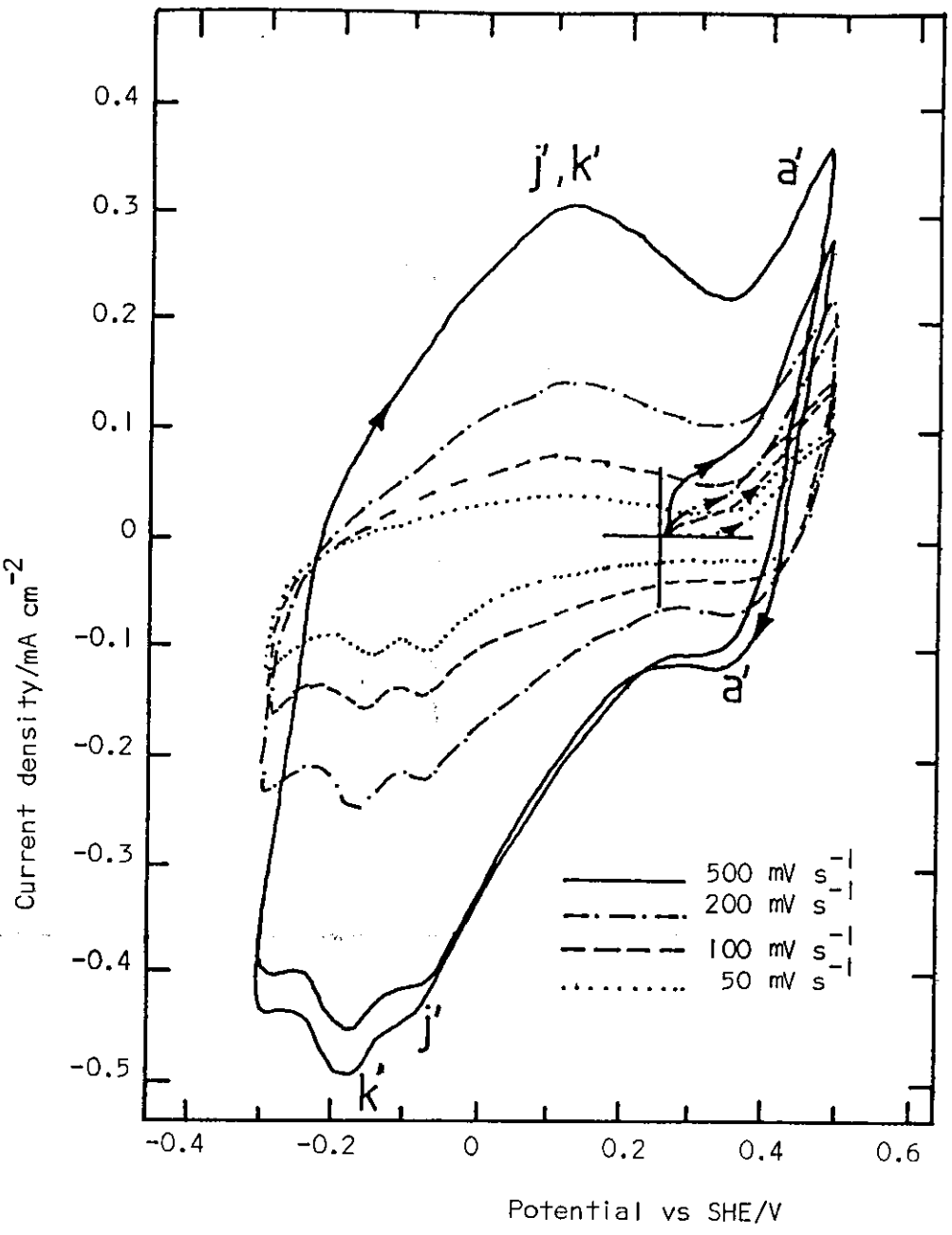

Figure 4.39. Cyclic voltammograms of a pyrite electrode as a function of potential scan rate

and

$$FeS_2 + 8H_2O \rightleftharpoons Fe^{2+} + 2SO_4^{2-} + 16H^+ + 14e \qquad (b')$$

$$Eh = 0.367 - 0.067\ pH + 0.008\ \log\left[SO_4^{2-}\right] + 0.004\ \log\left[Fe^{2+}\right]$$

The rate of reaction b' became appreciable only above 0.6 V[213] so that the anodic oxidation current above 0.3 V was due to reaction a'. The only oxidation product formed on the surface of pyrite was S^o since Fe^{2+} ions would have been removed by stirring due to bubbling nitrogen.

The cathodic peak at $\sim$ -0.1 V can be assigned to the reduction of sulphur formed by reaction a'. In acid solutions the reduction of sulphur produced H_2S by reaction j', the reversible potential of which is 0.229 V at pH 1. The more negative cathodic peak at $\sim$ -0.2 V arose from the reduction of the FeS_2 lattice by reaction k'.

With increase of scan rate, both anodic and cathodic currents increased. The currents for the cathodic peaks at $\sim$ -0.1 and $\sim$ -0.2 V have been plotted as a function of scan rate N in figure 4.40. The Ip vs N plots for both peaks are approximately linear indicating that surface transformations were involved[253] rather than diffusion controlled processes, which would have a Ip vs $N^{\frac{1}{2}}$ linear dependency.[249]

When the scan was reversed at -0.3 V, the H_2S formed by reaction j' and k' was oxidised by the reverse of the same reactions, forming S^o and FeS_2 respectively. These gave

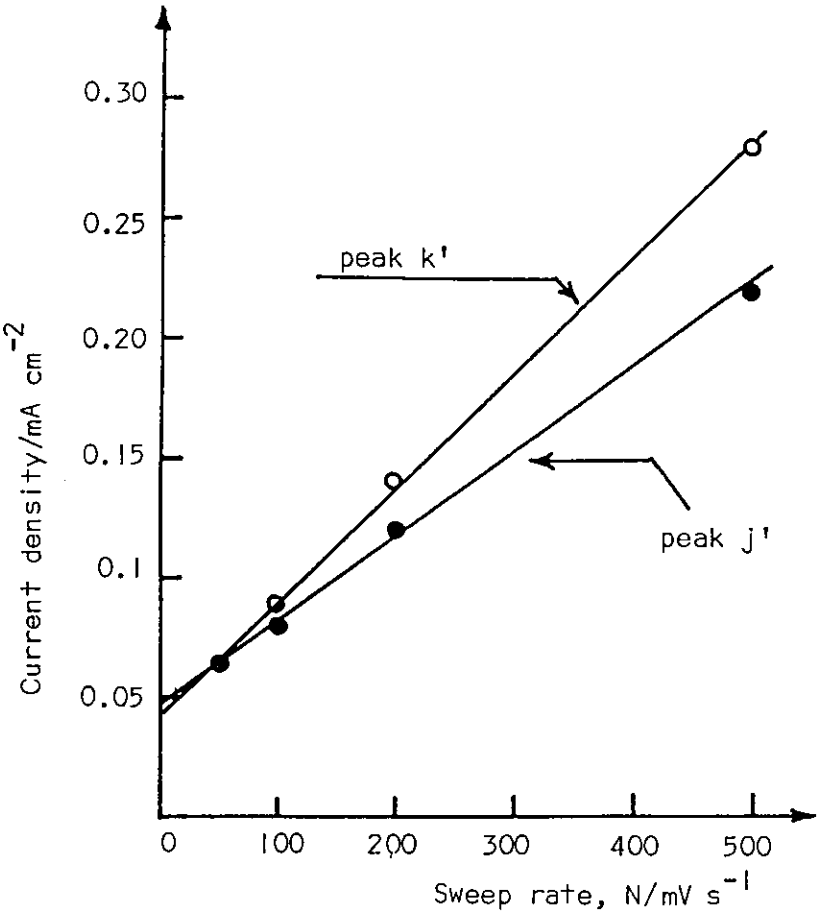

Figure 4.40. Currents of cathodic peaks due to reactions j' and k' against scan rate N

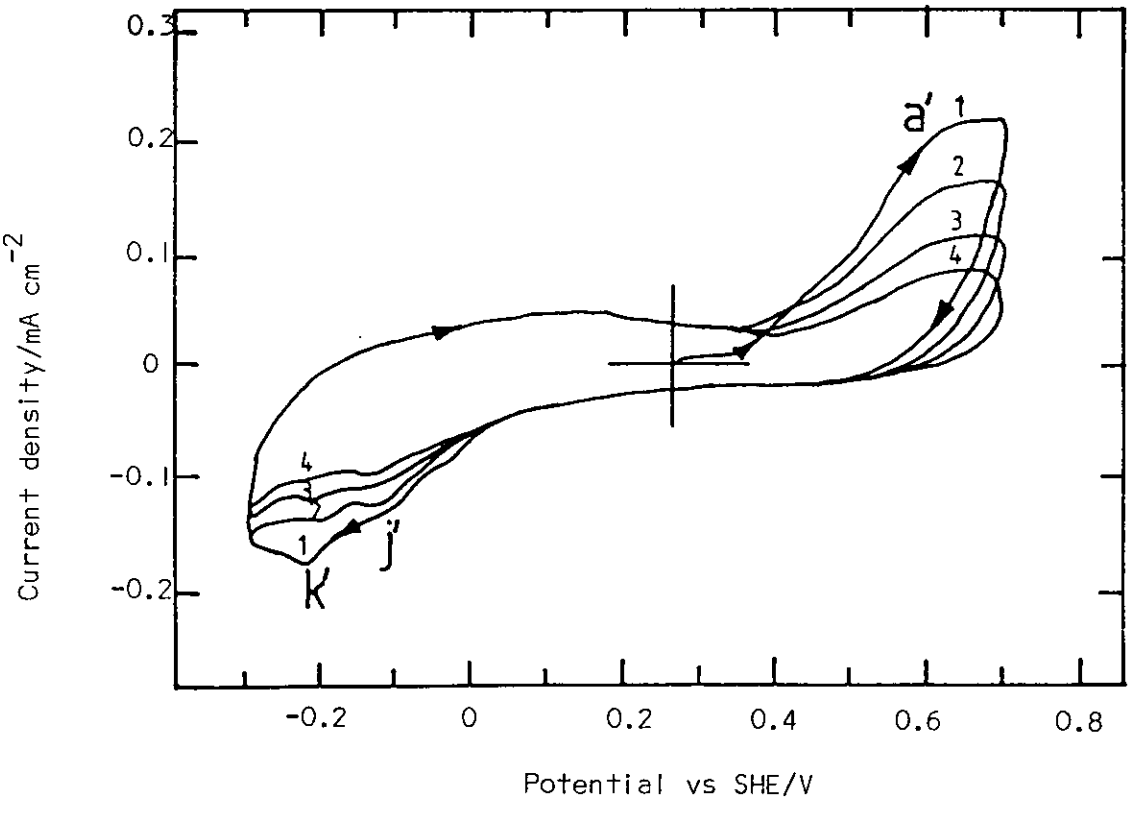

Figure 4.41. Cyclic voltammogram of pyrite electrode at 50 mV s^{-1} sweep rate in 0.1 M HCl

rise to the broad anodic peak j', k' in figure 4.39.

The cathodic peak at ∿ 0.35 V at high scan rates was probably due to the reverse of reaction a'. During the experiments nitrogen was bubbled through the electrolyte so that the Fe^{2+} and H_2S products were dispersed from the vicinity of the electrode. Therefore, the oxidation of H_2S by reactions j' and k' and the reverse of reaction a' were observed only at scan rates > 0.2 V s^{-1}.

When the anodic potential limit was extended to 0.7 V, the magnitude of the anodic and cathodic processes decreased on consecutive cycles as shown in figure 4.41. A similar phenomenon was observed with galena and was attributed to the formation by reaction a' of sulphur, which passivated the surface and was difficult to reduce due to its dielectric nature.[266] Hence the magnitude of the anodic and cathodic peaks decreased with potential cycling. This was also clear from the disappearance of the cathodic peak at ∿ -0.2 V due to the reduction of FeS_2 lattice, since with cycling the surface became coated with excess sulphur. Only on extending the anodic potential limit to 0.9 V (figure 4.42) did the influence of the sulphur layer diminish, since reaction b' became predominant and pyrite oxidised to SO_4^{2-} and Fe^{2+}. However, the amount of sulphur produced by reaction a' also increased, so the cathodic peaks at -0.1 and -0.2 V due to reactions j' and k' merged to give a single peak at -0.1 V, as the peak due to reaction j' increased in magnitude.

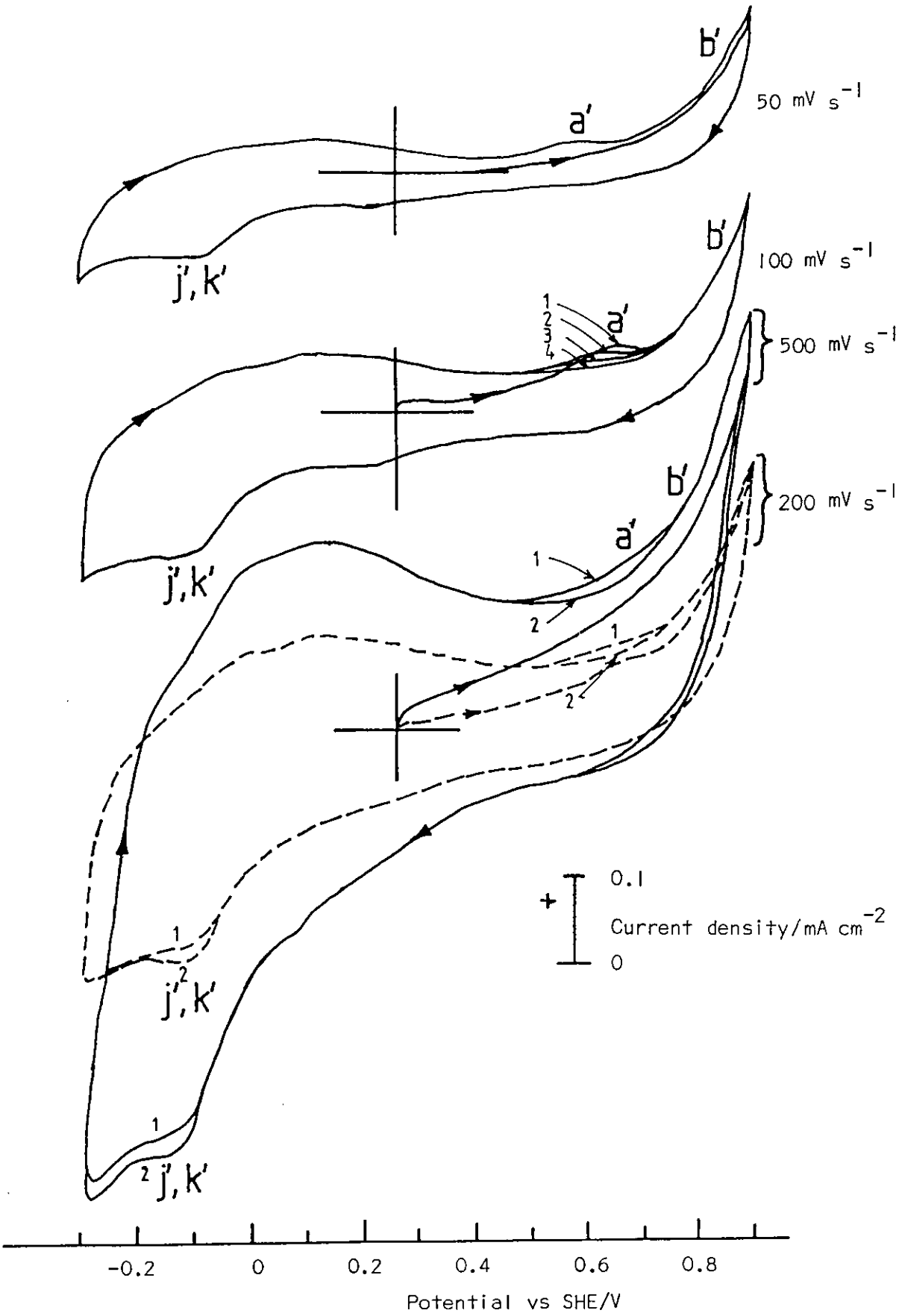

Figure 4.42. Linear sweep voltammogram of pyrite electrode at 50, 100, 200, 500 mV s^{-1} in 0.1 M HCl

With extension of the anodic potential limit to 0.9 V, the oxidation of Fe^{2+} to Fe^{3+} by reaction c' would also be observed on pyrite.

pH 4.6 (0.05 M CH_3COOH + 0.05 M CH_3COONa)

At pH 4.6 the initial anodic current on the first anodic-going scan starting from the rest potential and the anodic peak at 0.3 V on the second and subsequent anodic scans (figure 4.43) were again assigned to reaction a', the reversible potential of which is 0.246 V at 10^{-6} ion activity. According to the Eh-pH diagram of the Fe-H_2O system (figure 2.5), above $\sim$ 0.5 V pyrite oxidation should take place by reaction e' and f' such that all the iron would be in the ferric state:

$$FeS_2 + 3H_2O \rightleftharpoons Fe(OH)_3 + 2S + 3H^+ + 3e \qquad (e')$$

$$Eh = 0.64 - 0.059\ pH$$

and

$$FeS_2 + 11H_2O \rightleftharpoons Fe(OH)_3 + 2SO_4^{2-} + 19H^+ + 15e \qquad (f')$$

$$Eh = 0.412 - 0.0749\ pH + 0.0078 \log \left[SO_4^{2-}\right]$$

Although reaction f' was thermodynamically more favourable than reaction e', it was found[213] that the initial oxidation

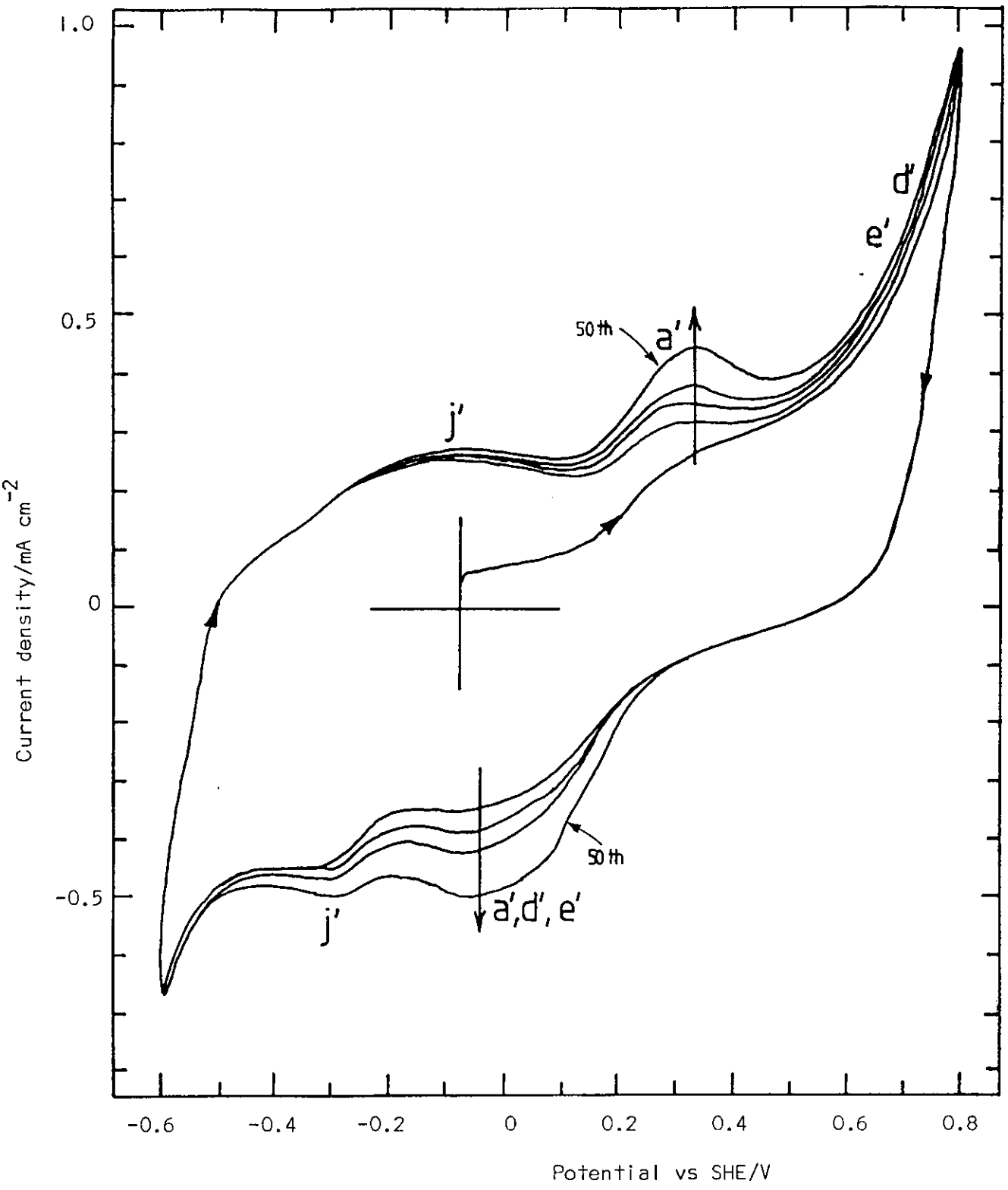

Figure 4.43. Cyclic voltammogram of pyrite electrode at pH 4.6 (0.05 M CH_3COOH + 0.05 M CH_3COONa) and a scan rate of 0.5 V s^{-1}

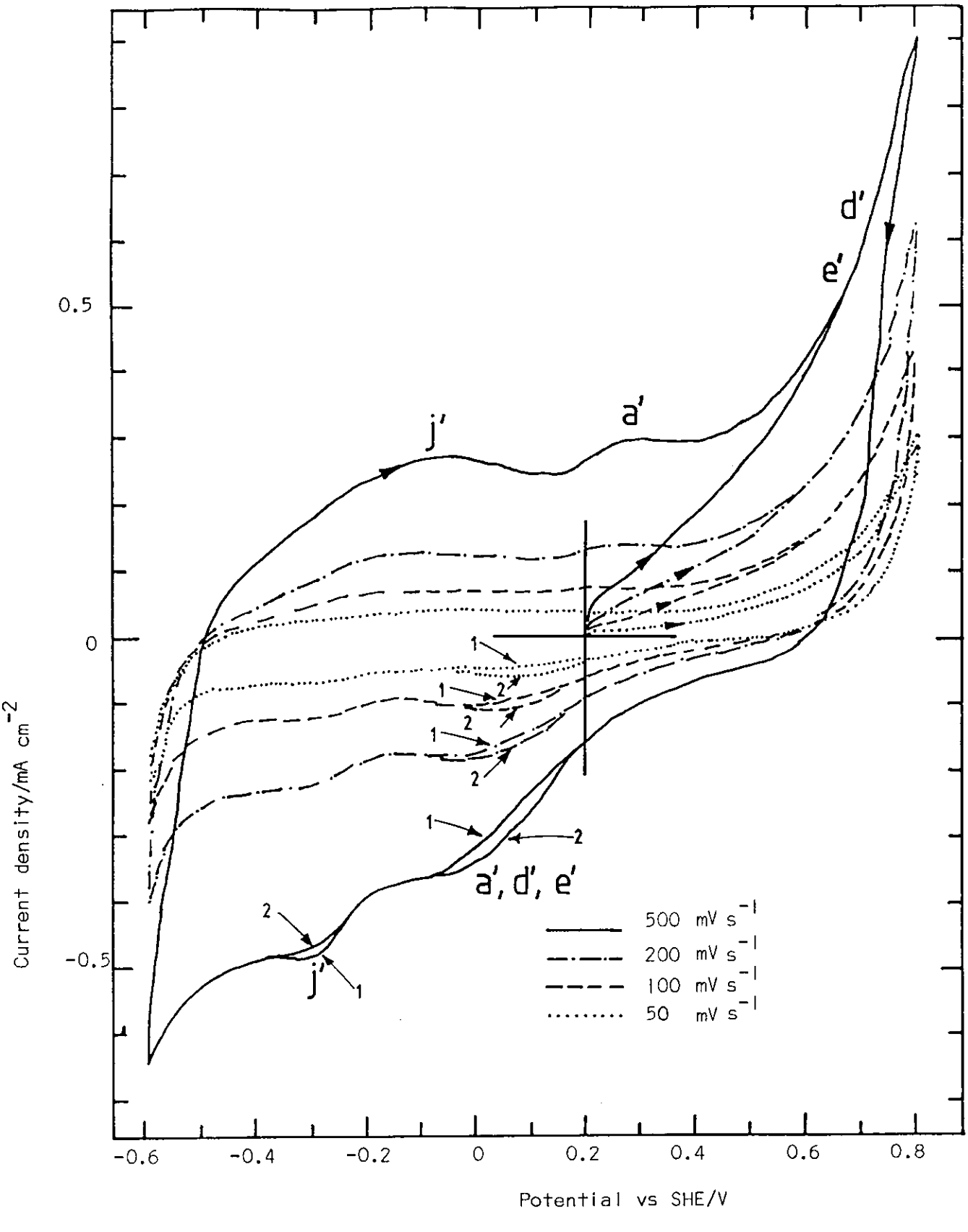

Figure 4.44. Cyclic voltammogram of pyrite electrode at various scan rates at pH 4.6 (0.05 M CH_3COOH + 0.05 M CH_3COONa)

product was sulphur with very little sulphate being formed. The proportion of sulphate increased as the potential was taken to higher values. A similar phenomenon was observed with galena oxidation to sulphate which occurs at higher overpotentials.[232] Some of the ferric hydroxide formed should dissolve at this pH to form species such as $Fe(OH)^{2+}$ and $Fe(OH)_2^+$, so excess sulphur would be present on the surface of pyrite.

The cathodic peak in figure 4.43 and 4.44 in the potential range +0.25 to -0.2 V corresponded to the reverse of reactions a', d' and e'. The more cathodic peak was due to the reduction of excess sulphur by reaction j' to give H_2S, which was oxidised on the subsequent anodic scan (figure 4.43) at high scan rates (figure 4.44), producing the anodic peak at $\sim$ -0.2 V.

pH 6.89 (0.025 M KH_2PO_4 + 0.025 M Na_2PO_4)

The initial oxidation process at pH 6.89 occurred by reaction e' which has a reversible potential of 0.23 V and gave rise to a peak at 0.25 V (figure 4.45) before reaction f' became the dominant anodic process. The anodic reactions were matched by a cathodic peak of similar magnitude on the cathodic sweep displaced by only 0.1 V.

$Fe(OH)_3$ was formed by reaction f' so that the second cathodic peak at 0.0 V can be assigned to the reduction of $Fe(OH)_2$ to Fe^{2+} by reaction d'. It is thermodynamically possible for the products of the anodic oxidation to be

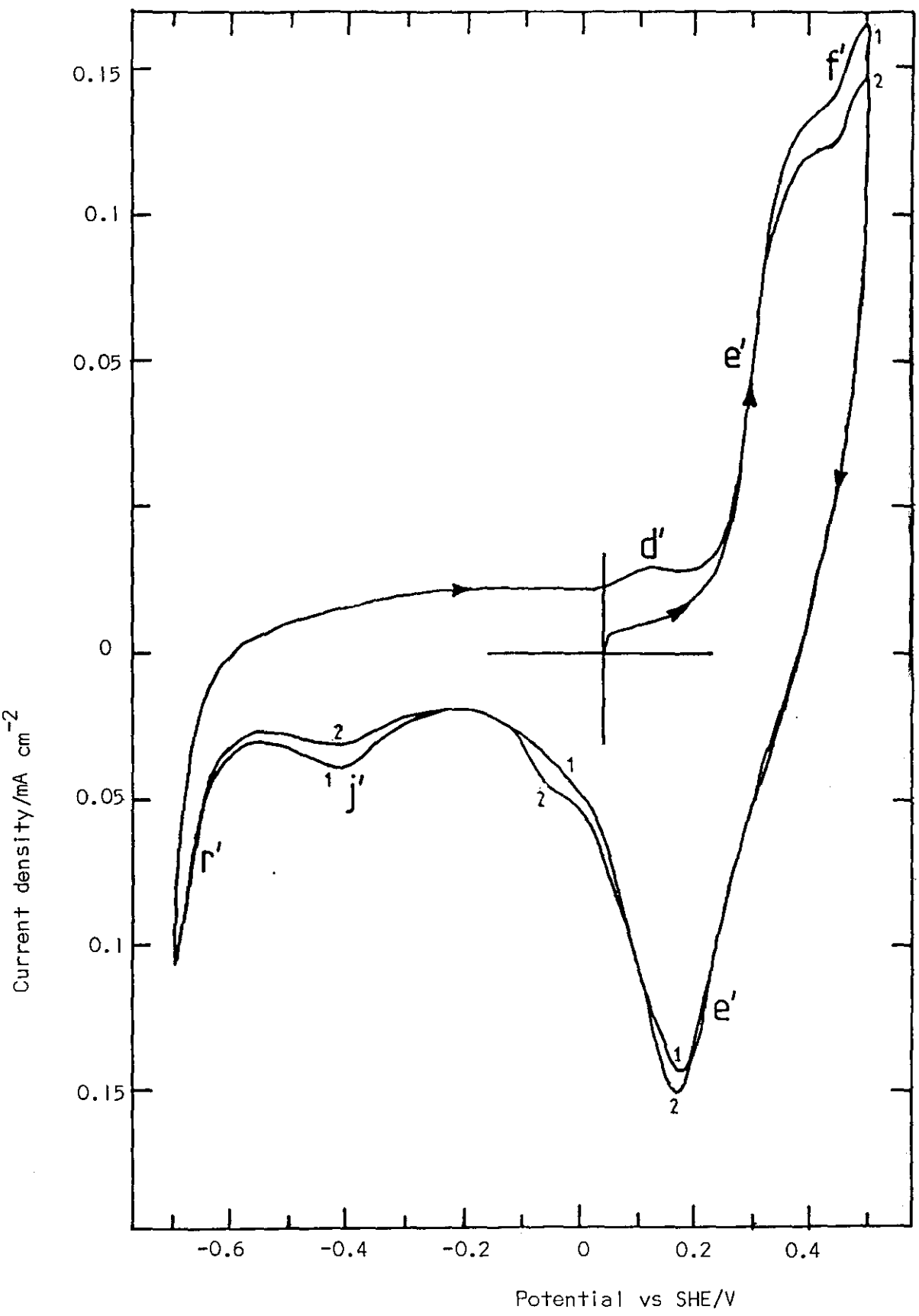

Figure 4.45. Cyclic voltammogram of pyrite at pH 6.89 (0.025 M KH_2PO_4 + 0.025 M Na_2HPO_4), at 50 mV s^{-1} sweep rate

reduced by reactions such as:

$$FeS + 3OH^- \rightleftharpoons Fe(OH)_3 + S + 3e^- \qquad (g')$$

$$Eh = 0.398 - 0.059\ pH$$

and

$$Fe(OH)_2 \rightleftharpoons Fe(OH)_3 + H^+ + e \qquad (h')$$

$$Eh = 0.271 - 0.059\ pH$$

for which the reversible potentials are -0.008 and -0.135 V respectively at pH 6.89. However, these reactions did not seem to occur because if any FeS or $Fe(OH)_2$ was formed by reactions g' and h', they would give rise to peaks on the cathodic and subsequent anodic sweep.

The anodic peak rising from 0.0 V, before the oxidation of pyrite by reaction e', is the oxidation of Fe^{2+} formed from the reduction of $Fe(OH)_3$ by reaction d' (figure 4.45). The cathodic peak at -0.4 V can be assigned to the reduction of excess sulphur on the surface by reaction j' which has a reversible potential of -0.26 V, at which the cathodic process starts. The cathodic current below -0.6 V was probably due to H_2 evolution on pyrite by reaction r'. However, the reduction of FeS_2 to FeS and then Fe are also possible by reactions l' and n'.

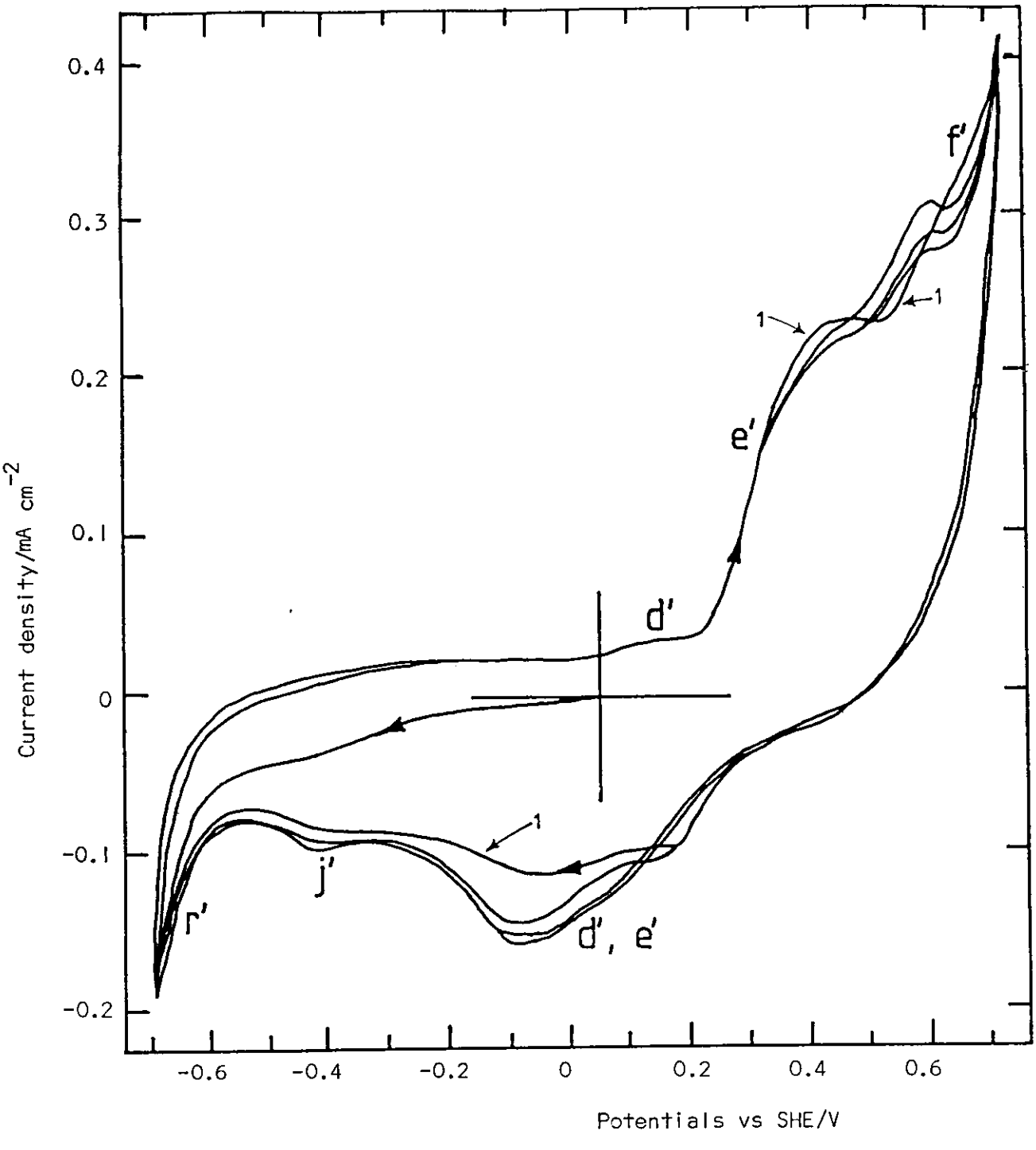

Figure 4.46. Cyclic voltammograms of pyrite at pH 6.89 (0.025 M KH_2PO_4 + 0.025 M Na_2HPO_4) and a potential sweep rate of 50 mV s^{-1}

Figure 4.46 shows the effect of continuous cycling at 50 MV s^{-1} and extending the potential limit to 0.7 V. The anodic peaks associated with reactions e' and f' and the cathodic peaks associated with reactions e' and d' shifted to more anodic and cathodic potentials respectively after the second potential cycle, and the cathodic peaks due to reactions e' and d' merged. This was probably due to the formation by reaction f' of more $Fe(OH)_3$, which would be reduced on the following cathodic scan by reaction d' and reoxidised on the subsequent anodic scan, forming a passive $Fe(OH)_3$ layer. This inhibited reactions e' and f' which then occurred at higher potentials. This did not happen on the first anodic scan because initial sweeping was in the cathodic direction.

pH 9.2 (0.05 M $Na_2B_4O_7$)

The voltammograms of pyrite at pH 9.2 are shown in figure 4.47-4.49 and were identical to those obtained by previous workers.[268,269] The anodic current at potentials > 0.2 V was due to reactions e' and f' which, at pH 9.2, have reversible potentials of 0.098 and -0.277 respectively. The cathodic peak at -0.2 V was due to the reverse of reaction e' and the reduction of $Fe(OH)_3$ to $Fe(OH)_2$ by reaction h', the reversible potential of which is -0.272 V. Michel and Woods[268] confirmed this by measuring the quantity of oxide-forming charge and by using X-ray emission spectroscopic analyses.

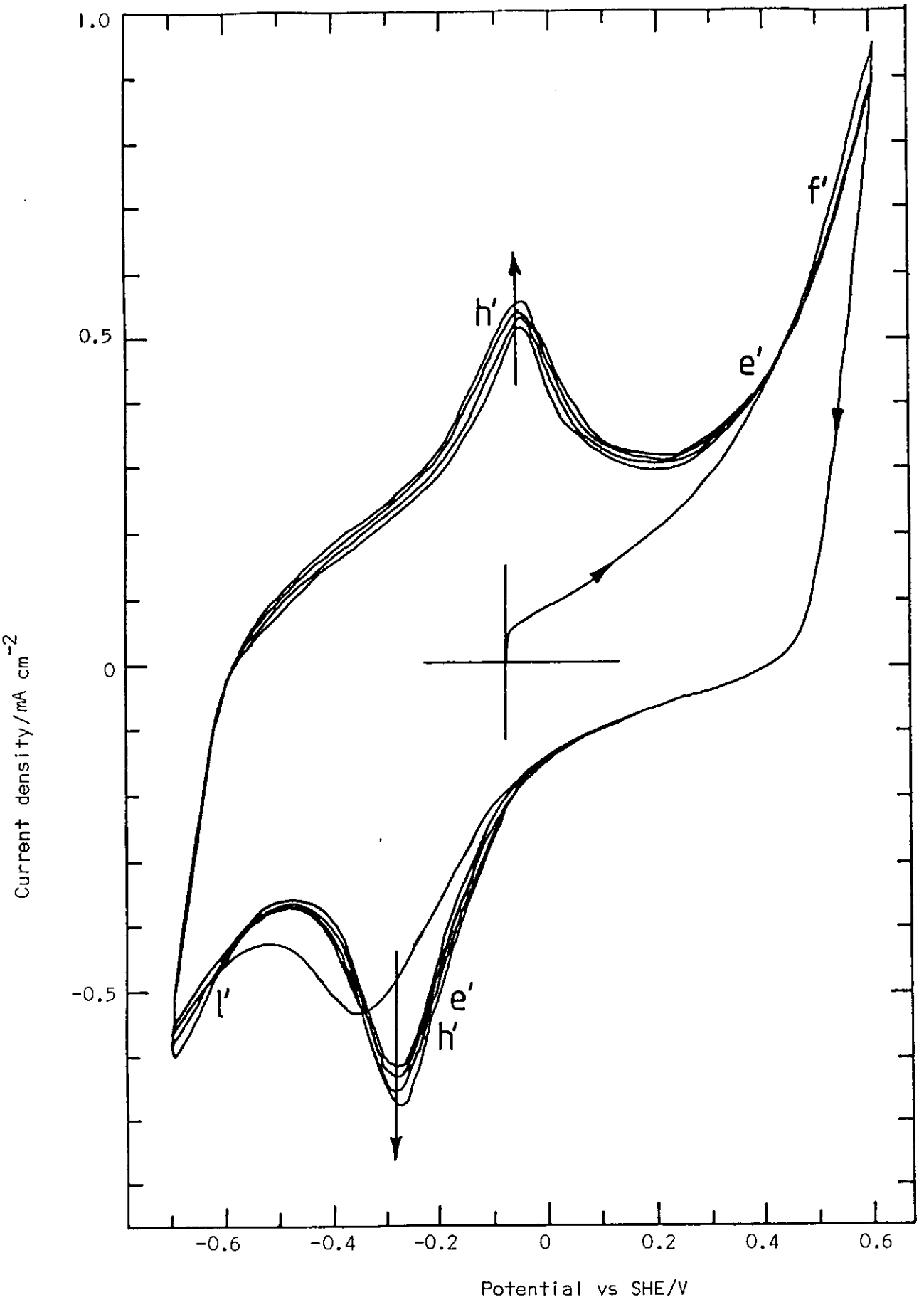

Figure 4.47. Cyclic voltammogram of pyrite at pH 9.2 (0.05 M $Na_2B_4O_7$) and a sweep rate of 0.5 V s^{-1}

Jenetski et al[269] suggested that the anodic peak at -0.1 V was due to the oxidation of an iron(II) hydroxide layer to the iron(III) state by reaction h'. After polishing the electrode and holding it at a cathodic potential for 60 seconds, sweeping cathodically from the rest potential (figure 4.48) produced a cathodic peak corresponding to reaction h'. This suggested that an oxide layer formed immediately on the pyrite surface even after cathodic treatment to remove it.

The voltammograms of pyrite at various sweep rates are shown in figure 4.49. A plot of the peak currents (Ip) against sweep rate (N) for the cathodic peak at -0.2 V and the anodic peak at -0.1 V gave a linear dependency (figure 4.50), confirming that surface transformations were occurring rather than diffusion controlled reactions.[249,253]

The reversible potential relationship for reaction g' suggests that the sulphur formed by reaction e' can be reduced by reaction g' which has a reversible potential of -0.145 V at pH 9.2. However, if this was the case then FeS would be oxidised to $Fe(OH)_3$ + S by reaction g', giving rise to an anodic current on the subsequent anodic scan. Alternatively, if it was oxidised in the potential range of the anodic peak at -0.1 V (which is thermodynamically possible), then the anodic peak charge should equal that for cathodic peak since both peaks were due to two 2-electron reactions. Therefore reaction g' does not take place on pyrite and the cathodic peak at -0.2 V was due only to the reverse of reactions d' and e'. The anodic peak at -0.1 V was due to reaction d'

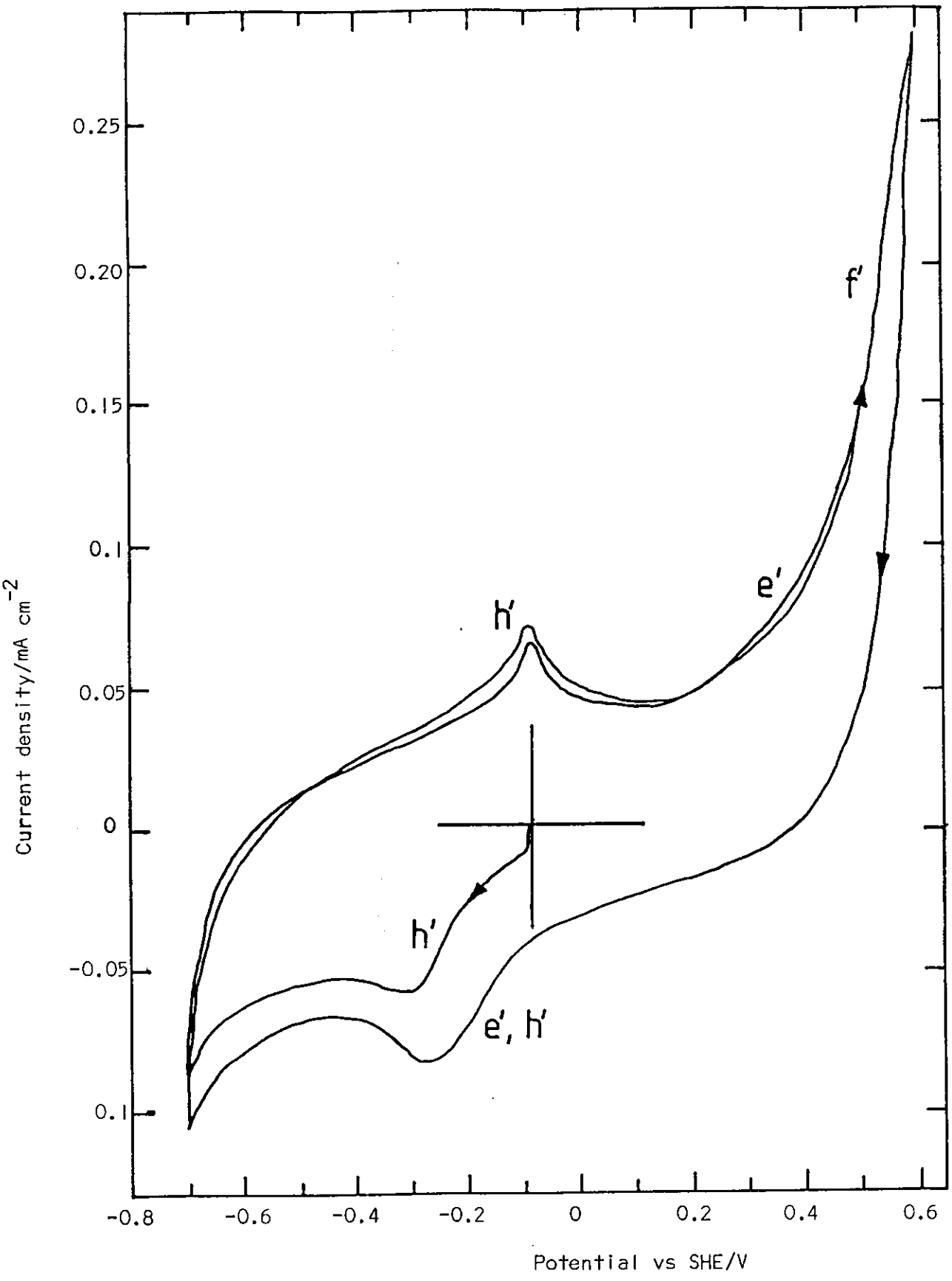

Figure 4.48. Cyclic voltammogram of pyrite at pH 9.2 (0.05 M $Na_2B_4O_7$), sweeping initially in the cathodic direction at 50 mV s^{-1}

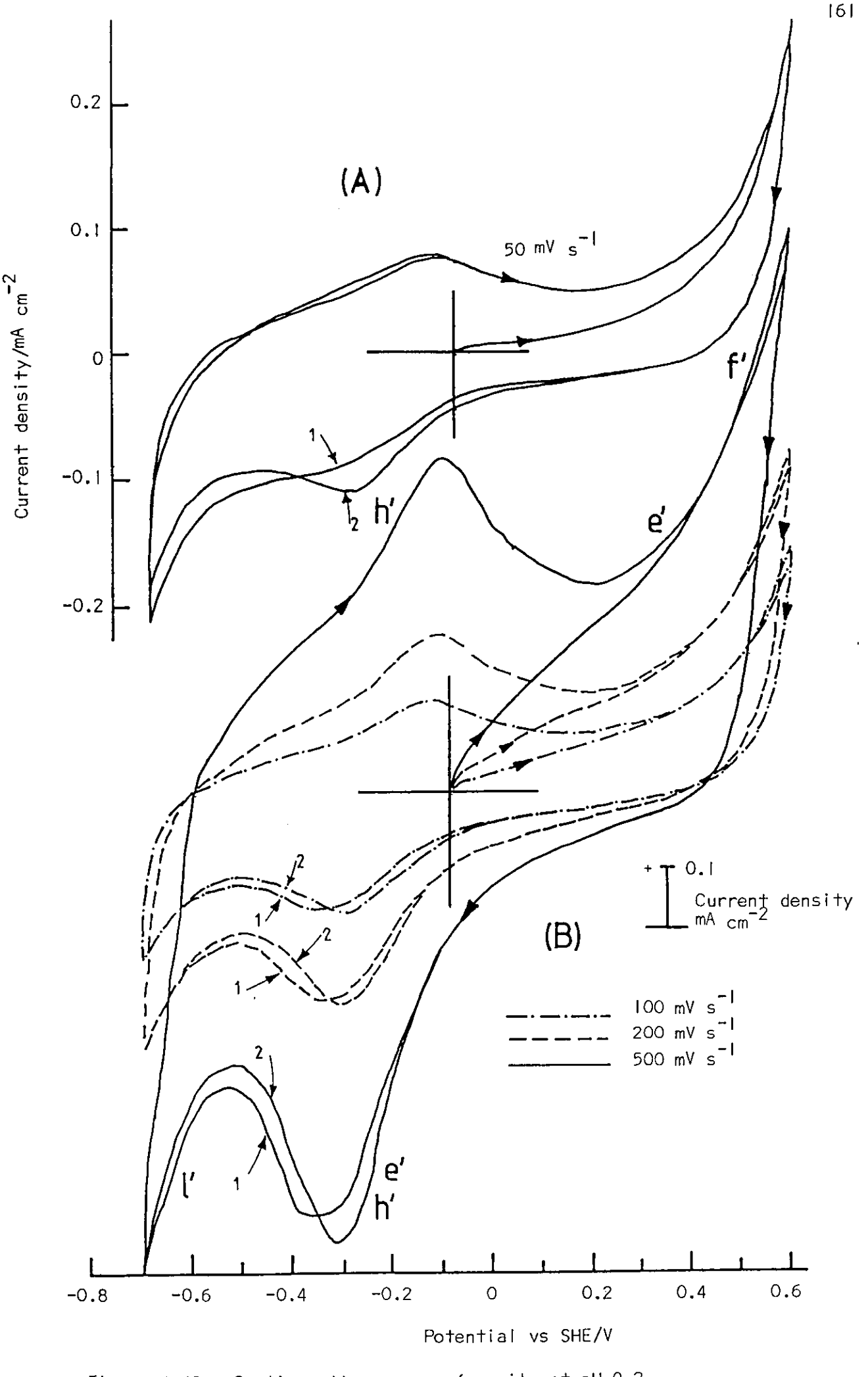

Figure 4.49. Cyclic voltammogram of pyrite at pH 9.2 (0.05 M $Na_2B_4O_7$) at various scan rates

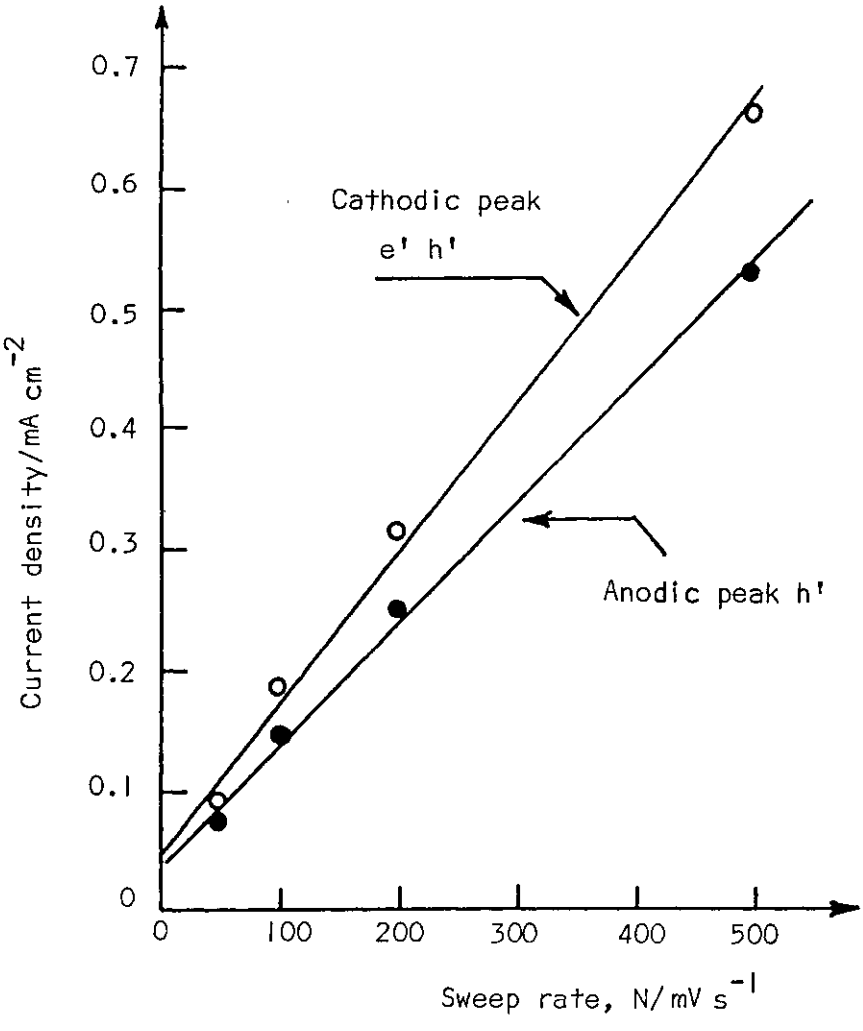

Figure 4.50. Currents of cathodic peak due to reactions e' and h' and anodic peak due to reaction h' against sweep rate

alone, so the anodic peak current is smaller than the cathodic peak current (figure 4.50).

Figure 4.47 shows that both the anodic peak due to reactions d' and e' grew with the number of potential cycles as more $Fe(OH)_3$ was formed by reaction f'. At more cathodic potentials the pyrite electrode was reduced by reaction l':

$$FeS + H_2S \rightleftharpoons FeS_2 + 2H^+ + 2e \qquad (l')$$

$$Eh = -0.133 - 0.059\ pH - 0.0295 \log [H_2S]$$

pH 11 (0.025 M $NaHCO_3$ + 0.023 NaOH

In the voltammogram of pyrite at pH 11 (figure 4.51), there was a large anodic peak on the anodic-going potential sweep and a large cathodic peak on the subsequent cathodic scan. The potential of the anodic peak corresponded to the oxidation of $Fe(OH)_2$ to $Fe(OH)_3$ by reaction h', which has a reversible potential of -0.378 V at pH 11. The Eh-pH diagram of the Fe-S-H_2O system (figure 2.7) suggests that above pH 9.5, $Fe(OH)_2$ is the thermodynamically favoured species in equilibrium with pyrite at its rest potential.

When the anodic potential limit was extended to 0.8 V a second anodic process appeared at potentials > 0.3 V (figure 4.52) due to reactions e' and f'. The shift of the potentials of these reactions to more anodic potentials was due to the presence of an oxide layer on the surface. The cathodic peak on the cathodic scan corresponded to the reverse of reaction g' and h', the reversible potential of which are -0.251 and -0.378 V respectively.

At more cathodic potentials the reduction of FeS_2 to FeS by reaction m' and the reduction of FeS to Fe by reaction o' could occur.

The anodic wave at -0.38, before the oxidation of $Fe(OH)_2$ to $Fe(OH)_3$ by reaction h', and the anodic peak at -0.65 V on the second anodic sweep (figure 4.52), could be due to reaction g' and oxidation of Fe to $Fe(OH)_2$ by reaction q':

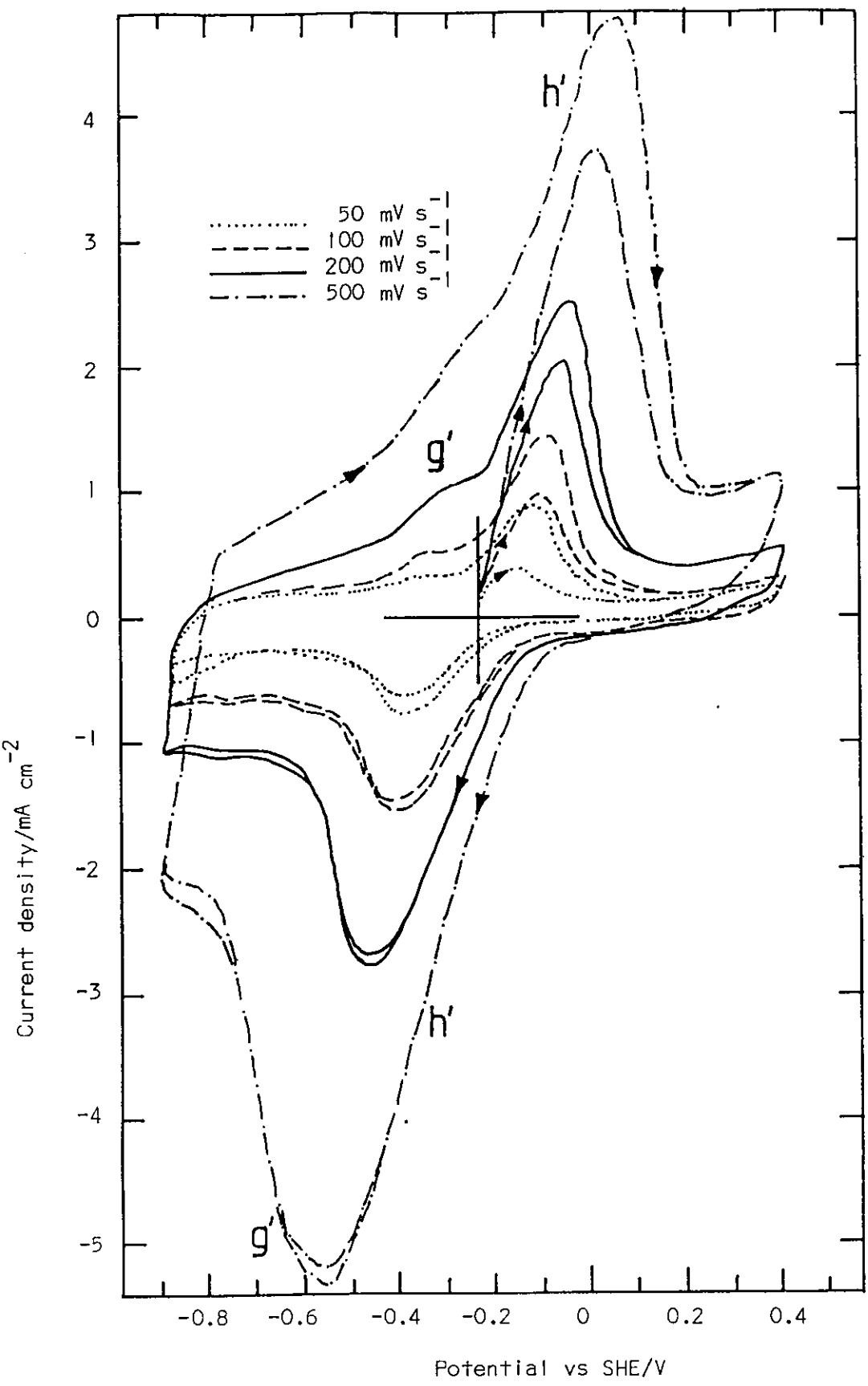

Figure 4.51. Cyclic voltammogram of pyrite at pH 11 (0.025M $NaHCO_3$ + 0.023M NaOH) at various scan rates

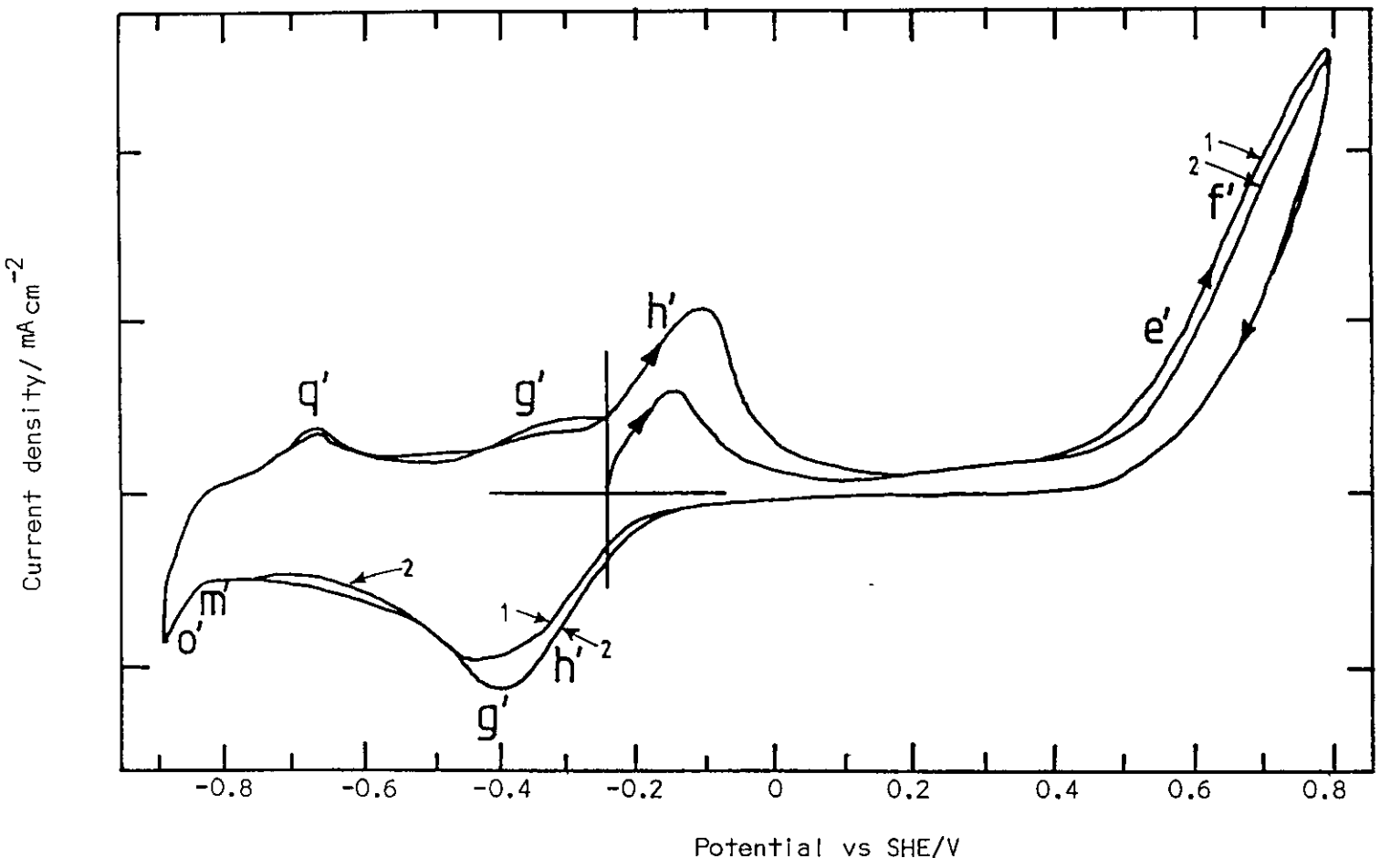

Figure 4.52. Cyclic voltammogram of pyrite at pH 11 (0.025 M $NaHCO_3$ + 0.023 M NaOH), the anodic potential limit extended to +0.8 V, and a scan rate of 50 mV s^{-1}

$$Fe + H_2O \rightleftharpoons Fe(OH)_2 + 2H^+ + 2e \qquad (q')$$

$$Eh = -0.047 - 0.059\ pH$$

the reversible potential of which is -0.696 V at pH 11.

4.5.5 Particulate bed electrode studies

Application of potentials using a 100 mm long flat spiral pt wire feeder electrode at the bottom of the first cell (figure 3.4) made no difference in the recovery as a function of potential at various pH values. The polarisation curves of the Pt-wire feeder electrode showed an unexpected decrease in the current in the presence of fine galena particles. After polarisation the wire was found to be covered by a black deposit which was easily removed from the surface by rubbing. It was attributed to coating of the electrode by very fine galena particles which caused passivation of the electrode.

A Pt-foil, about 10 mm wide formed into an open cylinder at the bottom of the cell, was found to be more effective as a feeder electrode. Polarisation curves showed an increase in the current in the presence of the mineral suspension (figure 4.53). The decrease in the current above +0.95 V was probably due to the formation of an oxide layer on the Pt electrode.[286]

Preliminary studies with coarse galena showed that sulphidised galena was oleophilic, but due to the coarse size (-300 + 106 μm) of the particles, oil drop/mineral composites sank to the bottom of the cell. Observations of

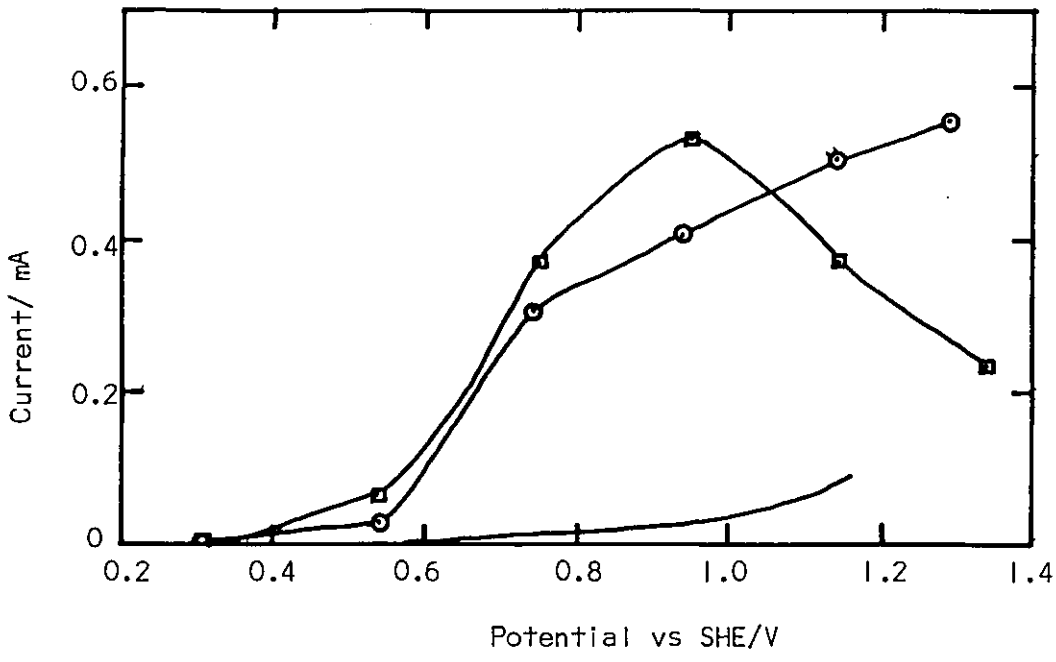

Figure 4.53. Polarisation curves for Pt foil electrode in the absence and presence of a galena particulate bed. ▣ fines, ⊙ -300 + 106 μm

the nature of settled oil drops at different potentials indicated that at pH I, 6.89 and II, the reduction increased oleophilicity whereas on oxidation, oleophilicity increased at pH I, disappeared at pH 6.89 and was unaffected at pH II.

Freshly ground fine galena was oleophobic probably due to oxidation forming $Pb(OH)_2$ on the surface. Neither reducing nor oxidising produced an oleophilic surface at pH 9.2 and II, whereas at pH 6.89 and I reducing the galena produced an oleophilic surface, as shown in figure 4.54-4.57. At pH I galena particles were partly oleophilic probably due to dissolution of surface oxide.

However, when galena was sulphidised it was oleophilic from pH I to II as shown in figure 4.60 and results were as expected from those obtained in the two-liquid flotation studies (figure 4.1). At pH 6.89, 9.2 and II (figure 4.55-4.57),

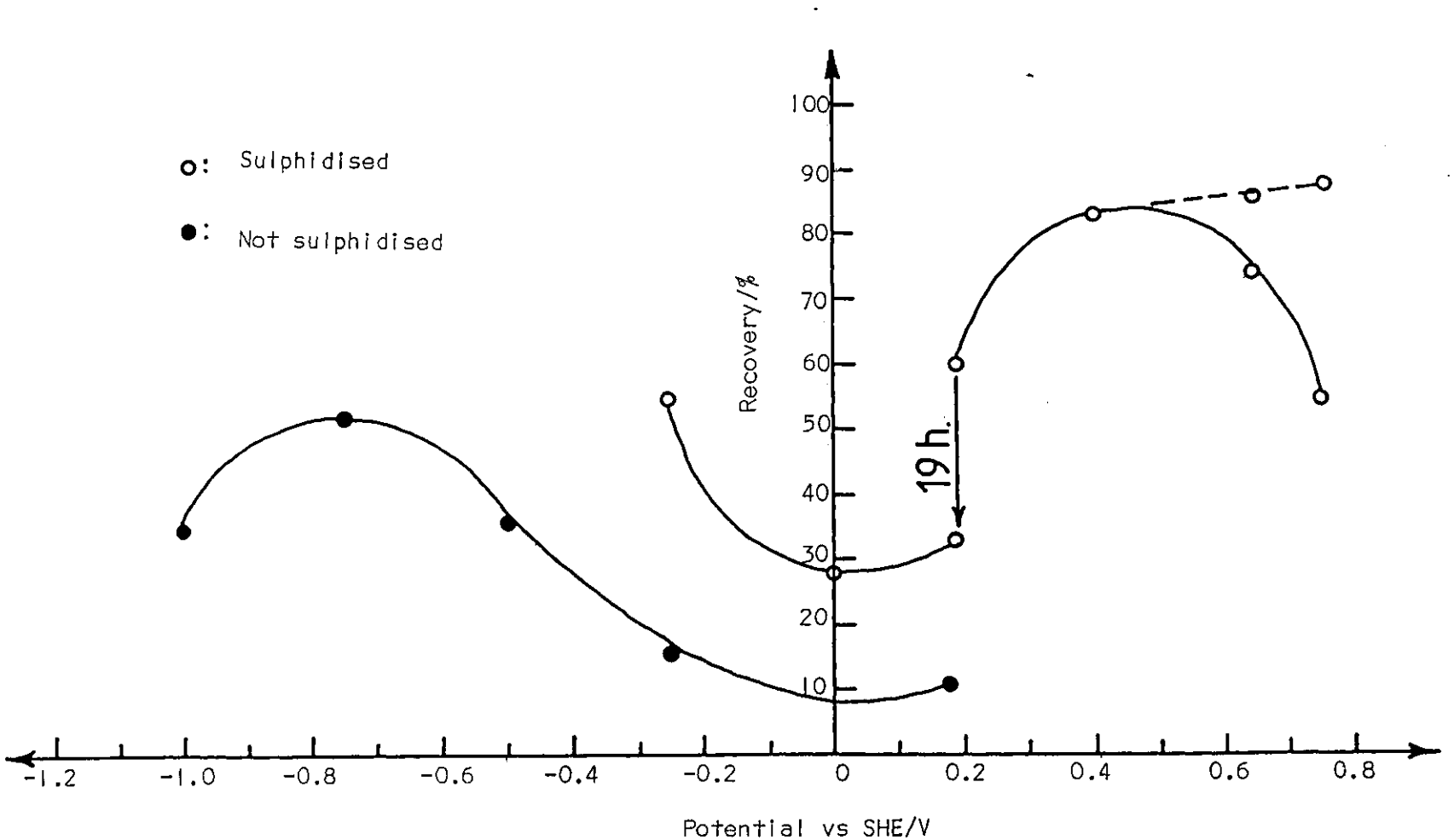

Figure 4.54. The change of galena recovery with potential at pH 1 (0.1 M $HClO_4$)

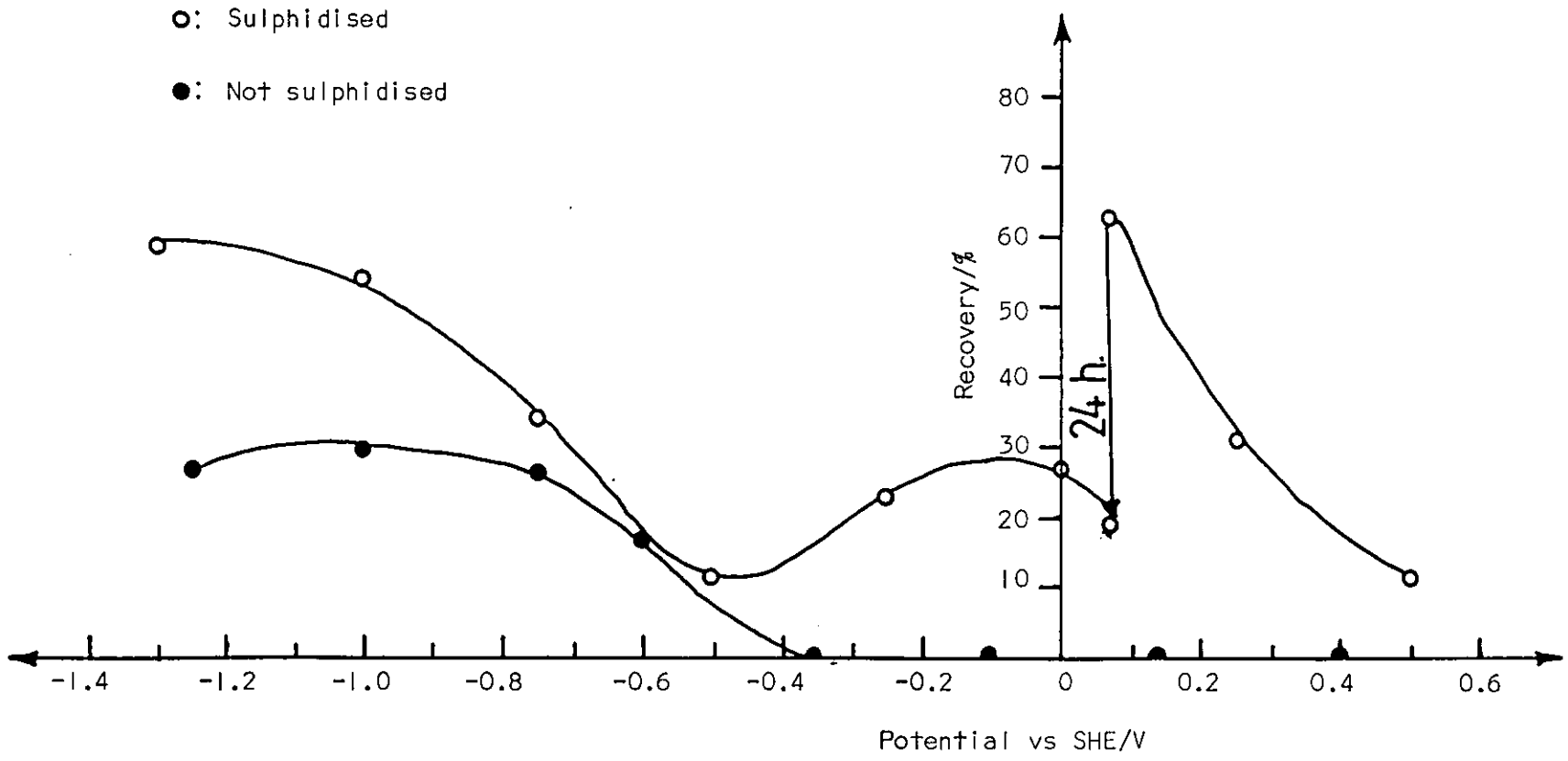

Figure 4.55. The change of galena recovery with potential at pH 6.89 (0.025 M KH_2PO_4 + 0.025 M Na_2HPO_4)

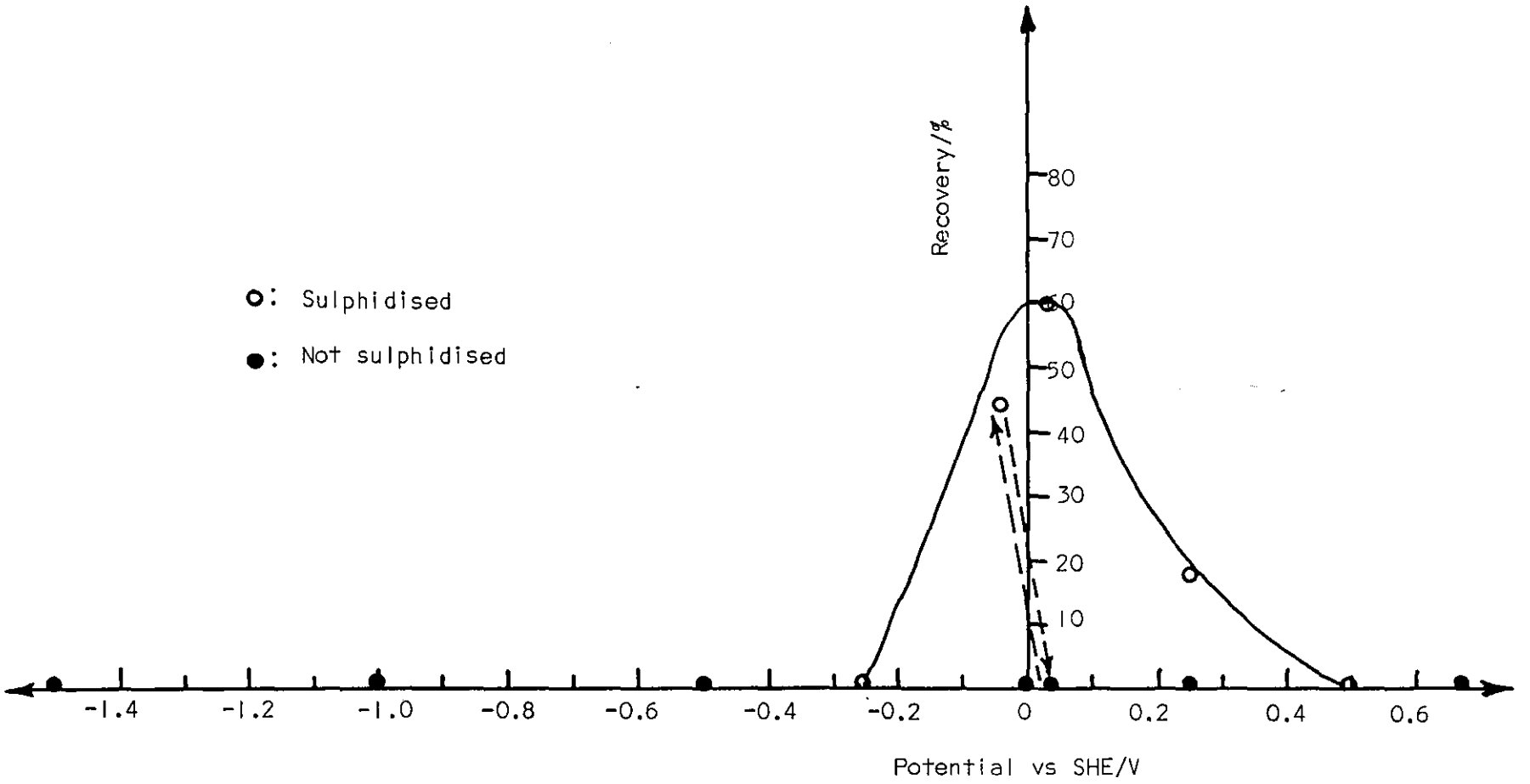

Figure 4.56. The change of galena recovery with potential at pH 9.2 (0.05 M $Na_2B_4O_7$)

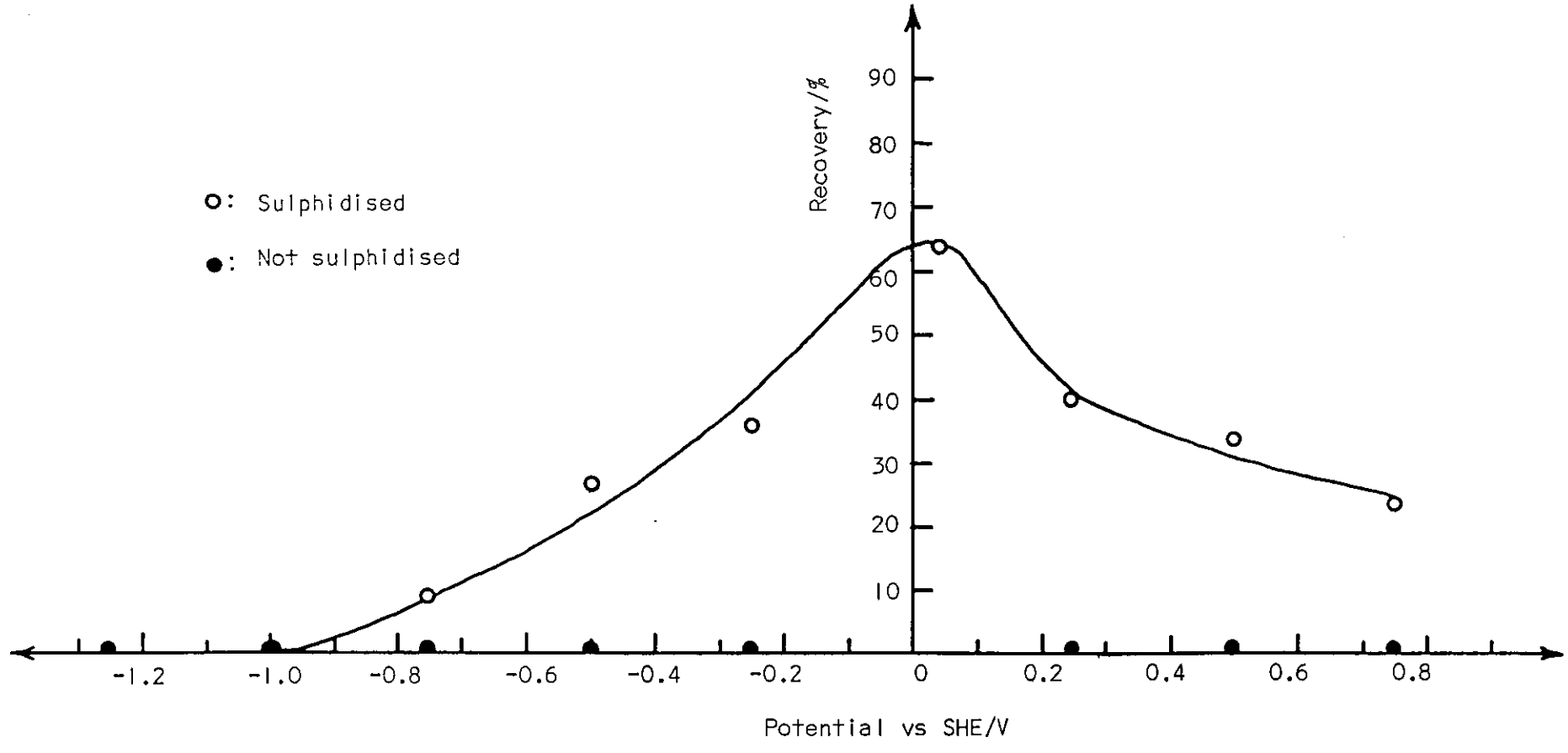

Figure 4.57. The change of galena recovery with potential at pH 11 (0.025 M $NaHCO_3$ + 0.023 M NaOH)

oleophilicity decreased with anodic oxidation whereas at pH I it increased, though at higher anodic potentials recovery decreased again. This was probably due to hydrophobic coagulation of particles because of increased amount of sulphur on the surface formed by oxidation. On reduction the recovery of sulphidised galena decreased at pH 9.2 and II and first decreased then increased at pH 6.89 and I as shown in figure 4.54-4.57.

The above results were reproducible qualitatively though not quantitatively, due to different amounts of sample in each test and different degrees of initial oxidation of the surface. However, for some unidentified reason, the dependency of the recoveries on potential disappeared and the system became ineffective. Platinised titanium gauze and a new Pt-foil were tested as feeder electrode and magnetic and mechanical stirring of the slurry were used to enhance the collision efficiency of particles with the feeder electrode. However, no improvement in the recovery/potential relationship was found.

To check whether the above results (figure 4.54-4.57) were due to contamination, the cell content was deliberately contaminated with oleic acid. However, this gave no recovery up to a concentration of 10^{-4}M with unsulphidised galena, and the recovery was independent of the potential. Therefore the increase in the recovery on reduction of the bed at pH I and 6.89 (figure 4.54 and 4.55) could not have been caused by contamination.

To obtain better control of the potential, the tests were repeated in the second cell (figure 3.5) incorporating a compacted bed electrode. The current was integrated for 30 minutes with a digital integrator in both the absence and presence of mineral at a constant applied potential of -1.0 V. The charge passed increased substantially in the presence of the mineral (figure 4.58) indicating changing of the particles. Charging of coarse galena particles was much more effective than with fine particles, in spite of the greater surface area of the fine particle bed ($A \alpha {}^{1}/r$), due to the better contact of coarse particles with the working electrode. The fine particle bed was difficult to compact because when the pressure was applied with the counter electrode chamber, the bed was destroyed. Therefore fine particles were allowed to sediment onto the working electrode and were not compacted by applying pressure.

The results were not reproducible. The only phase change obtained reproducibly was the cathodic reduction of PbS to $Pb + H_2S$ or $Pb + HS^-$ by reaction k and o (see Appendix I). When the galena bed electrode was cathodically polarised, i.e. at -0.75 V, -1.0 V and -1.25 V at pH 1, 6.89 and 11 respectively, the bed turned into a very porous mass and the current increased with time, due to the formation of Pb^o on the surface of the particles. Also the solution in the cell became a cloudy cream colour, and H_2S or HS^- was oxidised at the counter electrode forming a red-brown layer of sulphur.

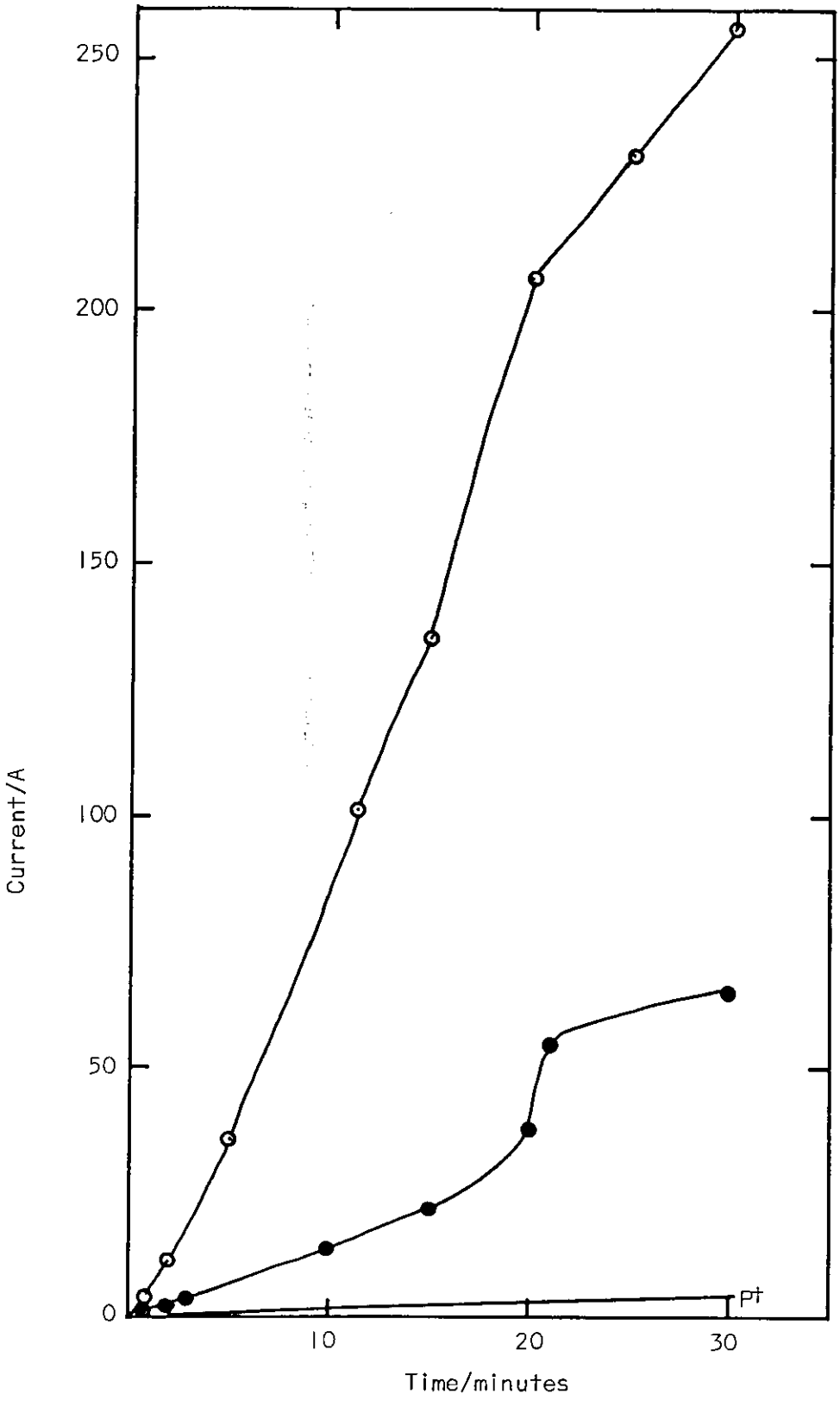

Figure 4.58. Pt feeder electrode current-time relationship when polarised to -1.0 V alone and with fine (●) and coarse galena (⊙) compacted beds present

Though particle-particle charge transfer was possible in a cathodically polarised bed, anodic oxidation tended to block inter particle charging due to formation of oxides on the surfaces of particles.

As shown in figure 4.59, the change of potential produced no change in the recovery of pyrite in the electro-Hallimond cell (figure 3.4). Unsulphidised pyrite was oleophobic due to the formation of an $Fe(OH)_2$ layer, except at pH I when the oxide dissolved and non-oxidative dissolution of pyrite took place yielding H_2S, which was evident by its smell in the outgoing gas. When pyrite was sulphidised, however, it was oleophilic below pH II as shown in figure 4.61 and the results were similar to those obtained in the two-liquid flotation experiments (figure 4.2).

The oleophilicity of both sulphidised pyrite and galena decreased with time and the minerals became oleophobic in deoxygenated water under a nitrogen atmosphere. Resulphidising restored their oleophilicity. This could be due to the diffusion of atmospheric oxygen into the system (or to residual O_2 in the N_2) forming an oxide layer on the mineral surface, in spite of the presence of a nitrogen overpressure. When the mineral was sulphidised in aqueous Na_2S solution,[225,287] the reaction

$$M(OH)_2 + HS^- \longrightarrow MS + H_2O + OH^- \qquad (4.3)$$

restored the sulphide surface.

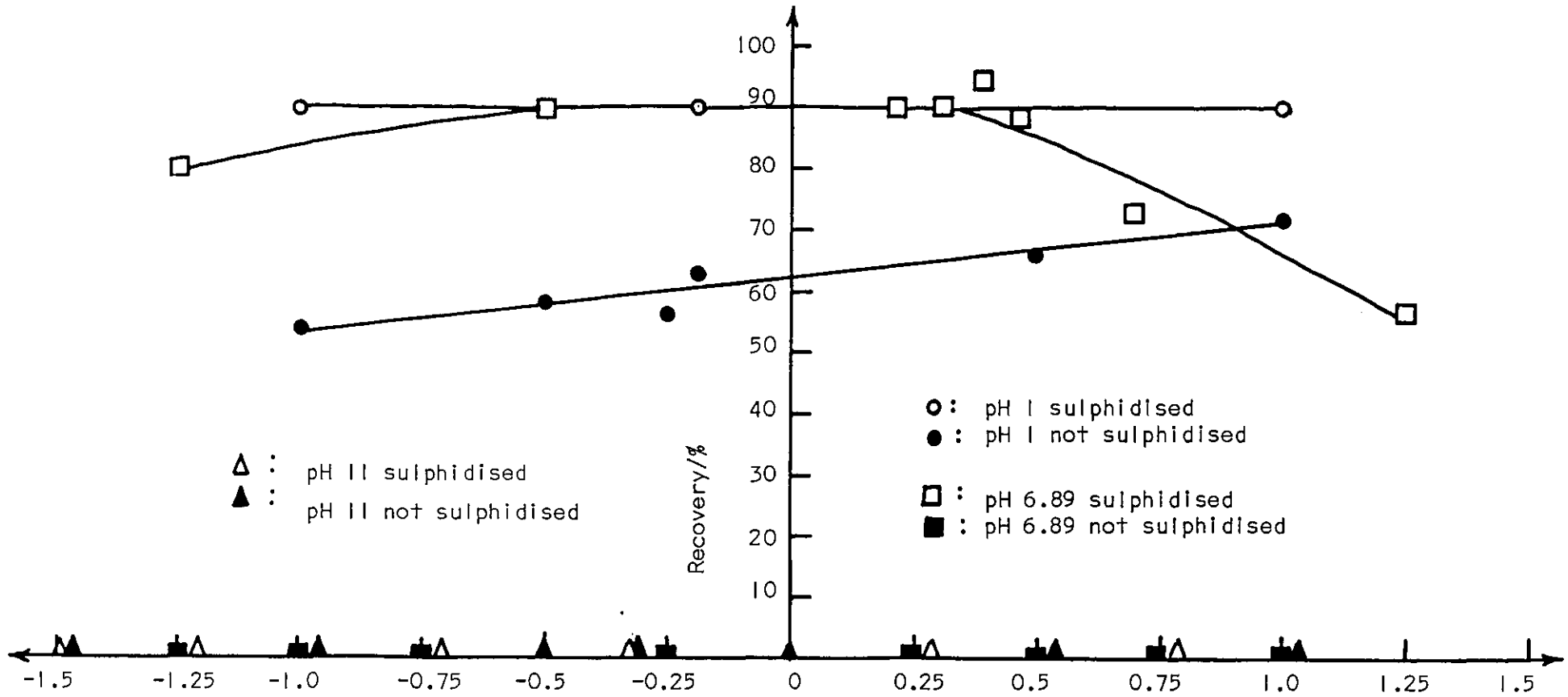

Figure 4.59. The change of pyrite recovery with potential as a function of pH

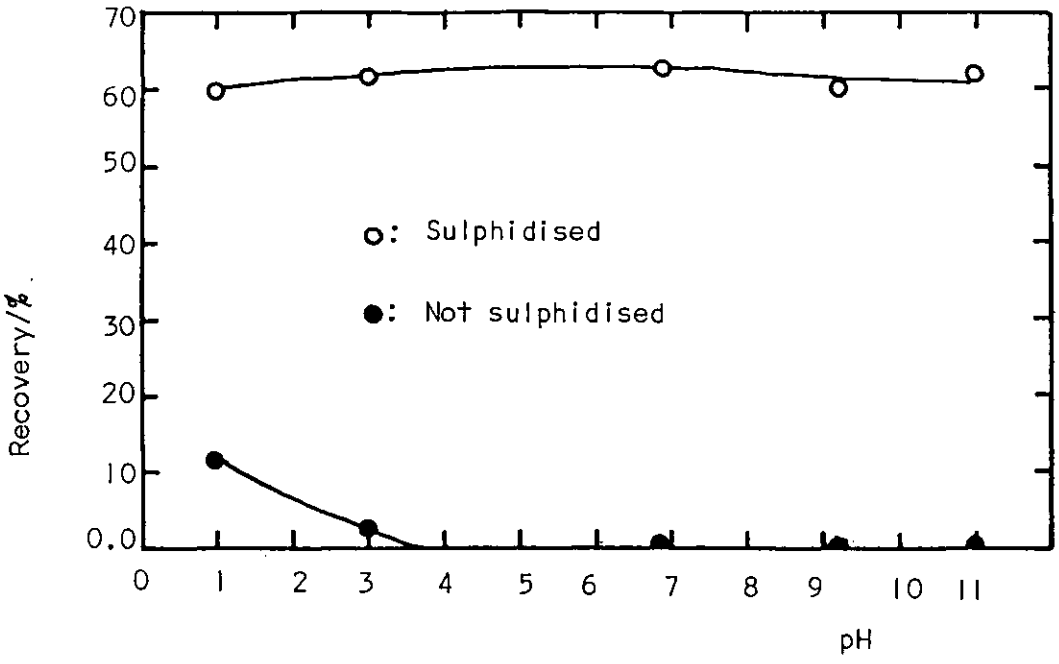

Figure 4.60. The change of galena recovery with pH after being sulphidised and without sulphidisation

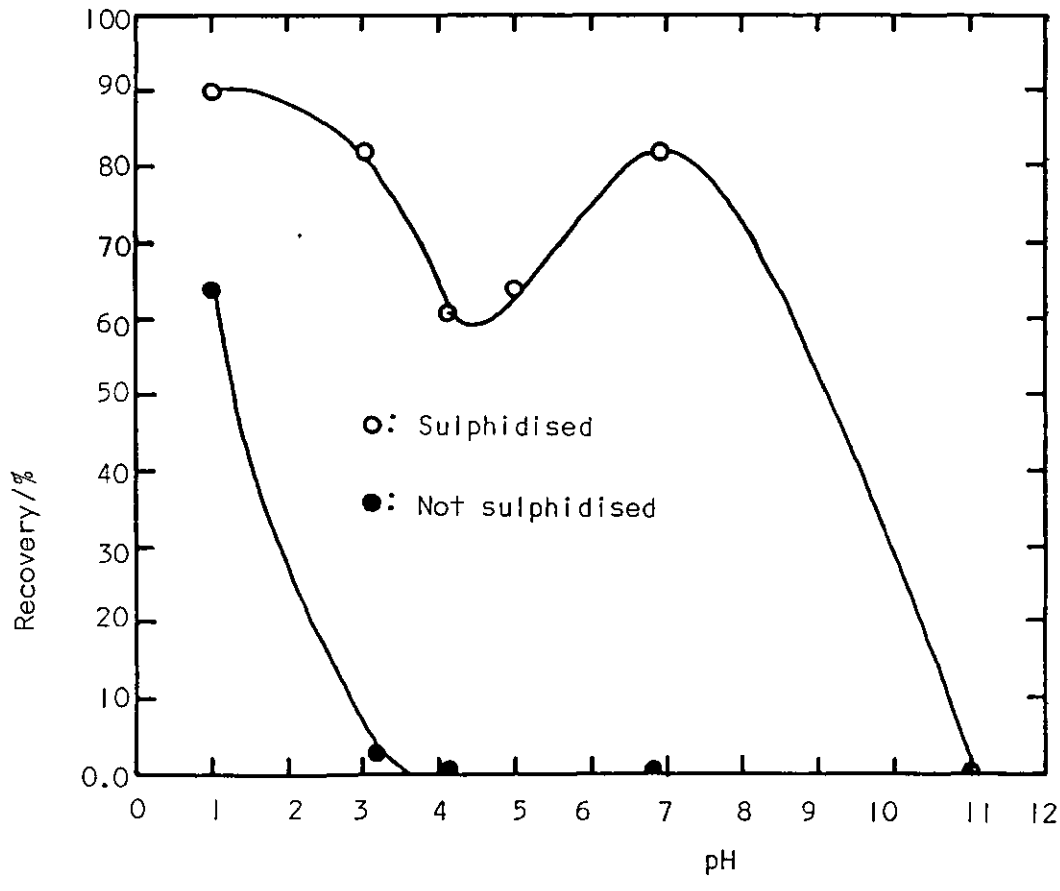

Figure 4.61. The change of pyrite recovery with pH after being sulphidised and without sulphidisation

4.5.6 Contact potential measurements

Figures 4.62 to 4.64 show typical galena electrode potential and feeder electrode current transients when a galena electrode was contacted to the Pt feeder electrode, polarised to different potentials. The potential of the galena electrode almost reached the applied potential in less than 2 seconds. As seen in figures 4.66 and 4.67 the change in the potential of pyrite was much less than that of galena, as was the pyrite charging current.

When the mineral and feeder electrodes were kept in contact for longer times, the potential of the galena electrode reached the feeder electrode potential in a few seconds, whereas pyrite had not achieved the feeder electrode potential even after 15 minutes. Increasing the pressure applied during contact was found to increase the rate of change of potential. Several consecutive contacts, as shown in figure 4.65, 4.66b and 4.67c, produced bigger changes in the potential of mineral electrodes.

When the mineral electrodes were separated from the feeder electrode, their potential decreased towards their initial potential though there was still some disparity, indicating that charge may leak away by electrochemical reactions/oxidation or reduction of the mineral electrodes. However, the final difference in the potential of pyrite was smaller than that of galena and the change caused by anodic oxidation was smaller than that following cathodic reduction (figure 4.68 and 4.69).

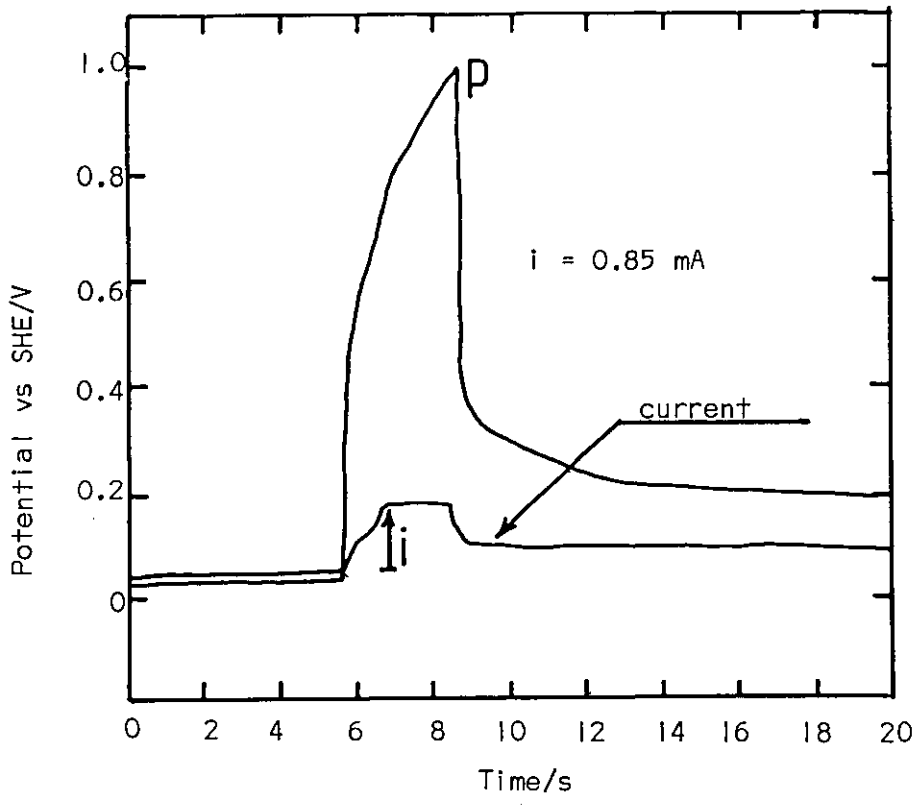

Figure 4.62. The change of galena potential and cell current in contact with Pt feeder electrode at 1.0 V. P - point of separation of the electrodes

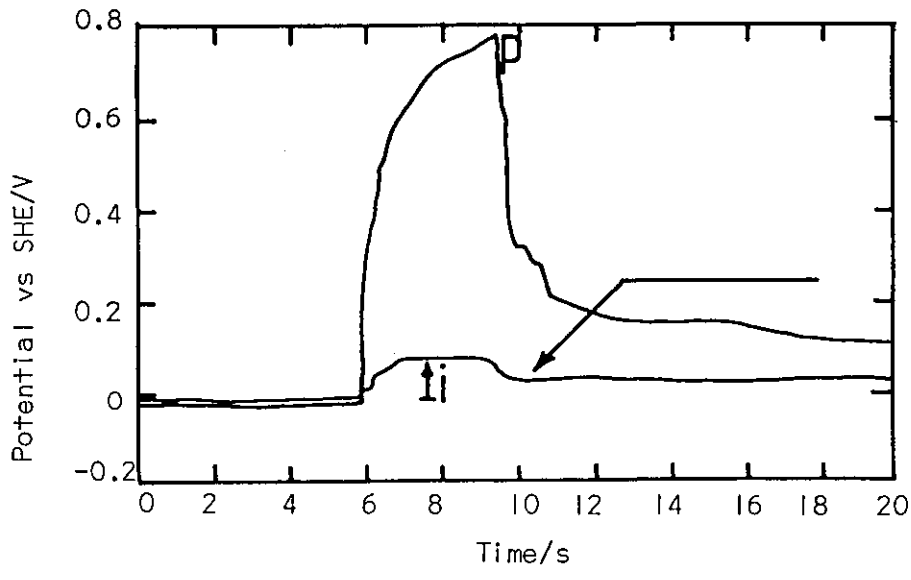

Figure 4.63. The change of galena potential and cell current in contact with a Pt feeder electrode at 0.8 V. P - point of separation of the electrodes

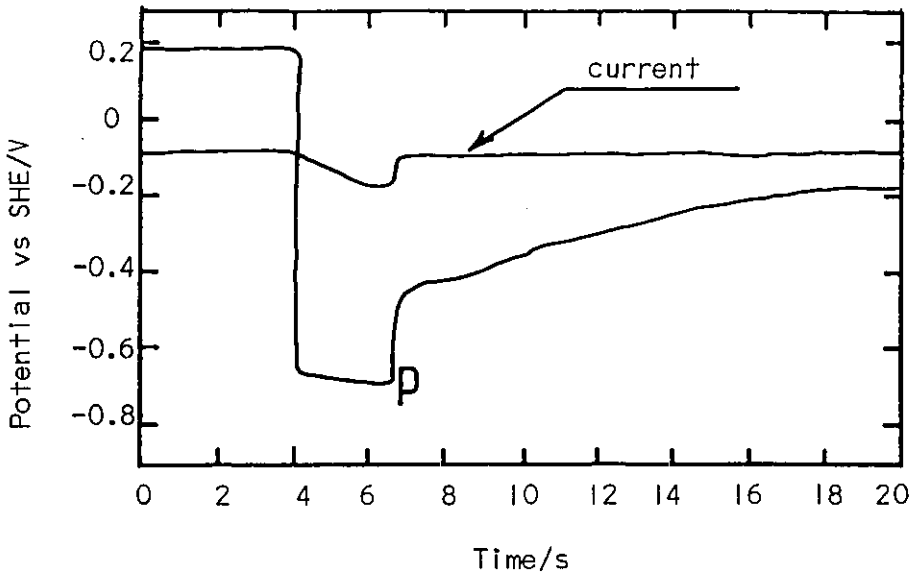

Figure 4.64. The change of galena potential and cell current in contact with a Pt feeder electrode at -0.8 V

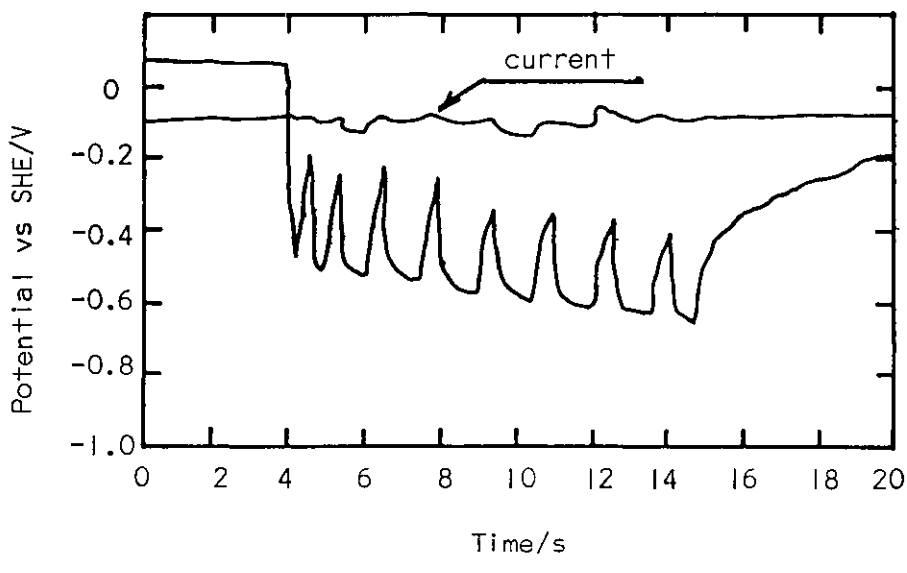

Figure 4.65. The change of galena potential and cell current in consecutive contacts with a Pt feeder electrode at -0.75 V

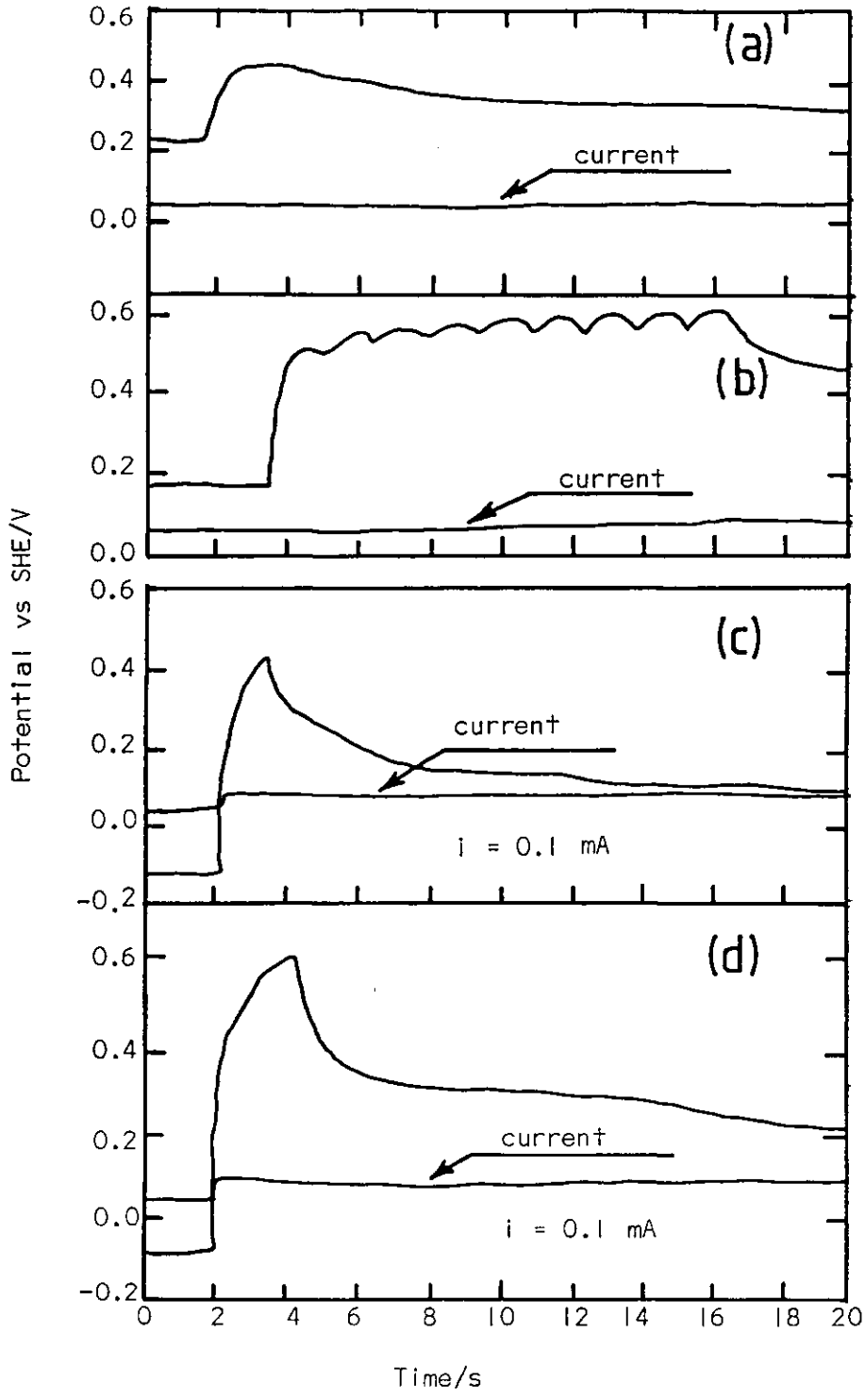

Figure 4.66. The change of pyrite potential and cell current in single and consecutive contacts with a Pt feeder electrode at a) 0.5 V, b) 0.75 V, c) 1.0 V, d) 1.25 V. i = the change in current

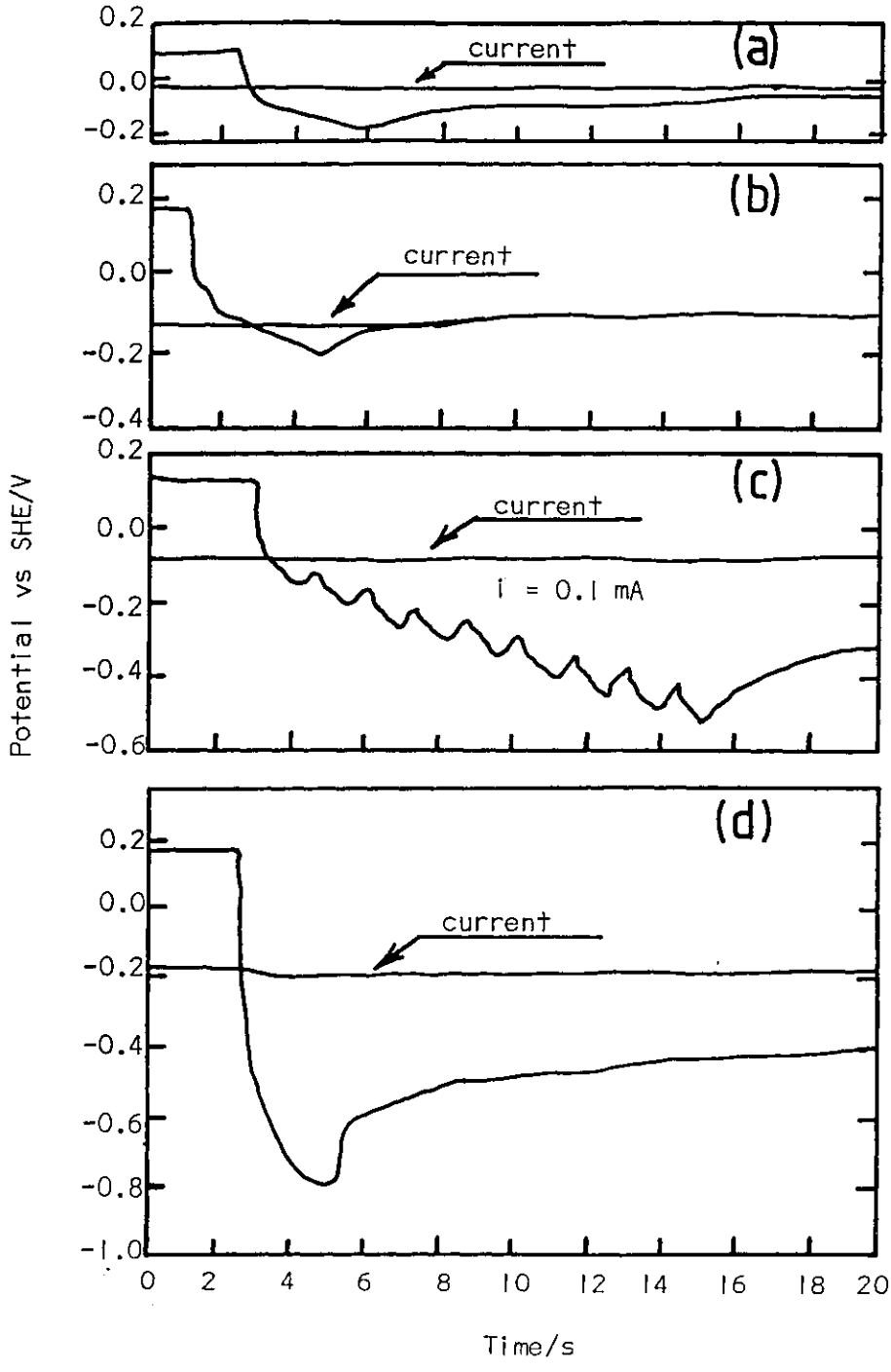

Figure 4.67. The change of pyrite potential and cell current in single and consecutive contacts with a Pt feeder electrode at a) -0.5 V, b) -1.0 V, c) -1.0, d) -1.5 V. i = the change in current

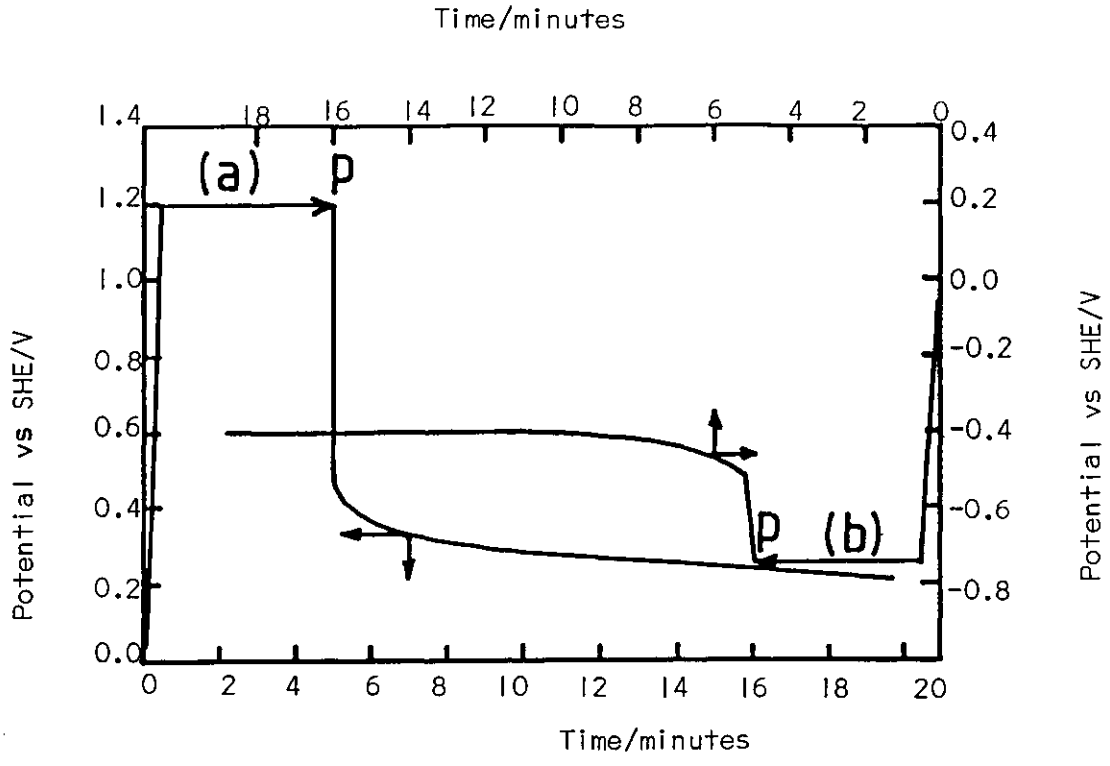

Figure 4.68. The change of galena potential during contact with and following separation from a Pt feeder electrode, polarised at a) 1.2 V, b) -0.75 V, electrodes were separated at p

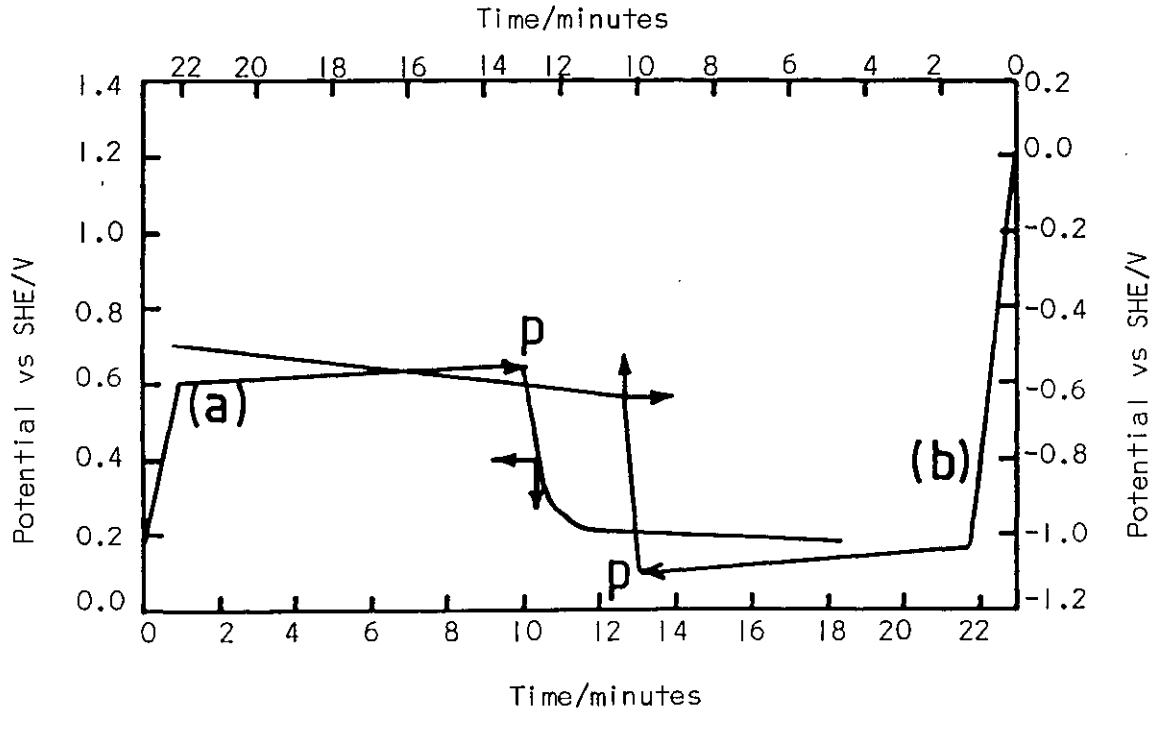

Figure 4.69. The change of pyrite potential during contact with and following separation from a Pt feeder electrode polarised at a) 0.75 V, b) -1.5 V. Electrodes were separated at p

Reduction of galena at < -0.75 V gave a final rest potential about -0.4 V and H_2S was detected by its smell, indicating a PbS/Pb phase transformation by reaction k. No such potential limit was observed with pyrite. This could mean that the increase in the flotation recovery of galena with cathodic reduction at pH I and 6.89 (figure 4.54 and 4.55) was due to the formation of lead on the galena surface, since in acidic solutions lead was found to be highly oleophilic by contact angle measurements (figure 4.22). However, the discrepancy at pH 6.89 is not understood.

The results of contact potential measurements indicate that the chemistry and physics of particle/electrode collision is important, i.e. the mineral particles should have a certain amount of energy for charging in a particulate bed electrode. It seems that the charging of galena particles should be easier than pyrite, which means that the chemistry of metal/mineral sulphide or oxide formation is also important.

CHAPTER FIVE

CONCLUSIONS

1 Both unoxidised galena and pyrite were oleophilic but hydrophilic with respect to gas bubbles.

2 The recovery of unoxidised galena at the oil/water interface was a maximum at pH 5.5 where almost 100% recovery was obtained. However, with increase and decrease of pH recovery decreased to about 70%.

3 A maximum contact angle at an unoxidised galena/oil/water interface was obtained at pH 5.5 ($\theta_{Ad} = 70^{o}$) where maximum flotation recovery was also obtained.

4 The oxidation of galena at the natural pH (5.5-6.5) reduced the recovery due to the formation of $Pb(OH)_2$ on the surface. The recovery was a minimum in neutral solutions, and increased with increasing or decreasing pH. The increase in alkaline solutions was due to the removal from the surface of $Pb(OH)_2$ as $HPbO_2^-$, whereas in acidic solutions it was due to the removal of $Pb(OH)_2$ as Pb^{2+}, as well as to the presence of sulphur formed by oxidation.

5 Contact angles measured at oxidised galena/oil/water interfaces were in agreement with the two-liquid flotation results. The contact angle was 0^{o} in neutral solutions and increased with decreasing or increasing pH.

6 The recovery of unoxidised pyrite at the oil/water interface was a maximum in the pH range 6.5-9.5, where 90% recovery was obtained. The recovery showed a minimum around pH 4 and increased again in acid solutions. The decrease in the recovery above pH 9.5 was due to the formation of $Fe(OH)_2$ on the surface. The minimum in the recovery around

pH 4 was attributed to the adsorption of solution ferric hydroxide species on the surface. With further decrease of pH below 3, the recovery increased again because ferric hydroxide does not form and/or S^{o} forms.

7 Oxidation at the natural pH decreased the recovery of pyrite, giving higher recoveries below pH 5.5. The increase in the recovery at lower pH values was due to the removal of $Fe(OH)_3$ from the surface as Fe^{3+}, as well as to the presence of sulphur formed by oxidation. The recovery of oxidised pyrite did not increase in alkaline solutions as with galena, because the $Fe(OH)_3$, the oxidation product of pyrite, was stable.

8 The results of contact angle measurements at unoxidised and oxidised pyrite/oil/water interfaces were as expected from the two-liquid flotation results. With unoxidised pyrite, the contact angle showed a maximum ($\theta_{Ad} = 90^{o}$) around pH 7 decreasing in alkaline solutions, whereas in acidic solutions it showed a minimum around pH 4 and increased again at lower pH values. The contact angle was 0^{o} with oxidised pyrite at pH > 6, but increased at lower pH values.

9 Suspensions of both galena and pyrite were reasonably stable at pH values where maximum recovery of minerals was obtained at the oil/water interface. Therefore, the recovery was not due to the entrapment of oil drops.

10 No direct relation was obtained between the interfacial tensions of various oil/water/ interfaces and the contact angle at the mineral/oil/water interface. However, pyrite gave larger contact angles.

11 Oxidation of galena in acidic solutions below pH 5 occurred by

$$Pb^{2+} + S + 2e \rightleftharpoons PbS \qquad (a)$$

$$Eh = 0.354 + 0.0295 \log \left[Pb^{2+}\right]$$

forming sulphur on the surface which increased the oleophilicity of galena.

12 Oxidation of galena in neutral and alkaline solutions occurred by

$$Pb(OH)_2 + S + 2H^{+} + 2e \rightleftharpoons PbS + 2H_2O \qquad (e)$$

$$Eh = 0.765 - 0.059\ pH$$

forming $Pb(OH)_2$ in addition to sulphur, so galena became oleophilic.

13 Lead was oleophilic when it was reduced, except at pH 6.89, and oleophobic when it was oxidised. The oleophilicity decreased with pH, the contact angle becoming zero at pH 6.89, and increased again at higher pH values but not to the same degree as in acidic solutions. The 0^{o} contact angle at pH 6.89, even after reduction of the lead, was due to the formation of a surface layer of $PbHPO_4$ at open circuit.

14 Initial oxidation of pyrite at pH 1 and 4.6 occurred by

$$Fe^{2+} + 2S + 2e \rightleftharpoons FeS_2 \qquad (a')$$

$$Eh = 0.423 + 0.0295 \log \left[Fe^{2+}\right]$$

forming sulphur, which increased the oleophilicity of pyrite. However, with the increase of anodic potential, the oxidation of pyrite at pH 1 occurred by

$$Fe^{2+} + 2SO_4^- + 16H^+ + 14e^- \rightleftharpoons FeS_2 + 8H_2O \qquad (b')$$

$$Eh = 0.367 - 0.067\ pH + 0.008 \log \left[SO_4^{2-}\right] + 0.004 \log \left[Fe^{2+}\right]$$

and at pH 4.6 by

$$Fe(OH)_3 + 2SO_4^{2-} + 19H^+ + 15e \rightleftharpoons FeS_2 + 11H_2O \qquad (f')$$

$$Eh = 0.412 - 0.0749\ pH + 0.0078 \log \left[SO_4^{2-}\right]$$

so the oleophilicity of pyrite decreased.

15 In neutral and alkaline solutions, the oxidation of pyrite occurred by

$$Fe(OH)_3 + 2S + 3H^+ + 3e^- \rightleftharpoons FeS_2 + 3H_2O \qquad (e')$$

$$Eh = 0.64 - 0.059\ pH$$

at lower potentials and at higher potentials by f', forming $Fe(OH)_3$ on the surface, so pyrite becomes oleophilic.

16 Sulphidising the oxidised galena and pyrite with aqueous sodium sulphide solution restored the oleophilicity of these minerals.

17 Freshly ground galena was oleophobic in a particulate bed electrode system. Anodic oxidation did not produce any change, whereas cathodic reduction at pH 6.89 and I produced an increase in oleophilicity, but not at pH 9.2 and II.

18 The recovery of unoxidised/sulphidised galena in a particulate bed electrode system was decreased by anodic oxidation at pH 6.89, 9.2 and II, but increased at pH I due to formation of sulphur. With reduction, recovery decreased at pH 9.2 and II whereas it first decreased then increased at pH 6.89 and I. The increase in recovery with increase of cathodic potential was probably due to the formation of lead, by the reduction of PbS.

19 The only phase change obtained reproducibly with a compacted bed electrode of galena and in contact measurements between a galena electrode and a feeder electrode, was the reduction of PbS to Pb + H_2S at pH 6.89.

20 Change of potential produced no change in the recovery of pyrite in a particulate bed electrode. Unsulphidised pyrite was oleophobic due to the formation of a $Fe(OH)_2$ layer except at pH I, where the oxide layer dissolved and non-oxidative dissolution of pyrite occurred. However, sulphidised pyrite was oleophilic below pH II.

21 Contact potential measurements indicated that, in a particulate bed electrode system, the chemistry of metal/metal sulphide or oxide formation was important as well as the physical conditions, i.e. particle-electrode collision. Charging of galena particles was easier than charging pyrite.

REFERENCES

1 FUERSTENAU, D W, in 'Fine particle processing', vol 1, Edt P Somasundaran, AIME (1980) pp 669-705

2 SHERGOLD, H L and LOFTHOUSE, C H, Proced. XII Int Min Process Congress, Sao Paulo (1977), vol II, pp 28-56

3 CHANDER, S, Trans. Ind. Inst. Met. 31 No 1, February 1978, pp 12-19

4 GAUDIN, A M, Principles of mineral dressing, McGraw-Hill (1939)

5 MOSLEY, R H, 'Technical Conference on Tin, London 1967', Vol 1, pp 79-98, London Int. Tin Council (1968)

6 FALCON, L M, J. South Afr. Ins. Min. Met. Spt. issue, October 1975, p 98

7 BURT, R O, Int. J. Min Processing 2 (1977) pp 219-34

8 BURT, R O, in 'Fine particle processing', edt. P Somasundaran, AIME (1980), vol 2, pp 1359-1375

9 COLLINS, D N and READ, A D, Mineral Sci. Eng. 3 (1971) pp 19-31

10 LAWYER, J E and HOPSTOCK, D M, Mineral Sci. Eng. 6, No 3, July 1974, pp 154-172

11 COHEN, H E and GOOD, J A, Proced. XIth Int. Min. Process. Congr., Cagliari, Italy, 1975, pp 777-793

12 CLARK, N O, Proced. Xth Int. Min. Process. Congr., IMM (1973) p 913

13 THOMTE, W L et al, in 'Milling Methods in Americas', Edt N Arbiter, Gordon and Breach Publishers, NY (1961) p 231

14 HOPSTOCK, D M and COLOMBO, F, in 'Fine particle processing', Vol 2, Edt P Somasundaran, AIME (1980) pp 1242-1260

15 HOPSTOCK, D M, in 'Research Needs in Mineral Processing', Report of workshop, NSF, August 1-3 1975, Edt P Somasundaran and D W Fuerstenau

16 CAVE, J M, High intensity wet magnetic separation for the Brightness Beneficiation of Caolin Clays. The City University, Centre for Information Science, February 1976

17 PRYOR, E J, Mineral Processing, Applied Science Publishers Ltd, London (1974) pp 571-599

18 FUERSTENAU, D W, CHANDER, S and ABOUZEID, A M, 1st Latin American Congr. Min. and Extractive Met., held Aug/Sept 1973, Santiago, Chile

19 US Patent 3.322.275, May 1967

20 OLOFINSKY, N F, NOVIKOVA, V A and BELOU, V I, Xth Int. Min. Process. Congr., IMM, London (1973) pp 926-948

21 REUNIVTSEV, V I and KHOPUNOV, E A, in 'Fine particle processing', Edt P Somasundaran, AIME (1980) vol 2, pp 1325-1341

22 GAUDIN, A M et al, AIME Tech Publ. No 414 (1931)

23 MEHROTRA, S P and KAPUR, P C, Powder Tech. 9 (1974) pp 213-219

24 TRAHAR, W J and WARREN, L J, Int. J. Min. Processing 3 (1976) pp 103-131

25 TRAHAR, W J, Int. J. Min. Processing 8 (1981) pp 289-327

26 REAY, D and RATCLIFF, G A, Can. J. Chem. Engr. 53 (1975) p 481

27 GLEMBOTSKY, V A, 'Flotation', NY 1963

28 WHELAN, P F and BROWN, D J, Trans. IMM 66 (1956) p 181

29 FLINT, L R and HOWARTH, W J, Chem. Engrg. Sci. 26 (1971) 1155-68

30 SCHULZE, H J and GOTTSCHALK, G, 13th Int. Min. Process. Congr., Warshow (1979)

31 DERJAGUIN, B V and DUKHIN, S S, Trans. IMM 70 (1961) pp 221-226

32 MOLEY, T P, in 'Froth Flotation - 50th Anniversary Volume' Edt D W Fuerstenau, AIME, NY (1962) pp 247-257

33 GAUDIN, A M, FUERSTENAU, D W and MIAW, H L, Trans. Can. Ins. Min. Met. 63 (1960), p 668

34 HEMMINGS, C E, Int. J. Min. Process. 5 (1978) 85-92

35 EDWARD, C R, KIPKIE, W B and AGAR, G E, Int. J. Min. Process. 7, (1980) 33-42

36 HEMMINGS, C E, Trans. IMM 89 (1980), pp C113-120

37 KLASSEN, V I and MOKROUSOV, V A, 'An Introduction to the Theory of Flotation', Butterworths, London (1963) p 407

38 BOGDANOV, O S et al, in 'Fine particle processing', Edt P Somasundaran, AIME (1980), Vol 1, pp 706-719

39 PHILIPPOFF, W, Trans. AIME 193, (1952), pp 386-390

40 DERJAGUIN, B V and DUKHIN, S S, Proced. XIIIth Int. Min. Process. Congr. Warshow (1979)

41 COLLINS, G L and JAMESON, G J, Chem. Engr. Sci. 31 (1976), pp 985-991

42 COLLINS, G L and JAMESON, G J, Chem. Engr. Sci. 32 (1977), pp 239-246

43 KIRCHBERG, H and TOPFER, E, Proced. VIIth Int. Min. Process. Congr., Edt N Arbiter, Gordon and Breach Sci. Publ., Inc, (1964) pp 157-168

44 WELCH, A J E, in 'Recent developments in mineral dressing', IMM London (1953) p 387

45 BURTON, T G, Trans. Ins. Chem. Engr. 44 (1966) T37-41

46 LIN, I J, NADIV, S and GRODZIAN, D J M, Min. Sci. Engr. 7, (1975) pp 313-336

47 KOCABAG, D, M.Sc thesis, University of Birmingham, UK (1978)

48 SOMASUNDARAN, P, in 'Research Needs in Mineral Processing', Report of workshop, NSF, Aug 1-3 1975. Edt P Somasundaran and D W Fuerstenau (1976)

49 FUERSTENAU, D W, HARPER, R W and MILLER, J W, Trans. AIME 247 (1970), p 69

50 RINELLI, G and MARABINI, A M, Proced. Xth Int. Min. Process. Congr., London (1973) p 20

51 WARREN, L J, Trans. IMM 84 (1975) p C99

52 WARREN, L J, J. Colloid Interface Sci, 50, (1975) p 307

53 COOKE, S R B, IWASAKI, I and CHOI, H S, Trans AIME 217 (1960), p 76

54 PARKINS, E J and SHERGOLD, H L, in 'Flotation - A M Gaudin Memorial Volume', Edt M C Fuerstenau, AIME, NY (1976) Ch 20, p 561

55 LAAPAS, H, Proced. XIth Int. Min. Process. Congr. Special Vol, Cagliari, Italy (1975) Paper 6

56 KUBOTA, T et al, Proced. XIth Int. Min. Process. Congr., Cagliari, Italy (1975) p 623-637

57 MILLER, J D and ACKERMAN, J B, in 'Fine particle processing', edt P Somasundaran, AIME, NY (1980) Vol I, p 832

58 LAI, R W M, in 'Fine particle processing', Edt P Somasundaran, AIME, NY (1980) Vol I, p 853

59 GREENE, G W, DUKE, J B and HUNTER, J L, US Patent 2.990.958 (1961)

60 GROUNDS, A, Min. & Quarry Engng, March (1964) p 128

61 GREENE, E W and DUKE, J B, Trans AIME 223, (1962) p 389

62 DERYAGIN, V D et al, Colloid J. of USSR (Colloid J - New York) 26 (1964) p 149

63 SAMYAGIN, V D et al, Colloid J. of USSR (Colloid J - New York) 30 (1968) p 435

64 GAUDIN, A M and MALEZEMOF, P, J. Phys. Chem. 37 (1933) pp 597-607

65 MARCADDE, W V, US Patent 3.915.391 (1975)

66 KOH, P T L and WARREN, L J, Trans. IMM 86 (1977) p C94

67 OSBORNE, D G, Trans. IMM 87, (1978) p C189

68 KHAVSKI, N N et al, Proced. XIth Int. Min. Process. Congr. Cagliari, Italy (1975), p 1345

69 JACOBS, H D and COLOMBO, A F, Rep. of Invest. US Bur.of Mines No 8482, 1980

70 THOMPSON, P and HULATT, J L, Rep. of Invest. US Bur.of Mines No 8516, 1981

71 ARFUNS, J F and KITCHENER, J A, Trans. IMM 86 (1977) p C9

72 GLEMBOTSKY, V A et al, Proced. XIth Int. Min. Process. Congr., Cagliari, Italy (1975), p 561-582

73 HOGAN, P, KUHN, A T and WILLS, B A, Camborne School of Mines J, 76, 1976, 48-54

74 GORODETSKII, M I et al, Xth Int. Min. Process. Congr. 1973, IMM, London (1973), p 689

75 HOGAN, P, KUHN, A T and TAYLOR, J F, Trans IMM 88, 1979, p C83

76 KUHN, A, Chemical Processing, 20, June 1974, p9

77 HOGAN, P and KUHN, A T, Oberflache - Surface 18, Oct 1977, 255-60

78 CIENSKI, T and COFFIN, V, Proced. 13th Annual Meeting of the Canadian Mineral Processors, Jan 1981, Paper 13

79 NARASIMHAN, K S, RAO, S B and CHAUDHURY, G S, Engineering and Mining J. 84, May 1972, p 84-85

80 BOUTIN, P and WHEELER, D A, Can.Min. J. 94, March 1967

81 SASTRY, K V S and FUERSTENAU, D W, Trans. AIME, 247 (1970), p 46

82 Reference 37, p 118

83 REAY, D and RATCLIFF, G A, Can. J. Chem. Engr. 51, April 1973, p 178

84 ZABEL, T, in 'The Scientific basis of flotation, Part 2', NATO Advanced Study Institute, 5-16 July 1982, Cambridge, England

85 NEIS, U and KIEFHABER, K P, in 'Fine particle processing', Edt P Somasundaran, AIME, NY (1980) Vol 1, p755

86 HAHN, H H, in 'Scientific Basis of Flotation, Part 2', NATO Advanced Study Institute, 5-16 July 1982, Cambridge, England

87 SAAVEDRA, J A S, Ph.D thesis, University of London (1980)

88 FAHRANWALD, A W, Mining Congress J. 43, August (1957) pp 72-4

89 KARJALAHTI, K, Trans. IMM 81, (1972), pp C219-226

90 GATES, E H, Trans. AIME, 208, 1957, pp 1368-1372

91 RUNOLINNA, U, RINNE, R and KURRONEN, S, 5th Int. Min. Process. Congr., IMM, London (1960), pp 447-475

92 LEPIDOT, M and MELLGREN, D, Trans. IMM 77 (1968) pp C149-165

93 GUTIEREZ, C, Trans. SME/AIME 262 (1977) pp 254-262

94 LI, K, LIVINGSTON, R W and LAMKE, L K, Trans. IMM 70, (1960-61), pp 19-31

95 McCARROLL, S J, Trans. AIME, Mining Engnr 6 (1-6) (1954), pp 289-93

96 KIHLSTEDT, P G, Proced. in Min. Process., Trans. Int. Min. Process. Congr., Stockholm (1957) p 559

97 MILLIKEN, F R, Trans. AIME, 183, (1949) pp 101-114

98 HOOVER, R M and MALHOTRA, D, in 'Flotation - A M Gaudin Memorial Volume', Edt M C Fuerstenau, AIME, NY (1976), Vol 1, p 485

99 LOWVER, J E and COOK, C C, Trans AIME 268 (1980), pp 1787-1801

100 BAARSON, R E, RAY, C L and TREWEEK, H B, in 'Froth Flotation - 50th Anniversary Volume', Edt D W Fuerstenau, AIME, NY (1962) pp 427-453

101 WANG, Y H C and SOMASUNDARAN, P, in 'Fine particle processing', Edt P Somasundaran, AIME, NY (1980), Vol 2, Ch 57, p 1112

102 READ, A D and HOLLICK, C T, Minerals Sci. Engng. 8, 3(1976), p 202

103 READ, A D, Trans IMM 80 (1971), C24-31

104 FRIEND, J P, ISKRA, J and KITCHENER, J A, Trans. IMM 82, (1973), C235-239

105 PUGH, R J and KITCHENER, J A, J. Colloid and Interface Sci. 35, (1971) pp 656-664

106 SLATER, R W, CLARK, J P and KITCHENER, J A, VIIIth Int. Min. Process. Congr., Leningrad (1968) C-5

107 FRIEND, J P and KITCHENER, J A, Chem. Engng. Sci. 26 (1973) 1071-80

108 YARAR, B and KITCHENER, J A, Trans. IMM 79 (1970), pp C23-33

109 FRIEND, J P and KITCHENER, J A, Filtration and Separation, vol 9, No 1, (1972) pp 25-28

110 SOMASUNDARAN, P, in 'Fine particle processing', Edt. P Somasundaran, AIME, NY (1980), vol 2, p 947

111 READ, A D and WHITEHEAD, A, Xth Int. Min. Process. Congr., IMM, London (1973), p 949-957

112 USONI, L, GRINELLI, G and MARABINI, A M, VIIIth Int. Min. Process. Congr., Leningrad (1968), D-13

113 DRZYMALA, J and FUERSTENAU, D W, Int. J. Min. Process. 8, (1981), 265-277

114 ATTIA, Y A I, and KITCHENER, J A, Proced. XIth Int. Min. Process. Congr., Cagliari, Italy (1975), p 1233-1248

115 APPLETON, E A et al, J. South Afr. Inst. Min. Met. Oct 1975, p 117

116 CLAUSS, C R A, APPLETON, E A and VINK, J J, Int. J. Min. Process. 3 (1976), 27-34

117 RUBIO, J and KITCHENER, J A, Trans. IMM 86 (1977) pp C97-100

118 SOMASUNDARAN, P, Information Circular 8818, US Bureau of Mines

119 BURURAJ, B et al, Proced. 13th Int. Min. Process. Congr., Warshow (1979), p 447

120 COLOMBO, A F, in 'Fine particle processing', Edt. P Somasundaran, AIME, NY (1980), Vol 2, p 1034

121 Tilden based on processing breakthrough, Engr. & Mining J., Nov 1974, pp 140-142

122 PAANANEN, A O and TURCOTTE, W A, Mining Engr, SME/AIME, August 1980, p 1244

123 KUZNETSOV, V P et al, Proced. 13th Int. Min. Process. Congr., Warshow 1979, p 370

124 EIGELES, M A et al, Proced. XIth Int. Min. Process. Congr., IMM, London (1973), p 42

125 SADOWSKI, Z and LASKOWSKI, J, in 'Fine particle processing', Edt P Somasundaran, AIME, NY (1980) Vol 2, p 1083

126 KITCHENER, J A, Chemistry and Industry, Jan 1975, p 54

127 BECHER, P, 'Emulsions: Theory and Practice', Reinhal Publ. Corp, New York (1965), p 260-61

128 SCHULMAN, J H and LEJA, J, Trans. Faraday Soc., 50, (1954), p 598

129 GOOLD, L A et al, J. South Afr. Ins. Min. Met., October 1975, p 132

130 FARNAND, J R, SMITH, H M and PUDDINGTON, I E, Can. J. Chem. Engng, April (1961), p 94

131 MULAR, A L and PUDDINGTON, I E, CIM Bulletin, June 1968, p 726

132 SIRIANNI, A F, CAPES, C E and PUDDINGTON, I E, Can. J. Chem. Engng. 47, (1969), p 166

133 PUDDINGTON, I E and SPARKS, B O, Min. Sci. Engng. 7, No 3, (1975), p 282

134 FINKELSTEIN, N P, 'Beneficiation of mineral fines - problems and research needs', Edts P Somasundaran and N Arbiter, AIME (1979) Ch 30, p 331

135 BHATTACHARYYA, R N, MOZA, A K and SARKAR, G G, in 'Agglomeration 77', Edt Sastry, K V S, AIME (1977) p 931

136 SWANSON, A R et al, Reference 135, p 939

137 KAVOURIDIS, C B, SHERGOLD, H L and AYERS, P, Trans. IMM 90, (1981), p C53

138 FARNAND, J R and PUDDINGTON, I E, CIM Bulletin, March 1969, p 267

139 FARNAND, J R et al, CIM Bulletin, Dec 1969, p 1327

140 SIRIANNI, A F et al, CIM Bulletin, June 1968, p 731

141 FARNAND, J R et al, Can. Met. Quarterly 3, No 2, 1964, p 123

142 MEADUS, F W et al, CIM Bulletin, August 1966, p 968

143 SPARKS, B D and WONG, R H T, CIM Bulletin, January 1973, p 73

144 MEADUS, R W and PUDDINGTON, I E, CIM Bulletin, June 1973, pp 123-126

145 MEADUS, F W et al, CIM Bulletin, 61 (1968), p 736

146 NICOL, S K, BENSLEY, C N and SWANSON, A R, Trans. IMM 86, 1977, p C92

147 RAO, T C, MANANGAMUOI, M and RAO, K H, Int. J. Min. Process. 9, 1982, 235-248

148 MELLGREN, O and SHERGOLD, H L, Trans. IMM 75, 1966, pp 267-268

149 TAKAKUWA, T and TAKAMORI, T, Proced. 6th Int. Min. Process. Congr., Cannes (1963), p 1

150 SHERGOLD, H L, Industrial Minerale - Minèralugie, 3, 1976, 192-205

151 STRATTON-CRAWLEY, R, in 'Beneficiation of mineral fines, problems and research needs', Edts P Somasundaran and A Arbiter, AIME (1979), Ch 29, p 317

152 SHERGOLD, H L and MELLGREN, O, Trans IMM, 78, 1969, p C121

153 SHERGOLD, H L and MELLGREN, O, Trans. SME/AIME, 247, 1970, p 149

154 LAI, R W M and FUERSTENAU, D W, Trans. SME/AIME, 241, 1968, p 549

155 RAGHAVAN, S and FUERSTENAU, D W, AIChE Symp. Series, 71, No 150 (1975), p 59

156 COLEMAN, R D, SUTHERLAND, J P and CAPES, C E, J. Appl. Chem. 17, 1967, p 89

157 ZAMBRANA, G Z et al, Int. J. Min. Process. 1, (1974) 335-345

158 YAP, S N, Ph.D thesis, Colorado School of Mines, May 1975

159 OLIVER, J P, US Patent 3.432.030 (1969)

160 STRATTON-CRAWLEY, R and SHERGOLD, H L, Colloids and Surfaces 2 (1981), 145-154

161 SHERGOLD, H L and STRATTON-CRAWLEY, R, Colloids and Surfaces 3 (1981), 253-265

162 APPLETON, E A, M.Sc thesis, University of Natal, South Africa (1973)

163 FINCH, J A and SMITH, G H, Min. Sci. Engng. 11, No 1, January 1979, p 36

164 VOYUTSKY, S, 'Colloid Chemistry', MIR Publ, Moscow 1978, p 171

165 GAUDIN, A M and MIAW, H L and SPEDDEN, H R, 2nd Int. Congr. of Surface Activity (1957), vol 2, p FS-451

166 FOWKES, F M, Ind. Engng. Chem. 56, No 12, Dec 1964, p 40

167 FOWKES, F M, A. Chem. Soc., Adv. in Chem. Seri. 43, 1964, p 99

168 MACKENZIE, J M W, Trans. SME/AIME 244, 1969, p 393

169 ARBITER, N et al, AIChE Symp Series 71, No 150, 1975, 176-182

170 LASKOWSKI, J and KITCHENER, J A, J. Colloid and Interface Sci. 29, No 4, 1969, p 670

171 FINKELSTEIN, N P et al, AICHE Symp Series 71, No 150, 1975, p 165

172 RAO, S R, Min. Sci. Engng. 6 No 1 (1974) p 45

173 KLASSEN, V I and MAKROUSOV, V A, 'An introduction to the theory of flotation', Butterworths, London (1963), pp 39-65

174 READ, A D and KITCHENER, J A, Society of chemical industry, Monograph No 25 (1967), pp 300-313

175 READ, A D and KITCHENER, J A, J. Colloid and Interface Sci., 30, 1969, p 391

176 SOMASUNDARAN, P, AIChE Symp. Series 71, No 150 (1975), p 1

177 ONODA, G Y and DE BRUYN, P L, Surface Science 4 (1966) 48-63

178 BOEHM, H P, Adv. Catal. Related Subjects 16 (1966) p 179

179 GRIOT, O and KITCHENER, J A, Trans. Faraday Soc. 61 (1965), p 1026

180 EVANS, R C, 'An introduction to crystal chemistry', 2nd ed, Cambridge University Press, 1979, p 157

181 PASHLEY, R M and KITCHENER, J A, J. Colloid and Interface Sci. 71 (1979), p 491

182 MELLGREN, O et al, Proced. XIth Int. Min. Process. Congr., IMM, London 1973, p 451-472

183 ZIZMAN, W A, Am. Chem. Soc., Advances in Chem. Series 43 (1964), pp 1-51

184 HUNTER, R J, 'Zeta potential in colloid science - principles and applications', Academic Press, 1981, pp 17-18

185 FUERSTENAU, D W, US Bureau of Mines Information Circular 8818 (1980), p 35-62

186 LAI, R W and FUERSTENAU, D W, Trans. SME/AIME 260 (1976), p 104

187 TADROS, T F and LYKLEMA, J, J. Electroanalytical Chem. and Interfacial Chem. 17, 1968, p 267

188 SHERGOLD, H L, in 'Scientific basis of flotation, Part 2', NATO Advanced Study Institute, 5-16 July (1982), Cambridge, England

189 FREYBERGER, W L and DE BRUYN, P L, J. Phys. Chem. 61 (1957), p 586

190 IWASAKI, I and DE BRUYN, P L, J. Phys. Chem. 62 (1958), p 594

191 HEALY, T W and MOIGNARD, M S, in 'Flotation - A M Gaudin Memorial Vol, Vol 1, AIME (1976) Ch 9, p 275

192 PARKS, G A, Am. Chem. Soc. - Advanced in Chem. Series, 67, (1967), p 121

193 DERJAGUIN, B, Faraday Soc. Trans. 36 (1940), p 203-215

194 DERJAGUIN, B V and SHUKAKIDSE, N D, Trans. IMM 70 (1961), p 569-574

195 MUSHIAKE, K, IMAIZUMI, T and INOUE, T, Proced. XIth Int. Min. Proces. Congr., Cagliari, Italy (1975), pp 405-425

196 BLAKE, T D and KITCHENER, J A, J. Chem. Soc., Faraday Trans - 1, 68, (1972) p 1435

197 CHANDER, S and FUERSTENAU, D W, Trans. AIME 252 (1972) pp 62-69

198 LUCASSEN-REYNDERS, E H and LUCASSEN, J, in 'The Scientific basis of flotation, Part I', NATO Advanced Study Institute, 5-16 July (1982), Cambridge, England

199 McCAFFERTY, E and ZETTLEMOYER, A C, Discussions of Faraday Soc. No 52 (1971), p 239

200 PAULING, L, Mineral. Soc. Amer., Spec. Pap 3 (1970), pp 125-131

201 HOBERG, H and SCHNEIDER, F U, Proced. XIth Int. Min. Proces. Congr., Cagliari, Italy (1975) p 468-492

202 BOGDANOV, D S et al, XIIth Int. Min. Process. Congr., Sao Paulo, Brazil, 28 Sept 1977, Meeting 7

203 BHATTACHARYYA, D et al, AIChE. Symp. Series 77 No 209 (1980)

204 SATO, M, Economic Geology 35 (1960), p 1202-1231

205 SATO, M and MOONEY, H M, Geophysics 25, No 1 (1960), 226-240

206 SATO, M, Electrochimica Acta 11 (1966), 361-373

207 VAUGHAN, D J and CRAIG, J R, Mineral Chemistry of Metal Sulphides, Cambridge Univ. Press (1978)

208 SHUEY, R T, 'Semiconducting ore minerals', Elsevier Sci. Publ. Camp. (1975)

209 POMIANOWSKI, A and CZARNECKI, J, J. Colloid and Interface Sci. 47, No 2, (1974), p 315

210 MEHTA, A P and MURR, L E, presented at the SME/AIME Meeting, Dallas, Texas, Feb 14-18 1982

211 GARDNER, J R and WOODS, R, Int. J. Min. Process. 6 (1979) 1-16

212 WOODS, R, in 'Flotation - A M Gaudin Memorial Vol, Vol 1, Edt M C Fuerstenau, AIME, NY (1976), p 298-333

213 HAMILTON, I C and WOODS, R, J. Electroanal. Chem. 118 (1981), pp 327-344

214 GAUDIN, A M, 'Flotation', McGraw-Hill Book Comp (1932), p 165 and 198

215 TAGGART, A F, DELGUIDICE, G R M and ZIEHL, D A, Trans. AIME 112 (1934) pp 348-381

216 SUTHERLAND, K L and WARK, I W, 'Principles of flotation', Aust. IMM (1955) p 104

217 HERD, H H and URE, W, J. Phys. Chem. 45 (1941), p 93-106

218 RANITZ, S F, Trans. AIME 153 (1943) p 528

219 PLAKSIN, I, Mining Engineering 11 (1-6) (1959) pp 319-324

220 STEWART, B V, NIM Report 1587 (1973)

221 FUERSTENAU, M C and SABACKY, B J, Int. J. Min. Process. 8 (1981) 79-84

222 LEPETIC, V M, CIM Bulletin, June (1974) p 71

223 HAYES, G W and TRAHAR, W J, Int. J. Min. Process. 4 (1977), 317-344

224 GARDNER, J R and WOODS, R, Int. J. Min. Process. 6 (1979) 1-16

225 YOON, R H, Int. J. Min. Process. 8 (1981) 31-48

226 HANNA, H S and SOMASUNDARAN, P, in 'Flotation - A M Gaudin Memorial Vol, Vol 1, Edt. M C Fuerstenau, AIME (1976) p 197-272

227 BOCKRIS, J O'M and REDDY, A K N, 'Modern Electrochemistry, Vol 2', Macdonald, London (1970) Ch 7, pp 623-634

228 SHERGOLD, H L, Ph.D thesis, University of London (1968)

229 MEITES, L and MEITES, T, Anal. Chem. 20 (1948) 984-985

230 GADDUM, J H, Proced. Roy. Soc. B109 (1931) pp 114-125

231 HARKINS, W D, in 'Physical Methods of organic chemistry', Part I, 2nd ed, Edt E Weissberger, Interscience Publ. Inc. NY (1949) p 374

232 BRODIE, J B, M.Sc thesis, University of British Colombia, March 1969

233 WOODS, R, J. Phys. Chem. 75, No 3 (1971), p 354

234 SATO, M, Electrochimica Acta 11 (1966) pp 361-373

235 RAND, D A J, J. Electroanal. Chem. 83 (1977) 19-32

236 WOODS, R, Proced. Aust. Ins. Min.Met. No 241, March 1972, p 53

237 PETERS, E, in 'Trends in Electrochemistry', Edts J O'M Bockris, D A J Rand and B J Welch, Plenum Press, NY (1977) p 267

238 MAJIMA, H, VIIIth Int. Min. Process. Congr. Leningrad (1968) E-1

239 SCOTT, P D and NICOL, M H, in 'Trends in Electrochemistry', Edts J O'M Bockris, D A J Rand and B J Welch, Plenum Press, NY (1977) p 303

240 BIEGLER, T, RAND, D A J and WOODS, R, J. Electroanal. Chem. 60 (1975) 151-162

241 BIEGLER, T, J. Electroanal. Chem. 70 (1976) 265-275

242 BIEGLER, T, RAND, D A J and WOODS, R, in 'Trends in Electrochemistry', edts J O'M Bockris, D A J Rand and B J Welch, Plenum Press, NY (1977), pp 267-90

243 POURBAIX, M, 'Atlas of Electrochemical Equilibria', Pergamon Press, London 1966

244 GARRELS, R M and CHRIST, C L, 'Solution Minerals and Equilibria', Harper and Row, New York 1965

245 PETERS, E, Metal Trans. AIME 7B, Dec 1976, p 505

246 SALAMY, S G and NIXON, J C, in 'Recent Developments in Mineral Processing', IMM (1953) pp 503-516

247 TOLUN, R and KITCHENER, J A, Trans. IMM 72 (1963-64) 313-322

248 USUL, A H and TOLUN, R, Int. J. Min. Process. 1 (1974) 135-140

249 HO, F C and CONWAY, B E, J. Colloid. Interface Sci. 65 (1978) pp 19-35

250 GARDNER, J R and WOODS, R, J. Electroanal. Chem. 100 (1979) pp 447-460

251 PAUL, R L and NICOL, M J et al, Electrochimica Acta 23 (1978) 625-633

252 NICOL, M J and PAUL, R L and DIGGLE, J W, Electrochimica Acta 23 (1978) 635-639

253 CONWAY, B E and KU, J C and HO, F C, J. Colloid and Interface Sci. 75 (1980) p 357

254 POWER, G P, Aust. J. Chem. 34 (1981) 2287-96

255 CHANDER, S and FUERSTENAU, D W, Proced. XIth Int. Min. Process. Congr., Cagliari, Italy (1975) p 584-604

256 GARDNER, J R and WOODS, R, Aust. J. Chem. 27 (1974), 2139-2148

257 CHANDER, S and FUERSTENAU, D W, Trans. SME/AIME 258 (1975) p 284

258 GARDNER, J R and WOODS, R, Aust. J. Chem. 26 (1973) 1635-1644

259 NATARJAN, K A and IWASAKI, I, Trans. SME/AIME 252 (1972) p 438

260 ONUCHUKWU, A, Electrochimica Acta 27 No 4 (1982) 529-533

261 HEADRIDGE, J B, 'Electrochemical Techniques for Inorganic Chemists', Academic Press, London 1969, Ch 5, pp 42-49

262 SAWYER, D T and ROBERTS, J L, 'Experimental Electrochemistry for Chemists', John Wiley & Sons (1974) Ch 7, pp 329-394

263 JOHNSON, J W et al, J. Applied Electrochemistry 8 (1978) 25-32

264 BIEGLER, T and SWIFT, D A, J. Applied Electrochemistry 9 (1979) 545-554

265 PAUL, R L et al, NIM Report No 1878 (1977)

266 GHALI, E and DANDAPANI, B, J. Applied Electrochemistry 10 (1980) 335-344

267 RICHARDSON, P E and MAUST, E E, in 'Flotation - A M Gaudin Memorial Volume', Vol 1, AIME (1976) pp 364-392

268 MICHELL, D and WOODS, R, Aust. J. Chem. 31 (1978) 27-34

269 JANETSKI, N D, WOODBURN, S I and WOODS, R, Int. J. Min. Process. 4 (1977) 227-239

270 YARAR, B, Ph.D thesis, Imperial College, London 1969

271 YUCESOY, A and YARAR, B, Trans. IMM 83 (1974) p C96-100

272 FUERSTENAU, M C, KHUN, M C and ELGILLANI, D A, Trans. SME/AIME, June 1968, p 148

273 Reference 214, pp 163-165

274 STRATTON-CRAWLEY, R, Ph.D thesis, University of London, 1977

275 HUH, C and MASON, S G, J. Colloid and Interface Sci. 60 (1977) 11-38

276 GAUDIN, A M et al, Proced. VIth Int. Min. Process. Congr., Pergamon Press (1963) p 527

277 WALKER, G W et al, Unpublished work

278 ALLISON, S A, NIM Report 1597, Jan 1974

279 AHMED, S M, Int. J. Min. Process. 5 (1978) 163-174

280 FUERSTENAU, D W and MISHRA, R K, in 'Complex sulphide ores', IMM, London (1980) p 271

281 PETERS, E and MAJIMA, H, Can. Met. Quart. 7 No 3 (1968) p 111

282 SATO, M, Economic Geology 55 (1960) 928-961

283 SEIDELL, A, 'Solubilities of Inorganic and Metalorganic Compounds', D van Nostrand Comp Inc, NY (1940) p 1383

284 BAILEY, L K and PETERS, E, Can. Met. Quart. 15, No 4 (1976) p 333

285 BIEGLER, T and SWIFT, D A, Electrochimica Acta 24 (1979) 415-420

286 ANGERSTEIN-KOZLOWSK, H, CONWAY, B E and SHARP, W B A, J. Electroanalytical Chem. and Interfacial Chem. 43, (1973), 9-36

287 MITROFANOV, S I, in 'Progress in Mineral Processing, Trans. IMPC, Stockholm (1957)', Almquist & Wiksell, Stockholm (1958) p 441

288 GARDNER, J R and WOODS, R, Aust. J. Chem. 30 (1977) 981-91

289 BHASKAR RAJU, G and KHANGAONKAR, P R, Int. J. Min. Process. 9 (1982) 133-143

290 DERJAGUIN, B V and CHUREAV, N V, J. Colloid Interface Sci. 49, No 2 (1974) p 249

291 'Comprehensive Inorganic Chemistry', vol 2, Edts J C Bailar et al, Pergamon Press, 1973, p 130-132

292 STEPHEN, H and STEPHEN, T, 'Solubility of Inorganic and Organic Compounds', Vol 1, Part 1, p 321, Pergamon Press (1963)

293 LATIMER, W M 'Oxidation potentials', 2nd ed, Prentice-Hall Inc. (1956)

294 AWAD, S A and ELHADY, Z A, J. Electroanal. Chem. 20 (1969) 79-87

APPENDIX I

Electrode reactions of the Pb-S-H_2O system

Electrode potentials were calculated using thermodynamic data given by Garrels and Christ[244] and by Latimer.[293]

a) $Pb^{2+} + S + 2e \rightleftharpoons PbS$

$Eh = 0.354 + 0.0295 \log [Pb^{2+}]$

b) $PbSO_4 + 8H^+ + 8e \rightleftharpoons PbS + 4H_2O$

$Eh = 0.289 - 0.059\ pH$

c) $SO_4^{2-} + 8H^+ + 6e^- \rightleftharpoons S + 4H_2O$

$Eh = 0.357 - 0.0788\ pH$

d) $PbO + S + 2H^+ + 2e^- \rightleftharpoons PbS + H_2O$

$Eh = 0.732 - 0.059\ pH$

e) $Pb(OH)_2 + S + 2H^+ + 2e^- \rightleftharpoons PbS + 2H_2O$

$Eh = 0.765 - 0.059\ pH$

f) $2PbO + S_2O_3^{2-} + 10H^+ + 8e \rightleftharpoons 2PbS + 5H_2O$

$Eh = 0.542 - 0.0737\ pH + 0.007 \log [S_2O_3^{2-}]$

g) $2Pb(OH)_2 + S_2O_3^{2-} + 10H^+ + 8e \rightleftharpoons 2PbS + 7H_2O$

$Eh = 0.61 - 0.074\ pH + 0.007 \log [S_2O_3^{2-}]$

h) $2HPbO_2^- + S_2O_3^{2-} + 12H^+ + 8e \rightleftharpoons 2PbS + 7H_2O$

$Eh = 0.82 - 0.0885\ pH + 0.007 \log [S_2O_3^{2-}]$

i) $2SO_4^{2-} + 10H^+ + 6e \rightleftharpoons S_2O_3^{2-} + 5H_2O$

$Eh = 1.60 - 0.098\ pH + 0.019 \log [SO_4^{2-}] - 0.009 \log [S_2O_3^{2-}]$

j) $S + 2H^+ + 2e \rightleftharpoons H_2S$

$Eh = 0.1418 - 0.059\ pH - 0.0295 \log [H_2S]$

k) $PbS + 2H^+ + 2e \rightleftharpoons Pb + H_2S$

$Eh = -0.338 - 0.059\ pH - 0.0295 \log [H_2S]$

l) $Pb^{2+} + 2e \rightleftharpoons Pb$

$Eh = -0.126 + 0.0295 \log [Pb^{2+}]$

m) $PbO + 2H^+ + 2e \rightleftharpoons Pb + H_2O$

$Eh = 0.313 - 0.059\ pH$

n) $S + H^+ + 2e \rightleftharpoons HS^-$

$Eh = 0.065 - 0.0295\ pH - 0.0295 \log [HS^-]$

o) $PbS + H^+ + 2e \rightleftharpoons Pb + HS^-$

$Eh = -0.575 - 0.0295\ pH - 0.0295 \log [HS^-]$

p) $PbO + H_2O = HPbO_2^- + H^+$

$\log [HPbO_2^-] = -14.32 + pH$

q) $Pb(OH)_2 + 2H^+ + 2e \rightleftharpoons Pb + 2H_2O$

$Eh = 0.277 - 0.059\ pH$

APPENDIX II

Electrode reactions of the Fe-S-H_2O system

Electrode potentials were calculated using thermodynamic data from Garrels and Christ[244] and from Latimer.[293]

a') $Fe^{2+} + 2S + 2e \rightleftharpoons FeS_2$

$Eh = 0.423 + 0.0295 \log [Fe^{2+}]$

b') $Fe^{2+} + 2SO_4^{2-} + 16H^+ + 14e \rightleftharpoons FeS_2 + 8H_2O$

$Eh = 0.367 - 0.067\ pH + 0.008 \log [SO_4^{2-}] + 0.004 \log [Fe^{2+}]$

c') $Fe^{3+} + e \rightleftharpoons Fe^{2+}$

$Eh = 0.771 + 0.059 \log [Fe^{3+}] - 0.059 \log [Fe^{2+}]$

d') $Fe(OH)_3 + 3H^+ + e \rightleftharpoons Fe^{2+} + 3H_2O$

$Eh = 1.056 - 0.177\ pH - 0.059 \log [Fe^{2+}]$

e') $Fe(OH)_3 + 2S + 3H^+ + 3e \rightleftharpoons FeS_2 + 3H_2O$

$Eh = 0.64 - 0.059\ pH$

f') $Fe(OH)_3 + 2SO_4^{2-} + 19H^+ + 15e \rightleftharpoons FeS_2 + 11H_2O$

$Eh = 0.412 - 0.0749\ pH + 0.0078 \log [SO_4^{2-}]$

g') $Fe(OH)_3 + S + 3e \rightleftharpoons FeS + 3OH^-$

$Eh = 0.398 - 0.059\ pH$

h') $Fe(OH)_3 + H^+ + e \rightleftharpoons Fe(OH)_2 + H_2O$

$Eh = 0.271 - 0.059\ pH$

i') $Fe(OH)_2 + SO_4^{2-} + 6H^+ + 2e \rightleftharpoons FeS_2 + 6H_2O$

$Eh = 1.80 - 0.177\ pH + 0.0295\ \log\ [SO_4^{2-}]$

j') $S + 2H^+ + 2e \rightleftharpoons H_2S$

$Eh = 0.1418 - 0.059\ pH - 0.0295\ \log\ [H_2S]$

k') $FeS_2 + 4H^+ + 2e \rightleftharpoons Fe^{2+} + 2H_2S$

$Eh = -0.106 - 0.118\ pH - 0.059\ \log\ [H_2S] - 0.0295\ \log\ [Fe^{2+}]$

l') $FeS_2 + 2H^+ + 2e \rightleftharpoons FeS + H_2S$

$Eh = -0.133 - 0.059\ pH - 0.0295\ \log\ [H_2S]$

m') $FeS_2 + H^+ + 2e \rightleftharpoons FeS + HS^-$

$Eh = -0.423 - 0.0295\ pH - 0.0295\ \log\ [HS^-]$

n') $FeS + 2H^+ + 2e \rightleftharpoons Fe + H_2S$

$Eh = -0.364 - 0.059\ pH - 0.0295\ \log\ [H_2S]$

o') $FeS + H^+ + 2e \rightleftharpoons Fe + HS^-$

$Eh = -0.571 - 0.0295\ pH - 0.0295\ \log\ [HS^-]$

p') $Fe^{2+} + 2e \rightleftharpoons Fe$

$Eh = -0.440 + 0.0295\ \log\ [Fe^{2+}]$

q') $Fe(OH)_2 + 2H^+ + 2e \rightleftharpoons Fe + H_2O$

$Eh = -0.047 - 0.059\ pH$

r') $2H^+ + 2e \rightleftharpoons H_2$

$Eh = 0.0 - 0.059\ pH$

s') $Fe^{3+} + H_2O \rightleftharpoons Fe(OH)^{2+} + H^+$

$$\log \frac{[Fe(OH)^{2+}]}{[Fe^{3+}]} = -2.43 + pH$$

t') $Fe(OH)^{2+} + H_2O = Fe(OH)_2^+ + H^+$

$$\log \frac{[Fe(OH)_2^+]}{[Fe(OH)^{2+}]} = -4.69 + pH$$

u') $Fe(OH)_2^+ + H_2O = Fe(OH)_3 + H^+$

$$\log [Fe(OH)_2^+] = -2.28 - pH$$

v') $Fe(OH)_3 + 3H^+ = Fe^{3+} + 3H_2O$

$$\log [Fe^{3+}] = 4.84 - 3\ pH$$